

University of Dundee

DOCTOR OF PHILOSOPHY

Novel semiconductor based broadly tunable light sources

Fedorova, Ksenia Alexandrovna

Award date:
2011

Awarding institution:
University of Dundee

[Link to publication](#)

General rights

Copyright and moral rights for the publications made accessible in the public portal are retained by the authors and/or other copyright owners and it is a condition of accessing publications that users recognise and abide by the legal requirements associated with these rights.

- Users may download and print one copy of any publication from the public portal for the purpose of private study or research.
- You may not further distribute the material or use it for any profit-making activity or commercial gain
- You may freely distribute the URL identifying the publication in the public portal

Take down policy

If you believe that this document breaches copyright please contact us providing details, and we will remove access to the work immediately and investigate your claim.

Download date: 17. Feb. 2017

DOCTOR OF PHILOSOPHY

Novel semiconductor based broadly tunable light sources

Ksenia Alexandrovna Fedorova

2011

University of Dundee

Conditions for Use and Duplication

Copyright of this work belongs to the author unless otherwise identified in the body of the thesis. It is permitted to use and duplicate this work only for personal and non-commercial research, study or criticism/review. You must obtain prior written consent from the author for any other use. Any quotation from this thesis must be acknowledged using the normal academic conventions. It is not permitted to supply the whole or part of this thesis to any other person or to post the same on any website or other online location without the prior written consent of the author. Contact the Discovery team (discovery@dundee.ac.uk) with any queries about the use or acknowledgement of this work.

NOVEL SEMICONDUCTOR BASED BROADLY TUNABLE LIGHT SOURCES

A Thesis presented for the degree of

Doctor of Philosophy

to the University of Dundee

by

Ksenia Alexandrovna Fedorova



Photonics and Nanoscience Group

School of Engineering, Physics and Mathematics

University of Dundee

September 2011

For my parents

Table of Contents

Contents	II
List of Figures	V
List of Tables	XI
Acknowledgements	XII
Declarations	XIV
Abstract	XV
List of Publications	XVII
<u>Chapter 1: Tunable External-Cavity Diode Lasers – Review</u>	1
1.1. Need for Tunable External-Cavity Diode Lasers.....	2
1.2. Brief History of Semiconductor Diode Lasers Development.....	3
1.3. Semiconductor Lasers.....	5
1.3.1. Semiconductor Diode Laser Structures.....	5
1.3.2. Growth Techniques and Materials.....	7
1.4. Review of Tunable Diode Lasers.....	10
1.4.1. Tunable Monolithic Semiconductor Lasers.....	10
1.4.2. Tunable External-Cavity Diode Lasers.....	11
1.4.2.1. Brief Introduction.....	11
1.4.2.2. Littrow Configuration.....	13
1.4.2.3. Littman-Metcalf Configuration.....	14
1.4.2.4. Quasi-Littrow Configuration.....	15
1.5. Summary.....	16
1.6. References.....	17
<u>Chapter 2: Tunable InGaAsP/InP Strained Multi-Quantum-Well External-Cavity Diode Laser</u>	24
2.1. Introduction.....	25
2.2. Design of InGaAsP/InP MQW Diode Laser.....	26
2.3. Experimental Setup.....	28
2.4. Results.....	30
2.5. Summary.....	34
2.6. References.....	36

<u>Chapter 3: Tunable InAs/GaAs Quantum Dot External-Cavity</u>	
Diode Lasers	38
3.1. Introduction.....	39
3.2. Semiconductor Optical Amplifier (Structure DO1866).....	41
3.2.1. Structure and Device Design of InAs/GaAs Quantum Dot Diode Laser.....	41
3.2.2. Experimental Setup.....	43
3.2.3. Results.....	45
3.3. Semiconductor Optical Amplifier (Structure DO1868).....	52
3.3.1. Structure and Device Design of InAs/GaAs Quantum Dot Diode Laser.....	52
3.3.2. Experimental Setup.....	53
3.3.3. Results.....	54
3.4. Gain Chip (Structure DO1868).....	61
3.4.1. Structure and Device Design of InAs/GaAs Quantum Dot Diode Laser.....	61
3.4.2. Experimental Setup.....	62
3.4.3. Results.....	63
3.4.4. Comparison of Different Configurations (SOA and Gain Chip).....	69
3.5. Gain Chips with Different Output Facet Reflectivities.....	69
3.6. Summary.....	72
3.7. References.....	74
<u>Chapter 4: Nonlinear Frequency Conversion Theory</u>	
4.1. Introduction.....	78
4.2. Second Order Nonlinear Optical Processes.....	79
4.3. Phase-Matching.....	82
4.3.1. Phase-Matching and Coherence Length.....	82
4.3.2. Birefringence Phase-Matching.....	82
4.3.3. Quasi-Phase-Matching.....	83
4.3.4. Mode Dispersion Phase-Matching.....	85
4.4. Summary.....	86
4.5. References.....	87
<u>Chapter 5: Frequency Doubling of Quantum Dot External-Cavity</u>	
Diode Laser in PPKTP Waveguides	89
5.1. Introduction.....	90
5.2. KTP Waveguide: Fabrication and Design.....	92
5.3. Loss Measurement in KTP Waveguides.....	93
5.4. Second Harmonic Generation at 612.9 nm.....	95
5.4.1. Experimental Setup.....	95
5.4.2. Results.....	96
5.5. Second Harmonic Generation at 591.5 nm.....	99

5.5.1.	Experimental Setup.....	99
5.5.2.	Results.....	100
5.6.	Tunable Visible Laser Source Based on Second Harmonic Generation in PPKTP Waveguide.....	103
5.6.1.	Discussion.....	103
5.6.2.	Experimental Results.....	110
5.7.	Summary.....	114
5.8.	References.....	116
Chapter 6: Frequency Conversion in OP-GaAs Waveguides.....		120
6.1.	Introduction.....	121
6.2.	Optical Parametric Oscillator Based on PP-MgO:CLN.....	125
6.2.1.	Experimental Setup.....	126
6.2.2.	Results and Discussion.....	128
6.3.	Orientation-Patterned GaAs Waveguides.....	134
6.3.1.	Sample Fabrication: First Structure.....	135
6.3.2.	Experimental Setup.....	138
6.3.3.	Sample Fabrication: Second structure.....	140
6.3.4.	Experimental Results.....	141
6.3.5.	Loss Measurement in OP-GaAs Waveguides.....	144
6.4.	Summary.....	145
6.5.	References.....	146
Chapter 7: Summary and Outlook.....		153

List of Figures

Fig. 1.1.	Evolution of the threshold current density of semiconductor diode lasers since their invention till the turn of the century. The image is adapted from [1.40].	4
Fig. 1.2.	Schematic morphology and density of states in bulk (3-D), quantum well (2-D), quantum wire (1-D) and quantum dot (0-D) material. The quantum dot case is for real dots which are not identical in size and exhibit size fluctuations leading to a broadening in energy level structure.	5
Fig. 1.3.	(a), A transmission electron microscopy (TEM) image of single plain of InAs quantum dots grown on GaAs substrate [1.59]; (b), A TEM image of a cross-section of 25-layer thick stack of InGaAs quantum dots grown on GaAs [1.60].	9
Fig. 1.4.	Schematic diagram of External-Cavity Diode Laser in Littrow configuration.	13
Fig. 1.5.	Schematic diagram of External-Cavity Diode Laser in Littman-Metcalf configuration.	14
Fig. 1.6.	Schematic diagram of External-Cavity Diode Laser in quasi-Littrow configuration.	15
Fig. 2.1.	Tunable External-Cavity Diode Lasers in the wavelength region of 1.5 μm .	26
Fig. 2.2.	The portion of the ridge waveguide mode reflected back from the as-cleaved facet into waveguide as a function of the incident angle.	27
Fig. 2.3.	InGaAs/InP strained MQW gain chip.	28
Fig. 2.4.	(a), Optical scheme of the experimental setup; (b), Simplified schematics of the ECDL configuration.	29
Fig. 2.5.	Electroluminescence spectra of the MQW gain chip at 450mA.	30
Fig. 2.6.	CW light-current characteristics for InGaAsP/InP MQW ECDL at grating positions providing wavelengths of 1550 nm and 1617 nm at 10°C and 20°C.	31
Fig. 2.7.	Tuning range limits for different temperatures and pump currents.	31

Fig. 2.8. Calculated gain spectra for InGaAsP/InP MQW structure for concentration $\sim 5 \cdot 10^{18} \text{ cm}^{-3}$. Dashed line shows the sum of the output losses and the internal losses.....	32
Fig. 2.9. Dependence of output power on wavelength measured in CW regime, at 450 mA drive current.....	33
Fig. 2.10. Spectra of the InGaAsP/InP MQW ECDL with the gain chip, tuned across the 1494 nm - 1667 nm wavelength range, under an applied constant current of 450 mA.....	33
Fig. 2.11. The resulting optical spectrum exhibited a bandwidth around 0.4 nm.....	34
Fig. 2.12. Telecommunication windows and tuning range of InGaAsP/InP MQW laser.....	35
Fig. 3.1. Tunable Quantum Dot External Cavity Diode Lasers.....	40
Fig. 3.2. PL spectrum of QD structure DO1866.....	41
Fig. 3.3. InAs/GaAs QD SOA (DO1866) chip design.....	42
Fig. 3.4. (a), Optical scheme of the experimental setup; (b), Simplified schematics of the ECDL configuration.....	43
Fig. 3.5. Transmittance of the 20% OC.....	44
Fig. 3.6. Electroluminescence spectra of the QD SOA for different bias and temperature conditions.....	45
Fig. 3.7. Light-current characteristics for InAs/GaAs QD-ECDL at grating positions providing wavelengths of 1160 nm and 1220 nm at 10°C.....	46
Fig. 3.8. Dependence of output power on wavelength for different temperatures and configurations, under an applied constant current of 1 A.....	48
Fig. 3.9. Dependence of output power on wavelength for different temperatures and configurations, under an applied constant current of 1.5 A.....	48
Fig. 3.10. Spectra of the QD ECDL with the SOA, tuned across the 1132 nm - 1310 nm wavelength range, in the configuration with the 20% OC.....	49
Fig. 3.11. The resulting optical spectrum exhibited a bandwidth around 0.12 nm.....	49
Fig. 3.12. Tuning range limits for the SOA (DO1866) for different temperatures and pump currents with the 96% OC.....	51

Fig. 3.13. Tuning range limits for the SOA (DO1866) for different temperatures and pump currents with the 20% OC.....	51
Fig. 3.14. PL spectrum of QD structure DO1868.....	52
Fig. 3.15. InAs/GaAs QD SOA (DO1868) chip design.....	53
Fig. 3.16. Electroluminescence spectra of the QD SOA chip (DO1868) for different bias and temperature conditions.....	54
Fig. 3.17. Light-current characteristics for InAs/GaAs QD-ECDL at grating positions providing wavelengths of 1180 nm and 1220 nm at 10°C.....	55
Fig. 3.18. Threshold current density of the SOA (DO1868) for different configurations.....	56
Fig. 3.19. Dependence of output power on wavelength for different temperatures and configurations of the QD-ECDL with the SOA, under an applied constant current of 1.7 A.....	57
Fig. 3.20. Spectra of the QD-ECDL with the SOA (DO1868), tuned across the 1125.5 nm – 1320 nm wavelength range, under an applied constant current of 1.7 A.....	58
Fig. 3.21. The resulting optical spectrum exhibited a bandwidth around 0.13 nm.....	58
Fig. 3.22. Tuning range limits for the SOA (DO1868) for different temperatures and pump currents with the 96% OC (a) and the 20% OC (b).....	59
Fig. 3.23. The prototype of the QD-ECDL.....	60
Fig. 3.24. InAs/GaAs QD gain chip (DO1868) design.....	61
Fig. 3.25. (a) Optical scheme of the experimental setup; (b) Simplified schematics of the ECDL configuration.....	62
Fig. 3.26. Electroluminescence spectra of the QD gain chip (DO1868) for different bias and temperature conditions.....	63
Fig. 3.27. Light-current characteristics for InAs/GaAs QD-ECDL at grating positions providing wavelengths of 1150 nm and 1220 nm at 10°C.....	64
Fig. 3.28. Threshold current density of the gain chip (DO1868) for different configurations.....	64
Fig. 3.29. Comparison of threshold current densities of the gain chip (DO1868) and the SOA (DO1868) in the configuration with 20% OC at 10°C.....	65

Fig. 3.30. Dependence of output power on wavelength for different temperatures and configurations of the QD-ECDL with the gain chip, under an applied constant current of 1.7 A.....	66
Fig. 3.31. Spectra of the QD-ECDL with the gain chip (DO1868), tuned across the 1122.5 nm – 1324.5 nm wavelength range, under an applied constant current of 1.7 A.....	67
Fig. 3.32. The resulting optical spectrum exhibited a bandwidth around 0.13 nm.....	67
Fig. 3.33. Tuning range limits for the gain chip (DO1868) for different pump currents and temperatures without an output coupler (a) and with the 20% output coupler (b).....	68
Fig. 3.34. Dependence of output power on wavelength for different configurations of the QD-ECDL with the gain chips with 3 different values of the output facet reflectivity ($2 \cdot 10^{-3}$, 10^{-2} and $3 \cdot 10^{-2}$), under an applied constant current of 1.5 A at 10°C	70
Fig. 3.35. Tuning range limits for the gain chips (DO1868) with 3 different values of the output facet reflectivity ($2 \cdot 10^{-3}$, 10^{-2} and $3 \cdot 10^{-2}$) for different pump currents and temperatures without an output coupler and with the 20% output coupler.....	71
Fig. 3.36. Tuning range of the demonstrated InAs/GaAs QD ECDL.....	72
Fig. 4.1. Sum frequency and second harmonic generation.....	80
Fig. 4.2. Optical parametric generation.....	80
Fig. 4.3. Basic OPO cavity.....	81
Fig. 4.4. Wave vector diagram of various phase-matching schemes: (a) and (b) Birefringence Phase-Matching, (c) Quasi-Phase-Matching, (d) Mode Dispersion Phase-Matching [4.8].....	83
Fig. 4.5 Second harmonic intensity as a function of the propagation distance inside the crystal in units of the coherence length l_C	84
Fig. 4.6. Waveguide dispersion curves showing mode dispersion phase-matching [4.8].....	85
Fig. 5.1. Microscope photograph of the cross section of a Ba/Rb-exchanged channel waveguide in KTP crystal.....	92
Fig. 5.2. Optical scheme of the experimental setup (including diffraction grating, gain chip, KTP waveguide, half-wave plate ($\lambda/2$) and 40x AR coated aspheric lenses).....	93

Fig. 5.3.	Total insertion loss measured using the cutback method.....	94
Fig. 5.4.	Optical scheme of the experimental setup (including diffraction grating, semiconductor optical amplifier (SOA), 96% output coupler (96% OC), PPKTP waveguide, half-wave plate ($\lambda/2$), 30x and 40x lenses and filter at the fundamental wavelength).....	95
Fig. 5.5.	Frequency-doubled output power at 612.9 nm and 613.6 nm versus launched pump power from gain chip at 1225.8 nm (<i>triangles</i>) and 1227.2 nm (<i>squares</i>), respectively.....	97
Fig. 5.6.	Photograph of the efficient SHG at 612.9 nm from the QD-ECDL and the PPKTP waveguide.....	97
Fig. 5.7.	Optical spectrum of the generated second harmonic (612.9 nm). <i>Inset:</i> Spectrum of the fundamental wavelength (1225.8 nm).....	98
Fig. 5.8.	Spectra of SHG tuned across the 612.9 – 616.3 nm wavelength range.....	98
Fig. 5.9.	Optical scheme of the experimental setup (including diffraction grating, gain chip, PPKTP waveguide, half-wave plate ($\lambda/2$), 40x lenses and filter at the fundamental wavelength).....	99
Fig. 5.10.	Frequency-doubled output power at 591.5 nm versus launched pump power from gain chip at 1183 nm.....	100
Fig. 5.11.	Photograph of the efficient SHG at 591.5 nm from the QD-ECDL and the PPKTP waveguide.....	101
Fig. 5.12.	Optical spectrum of the generated second harmonic (591.5 nm). <i>Inset:</i> Spectrum of the fundamental wavelength (1183 nm).....	101
Fig. 5.13.	Spectra of SHG tuned across the 591.5 – 594.2 nm wavelength range.....	102
Fig. 5.14.	Simplified schematic of the effective refractive indices for the fundamental and SH modes of different order.....	106
Fig. 5.15.	Calculated SHG tunability in a multi-mode PPKTP waveguide.....	108
Fig. 5.16.	Calculated SHG tunability for the PPKTP waveguides with $\Delta n = 0.01$ (solid lines) and 0.025 (dashed lines). Horizontal dashed line represents the physical poling period of $\sim 9.7 \mu\text{m}$, which corresponds to the QPM in the spectral region between 480 and 640 nm for $\Delta n=0.025$	109
Fig. 5.17.	Calculated dependence of the total tunable range $\Delta\lambda$ on waveguide refractive index step Δn for some nonlinear crystals (peak fundamental wavelength: 1183 nm).....	109

Fig. 5.18. Frequency doubled output power versus launched pump power for several SHG peaks corresponding to phase-matching between fundamental and SHG modes of different orders. Inset: zoom in.....	110
Fig. 5.19. Dependence of SHG conversion efficiency (black curve) and launched pump power (red curve) on wavelength.....	111
Fig. 5.20. Observed intensity profiles of the second-harmonic (colour images) and fundamental modes (red images) in the spectral region between 567.7 and 629.1 nm. In the centre: dependence of poling period on wavelength for different-order waveguide modes for frequency-doubling in a PPKTP waveguide.....	112
Fig. 5.21. Zoom in and observed intensity profiles of second-harmonic (colour images) and fundamental modes (red images).....	113
Fig. 6.1. Fabrication of a GaAs QPM grating: (a), GaAs/Ge/GaAs sublattice reversal epitaxy; (b), template formation by patterned etching; (c), GaAs overgrowth [6.34].....	123
Fig. 6.2. Calculated output SHG power versus pump wavelength for optimal crystal length with (a) a femtosecond pump beam and (b) a CW pump beam.....	124
Fig. 6.3. Simplified schematics of the experimental setup (including Nd:YAG laser, Faraday isolator, lens with $F=50\text{cm}$, half-wave plate ($\lambda/2$), PP-MgO:CLN and mirrors M1 and M2).....	126
Fig. 6.4. PP-MgO:CLN crystal configuration.....	127
Fig. 6.5. Dependence of reflectance of the PP-MgO:CLN crystal facets on wavelength.....	128
Fig. 6.6. Dependence of the idler wavelength on the signal wavelength for pump at 1064 nm.....	129
Fig. 6.7. Dependence of the signal and idler wavelengths on temperature ($24^\circ\text{-}201.3^\circ\text{C}$) for the PP-MgO:CLN crystal with seven grating periods ($\Lambda=28.5\text{-}31.5\mu\text{m}$). Results are compared with theoretical curves according to the Sellmeier equation [6.49].....	130
Fig. 6.8. Output power of the signal and idler waves and the total down-converted power as a function of the pump power (grating period = $31.5\mu\text{m}$).....	132
Fig. 6.9. Output power of the signal and idler waves and total down-converted power as a function of the pump power (grating period = $30.5\mu\text{m}$).....	132

Fig. 6.10. Measured spectra of the pump, signal and idler waves (grating period = 30.5 μm).....	133
Fig. 6.11. Fabrication process of OP-GaAs waveguide.....	136
Fig. 6.12. First epitaxial layer structure.....	137
Fig. 6.13. High quality re-orientated GaAs material with waveguides.....	138
Fig. 6.14. Completed OP-GaAs waveguide device.....	138
Fig. 6.15. Simplified schematic of the experimental setup for SHG in OP-GaAs waveguides.....	139
Fig. 6.16. Second epitaxial layer structure.....	140
Fig. 6.17. High quality re-orientated GaAs material with waveguides.....	141
Fig. 6.18. Completed OP-GaAs waveguide device.....	141
Fig. 6.19. Photographs of output facets of devices demonstrating guiding in ridge waveguide (left picture) and bulk material (right picture).....	142
Fig. 6.20. Second harmonic intensity as a function of fundamental input power.....	143
Fig. 6.21. Spectra of the fundamental and SHG waves.....	143
Fig. 6.22. Total insertion loss measured using the cutback method.....	144
Fig. 7.1. Spectral range covered by tunable light sources demonstrated in the thesis and potential frequency conversion device based on presented results.....	153

List of Tables

Table 3.1. Tuning range limits for the SOA (DO1866) for different configurations at 10°C and 20°C, under an applied constant current of 1 A and 1.5 A.....	50
Table 6.1. Coherence lengths required for SHG and OPO.....	134

Acknowledgements

I would like to acknowledge a number of people without whom this thesis would never have been completed.

First and foremost, I would like to thank my supervisor Professor Edik Rafailov for giving me the opportunity to work in his group in Dundee and for his incessant guidance, availability, advice, support and encouragement throughout these years.

Many special thanks also go to Dr. Grigorii Sokolovskii whose knowledge, help and encouragement were invaluable during my studies. I greatly appreciate the many fruitful discussions we have had throughout these years.

I am also indebted to Dr. Douglas McRobbie who assisted with the ion beam etching work.

I also would like to thank Dr. Daniil Livshits and Dr. Igor Krestnikov (Innolume GmbH) and Dr. Igor Kudryashov (Princeton Lightwave Inc.) for providing the laser sources and Dr. Philip Battle (AdvR Inc.) and Dr. Peter Schunemann (BAE Systems) for providing nonlinear crystals here studied.

I greatly acknowledge the EPSRC for the essential financial support that has enabled this research.

Special thanks must also go to the members of the Photonics and Nanoscience Group for their friendship, advice and empathy, and especially Dr. Natalia Bazieva and Dr. Sergei Sokolovski.

Throughout the course of my PhD I have been in the constant debt of the technical staff of the School of Electronic Engineering and Physics. I am particularly grateful to Mr. Callum Moore and Dr. Gary Callon.

I also would like to express my gratitude to my two examiners Prof. Richard Hogg (University of Sheffield) and Dr. Stephen Reynolds (University of Dundee) who kindly agreed to spend their time and efforts reading and improving my thesis.

I would like to thank all my friends, and especially Alesha, Maxim, Serega and Polina for their support all the time, for their patience and for hearing me.

And finally but most importantly, I am very grateful to my parents for their unwavering support throughout all my life which has only reinforced my desire to make them proud of me, and there will never be enough words to thank them. Dear Mum and Dad, I love you so much!

Declarations

I, Ksenia Alexandrovna Fedorova, hereby certify that this thesis has been written by me, that it is a record of work carried out by me, that it has not been submitted in any previous application for a higher degree and that all references cited have been consulted by myself.

Date

Signature of candidate

Ksenia A. Fedorova

I hereby certify that Ksenia A. Fedorova has fulfilled the conditions of the Ordinance and Regulations appropriate for the degree of Doctor of Philosophy in the University of Dundee and that she is qualified to submit this thesis in the application for that degree.

Date

Signature of supervisor

Professor Edik U. Rafailov

Abstract

The development of compact and low-cost coherent sources in visible and infrared wavelength range can provide indispensable tools for a variety of scientific, technological and industrial applications. Great progress over the last years in material science, crystal growth and semiconductor material processing in combination with recent advances in some of the more traditional technologies, in particular nonlinear frequency conversion and parametric sources, have led to the realisation of a new generation of laser sources. Furthermore, the advent of a new generation of quasi-phase-matched, waveguided and semiconductor nonlinear materials together with novel semiconductor lasers have led to the development of new frequency conversion and parametric sources with previously unattainable performance capabilities.

The research described in this thesis relates to the development and characterisation of novel semiconductor based laser sources tunable in the broad spectral ranges which are unattainable for conventional lasers due to a lack of suitable laser gain materials.

In the first part of the thesis the subject matter is concerned with the direct emission from laser devices. In particular, a broadly tunable InGaAs/InP strained multi-quantum well external cavity diode laser, operating in the spectral range of 1494 nm – 1667 nm with a maximum CW output power in excess of 81 mW and side-mode suppression ratio higher than 50 dB is demonstrated. This represents the highest output power and side-mode suppression ratio ever to be generated in this spectral region.

A record broadly tunable high-power external cavity InAs/GaAs quantum-dot diode laser with a tuning range of 202 nm (1122 nm - 1324 nm), a maximum output

power of 480 mW and a side-mode suppression ratio greater than 45 dB, is also demonstrated. This represents a promising achievement for the development of a high-power fast swept tunable laser and compact nonlinear frequency generation schemes for the green-yellow-orange-red spectral range.

The second part of the thesis relates to induced nonlinear processes, focusing on frequency doubling and optical parametric oscillation. In particular, an all-room-temperature CW second harmonic generation at 612.9 nm and 591.5 nm in periodically poled potassium titanyl phosphate waveguides pumped by a broadly-tunable quantum-dot external cavity diode laser with a conversion efficiency of 10.5% and 7.9%, respectively, is demonstrated.

For the first time, a green-to-red tunable laser source with tunability of over 60 nm (567.7 nm – 629.1 nm) based on frequency doubling in a single periodically poled potassium titanyl phosphate waveguide pumped by a single broadly-tunable quantum dot laser is demonstrated. These results are an important step towards a compact tunable coherent visible light source, operating at room temperature.

The possibility of nonlinear frequency conversion in orientation-patterned GaAs waveguides is also investigated. The technology of low-loss periodically poled GaAs waveguided crystals is developed and such crystals are fabricated. Second harmonic generation at 1621 nm in low-loss periodically poled GaAs waveguide is demonstrated. An optical parametric oscillator system used as the pump source for GaAs devices and based on the periodically poled 5 mol% MgO-doped Congruent Lithium Niobate crystal, generating light in the wavelength range between 1430 nm and 4157 nm, is presented. The obtained results show a great promise for realisation of efficient quasi-phase-matched optical parametric oscillator devices based on orientation-patterned GaAs waveguides, which enables the extending generated wavelength up to 16 μm .

List of Publications

Publications in Peer-reviewed Journals

1. **Green-to-red tunable SHG of a quantum-dot laser in a PPKTP waveguide**
K.A. Fedorova, G.S. Sokolovskii, E.U. Rafailov
Nature Physics (submitted).
2. **High-Power Versatile Picosecond Pulse Generation from Mode-Locked Quantum-Dot Laser Diodes**
 M.A. Cataluna, Y. Ding, D.I. Nikitichev, K.A. Fedorova, E.U. Rafailov
IEEE Journal of Selected Topics in Quantum Electronics, 17(5), pp.1302-1310 (2011).
3. **Orange light generation from a PPKTP waveguide end-pumped by a cw quantum-dot tunable laser diode**
K.A. Fedorova, M.A. Cataluna, P.R. Battle, C.M. Kaleva, I.L. Krestnikov, D.A. Livshits, E.U. Rafailov
Applied Physics B, 103, pp.41-43 (2011).
4. **Broadly Tunable High-Power InAs/GaAs Quantum-Dot External Cavity Diode Lasers**
K.A. Fedorova, M.A. Cataluna, I.L. Krestnikov, D.A. Livshits, E.U. Rafailov
Optics Express, 18(18), pp.19438-19443 (2010).
5. **Broadly Tunable InGaAsP/InP Strained Multiquantum-Well External Cavity Diode Laser**
K.A. Fedorova, M.A. Cataluna, I. Kudryashov, V. Khalfin, E.U. Rafailov
Photonics Technology Letters, 22(16), pp.1205-1207 (2010).
6. **1.2-um Semiconductor Disk Laser Frequency Doubled With Periodically Poled Lithium Tantalate Crystal**
 J. Rautiainen, K.A. Fedorova, J. Nikkinen, D. Eger, V.-M. Korpijärvi, E.U. Rafailov, O.G. Okhotnikov
Photonics Technology Letters, 22(7), pp.453-455 (2010).
7. **Electronic and thermal lensing in diode end-pumped Yb:YAG laser rods and discs**
 O.L. Antipov, E.A. Anashkina, K.A. Fedorova
Quantum Electronics, 39(12), pp. 1131- 1136 (2009).
8. **Intracavity generation of 610 nm light by periodically poled near-Stoichiometric Lithium Tantalate**
 J. Rautiainen, O.G. Okhotnikov, D. Eger, S.A. Zolotovskaya, K.A. Fedorova, E.U. Rafailov
Electronics Letters, 45(3), pp.177-178 (2009).
9. **Efficiency Enhancement of Components Based on Talbot Effect**
 G.G. Denisov, K.A. Fedorova, Yu.Yu. Danilov, S.V. Kuzikov, M.Yu. Shmelev, M.E. Plotkin
International Journal of Infrared and Millimeter Waves 28(11), pp.923-935 (2007).

Contributions to Peer-reviewed Conferences

1. **Broadly tunable CW green-to-red laser source based on frequency doubling of a quantum-dot external cavity diode laser in a PPKTP waveguide**
K.A. Fedorova, M.A. Cataluna, P.R. Battle, I.L. Krestnikov, D.A. Livshits, E.U. Rafailov
CLEO/Europe-EQEC 2011, CD3.3, Munich, Germany (2011).
2. **High-power spectral bistability in a multi-section quantum dot laser under continuous-wave or mode-locked operation**
 D.I. Nikitichev, M.A. Cataluna, Y. Ding, K.A. Fedorova, I. Krestnikov, D.A. Livshits, E.U. Rafailov
CLEO:2011, CThG1, Baltimore, USA (2011).
3. **Basic principles of design and functioning of multifunctional laser diagnostic system for non-invasive medical spectrophotometry**
 D.A. Rogatkin, S.G. Sokolovski, K.A. Fedorova, V.V. Sidorov, N.Z. Stewart, E.U. Rafailov
Proceedings of SPIE Vol. 7890, art. no.78901H (2011).
4. **202nm Continuous Tuning from High-Power External-Cavity InAs/GaAs Quantum-Dot Laser**
K.A. Fedorova, M.A. Cataluna, I. Krestnikov, D. Livshits, E.U. Rafailov
ISLC 2010, WD 3, Kyoto, Japan (2010).
5. **Broadband tunable InAs/GaAs quantum-dot lasers**
K.A. Fedorova, M.A. Cataluna, I. Krestnikov, D. Livshits, E.U. Rafailov
Photon 10, Southampton (2010).
6. **Tuning range enhancement in external-cavity InAs/GaAs quantum-dot lasers: temperature, bias and cavity loss dependence**
K.A. Fedorova, M.A. Cataluna, I. Krestnikov, D. Livshits, E.U. Rafailov
The 1st EOS Topical Meeting in Lasers, p. 2194, Capri, Italy (2009).
7. **Generation of orange light from a PPKTP waveguide end-pumped by a quantum-dot tuneable laser**
K.A. Fedorova, M.A. Cataluna, A. Abdolvand, P. Battle, I. Krestnikov, D.A. Livshits, M. Khomylev, E.U. Rafailov
CLEO/Europe-EQEC 2009, CD.P.26, Munich, Germany (2009).
8. **Population lensing vs thermal lensing in Yb:YAG rods and disks**
 E.A. Anashkina, O.L. Antipov, K.A. Fedorova
CLEO/Europe-EQEC 2009, CA.P19, Munich, Germany (2009).
9. **Periodically poled lithium tantalate crystals for efficient SHG generation**
 J. Rautiainen, K.A. Fedorova, D. Eger, V.-M. Korpijärvi, O.G. Okhotnikov, A. Abdolvand, E.U. Rafailov
CLEO/Europe-EQEC 2009, CD.P36, Munich, Germany (2009).

OTHER CONTRIBUTIONS

1. **Tuning range enhancement in external-cavity InAs/GaAs quantum-dot lasers**
K.A. Fedorova, M.A. Cataluna, I. Krestnikov, D. Livshits, E.U. Rafailov
SUSSP 66, Edinburgh, UK (2010).

1. Tunable External-Cavity Diode Lasers – Review

This Chapter presents a review of tunable diode lasers and describes the need for compact tunable external-cavity diode lasers and the brief history of their development. The growth techniques, possible semiconductor diode laser structures and commonly used external-cavity configurations are also discussed.

1.1. Need for Tunable External-Cavity Diode Lasers

Tunable compact laser sources emitting in the 1.1 - 1.3 μm and 1.55 μm spectral regions are of considerable interest for a wide range of applications, such as spectroscopy [1.1], interferometry [1.2] and telecommunication systems [1.3]. Longer distances and higher speeds of information transmission dictate the move toward these wavelengths, which correspond to the minimum dispersion and minimum loss in the standard glass fibre at 1.3 μm and 1.55 μm , respectively. Tunable diode lasers utilising an external-cavity diode laser (ECDL) design can provide many attractive features needed for wavelength-division-multiplexing (WDM) applications such as a very narrow linewidth, wide continuous tuning range, high output power, and considerable inventory reduction [1.4]. In recent years, there has also been a growing interest in the development of broadly-swept tunable laser sources, which are of interest for optical coherence tomography due to their high spectral bandwidth and output power [1.5-1.7]. Furthermore, the spectral region encompassing 1.1 - 1.3 μm is particularly useful for biomedical imaging due to the minimal absorption and scattering in human tissue, which can significantly enhance the penetration depth [1.8]. Other important applications for this spectral range include the generation of coherent radiation in the visible spectral region via second harmonic generation or sum frequency generation, particularly into the yellow-orange spectral region [1.9,1.10], for which compact and efficient sources are relatively scarce. Tunable compact laser sources emitting in the visible spectral region at around 550 nm - 650 nm are of considerable interest for various applications, such as biophotonic [1.11] and medical [1.12] applications, photodynamic therapy [1.13], laser projection displays [1.14] and optical atomic clock in ytterbium [1.15]. Commercially available lasers of this spectral range are in practice bulky and inconvenient in use. In this respect, the

ECDL is very promising for the realisation of a compact laser source in the visible spectral region by frequency doubling of infrared light in a nonlinear crystal.

1.2. Brief History of Semiconductor Diode Lasers Development

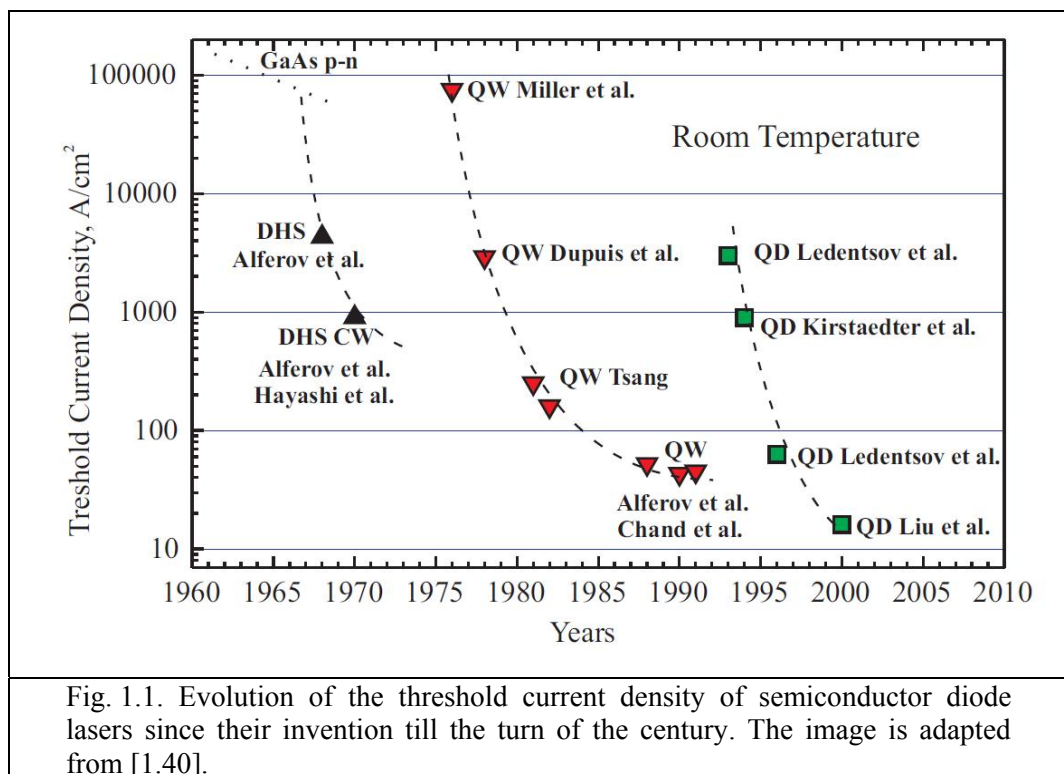
Since their first demonstration by Basov *et al.* in 1961 [1.16] and following experimental realisations by other scientific groups [1.17-1.20], semiconductor diode lasers were of great interest for many applications such as optical data storage, fibre optics and free space communication. However, the simple p-n junction semiconductor lasers fabricated at that time suffered from high threshold current density ($\sim 10^5 \text{ A/cm}^2$) and were able to operate only at cryogenic temperature.

In 1963, a double heterostructure laser, consisting of a lower bandgap layer surrounded by a higher bandgap semiconductor material, was suggested by Alferov [1.21] and Kroemer [1.22]. The development of the double heterostructure in 1968 [1.23] made possible to fabricate reliable diode lasers, which operate at room temperature with sufficiently low current [1.24,1.25].

A new hope appeared in the middle 1970s, when it had been predicted that reducing the dimensionality of the active region can significantly improve the performance of semiconductor lasers [1.26]. The development of new growth techniques: metal organic chemical vapour deposition (MOCVD) [1.27] and molecular beam epitaxy (MBE) [1.28], enabled the crystal deposition to be controlled on an atomic scale and led to growth of quantum well (QW) [1.29-33] and quantum dot (QD) [1.35-1.39] laser structures. The utilisation of these lower dimensional semiconductor

structures made it possible to operate QW [1.33,1.39] and QD [1.38] diode lasers at very low threshold current with higher efficiencies. The evolution of semiconductor diode lasers from their invention until the turn of the century is shown in Fig. 1.1 [1.40].

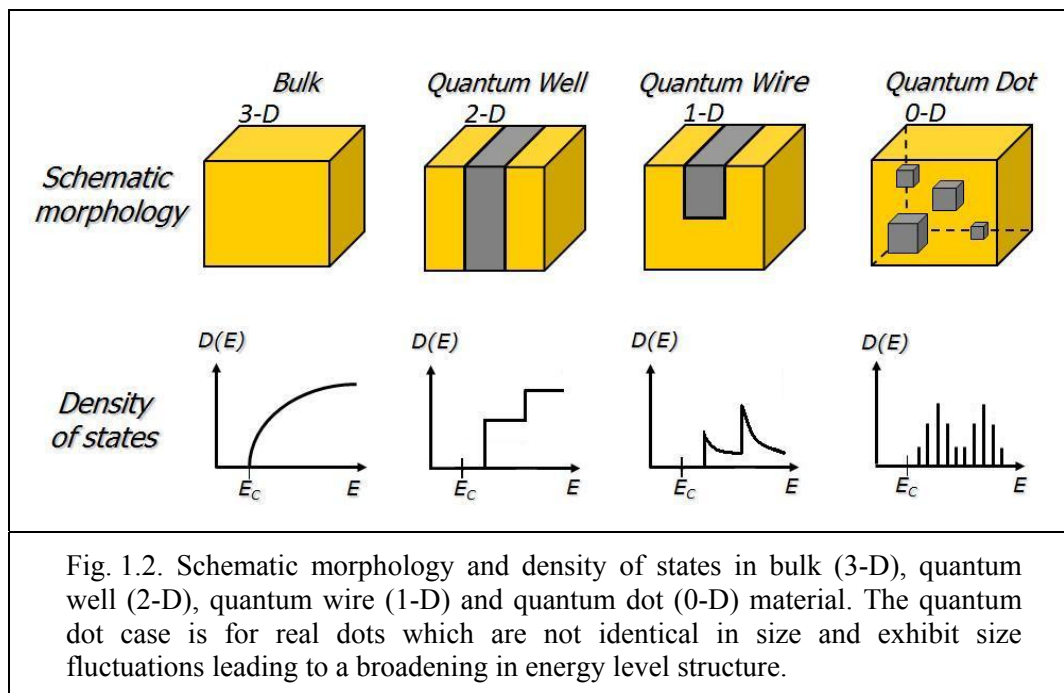
Up until now, QD and QW lasers were of great interest for research, because the flexibility in choice of semiconductor material compounds allowed a wide spectral range, from visible to infrared, to be covered [1.41]. Nowadays, diode lasers are widely used as compact and cheap coherent light sources in broad range of applications including biophotonic and medical applications, spectroscopy, interferometry, telecommunications, optical storage, laser printing, laser projection displays etc.



1.3. Semiconductor Lasers

1.3.1. Semiconductor Diode Laser Structures

Semiconductor lasers are compact low-cost sources for generating light in a broad wavelength range. Owing to the flexibility in choice of semiconductor material compounds, the emission wavelength can be engineered over a wide spectral range from visible to infrared [1.41]. Semiconductor diode laser characteristics are strongly connected with the band structure of their active region and can be optimized by the use of artificial structures. The family of possible dimensionalities of the laser active region involves bulk semiconductor epilayer (three-dimensional), thin epitaxial layer of quantum well (two-dimensional), elongated tube of quantum wire (one-dimensional) and isolated island of quantum dot (zero-dimensional) [1.42]. All these four cases are shown schematically in Fig. 1.2.



When the freedom of electron motion is restricted by reducing the dimensionality of the active region from bulk to QW, quantum wire and QD array, the density of states (DOS) is strongly modified, and as dimensionality decreases, the DOS is no longer continuous or quasi-continuous but become quantised (Fig. 1.2). In the ultimate case of a QD ensemble (confinement on the order of the de Broglie wavelength in all 3 dimensions), DOS represents a set of delta-function peaks centred at the atomic-like energy level.

In contrast to QW lasers which offer only 1-D carrier confinement and exhibit strain limits, semiconductor lasers based on self-assembled QDs provide valuable laser performance advantages. Increasing carrier confinement results in less temperature sensitivity and reduction of threshold current density. The inhomogeneous broadening associated with the strain and size dispersion of the QDs (inherent to the Stranski-Krastanow growth techniques) results in a distribution of energies which, to some extent, parallels the distribution of QD sizes. This feature, together with the manipulation of the chemistry and strain of the capping layers and barriers, can be flexibly engineered to widen the emission spectral bandwidth. By exploiting such broad gain bandwidths, QD based laser have demonstrated widely tunable high power output [1.43].

1.3.2. Growth Techniques and Materials

There are two main epitaxial growth techniques used for fabrication of epitaxially grown layers. These are Metal Organic Chemical Vapour Deposition (MOCVD), also known as Metal Organic Vapour Phase Epitaxy (MOVPE), and Molecular Beam Epitaxy (MBE). These techniques differ considerably in the sources used and surface growth kinetics. MOCVD is particularly complex with many factors, such as precursor chemistry, growth kinetics, hydrodynamics, mass transport and surface chemistry influencing growth [1.44]. In contrast to MBE, MOCVD uses chemical reactions and not physical deposition. Also, while MBE growth is conducted at very low pressures (10^{-8} to 10^{-9} Pa), MOCVD takes place at pressures that are much more comparable to atmospheric pressure (10^5 to 10^4 Pa for low-pressure MOCVD and 10^{-2} to 10^{-4} Pa for so-called vacuum MOCVD [1.45]). MOCVD technique is widely used in the manufacture of laser diodes.

For a long time, MBE [1.46] or MOCVD [1.47] techniques are used for growth of Single Quantum Well (SQW) or Multiple Quantum Well (MQW) structures, which required thin layers with typically thickness of 10nm or less [1.48]. In this respect, MOCVD technique can offer precise control of film thickness and alloy composition.

In the growth of MQW laser structures, the usual practice is to control the compositions of adjacent layers appropriately so as to produce lattice matching and eliminate internal strain. However, recent work has shown that in case of high power lasers, it may be desirable to introduce an amount of controlled strain [1.48]. Strain in the active region of QW semiconductor lasers has improved several important laser parameters as compared with lattice matched-well lasers [1.49]. InGaAsP/InP strained MQW structures are widely used in semiconductor lasers operating in the wavelength

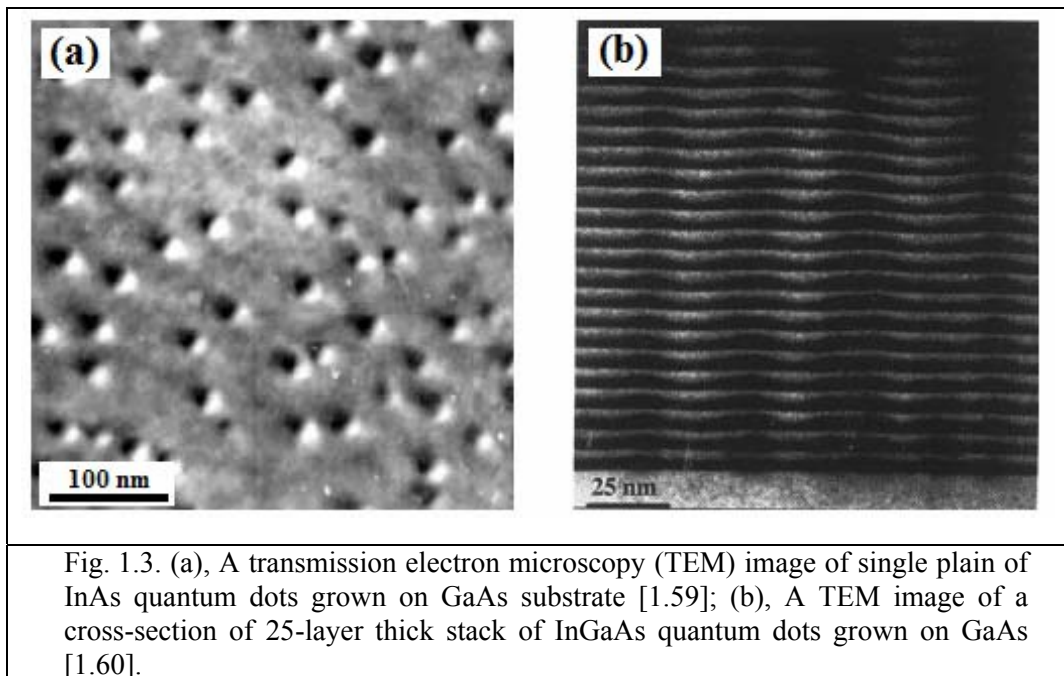
region of 1.5 μm , and they are currently of considerable interest for telecommunication applications as transmitters (digital and analogue systems) and also WDM pump sources for C- and L-band Raman amplifiers [1.50].

The recent achievements in quantum dot (QD) epitaxial growth have enabled the fabrication of QD lasers. The most effective method for the fabrication of three-dimensional islands (or QDs) is the strained-layer epitaxial growth in the Stranski-Krastanow mode [1.51-1.53]. In this growth mode, when a film is epitaxially grown over a substrate, the initial growth occurs layer by layer, but beyond a certain critical thickness, QDs start to form on top of a continuous film called the wetting layer. A crucial requirement of this technique is that the lattice constant of the deposited material is larger than that of the substrate, so that the additional strain leads to the formation of dots [1.54]. This is the case in an InAs film with the lattice constant of 6.06Å deposited on a GaAs substrate (lattice constant of 5.64Å). An advantage of this technique is that films can be grown using MBE and MOCVD. Fabrication of QDs by applying Stranski-Krastanow growth is accompanied by a distribution in dot size, height, shape and composition, due to the statistical fluctuations occurring during growth, but, at the moment, epitaxy techniques have evolved to such an extent that the amount of fluctuations can be reasonably controlled, and can be as small as a few percentage points.

Lateral positions of QDs grown in a plane surface are random, as shown in Fig. 1.3(a). In the self-assembly process, there is not a standard way of arranging the dots in a planar ordered way. The typical sizes of quantum dots are 15-20 nm in diameter and ~5 nm in height. The dot size, the shape and the surface density depend on the growth temperature and other growth conditions. The size of the quantum dots can be varied by changing the thickness of the capping layer. The average size of the QDs

capped with thicker layer is larger. By changing the thickness of the capping layers for different groups of QD layers, a broad spectral emission can be achieved.

At present, the densities of quantum dots lie typically between 10^9 cm^{-2} and 10^{11} cm^{-2} [1.55]. Typically a single layer of quantum dots provides insufficient gain for lasing so that stacked quantum dot layers are needed [1.56,1.57]. Growth of QDs in stacks allows an increase in the modal gain without increasing the internal optical mode loss [1.58]. A cross-section of a multi-stacked structure is shown in Fig. 1.3(b).



In this figure, InGaAs quantum dots are shown as thicker dark regions, which are connected within the layers by the wetting layers (thin dark regions). The various layers are separated by GaAs (lighter regions). The GaAs separators are responsible for transmitting the tensile strain from layer to layer, inducing the formation of ordered arrays of quantum dots aligned on the top of each other.

1.4. Review of Tunable Diode Lasers

1.4.1. Tunable Monolithic Semiconductor Lasers

There are several types of diode lasers which operate in single mode and can be continuously tuned. Distributed feedback (DFB) lasers and distributed Bragg reflector (DBR) lasers use integrated grating to achieve single mode operation [1.61]. They are very compact and easy to operate, but their wavelengths are usually limited to 1.3 μm and 1.55 μm , which correspond to the minimum dispersion and minimum loss in the standard glass fibre at 1.3 μm and 1.55 μm , respectively. DFB and DBR lasers at other wavelengths are rarely available and expensive. The design of these lasers is very specialised and their fabrication requires sophisticated equipment. Broadband tuning of DFB and DBR lasers has been obtained [1.62,1.63]. However, the linewidth of these lasers is 2 to 3 orders of magnitude broader [1.64] than that obtained with external cavity diode lasers (ECDL). Another type is a vertical-cavity surface emitting laser (VCSEL) [1.65,1.66]. These lasers well suited to low-cost, high-density uses in computer network and can be widely tunable [1.67], but their tuning range is relatively smaller than that offered by ECDLs [1.43,1.68].

Monolithic semiconductor diode lasers are compact and robust, but they have some limitations for certain applications. Ordinary solitary diode lasers usually operate in multi-mode and exhibit broad spectral linewidth. Moreover, such lasers can be tuned over only a limited spectral range by varying temperature or current of the diode, but the small tuning range cannot meet many applications.

The ECDL is an alternative to monolithic semiconductor diode laser for the development of widely tunable laser source. The ECDLs offer very attractive linewidth

as narrow as a few kilohertz, wide continuous tuning range of hundreds of nanometres, good single mode and high stability [1.69].

1.4.2. Tunable External-Cavity Diode Lasers

1.4.2.1. Brief Introduction

The first demonstration of laser diode coupled to external cavity was realised in 1964 by Crowe and Craig [1.70]. In the early and late 1970s, several papers on external cavity diode lasers were published by two Soviet research groups [1.71-1.74]. In 1972 Ludeke and Harris [1.75] reported the tunability of CW radiation from GaAs injection laser in an external dispersive cavity over a range of 15 nm about the centre wavelength of 825.5 nm at a temperature of 77K. Single mode operation with CW output power as large as 17 mW with a linewidth of 350 MHz was observed. In 1981 Fleming and Mooradian [1.76] were the first to study the spectral properties of ECDLs in detail. In the early to mid-1980s, the prospect of applying external cavity diode lasers as a transmitter and local oscillator in coherent optical telecommunications [1.68,1.77] motivated British Telecom Research Laboratories for study of ECDL. In the same time, a lot of research was done at AT&T Bell Laboratories and Centre National d'Etudes des Telecommunications (CNET) [1.78]. At the end of the 1980's and the beginning of the 1990's, there was a growing interest in ECDLs as coherent radiation sources for spectroscopic research and in commercial fibre optic test and measurement equipment [1.79]. Nowadays, broadly tunable, compact and low-cost ECDLs are being developed for the applications in telecommunications and wavelength division multiplexing (WDM) systems [1.3]. In recent years, there has also been a growing interest in the

development of broadly-swept tunable laser sources, which are of interest for optical coherence tomography due to their high spectral bandwidth and output power [1.5-1.7].

The classic ECDL consists of a semiconductor diode laser with or without the antireflection coatings on one or two facets, beam collimators and an external wavelength-selective optical element. One of the commonly used optical elements placed within an external cavity is a diffraction grating, which can accomplish the tuning of laser wavelength in the broad wavelength range and the narrowing of laser linewidth [1.80]. A diffraction grating reflects different wavelengths at slightly different angles, similar to a prism, spatially separating the light by wavelength. The Littman-Metcalf [1.81,1.82] and the Littrow [1.80] cavity configurations are typically used for implementation of tunable ECDLs. In both configurations a diffraction grating is used to control the emission wavelength and the selection of a single longitudinal mode of laser oscillation.

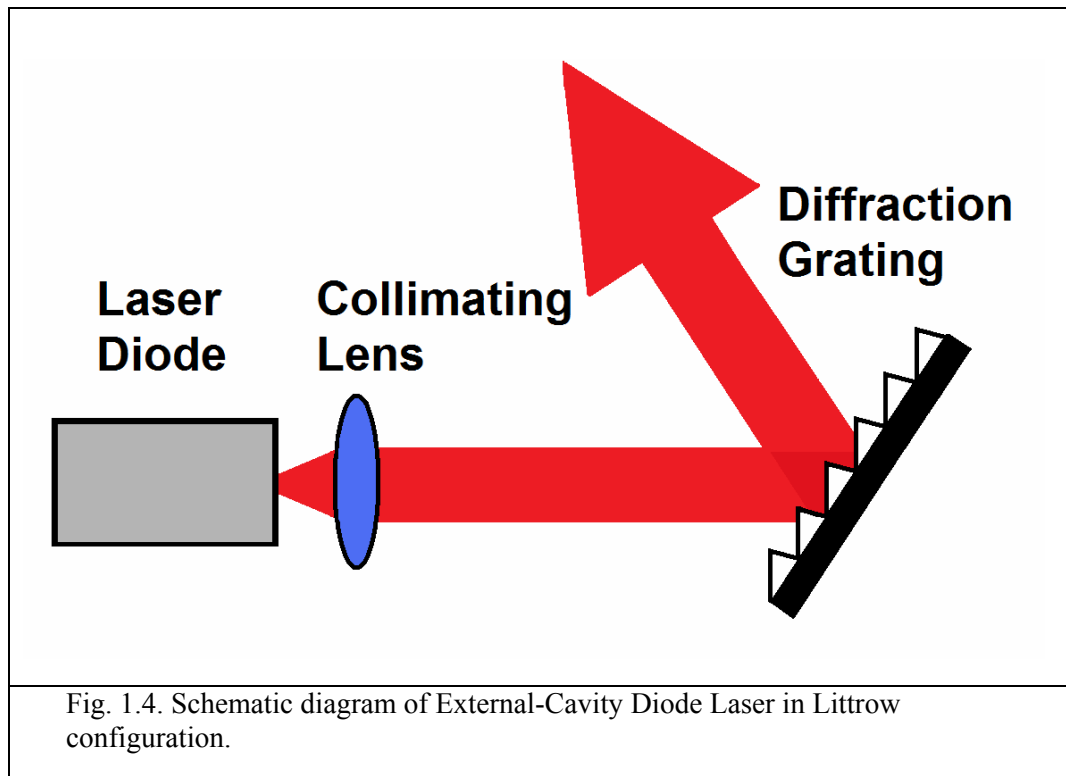
The lasing wavelength of ECDL in configuration containing a diffraction grating is determined by the centre of the grating dispersion curve, which is governed by the grating equation:

$$m\lambda = d(\sin\alpha + \sin\beta), \quad (1.1)$$

where λ is the wavelength of incident light, m is the diffraction order, d is the grating groove spacing, α and β are the incident and diffracted angles, respectively.

1.4.2.2. Littrow Configuration

In the Littrow configuration, the diffraction grating is used as the end mirror, which reflects the first order diffraction beam back to the laser diode to provide optical feedback, and the zeroth order diffraction beam is coupled out of the laser (Fig. 1.4).



The emission wavelength can be tuned by changing the incidence angle of the diffraction grating. For this configuration, the incident and diffracted angles are equal:

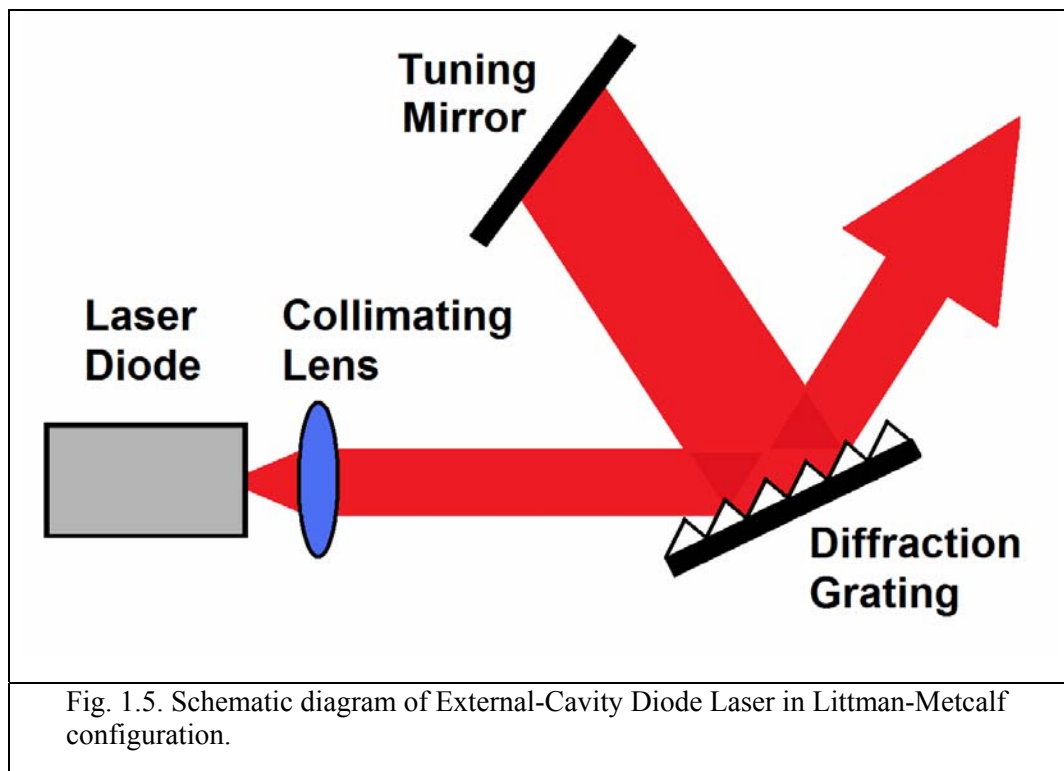
$\alpha = \beta = \theta$, and the grating Equation (1.1) reduces then to the following:

$$m\lambda = 2d(\sin\alpha). \quad (1.2)$$

One of the advantages of the Littrow configuration is that it is possible to achieve much higher output power than that for the Littman-Metcalf configuration. The major disadvantage, however, is a shift in the position of the beam as wavelength tuning is achieved via changing the incidence angle of the diffraction grating.

1.4.2.3. Littman-Metcalf Configuration

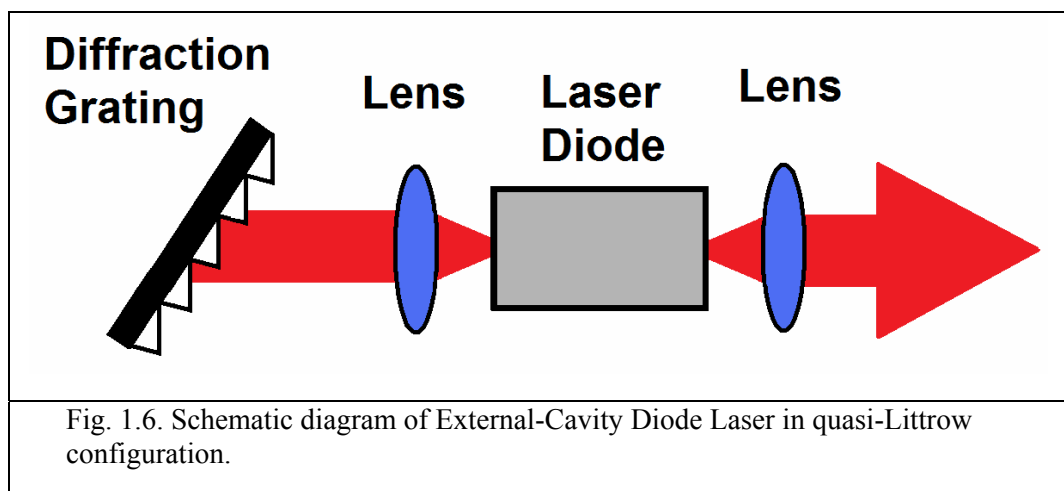
In the Littman-Metcalf configuration, the diffraction grating reflects the first order diffraction beam towards the tuning mirror, which reflects it back to the laser diode (Fig. 1.5). The emission wavelength can be tuned by rotating this mirror. The zeroth order diffraction beam is coupled out of the laser.



The benefit of the Littman-Metcalf configuration is that the position of the output beam remains fixed whilst rotation of the tuning mirror, and also the linewidth is smaller, as the wavelength selectivity is stronger. The main disadvantage is that the zeroth order reflection of the beam reflected by the tuning mirror is lost, so that the output power is lower than that for the Littrow configuration. As a consequence of the higher losses in the Littman-Metcalf configuration, the tuning range is also reduced.

1.4.2.4. Quasi-Littrow Configuration

In the quasi-Littrow configuration, the radiation emitted from the back facet of the laser diode is directed to a diffraction grating, which reflects the first order diffraction beam back to the laser diode, and the output of the front facet is collimated with an aspheric lens, as schematically represented in Fig. 1.6. Coarse wavelength tuning is made possible by changing the incidence angle of the grating.



The quasi-Littrow configuration offers a fixed position of the output beam, higher output power and tuning range, when compared to the alternative Littman-Metcalf configuration. Moreover, the quasi-Littrow configuration is simpler and more compact in comparison with the Littman-Metcalf configuration.

Therefore, as one of the aims of my work was to demonstrate high-power broadly-tunable ECDLs, a quasi-Littrow configuration was implemented in the experiments.

Tuning of the ECDLs in these configurations is realised via wavelength selective properties of the grating feedback. As the grating rotates, the laser tunes by hopping from one longitudinal mode to the next one. To avoid mode-hops and obtain wide continuous tuning, the external-cavity length and the diffraction angle should be changed simultaneously. A continuous tuning range can be realised by adjusting the

tuning element around a carefully chosen pivot point, located at the intersection of the grating plane and the diode laser back facet plane.

1.5. Summary

This Chapter has described the brief history of semiconductor diode lasers development, provided a review of tunable diode lasers and presented their potential applications. It also provided a summary of the main growth techniques and commonly used external-cavity diode laser configurations and their comparisons.

1.6. References

- [1.1] S.C. Woodworth, D.T. Cassidy, M.J. Hamp, “Sensitive absorption spectroscopy by use of an asymmetric multiple-quantum-well diode laser in an external cavity,” *Appl. Opt.* **40**(36), pp.6719–6724 (2001).
- [1.2] N. Kuramoto, K. Fujii, “Volume determination of a silicon sphere using an improved interferometer with optical frequency tuning,” *IEEE Trans. Instrum. Meas.* **54**(2), pp.868–871 (2005).
- [1.3] S.J.B. Yoo, “Wavelength conversion technologies for WDM network applications,” *J. Lightwave Technol.* **14**(6), pp.955–966 (1996).
- [1.4] J.D. Berger, Y. Zhang, J.D. Grade, H. Lee, S. Hrinya, H. Jerman, “Widely tunable external cavity diode laser based on a MEMS electrostatic rotary actuator,” in Proc. Optical Fiber Communication Conf., Washington, DC, 2001, OSA Technical Digest Series, Paper TuJ2-1 (2001).
- [1.5] N. Krstajic, D.T.D. Childs, S.J. Matcher, D. Livshits, A. Shkolnik, I. Krestnikov, R.A. Hogg, “Swept-source laser based on quantum-dot semiconductor optical amplifier – applications in optical coherence tomography,” *IEEE Photon. Tech. Lett.* **23**(11), pp.739-741 (2011).
- [1.6] B.J. Stevens, D.T.D. Childs, K.M. Groom, M. Hopkinson, R.A. Hogg, “All semiconductor swept laser source utilizing quantum dots,” *Appl. Phys. Lett.* **91**(12), pp.121119 (2007).
- [1.7] S.H. Yun, C. Boudoux, G.J. Tearney, and B.E. Bouma, “High-speed wavelength-swept semiconductor laser with a polygon-scanner-based wavelength filter,” *Opt. Lett.* **28**(20), pp.1981–1983 (2003).
- [1.8] M.E. Brezinski, and J.G. Fujimoto, “Optical coherence tomography: High-resolution imaging in nontransparent tissue,” *IEEE J. Sel. Top. Quantum Electron.* **5**(4), pp.1185–1192 (1999).
- [1.9] K.A. Fedorova, M.A. Cataluna, P.R. Battle, C.M. Kaleva, I.L. Krestnikov, D.A. Livshits, E.U. Rafailov, “Orange light generation from a PPKTP waveguide end-pumped by a cw quantum-dot tunable laser diode”, *Appl. Phys. B* **103**, pp.41-43 (2011).
- [1.10] A.Yu. Nevsky, U. Bressel, I. Ernsting, Ch. Eisele, M. Okhapkin, S. Schiller, A. Gubenko, D. Livshits, S. Mikhrin, I. Krestnikov, A. Kovsh, “A narrow-line-

- width external cavity quantum dot laser for high-resolution spectroscopy in the near-infrared and yellow spectral range,” *Appl. Phys. B* **92**, pp.501 (2008).
- [1.11] V. Kapoor, F.V. Subach, V.G. Kozlov, A. Grudinin, V.V. Verkhusha, W.G. Telford, “New lasers for flow cytometry: filling the gaps,” *Nat. Methods* **4**, pp.678-679 (2007).
- [1.12] R. E. Fitzpatrick, “Lasers in dermatology & plastic surgery,” *Opt. Photon. News* **6**, pp.24, (1995).
- [1.13] S. Karrer, W. Baumler, C. Abels, U. Hohenleutner, M. Landthaler, R.M. Szeimies, “Long-pulse dye laser for photodynamic therapy: investigations in vitro and in vivo,” *Lasers Surg. Med.* **25**, pp.51 (1999).
- [1.14] Z. Xu, & Y. Bi, “Large laser projection displays utilizing all-solid-state RGB lasers,” *Proc. SPIE* **5632**, pp.114-122 (2005).
- [1.15] C.W. Hoyt, Z.W. Barber, C.W. Oates, T.M. Fortier, S.A. Diddams, L. Hollberg, *Phys. Rev. Lett.* **95**, pp. 083003 (2005).
- [1.16] N.G. Basov, O.N. Krokhin, Y.M. Popov, “The possibility of use of indirect transmissions to obtain negative temperature in semiconductors”, *Soviet Physics JETP* **12**, pp.1033 (1961).
- [1.17] M.G.A. Bernard, D. Durraffoug, “Laser conditions in semiconductors”, *Phys. Status Solidi* **1**, pp.669 (1961).
- [1.18] R.N. Hall, G.E. Fenner, J.D. Kingsley, T.J. Soltys, R.O. Carlson, “Coherent light emission from GaAs junction,” *Phys. Rev. Lett.* **9**(9), pp.366-368 (1962).
- [1.19] M.I. Nathan, W.P. Dumke, G. Burns, F.H. Dill Jr., G.J. Lasher, “Stimulated emission of radiation from GaAs p-n junctions,” *Appl. Phys. Lett.* **1**(3), pp.62-64 (1962).
- [1.20] N. Holonyak Jr., S.F. Bevacqua, “Coherent (visible) light emission from Ga(As_{1-x}P_x) junctions,” *Appl. Phys. Lett.* **1**(4), pp.82-83 (1962).
- [1.21] Zh. I. Alferov and R. F. Kazarinov, Semiconductor laser with electrical pumping. Inventor’s Certificate 181737 (1963).
- [1.22] H. Kroemer, “A proposed class of heterojunction injection lasers,” *Proc. IEEE*, vol. **51**(12), pp.1782–1783 (1963).
- [1.23] Zh.I. Alferov, V.M. Andreev, V.I. Korol’kov, D.N. Tret’yakov, V.M. Tuchkevich, “High-voltage p-n junctions in Ga_xAl_{1-x}As crystals,” *Sov. Phys. Semicond.* **1**, pp.1313-1314 (1968).

- [1.24] Zh.I. Alferov, V.M. Andreev, E.L. Portnoi, M.K. Trukan, "AlAs-GaAs heterojunction injection lasers with a low room-temperature threshold," *Sov. Phys. Semicond.* **3**, pp.1107-1110 (1970).
- [1.25] I. Hayashi, M.B. Panish, P.W. Foy, S. Sumski, "Junction lasers which operate continuously at room temperature," *Appl. Phys. Lett.* **17**(3), pp.109-111 (1970).
- [1.26] R. Dingle and C. H. Henry, Quantum effects in heterostructure lasers. U.S. Patent 3982207 (Sept. 1976).
- [1.27] R.D. Dupuis, "AlGaAs-GaAs lasers grown by Metelorganic chemical vapor deposition - A review," *J. Crystal Growth* **55**, pp.213-221 (1981).
- [1.28] M.A. Herman, H. Sitter, Molecular beam epitaxy (Springer-Verlag, Berlin, 1989).
- [1.29] R.C. Miller, R. Dingle, A.C. Gossard, R.A. Logan, W.A. Nordland, Jr., W. Weigmann, "Laser oscillation with optically pumped very thin GaAs-Al_xGa_{1-x}As multilayer structures and conventional double heterostructures," *J. Appl. Phys.* **47**, pp.4509 (1976).
- [1.30] R.D. Dupuis, P.D. Dapkus, R.M. Kolbas, N. Holonyak, Jr., H. Shichijo, "Photopumped laser operation of MO-CVD Al_xGa_{1-x}As near a GaAs quantum well ($\lambda=6200\text{\AA}$, 77°K)," *Appl. Phys. Lett.* **33**, pp.596 (1978).
- [1.31] W.T. Tsang "Extremely low threshold (AlGa)As modified multi-quantum well heterostructure lasers grown by molecular beam epitaxy," *Appl. Phys. Lett.* **39**, pp.786-788 (1981).
- [1.32] Zh.I. Alferov, A.M. Vasiliev, S.V. Ivanov, P.S. Kop'ev, N.N. Ledentsov, B.Ya. Mel'tser, V.M. Ustinov, "Reduction of the threshold current density (52A/cm^{-2} , 300K) in SCH GaAs-AlGaAs lasers by using a quantum well confined by a variable-step short-period superlattice," *Sov. Phys.: Tech. Phys. Lett.* **14**, p.782 (1988).
- [1.33] Zh.I. Alferov, S.V. Ivanov, P.S. Kop'ev, N.N. Ledentsov, M.E. Lutsenko, M.I. Nemenov, B.Ya. Meltser, V.M. Ustinov and S.V. Shaposhnikov, "Spreading and surface recombination in quantum well (Al,Ga)As double heterostructure separate confinement lasers with a broad stripe," *Sov. Phys. Semicond.* **24**, pp.92-95 (1990).
- [1.34] N.N. Ledentsov, V.M. Ustinov, A.Yu. Egorov, A.E. Zhukov, M.V. Maximov, I.G. Tabatadze, P.S. Kop'ev, "Optical properties of heterostructures with InGaAs-GaAs quantum clusters," *Sov. Phys. Semicond.* **28**, pp.832-834 (1994).

- [1.35] N. Kirstaedter, N.N. Ledentsov, M. Grundmann, D. Bimberg, U. Richter, S.S. Ruvimov, P. Werner, J. Heydenreich, V.M. Ustinov, M.V. Maximov, P.S. Kop'ev, Zh.I. Alferov, "Low threshold, large T_0 injection laser emission from (InGa)As quantum dots," *Electron. Lett.* **30**, pp.1416 (1994)
- [1.36] N.N. Ledentsov, V.A. Shchukin, M. Grundmann, N. Kirstaedter, J. Böhrer, O. Schmidt, D. Bimberg, S.V. Zaitsev, V.M. Ustinov, A.E. Zhukov, P.S. Kop'ev, Zh.I. Alferov, A.O. Kosogov, S.S. Ruvimov, P. Werner, U. Gösele, J. Heydenreich, "Direct formation of vertically coupled quantum dots in Stranski-Krastanow growth," *Phys. Rev. B* **54**, pp.8743-8750 (1996).
- [1.37] G.T. Liu, A. Stintz, H. Li, T.C. Newell, A.L. Gray, P.M. Varangis, K.J. Malloy and L.F. Lester, "The Influence of Quantum-Well Composition on the Performance of Quantum Dot Lasers Using InAs/InGaAs Dots-in-a-Well (DWELL) Structures," *IEEE J. Quant. Electron.* **36**, pp.1272 (2000).
- [1.38] G. Park, O. B. Schekin, D. L. Huffaker, D. G. Deppe, "1.3- μm quantum-dot laser," *IEEE Photon. Tech. Lett.* **12**, pp.230-232 (2000).
- [1.39] D.Z. Garbuzov, N.Y. Antonishkis, A.D. Bondarev, A.B. Gulakov, S.N. Zhigulin, N.I. Katsavets, A.V. Kochergin, E.U. Rafailov, "High power $\lambda = 0.81 \mu\text{m}$ InGaAsP/GaAs SCH SQW lasers", *IEEE J. Quantum Electron.* **27**(6), p.1531 (1991).
- [1.40] N.N. Ledentsov, "The way to quantum dot lasers," *Window to Microworld* **1**(5), pp.17-25 (2002). <http://wmw-magazine.ru/uploads/volumes/05/17.pdf>
- [1.41] E. Kapon, ed., *Semiconductor lasers: Materials and structures* (Academic Press, San Diego, 1999).
- [1.42] V.M. Ustinov, A.E. Zhukov, A.Yu. Egorov, N.A. Maleev, *Quantum Dot Lasers* (Oxford University Press Inc., New York, 2003).
- [1.43] K.A. Fedorova, M.A. Cataluna, I. Krestnikov, D. Livshits, E.U. Rafailov, "Broadly-tunable high-power InAs/GaAs quantum-dot external-cavity diode lasers," *Opt. Exp.* **18**(18), pp.19438–19443 (2010).
- [1.44] Z.M. Wang, *Self-Assembled Quantum Dots* (Springer, New York, 2008).
- [1.45] H.P. Zappe, *Introduction to Semiconductor Integrated Optics* (Artech House, Norwood, 1995).
- [1.46] W.T. Tsang "Extremely low threshold (AlGa)As modified multi-quantum well heterostructure lasers grown by molecular beam epitaxy", *Appl. Phys. Lett.* **39**, pp.786-788 (1981).

- [1.47] M. Morisaki, M. Ogura, N. Hase, T. Kajiwara “InGaAsP/InP Multi-quantum-Well Structure grown by MOCVD”, *Electron. Lett.* **21**(4), pp.164-165 (1985).
- [1.48] G. Hunsperger, *Integrated optics: Theory and Technology* (Springer-Verlag, Berlin, 2009).
- [1.49] P.J.A. Thijs, L.F. Tiemeijer, J.J.M. Binsma, T. Van Dongen “Progress in long-wavelength strained-layer InGaAs(P) quantum-well semiconductor lasers and amplifiers”, *IEEE J. Quantum Electron.*, QE-**30**(2), pp.477-499 (1994).
- [1.50] R. Menna, A. Komissarov, M. Maiorov, V. Khalfin, L. DiMarco, J. Connolly and D. Garbuzov, “High Power 1550 nm Distributed Feedback Lasers with 440 mW CW Output Power for Telecommunication Applications”: Conference on Lasers and Electro-Optics post-deadline paper, CPD12-1, (IEEE/LEOS and OSA, 2001).
- [1.51] L. Goldstein, F. Glas, J.Y. Marzin, M.N. Charasse, G.L. Roux “Growth by molecular beam epitaxy and characterization of InAs/GaAs strained-layer superlattices”, *Appl. Phys. Lett.* **47**, pp.1099-1101, (1985).
- [1.52] D. Leonard, K. Pond, P.M. Petroff, “Critical layer thickness for self-assembled InAs island on GaAs,” *Phys. Rev. B* **50**, pp.11687-11696 (1994).
- [1.53] M. Grundmann, *Nano-Optoelectronics. Concepts, Physics and Devices* (Springer-Verlag, Berlin, 2002).
- [1.54] E.U. Rafailov, M.A. Cataluna, E.A. Avrutin, *Ultrafast Lasers Based on Quantum Dot Structures: Physics and Devices*, (Wiley-VCH Verlag GmbH & Co. KGaA, Weinheim, Germany, 2011).
- [1.55] M.A. Cataluna, “Ultra-short pulse generation from quantum-dot semiconductor diode lasers”, PhD Thesis, St. Andrews (2007).
- [1.56] A. R. Kovsh, N.A. Maleev, A.E. Zhukov, S.S. Mikhrin, A.P. Vasil’ev, Yu.M. Shernyakov, M.V. Maximov, D.A. Livshits, V.M. Ustinov, Zh.I. Alferov, N.N. Ledentsov, D.M. Bimberg, “InAs/InGaAs/GaAs quantum dot lasers of 1.3 μm range with high (88%) differential efficiency”, *IEEE Electron. Lett.* **38**(19), pp.1104-1106 (2002).
- [1.57] O.G. Schmidt, N. Kirstaedter, N.N. Ledentsov, M.H. Mao, D. Bimberg, V.M. Ustinov, A.Yu. Egorov, A.E. Zhukov, M.V. Maximov, P.S. Kop’ev, Zh.I. Alferov, “Prevention of gain saturation by multi-layer quantum dot lasers”, *IEEE Electron. Lett.* **32**(14), pp.1302-1303 (1996).

- [1.58] P.M. Smowton, E. Herrmann, Y. Ning, H.D. Summers, P. Blood, M. Hopkinson, "Optical mode loss and gain of multiple-layer quantum-dot lasers," *Appl. Phys. Lett.* **78**, pp.2629-2631 (2001).
- [1.59] A.E. Zhukov, A.R. Kovsh "Quantum dot diode lasers for optical communication systems", *Quantum Electronics* **38**(5), pp.409-423 (2008).
- [1.60] D. Bimberg, M. Grundmann, N.N. Ledentsov, "Growth, Spectroscopy, and Laser Application of Self-ordered III-V Quantum Dots", *Bulletin of the Materials Research Society* **23**, pp.31 (1998).
- [1.61] J. Buus, Single Frequency Semiconductor Lasers (SPIE Optical Engineering Press, Bellingham, 1991).
- [1.62] Y. Tohromi, F. Kano, H. Ishii, Y. Yoshikuni, Y. Kondo, "Wide tuning with narrow linewidth in DFB lasers with superstructure grating (SSG)," *Electron. Lett.* **29**, pp.1350-1351 (1993).
- [1.63] L.A. Coldren, S.W. Corzine, "Continuously-tunable single-frequency semiconductor lasers," *IEEE Journal of Quantum Electronics*, QE-**23**, pp.903-908 (1987).
- [1.64] F.J. Duarte, ed., Tunable lasers handbook (Academic Press, San Diego, 1995).
- [1.65] C.J. Chang-Hasnain, "Tunable VCSEL," *IEEE J. Select. Topics in Quantum Electron.* **6**(6), pp.978-987 (2000).
- [1.66] H. Li, K. Iga, Vertical-cavity surface-emitting laser devices (Springer-Verlag, Berlin, 2003).
- [1.67] M. Butkus, J. Rautiainen, O.G. Okhotnikov, C.J. Hamilton, G.P.A. Malcolm, S.S. Mikhlin, I.L. Krestnikov, D.A. Livshits, E.U. Rafailov, "Quantum dot based semiconductor disk lasers for 1-1.3 μm ," *IEEE J. Select. Topics in Quantum Electron.* **17**(6), pp.1763-1771 (2011).
- [1.68] M. Bagley, R. Wyatt, D.J. Elton, H.J. Wickes, P. C. Srundens, C. P. Seltzer, D.M. Cooper, and W.J. Devlin, "242 nm continuous tuning from a GRIN-SC-MQW-BH InGaAsP laser in an extended cavity," *Electron. Lett.* **26**(4), pp.267-269 (1990).
- [1.69] C. Ye, Tunable External Cavity Diode lasers (World Scientific, Singapore, 2004).
- [1.70] J.W. Crowe, R.M. Craig, "GaAs laser linewidth measurements by heterodyne detection," *Appl. Phys. Lett.* **5**, pp.72-74 (1964).

- [1.71] P.G. Eliseev, I. Ismailov, Yu.F. Fedorov, "Injection lasers for multichannel optical communication," *IEEE J. Quantum Electron.* **QE-6(1)**, pp.38-41 (1970).
- [1.72] A.P. Bogatov, P.G. Eliseev, L.P. Ivanov, A.S. Logginov, M.A. Manko, K.Ya. Senatorov, "Study of the single-mode injection laser," *IEEE J. Quantum Electron.* **QE-9(2)**, pp.392-394 (1973).
- [1.73] O.V. Bogdashevich, B.I. Vasil'ev, A.S. Nasibov, A.Z. Obidin, A.N. Pechenov, M.M. Zverev, "Investigation of the dynamics of emission from "radiating mirror" semiconductor laser with an external resonator," *Quantum Electronics* **4(1)**, pp.84-85 (1974).
- [1.74] S.A. Darznez, M.M. Zverev, V.A. Ushakhin, "Investigation of a multielement electron-beam-pumped semiconductor laser with an external mirror," *Quantum Electronics* **4(10)**, pp.1272-1274 (1975).
- [1.75] R. Ludeke, E.P. Harris, "Tunable GaAs laser in an external cavity dispersive cavity," *Appl. Phys. Lett.* **20(12)**, pp.499-500 (1972).
- [1.76] M.W. Fleming, A. Mooradian, "Spectral characteristics of external cavity controlled semiconductor lasers," *IEEE J. Quantum Electron.* **QE-17(1)**, pp.44-59 (1981).
- [1.77] R. Wyatt, W.J. Devlin, "10 kHz linewidth 1.5 μ m InGaAsP external cavity laser with 55 nm tuning range," *Electron. Lett.* **19(3)**, pp.110-112 (1983).
- [1.78] F. Favre, D. Le Guen, J.C. Simon, B. Landousies, "External-cavity semiconductor laser with 15 nm continuous tuning range," *Electron. Lett.* **22**, pp.795-796 (1986).
- [1.79] F. Favre, D. Le Guen, "82 nm of continuous tunability for an external cavity semiconductor laser," *Electron. Lett.* **27(2)**, pp.183-184 (1991).
- [1.80] C.J Hawthorn, K.P. Weber, R.E. Scholten, "Littrow configuration tunable external cavity diode laser with fixed direction output beam," *Review of Scientific Instruments* **72(12)**, p.4477-4479 (2001).
- [1.81] M.G. Littman, H.J. Metcalf, "Spectrally narrow pulsed dye laser without beam expander," *Appl. Opt.* **17(14)**, pp.2224-2227 (1978).
- [1.82] K. Liu, M. G. Littman, "Novel geometry for single-mode scanning of tunable lasers," *Opt. Lett.* **6(3)**, pp.117-118 (1981).

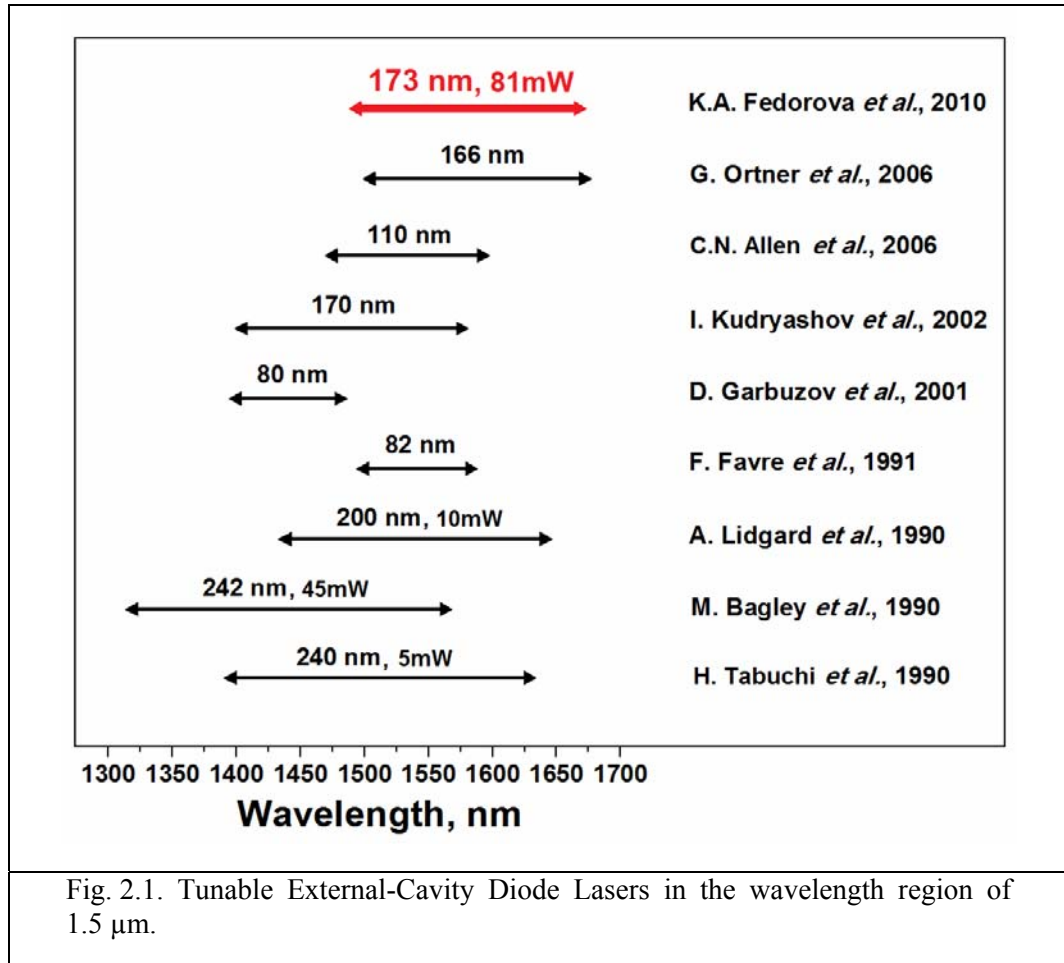
2. Tunable InGaAsP/InP Strained Multi-Quantum-Well External-Cavity Diode Laser

In this Chapter, a broadly tunable InGaAsP/InP strained multi-quantum well external-cavity diode laser, which operates in the spectral range of 1494 nm – 1667 nm is demonstrated. A maximum CW output power in excess of 81 mW and a side-mode suppression ratio higher than 50 dB were achieved in the central part of the tuning range. Different pump current and temperature regimes are investigated.

2.1. Introduction

Semiconductor lasers emitting within the 1.3 μm and 1.55 μm spectral regions are extremely relevant for applications in telecommunication systems [2.1]. Longer distances and higher speeds of information transmission dictate the move toward these wavelengths, which correspond to the minimum dispersion and minimum loss in the standard glass fibre at 1.3 μm and 1.55 μm , respectively. Tunable diode lasers utilising an external diode cavity laser (ECDL) design can provide many attractive features needed for wavelength division multiplexing (WDM) applications such as a very narrow linewidth, wide continuous tuning range, high output power and considerable inventory reduction [2.2]. Laser sources based on quantum well (QW) or quantum dot structures grown on InP substrates are very useful in this respect.

In the last 20 years several groups presented their results [2.3-2.11] on broadly tunable lasers in the wavelength region of 1.5 μm , as shown in Fig. 2.1. Most frequently, broadly tunable QW lasers have been mainly focused on materials which contain multiple quantum wells (MQW). MQW lasers have demonstrated wide tuning ranges up to 242 nm, for the spectral range between 1320 nm and 1562 nm with the maximum output power of 45 mW [2.3] or operating from 1390 nm to 1630 nm with the output power up to 5mW [2.4]. High-power MQW laser operating at high current and tunable in the wavelength range between 1400nm and 1480nm has also been reported [2.5]. Very recently, external cavity lasers with tuning ranges shifted towards the longer wavelength of the telecommunication window have been demonstrated [2.6-2.9]. However, the power emitted from these lasers was extremely low (typically of the order of 10's of μW).

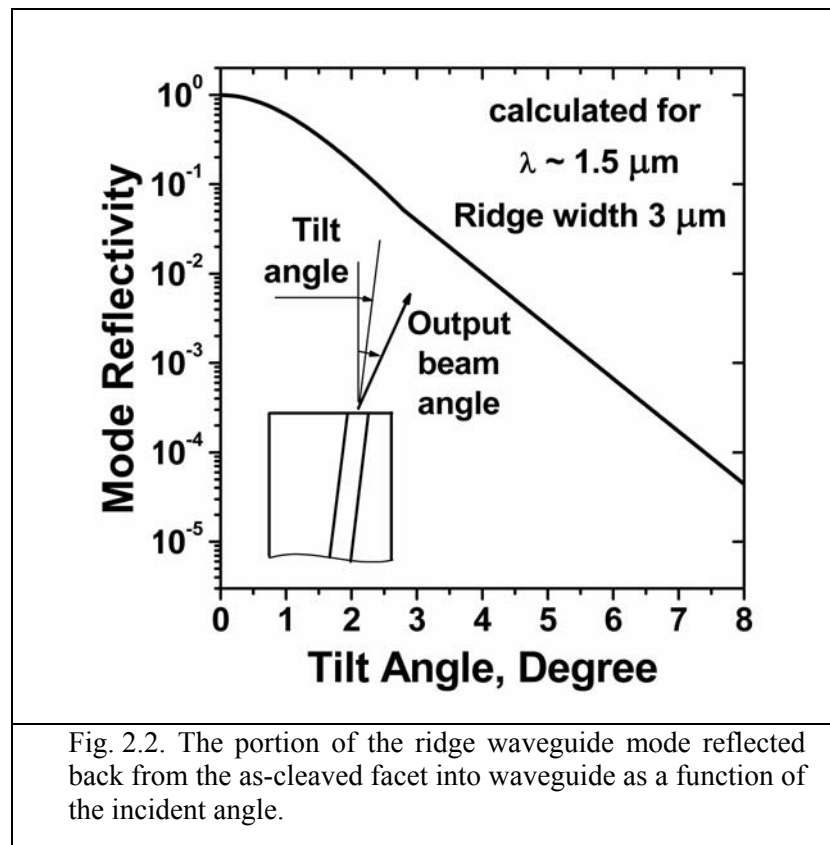


2.2. Design of InGaAsP/InP MQW Diode Laser

In this work InGaAsP/InP strained MQW structures similar to those described in [2.12] were used for bent ridge waveguide gain chip fabrication. Because the laser chip provided by Princeton Lightwave, Inc. (Cranbury, USA) commercially available, the disclosed information about this device was very limited. The InGaAsP/InP laser structures were grown by low-pressure metal-organic chemical vapor deposition (LP-MOCVD) on n-InP substrates. Quaternary InGaAsP compounds of different compositions were used as the material for the confinement, barrier (with photoluminescence at ~ 1250 nm) and compressively strained three QW layers of 9 nm width. Single mode operation was maintained for ridge widths from 3 to 5 μm by accurate control of channel etch depth. The channel depth control was aided by the use

of a grown-in etch-stop layer. Waveguide thickness design provided the fast axis divergence lower than 30 degrees for effective coupling into single mode fibre. Lateral mode confinement was provided by a dual-channel ridge waveguide structure prepared by conventional photolithography in conjunction with chemical etching [2.12].

The rear and front facets of the gain chip had conventional anti-reflective (AR) coating ($R \leq 2\%$) and reflective coatings (10%), respectively. The use of bent or tilted waveguide gain chips [2.13-2.15] for ECDL fabrication eliminates the need for very accurate thickness and refractive index material deposition on one or more of the emitting facets. The elimination of this very low-reflective coating ($R < 10^{-4}$) deposition procedure makes possible mass production of low-cost gain chips. Bent ridge waveguide gain chips even with an as-cleaved facet can have effective reflective coefficient as low as $6 \cdot 10^{-4}$ if the waveguide axis is tilted only by 6° relative to the chip facet [2.10,2.11] (Fig. 2.2).



Effective reflective coefficient in Fig. 2.2 was estimated as an overlap of the ridge waveguide mode with the mode reflected from the bent chip facet. The ridge mode near-field used for this calculation (similar to those described in [2.16,2.17]) was derived in Gauss approximation from experimental data on the chip far field.

The design of InGaAsP/InP strained MQW gain chip is presented in Fig. 2.3.

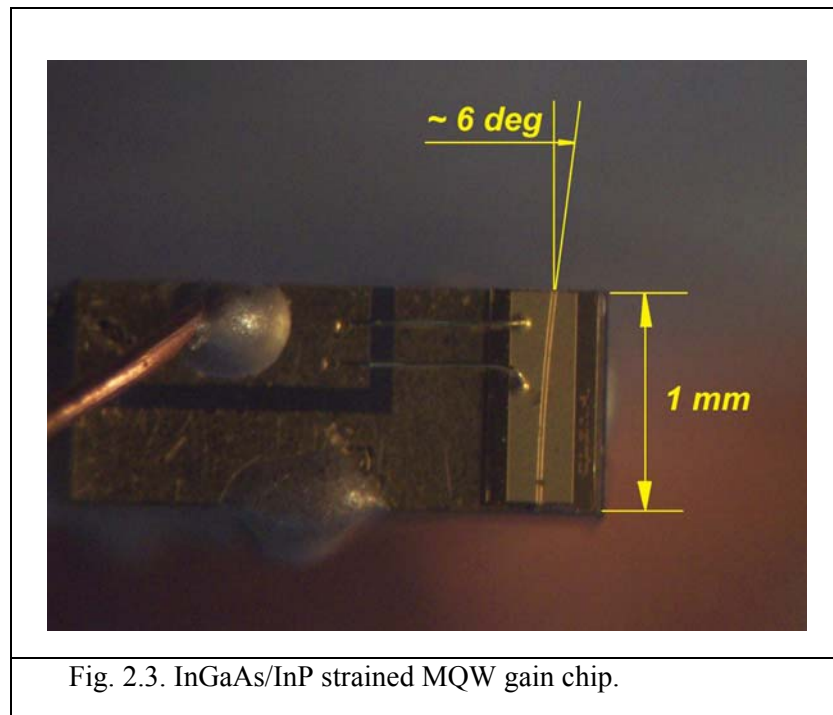


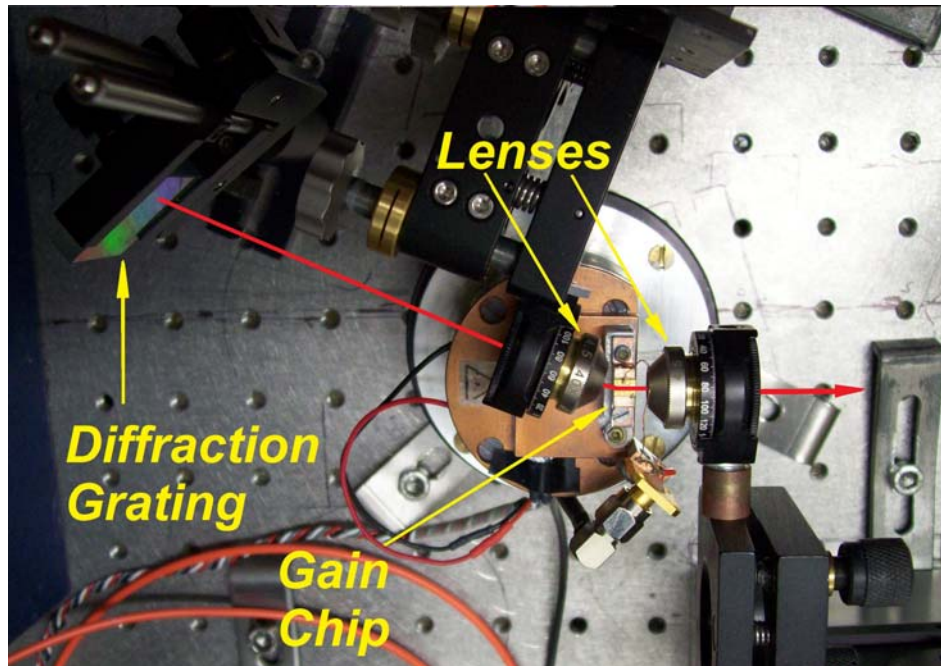
Fig. 2.3. InGaAs/InP strained MQW gain chip.

2.3. Experimental Setup

The experimental setup is shown in Fig. 2.4. A gain chip with a cavity length of 1 mm and a ridge width of $3\ \mu\text{m}$ (Fig. 2.3) was mounted on a copper heat sink and its temperature was controlled by a thermo-electric cooler. The ECDL cavity consisted of a standard 600 grooves/mm ($1.6\ \mu\text{m}$ blaze) diffraction grating in a quasi-Littrow configuration and 40x (NA~0.55) AR-coated aspheric lenses. The distance between the gain chip and the diffraction grating was 10 cm. Tuning was achieved by rotating the

grating to select a certain wavelength emission to be reflected back to the laser. The output of the front facet was collimated with an aspheric lens, as represented in Fig. 2.4.

(a)



(b)

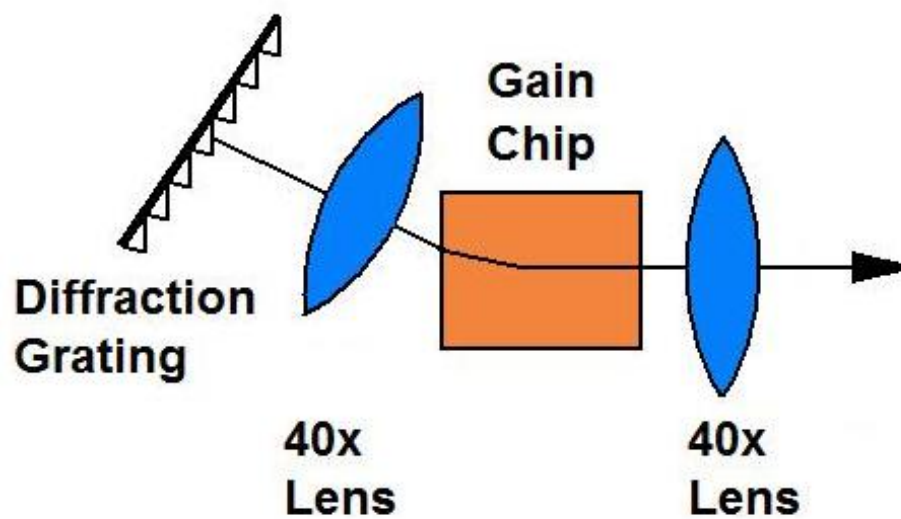
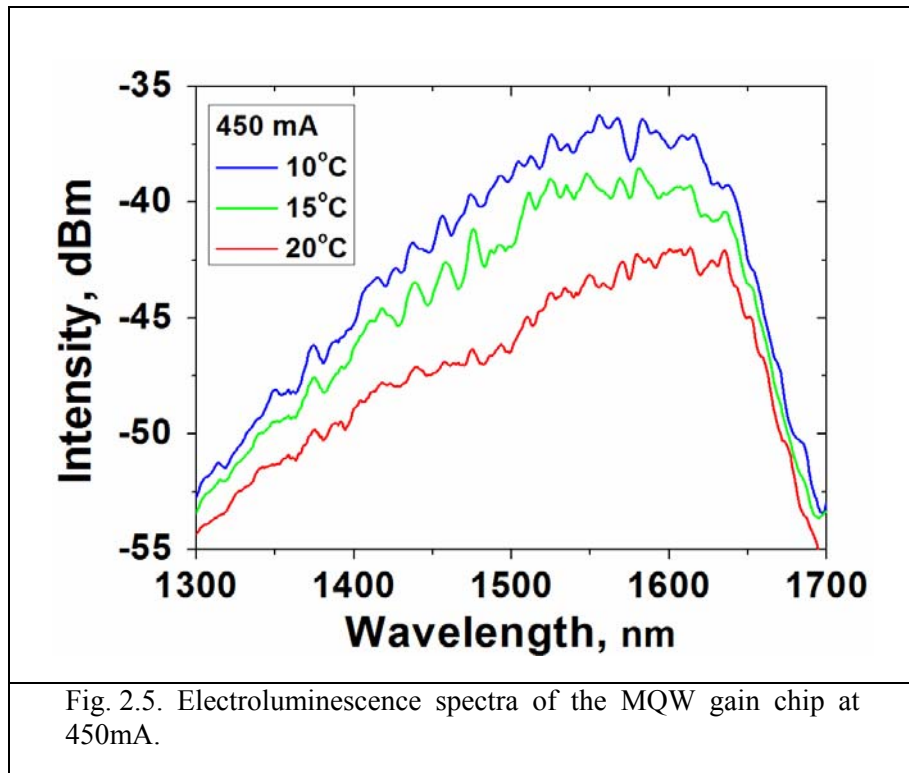


Fig. 2.4. (a), Optical scheme of the experimental setup; (b), Simplified schematics of the ECDL configuration.

2.4. Results

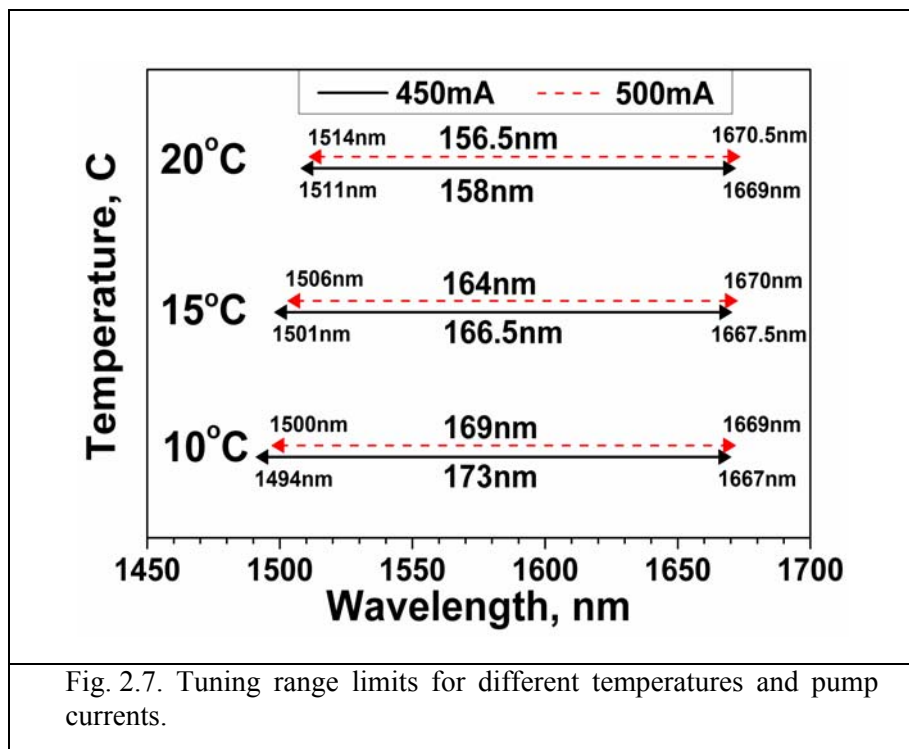
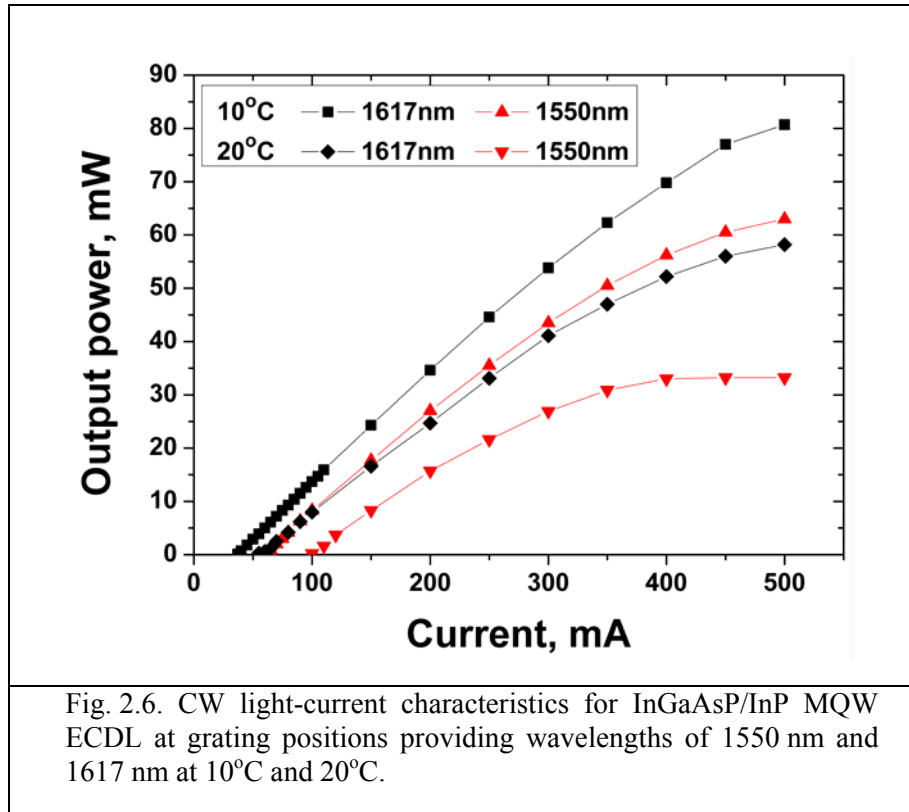
First investigations into the performance of this laser began by obtaining the electroluminescence (EL) spectra of the MQW gain chip. The EL spectra of the gain chip for various temperature conditions are shown in Fig. 2.5. For a fixed injected current ($I = 450$ mA), the measured EL spectra broaden with decreasing temperature (from 20°C to 10°C), predominantly on the short wavelength side of the spectrum.

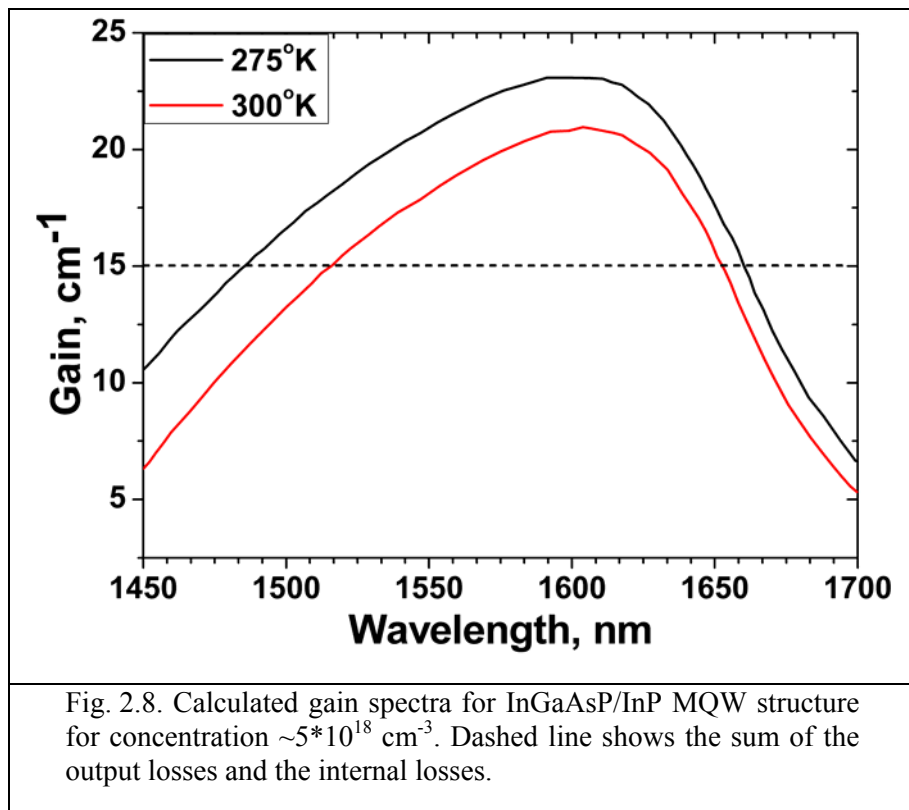


The light-current characteristics shown in Fig. 2.6 were taken with the grating positions providing single frequency output with wavelength of 1550 nm and 1617 nm. A maximum optical output power of 81 mW for a CW-pump current of 500 mA, at a heat sink temperature of 10°C (when tuned to $\lambda=1617$ nm) was observed.

The tuning range for different pump currents (450 mA and 500 mA) and temperature conditions (10°C - 20°C) were investigated, as depicted in Fig. 2.7. In agreement with the EL spectra depicted in Fig. 2.5, an enhancement of the tuning range was observed mostly on the blue side of the spectrum for low temperature (Fig. 2.7).

It can be explained by increasing the gain at a fixed current with temperature decreasing (Fig. 2.8). Optical gain spectra for InGaAsP/InP MQW structure (Fig. 2.8) was calculated using equations given in [2.18,2.19].





The observed saturation of the light-current characteristics for short-wavelength side of the spectrum with the increase of the pump current above 450 mA (Fig. 2.6) affected the reduction of tuning range on the blue side of the spectrum for the pump current above 450 mA. A maximum tuning range of 173 nm with side-mode suppression ratio higher than 45 dB in the spectral range from 1494 nm to 1667 nm was possible for a CW-current of 450 mA, and at an operating temperature of 10°C.

Fig. 2.9 depicts the CW power dependence on the wavelength at 10°C and 20°C achieved in the experiment by rotating the grating for a pump current of 450 mA. The actual tuning range at 10°C is shown in Fig. 2.10. At each step the spectrum was measured by an optical spectrum analyser (OSA Advantest Q8383). The side-mode suppression ratio was higher than 50 dB in the central part of the tuning range. The resulting optical spectrum exhibited a bandwidth around 0.4 nm (Fig. 2.11), limited only by the spectrometer's resolution.

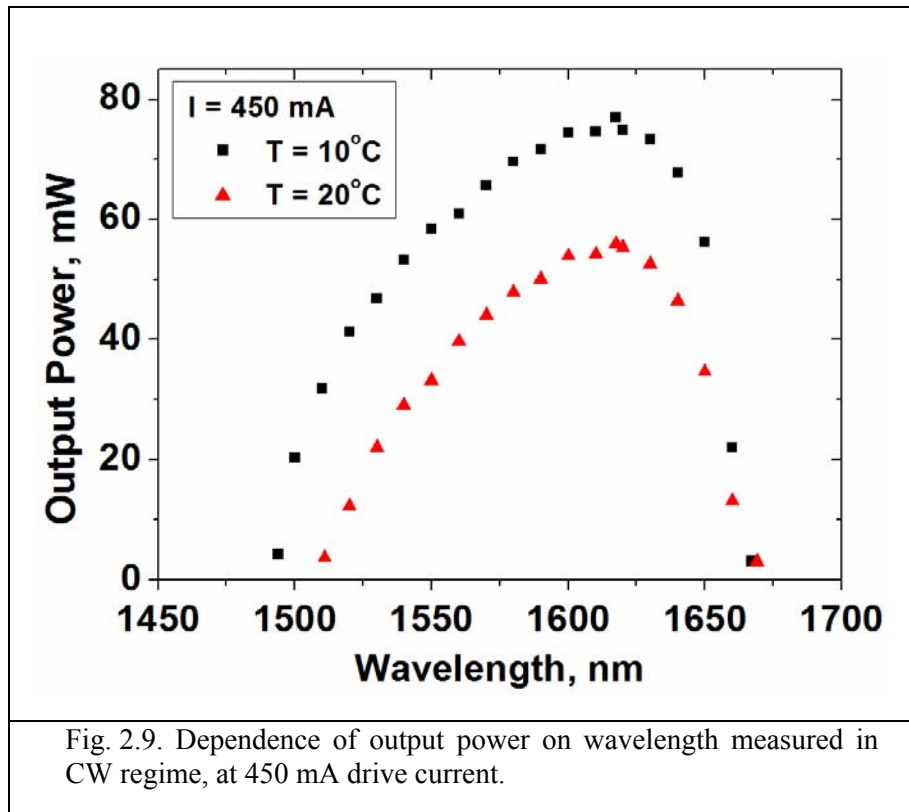


Fig. 2.9. Dependence of output power on wavelength measured in CW regime, at 450 mA drive current.

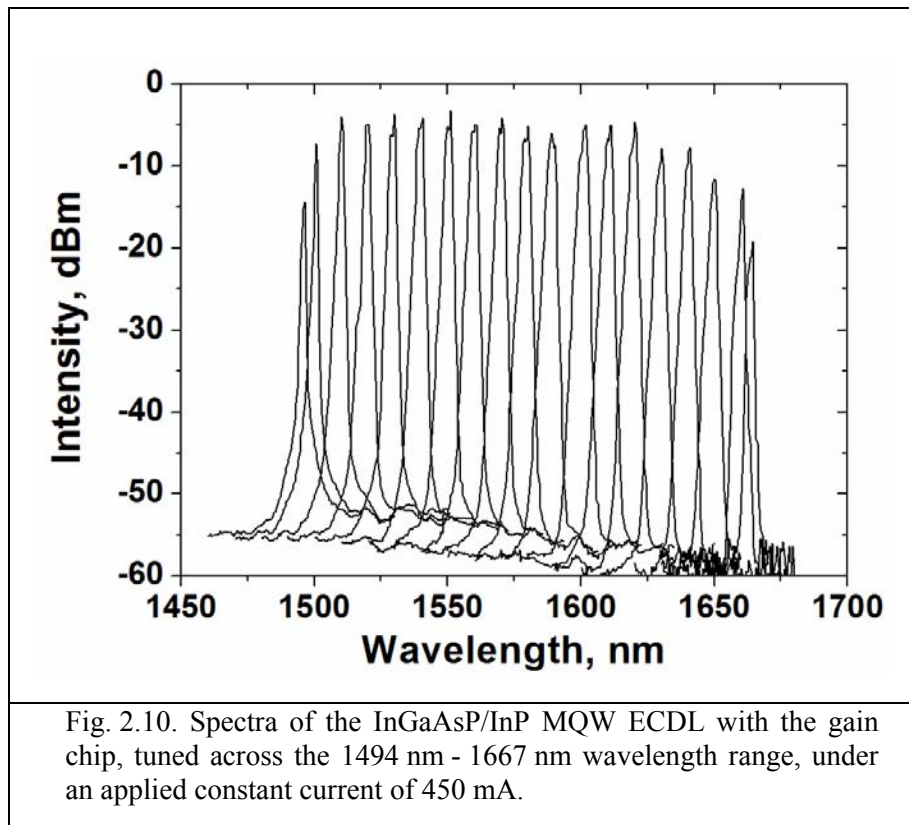
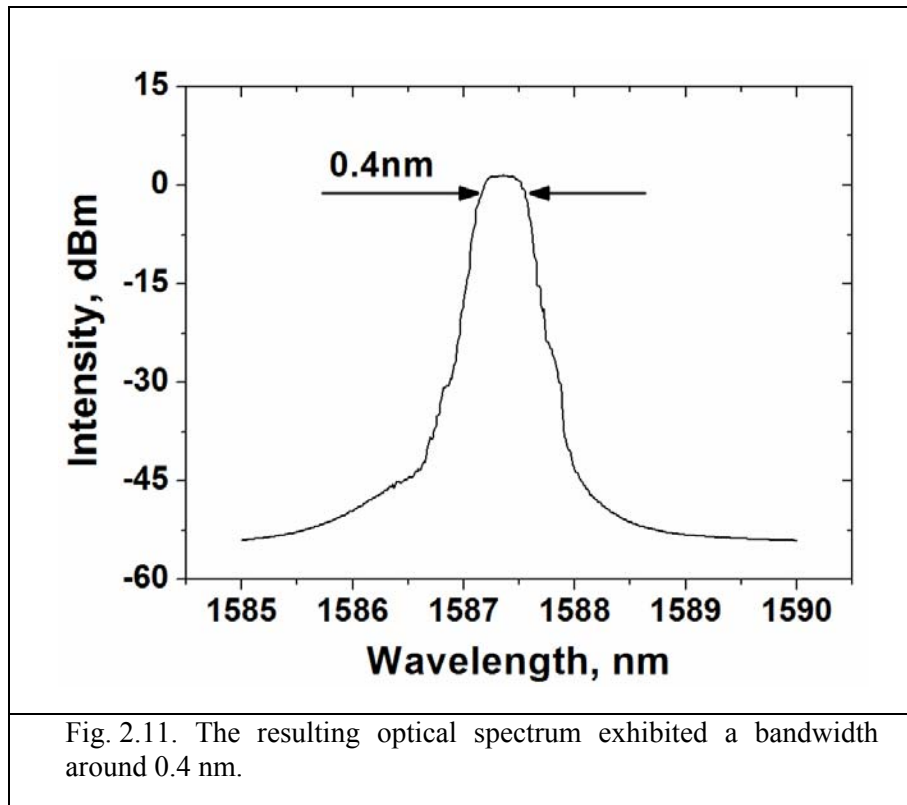


Fig. 2.10. Spectra of the InGaAsP/InP MQW ECDL with the gain chip, tuned across the 1494 nm - 1667 nm wavelength range, under an applied constant current of 450 mA.

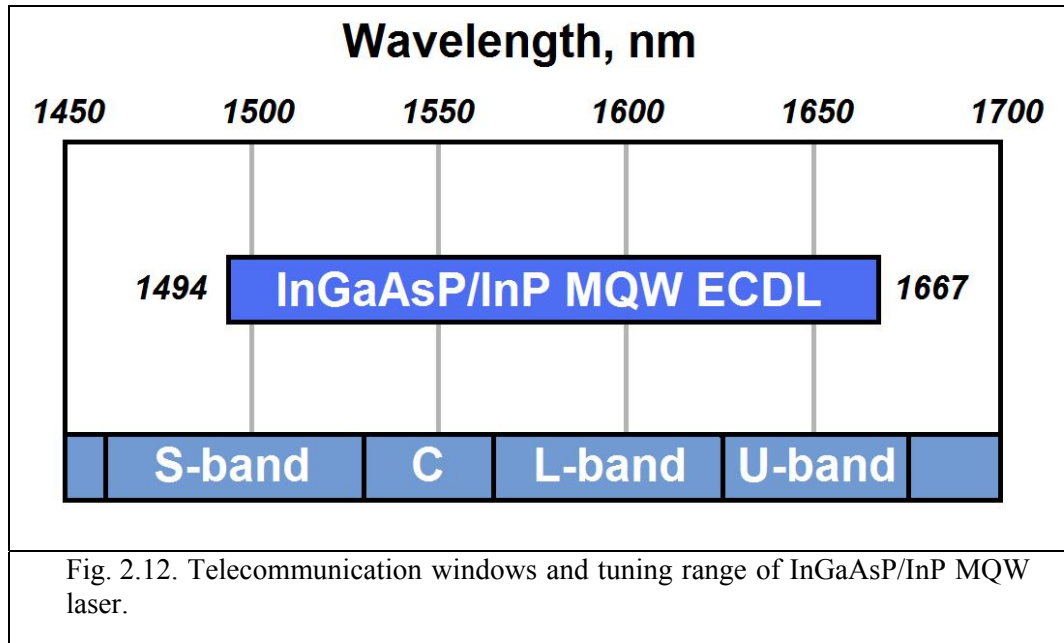


2.5. Summary

In this Chapter, an external cavity laser based on an InGaAsP/InP strained MQW structure, which is tunable between 1494 nm and 1667 nm was demonstrated. This represents an extremely versatile source which can encompass the four telecommunication windows S, C, L and U (1460 - 1530 nm, 1530 - 1565 nm, 1565 - 1625 nm, 1625 - 1675 nm, respectively), as defined by the International Telecommunication Union (ITU-T) (Fig. 2.12).

A maximum CW output power in excess of 81 mW was demonstrated and a maximum side-mode suppression ratio in excess of 50 dB was achieved, with more than 45 dB attained in most of the tuning range of the ECDL. This represents the highest output power and side-mode suppression ratio ever to be generated by a diode laser in this spectral region - which due to its extended coverage, could prove extremely useful

for the deployment of these sources in dense wavelength division multiplexing applications, and also for high-speed swept sources.



Future work which could yield improved performance of this MQW ECDL relates to the re-design of gain chip and its modification for higher current operation and the use of optimised lens AR-coatings and optimally blazed diffraction grating. There is also the option to incorporate a slit in the cavity to improve a laser linewidth.

2.6. References

- [2.1] S.J.B. Yoo, "Wavelength conversion technologies for WDM network applications", *IEEE J. Lightwave Technol.* **14**, p.955 (1996).
- [2.2] J.D. Berger, Y. Zhang, J.D. Grade, H. Lee, S. Hrinya, and H. Jerman, "Widely tunable external cavity diode laser based on a MEMS electrostatic rotary actuator", Optical Fiber Communication Conference, OSA Technical Digest Series, p.TuJ2-1 (Optical Society of America, Washington, D.C., 2001).
- [2.3] M. Bagley, R. Wyatt, D.J. Elton, H.J. Wickes, P.C. Srundens, C.P. Seltzer, D.M. Cooper, and W.J. Devlin, "242nm continuous tuning from a GRIN-SCH-MQW-BH InGaAsP laser in an extended cavity", *Electron. Lett.* **26**, pp.267-269 (1990).
- [2.4] H. Tabuchi, H. Ishikawa, "External grating tunable MQW laser with wide tuning range of 240nm," *Electron. Lett.* **26**(11), pp.742-743 (1990).
- [2.5] D. Garbuzov, R. Menna, A. Komissarov, M. Maiorov, V. Khalfin, A. Tsekoun, S. Todorov, J. Connolly "1400-1480nm ridge-waveguide pump lasers with 1 Watt CW output power for EDFA and Raman amplification", Optical Fiber Communication Conference post deadline papers, OSA Technical Digest series, PD18 (OSA, Washington, D.C., 2001).
- [2.6] G. Ortner, C.Ni. Allen, C. Dion, D. Poitras, D. Dalacu, G. Pakulski, J. Lapointe, P.J. Poole, W. Render, and S. Raymond, "External cavity InAs/InP quantum dot with a tuning range of 166nm", *Appl. Phys. Lett.* **88**, pp.121119 (2006).
- [2.7] F. Favre and D. Le Guen, "82 nm of continuous tunability for an external cavity semiconductor laser", *Electron. Lett.* **27**, pp.183-184 (1991).
- [2.8] C.N. Allen, G. Ortner, C. Dion, P.J. Poole, P. Barrios, J. Lapointe, G. Pakulski, W. Render, S. Fafard, S. Raymond "External-cavity quantum-dot laser tunable through 1.55um", *Appl. Phys. Lett.* **88**, pp.113109 (2006).
- [2.9] A. Lidgard, T. Tanbun-Ek, R.A. Logan, H. Temkin, K.W. Wecht, N.A. Olsson "External-cavity InGaAs/InP graded index multiquantum well laser with a 200 nm tuning range", *Appl. Phys. Lett.* **56**(9), pp.816-817 (1990).
- [2.10] I. Kudryashov, A. Komissarov, N. Morris, M. Maiorov, J. Connolly, D. Garbuzov, V. Khalfin, A. Braun, G. Alphonse "100mW External cavity laser with a 1405-1575nm tuning range", CLEO2002, CWK3 (2002).

- [2.11] K.A. Fedorova, M.A. Cataluna, I. Kudryashov, V. Khalfin, E.U. Rafailov “Broadly Tunable InGaAsP/InP Strained Multi-quantum-Well External Cavity Diode Laser” *Photon. Tech. Lett.* **22**(16), pp.1205-1207 (2010).
- [2.12] R. Menna, A. Komissarov, M. Maiorov, V. Khalfin, L. DiMarco, J. Connolly and D. Garbuzov, “High Power 1550 nm Distributed Feedback Lasers with 440 mW CW Output Power for Telecommunication Applications“, Conference on Lasers and Electro-Optics post deadline papers, CPD12-1, (IEEE/LEOS and OSA, 2001).
- [2.13] P.J. Delfyett, C.-H. Lee, G.A. Alphonse, and J.C. Connolly, “High peak power picosecond pulse generation from AlGaAs external cavity mode-locked semiconductor-laser and travelling-wave amplifier”, *Appl. Phys. Lett.* **57**, pp.971-973 (1990).
- [2.14] H. Hillmer, K. Magari, and Y.Suzuki, “Chirped gratings for DFB laser diodes using bent waveguides”, *IEEE Photon. Technol. Lett.* **5**, pp.10-12 (1993).
- [2.15] R. Helkey, W.X. Zou, A. Mar, D.B. Young, J. Bowers, “Curved and tapered waveguide mode-locked InGaAs/AlGaAs semiconductor lasers fabricated by impurity induced disordering”, *IEEE Trans. Electron Dev.* **40**, p.2107 (1993).
- [2.16] I.A. Kostko, V.P. Evtikhiev, E.Yu. Kotelkov, G.G. Zegrya, “Power rise in broad-waveguide diode laser with inclined facet,” *Appl. Phys. Lett.* **74**(7), pp.905-907 (1999).
- [2.17] I.A. Kostko, V.P. Evtikhiev, E.Yu. Kotelkov, G.G. Zegrya, “Increasing the power of broad-waveguide lasers by additional selection of transverse modes,” *Semiconductors* **33**(6), pp.693-699 (1999).
- [2.18] L.A. Coldren, S.W. Corzine, Diode Lasers and Photonic Integrated Circuits (Wiley, New York, 1995).
- [2.19] Z.N. Sokolova, I.S. Tarasov, L.V. Asryan, “Capture of carriers and output power of a quantum well laser,” *Fiz. Tekh. Poluprovod.* (in Russian) **45**(11), pp.1553-1559 (2011).

3. Tunable InAs/GaAs Quantum Dot External-Cavity Diode Lasers

In this Chapter, a range of diode lasers with two waveguide designs (gain chip and semiconductor optical amplifier), processed from two different structures with chirped QD layers, are characterised. A comparison of their performance is undertaken.

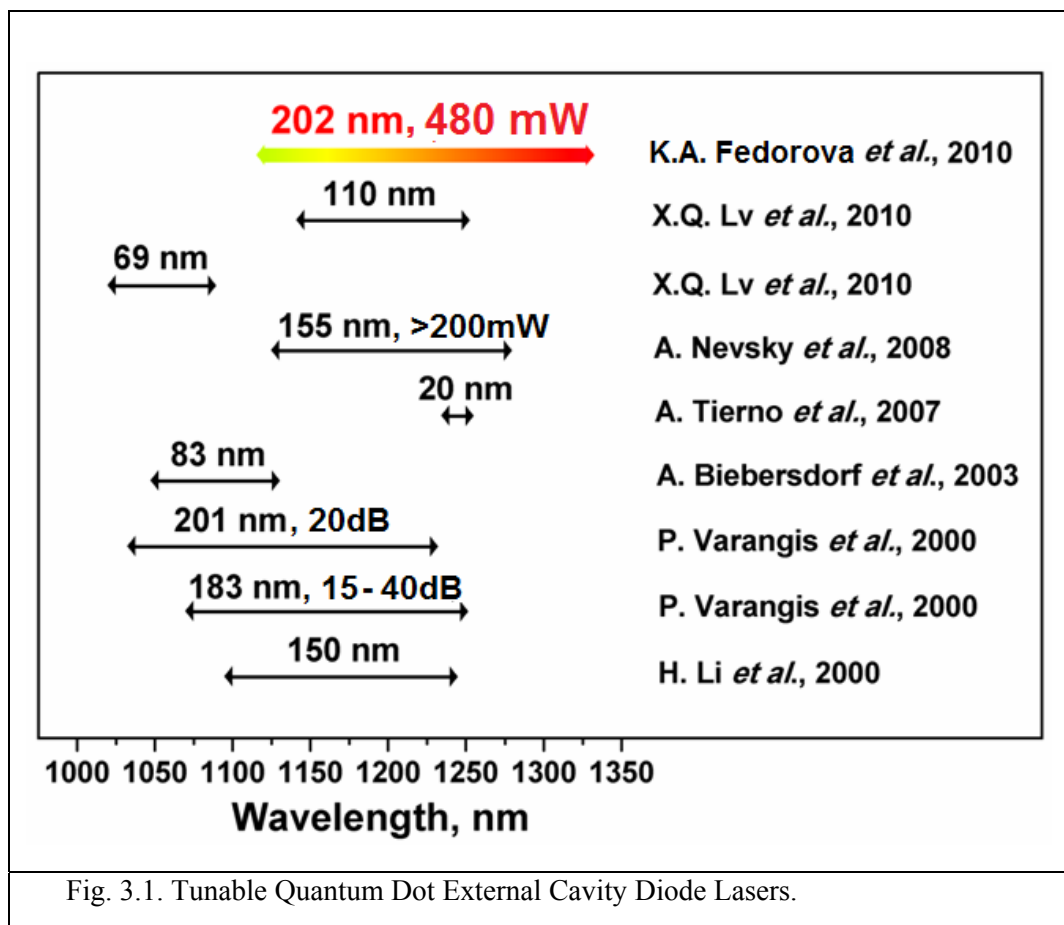
A record broadly tunable high-power external-cavity InAs/GaAs quantum-dot diode laser, with a tuning range of 202 nm (1122 nm-1324 nm) is demonstrated. A maximum output power of 480 mW and a side-mode suppression ratio greater than 45 dB are achieved in the central part of the tuning range. A number of strategies for enhancing the tuning range of external cavity quantum-dot lasers are exploited. Different waveguide designs, output facet reflectivities, laser configurations and operation conditions (pump current and temperature) are investigated for optimization of output power and tunability.

3.1. Introduction

The development of high-power, broadly tunable, compact and low-cost external-cavity diode lasers (ECDLs) is an important research area for a wide range of applications, such as spectroscopy [3.1], interferometry [3.2] and testing of telecommunication and wavelength division multiplexing (WDM) systems [3.3]. In recent years, there has also been a growing interest in the development of broadly-swept tunable laser sources, which are of interest for optical coherence tomography due to their high spectral bandwidth and output power [3.4-3.6]. Furthermore, the spectral region encompassing 1.1 - 1.3 μm is particularly useful for biomedical imaging due to the minimal absorption and scattering in human tissue, which can significantly enhance the penetration depth [3.7]. Other important applications for this spectral range include the generation of coherent radiation in the visible spectral region via second harmonic generation or sum frequency generation, particularly into the yellow-orange spectral region [3.8,3.9], for which compact and efficient sources are relatively scarce.

However, the spectral range between 1.1 - 1.3 μm has been difficult to access with semiconductor lasers based on quantum well (QW) technology. In this respect, quantum dot (QD) materials have shown great promise for a new generation of optoelectronic devices and ultrafast technology [3.10]. Recently developed growth techniques have been able to control the fabrication of InAs/GaAs QDs with different transition energies, allowing the coverage of a broad spectral range between 1.0 μm and 1.3 μm [3.11]. For instance, the inhomogeneous broadening associated with the strain and size dispersion of the QDs (inherent to the Stranski-Krastanow growth techniques) results in a distribution of energies which, to some extent, parallels the distribution of QD sizes. This feature, together with the manipulation of the chemistry and strain of the capping layers and barriers, can be flexibly engineered to widen the emission spectral

bandwidth. By exploiting such broad gain bandwidths, QD external cavity diode lasers (QD-ECDLs) have demonstrated impressive tuning ranges up to 200 nm, for the spectral range between 1095 and 1245 nm [3.12] or between 1033 and 1234 nm [3.13]. However, the power emitted from these previously reported lasers was reasonably low (of the order of a few tens of mW). Nevsky *et al.* have demonstrated output power higher than 200 mW from a QD-ECDL, within a tuning range of 155 nm (between 1125 nm and 1280 nm) [3.14]. However, this tuning range was not realised at the same injection current. Very recently, a low-threshold tunable QD-ECDL in the spectral range 1141.6 – 1251.7 nm, with a maximum output power of 53 mW has been reported [3.15]. Significant results on QD-ECDLs published during the last 10 years [3.12-3.20] are presented in Fig. 3.1.

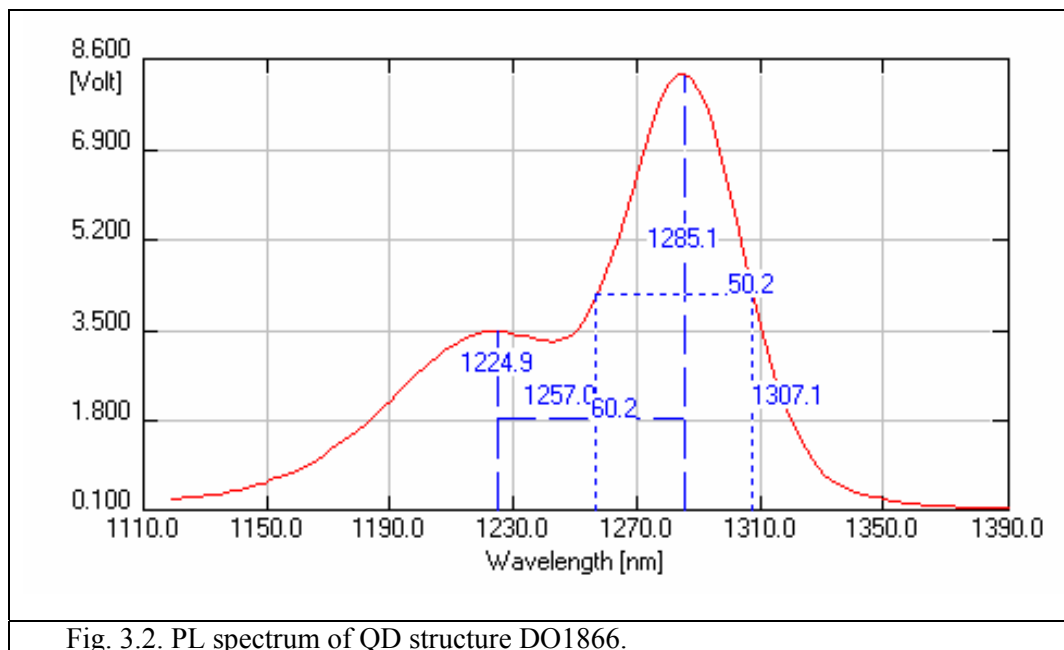


3.2. Semiconductor Optical Amplifier (Structure DO1866)

3.2.1. Structure and Device Design of InAs/GaAs Quantum Dot Diode

Laser

The semiconductor optical amplifier (SOA) was fabricated by Innolume GmbH (Dortmund, Germany) from the QD wafer structure (DO1866), with an active region which contained 10 non-identical InAs QD layers, incorporated into $\text{Al}_{0.35}\text{Ga}_{0.65}\text{As}$ cladding layers and grown on a GaAs substrate by MBE. These 10 layers were made up of 3 groups of QDs: Group 1 consisted of 4 QD layers while Groups 2 and 3 consisted of 3 QD layers each with different photoluminescence (PL) peak positions (1285 nm, 1243 nm and 1211 nm, respectively). The PL spectrum of QD structure DO1866 is presented in Fig. 3.2. On this PL spectrum, one can clearly see that there is no dip between ground and excited states as these energies are filled with QDs having different position of ground and excited states.



A broad spectral emission was achieved by changing the thickness of the $\text{In}_{0.15}\text{Ga}_{0.85}\text{As}$ capping layers for different groups of QD layers. This approach results in increased indium segregation into the quantum dots that have thicker capping layers and as such, the average size of the quantum dots capped with thicker layers becomes larger. Furthermore, the level of confinement in these quantum dots allows for the existence of not only a ground-state energy level but also of a first excited-state transition, which in combination with the distribution of different QD sizes, results in a structure specifically designed for continuous tuning between the ground and excited-state optical transitions of the different QD groups.

In an ECDL setup, it is crucial to minimise as much as possible the effective facet reflectivity of the gain element. This can be attained with the fabrication of devices where the waveguide is at a particular angle with the facet. In this work, the SOA ridge waveguide has a width of $5\ \mu\text{m}$ and length of 4mm (Fig. 3.3) and was angled at 6.5° relative to the normal of the facets, in order to significantly reduce its reflectivity. Additionally, both facets also had conventional anti-reflective (AR) coatings, resulting in total estimated reflectivities of 10^{-5} for each.

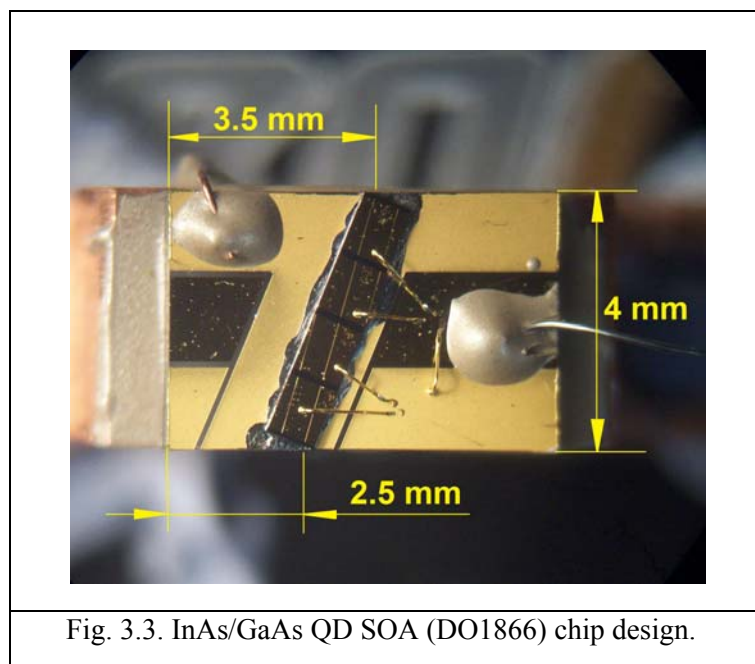
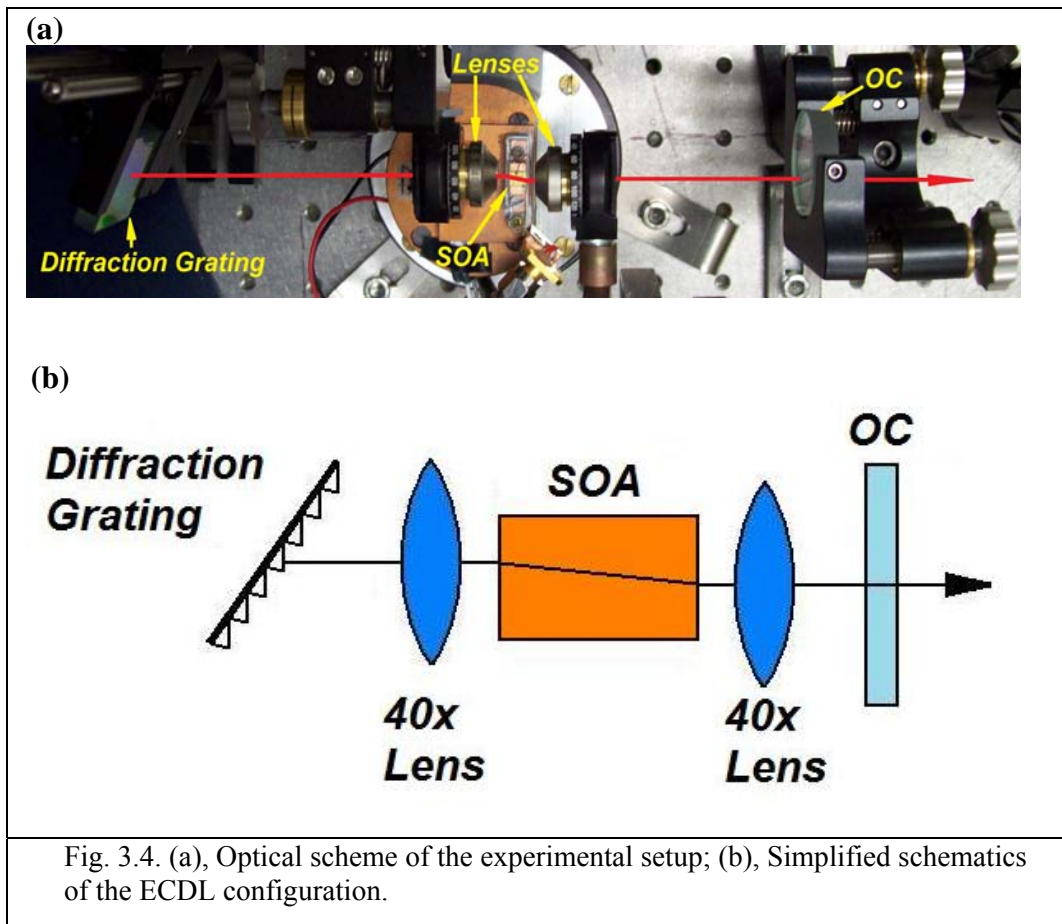


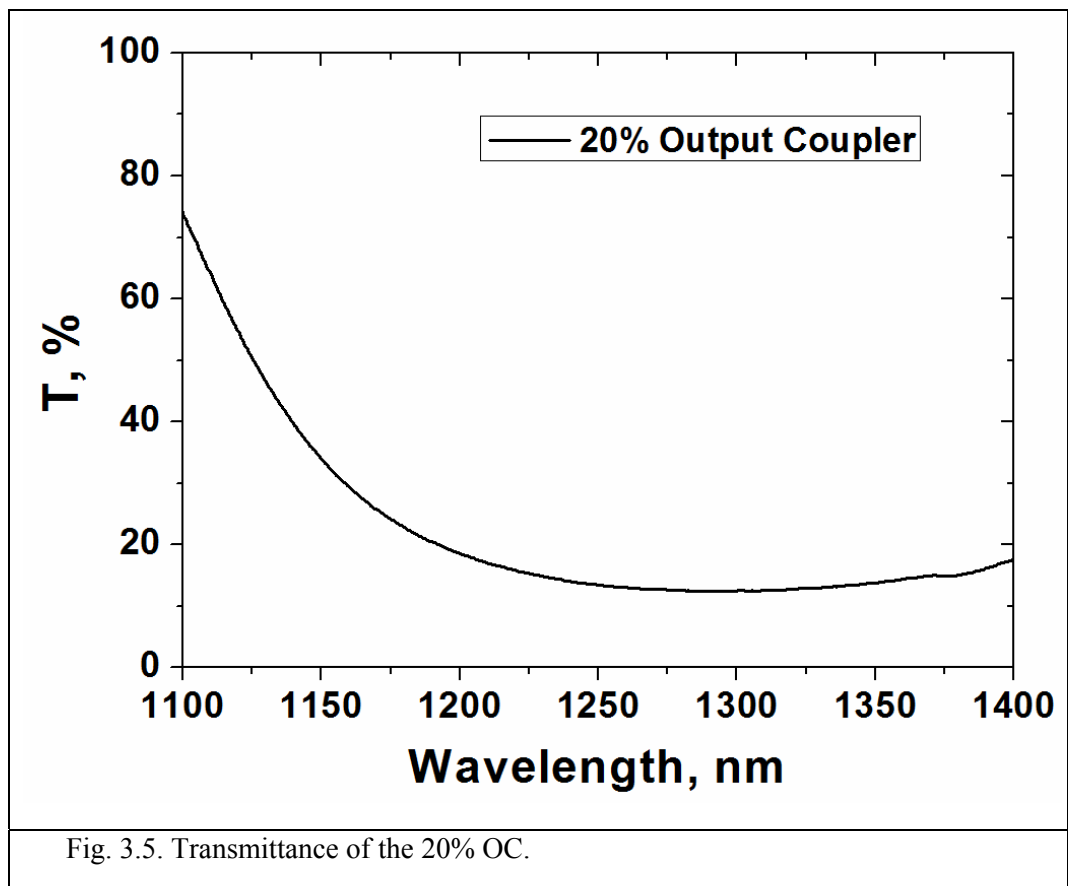
Fig. 3.3. InAs/GaAs QD SOA (DO1866) chip design.

3.2.2. Experimental Setup

The SOA operated under continuous wave (CW) forward bias and was mounted on a copper heat sink, with its temperature controlled by a thermo-electric cooler. As the aim of this work was to demonstrate a high-power broadly-tunable quantum-dot external cavity diode laser, a quasi-Littrow configuration was implemented due to its superiority in terms of output power and tuning range, when compared to the alternative Littman-Metcalf configuration. Moreover, the quasi-Littrow configuration is simpler and more compact in comparison with the Littman-Metcalf configuration. Therefore, the QD-ECDL was set-up in a quasi-Littrow configuration (Fig. 3.4), which consisted of a diffraction grating with 1200 grooves/mm, 40x (numerical aperture of 0.55) AR-coated aspheric lenses and an output coupler (OC). Coarse wavelength tuning was made possible by changing the incidence angle of the grating.

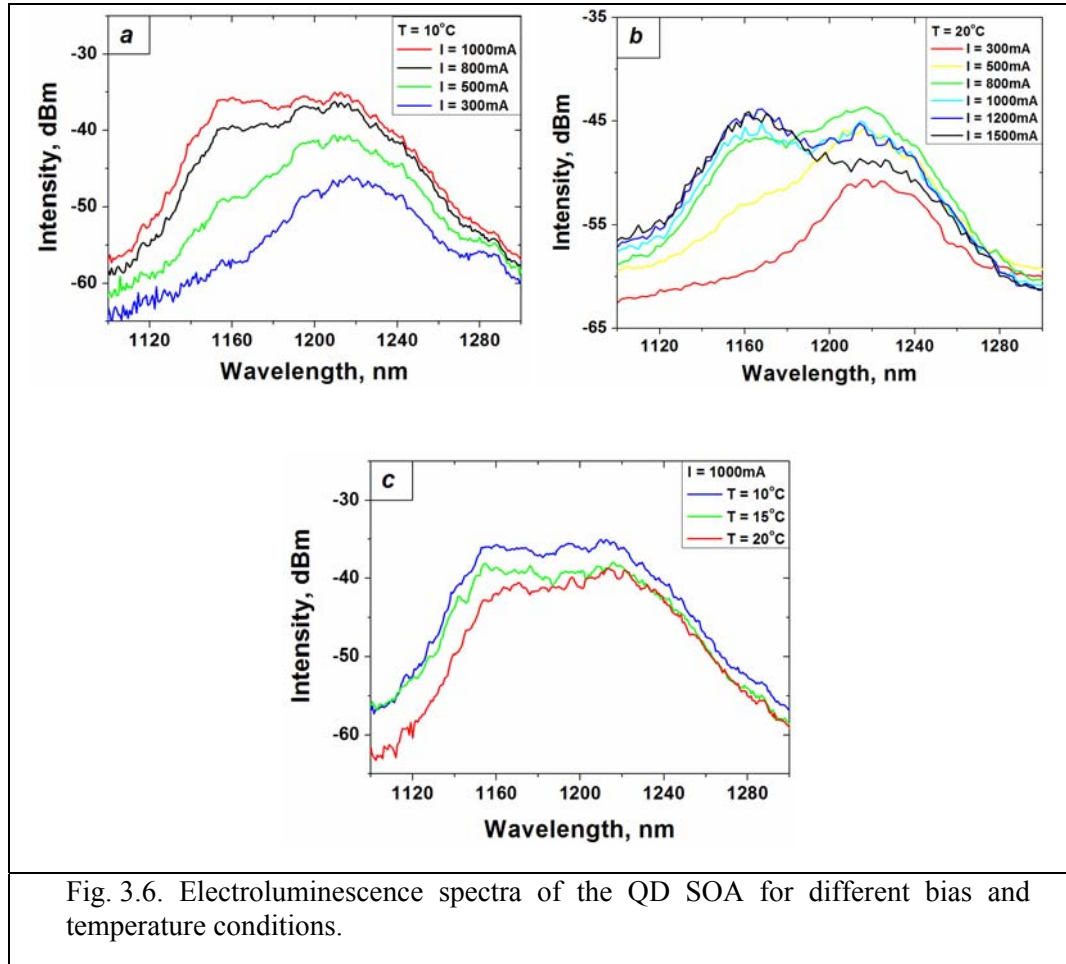


The output of the front facet was collimated with an aspheric lens, as represented in Fig. 3.4, and then coupled via an optical fibre into an optical spectrum analyser (OSA Advantest Q8383) and a broadband thermopile power meter. The QD-ECDL with the SOA was examined in two configurations by utilising a 20% OC and a 96% OC. The 96% OC had the same reflectivity across all of the tuning range. The reflectivity of the 20% OC unfortunately differed over the tuning range, becoming slightly lower with decreasing wavelength, from approximately 1190 nm to 1120 nm, as can be seen in Fig. 3.5.



3.2.3. Results

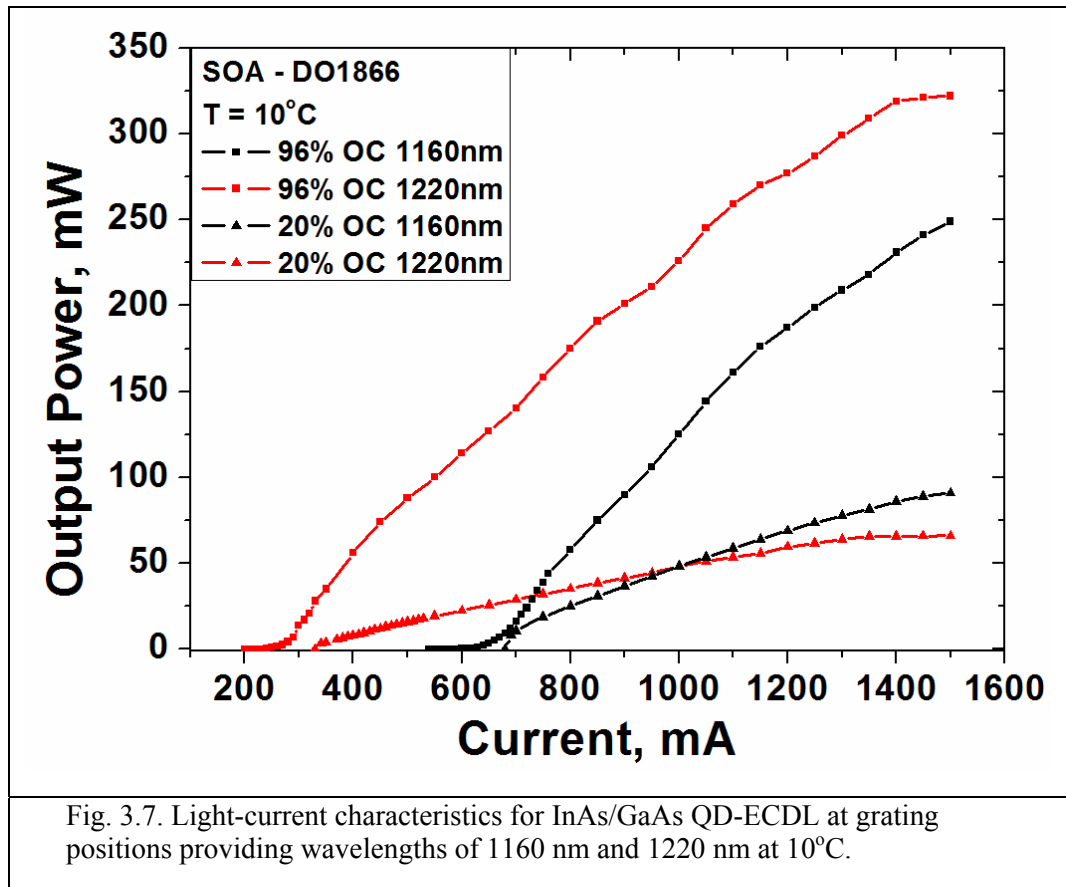
The broad electroluminescence (EL) spectra obtained from the SOA for various bias and temperature conditions are shown in Fig. 3.6.



The measured EL spectra broaden with decreasing temperature, predominantly on the blue side of the spectrum. Similar behaviour was observed for increasing current, for a fixed temperature. These results imply that QD filling in the excited state transitions is stronger for higher pump currents, therefore boosting the emission on the blue side. Furthermore, the interplay between homogeneous and inhomogeneous broadening cannot be neglected in QD materials [3.21]. Due to the increase of the QD homogeneous broadening with increasing temperature, the emission spectrum becomes

narrower, thus being detrimental to the tuning range of QD-ECDL. This result is perhaps counter intuitive when comparing with other QW and bulk ECDLs, where temperature is routinely used to further tune the emission wavelength.

The light-current characteristics of the external cavity laser - as shown in Fig. 3.7 were taken with the QD-ECDL tuned at the wavelengths providing a maximum output power. This corresponded to 1220 nm with the 96% OC and to 1160 nm, with the 20% OC. For a CW-pump current of 1500 mA, a maximum optical output power of 322 mW for the 20% OC, at a heat sink temperature of 10°C was observed.



The dependences of output power on wavelength for the SOA QD-ECDL are represented in Fig. 3.8 and Fig. 3.9, for the configurations with 20% OC and 96% OC, for two distinct temperatures of 10°C and 20°C, under applied constant current of 1 A and 1.5 A. Notably, for the QD-ECDL configuration with the 96% OC, a maximum optical output power of 322 mW was achieved for a CW-pump current of 1.5 A, at 10°C (when tuned to $\lambda=1220$ nm, as previously shown in Fig. 3.7). In comparison, only 91 mW was achieved (when tuned to $\lambda=1160$ nm), when a 20% OC was included in the cavity (Figures 3.7 and 3.9). The slightly different shape of the output power vs. wavelength curve (Fig. 3.8 and Fig. 3.9) for the configuration with the 20% OC compared to the 96% OC was obtained as a result of the reflectivity of the 20% OC, which becomes slightly lower with decreasing wavelength from approximately 1190 nm to 1120 nm (Fig. 3.5).

The various optical spectra obtained while tuning this laser across the 1132 nm – 1310 nm wavelength range, are presented in Fig. 3.10. The emission spectrum exhibited a side-mode suppression ratio in excess of 40 dB in the central part of the tuning range. The resulting optical spectrum exhibited a full-width half-maximum spectral bandwidth around 0.12 nm (Fig. 3.11), limited only by the instrumental resolution of the spectrometer.

Using a CW-pump current of 1.2 A, a tuning range of 147 nm was achieved in the configuration with the 96% OC at 10°C. The tuning range can be extended by changing the configuration of the cavity by the addition of the 20% OC instead of the 96% OC. It should be noted that the same laser demonstrated a 178 nm continuous tuning (1132nm – 1310nm) in the configuration with the 20% OC (Fig. 3.10). Using a CW-pump current of 1 A, a tuning range of 172 nm has been achieved for InAs/GaAs QD-ECDL in the SOA configuration with the 20% OC at 10°C.

Tuning range limits for the SOA (DO1866) for different configurations at 10°C and 20°C, under an applied constant current of 1 A and 1.5 A, are shown in Table 3.1.

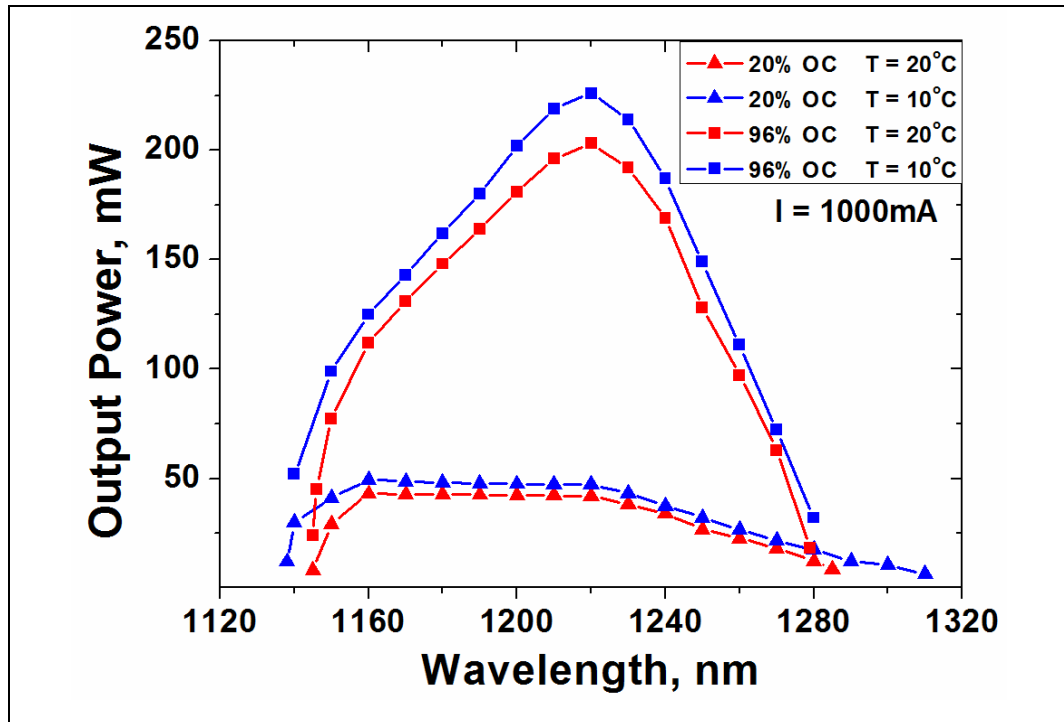


Fig. 3.8. Dependence of output power on wavelength for different temperatures and configurations, under an applied constant current of 1 A.

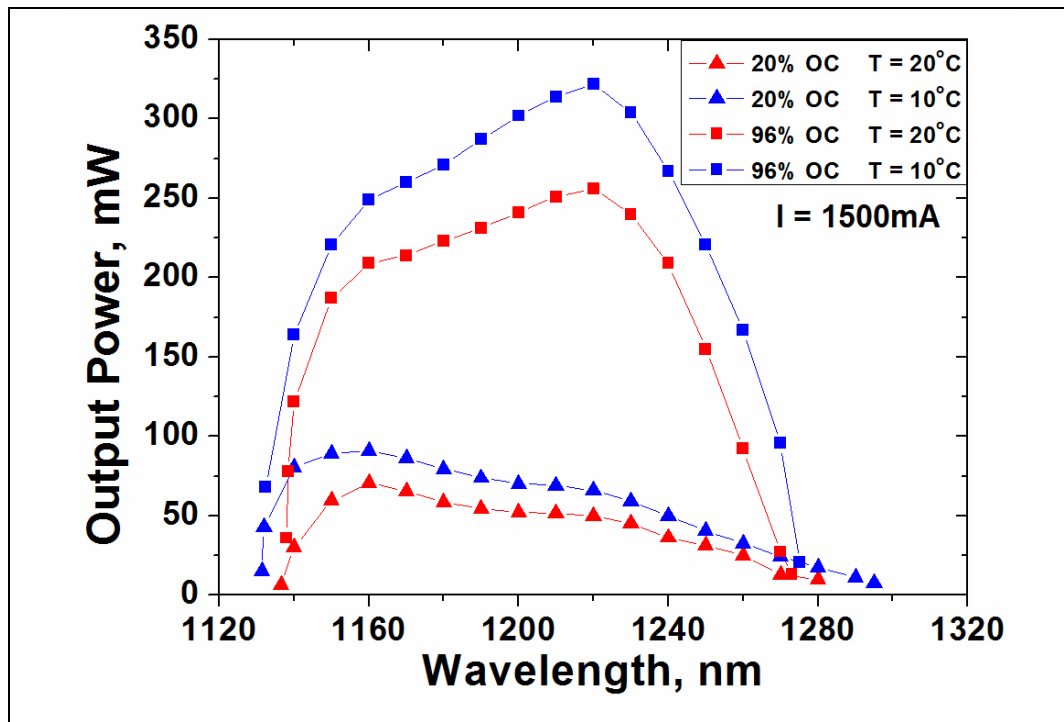


Fig. 3.9. Dependence of output power on wavelength for different temperatures and configurations, under an applied constant current of 1.5 A.

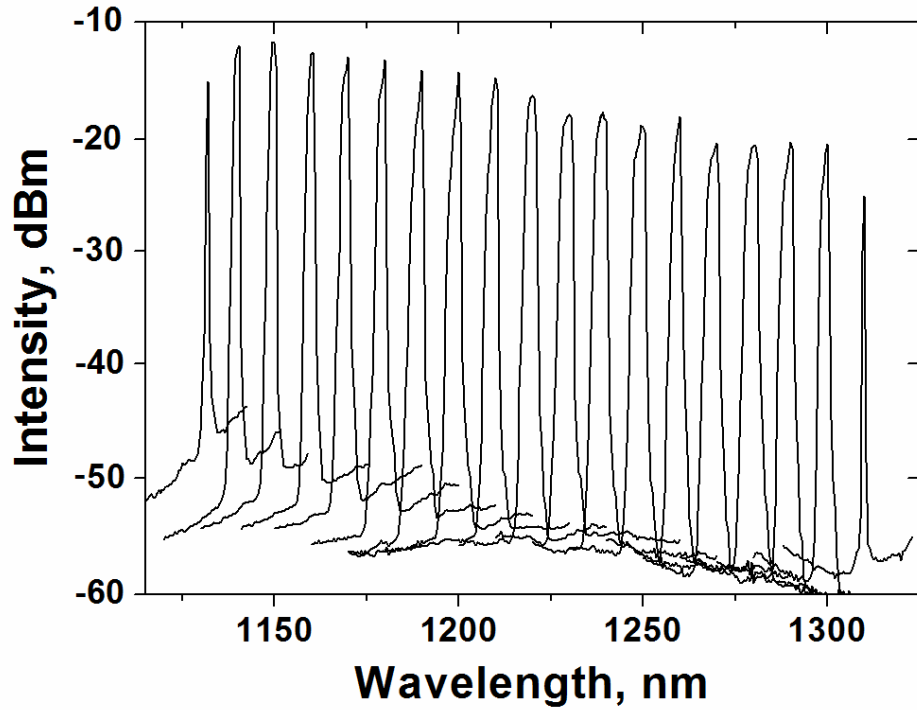


Fig. 3.10. Spectra of the QD ECDL with the SOA, tuned across the 1132 nm - 1310 nm wavelength range, in the configuration with the 20% OC.

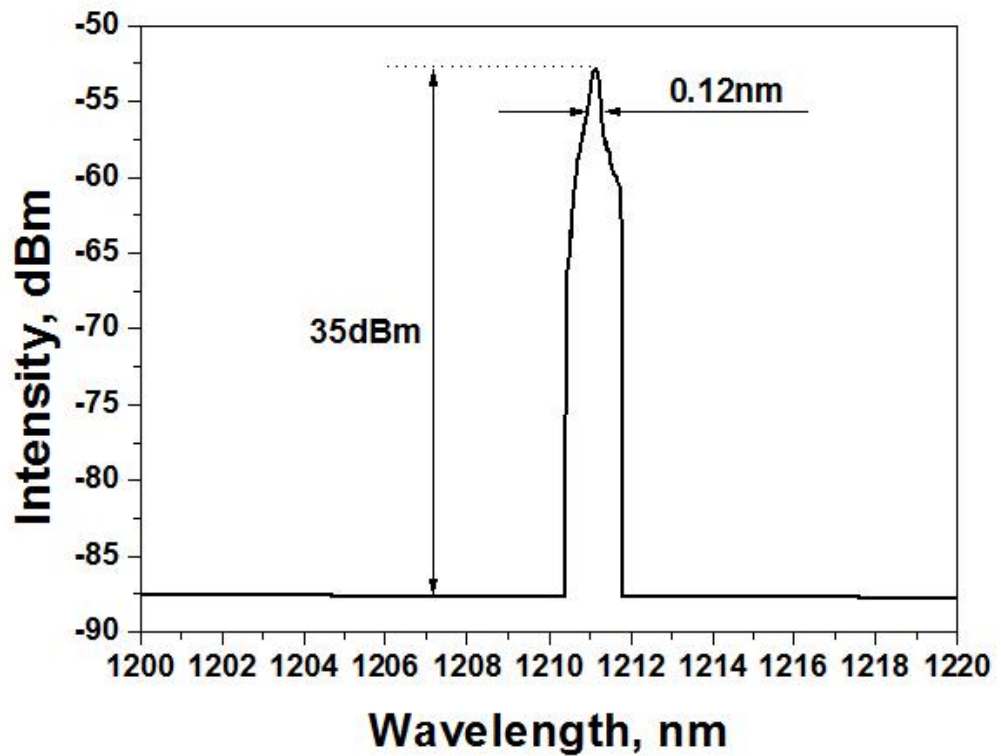


Fig. 3.11. The resulting optical spectrum exhibited a bandwidth around 0.12 nm.

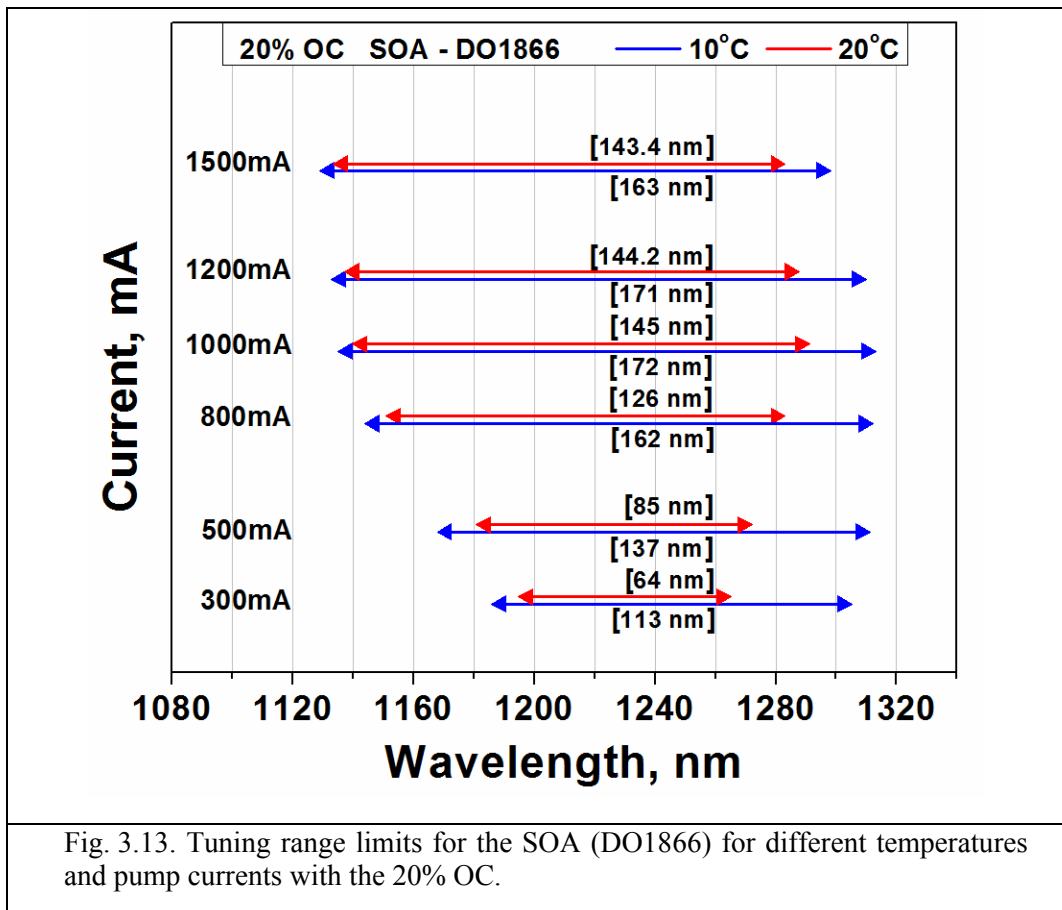
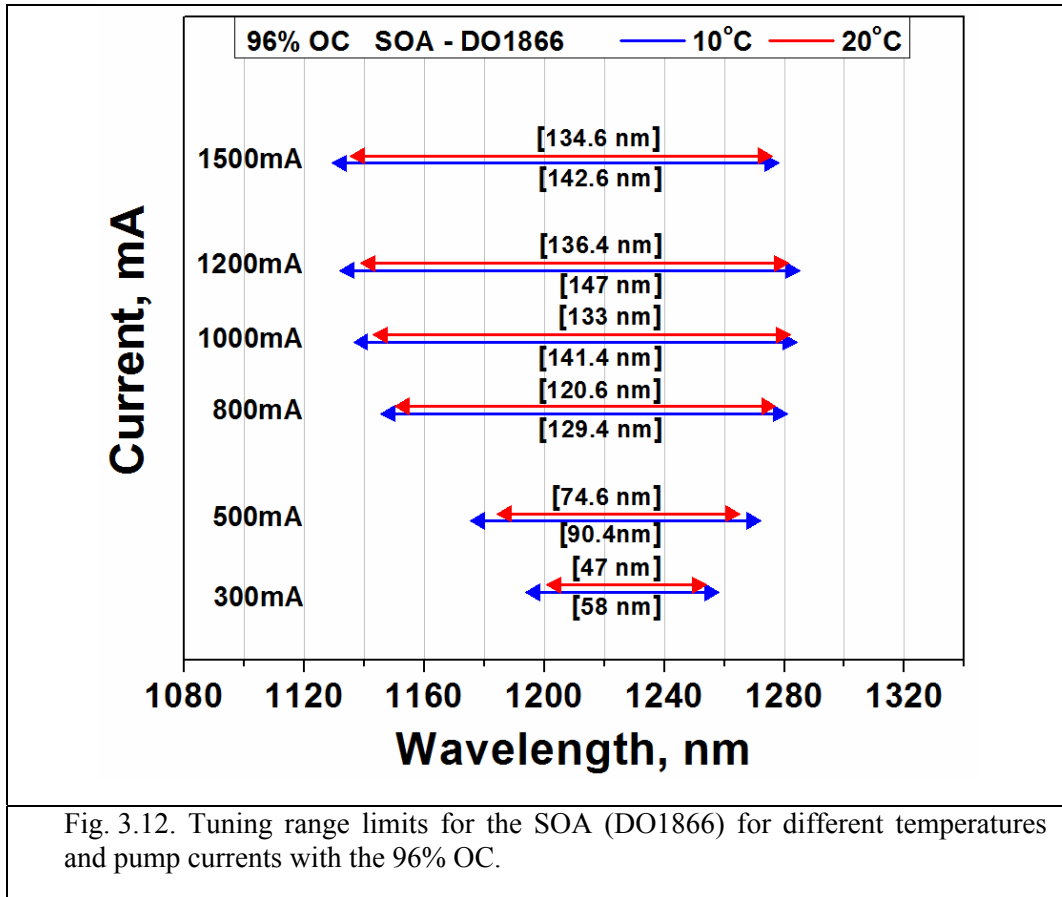
Table 3.1. Tuning range limits for the SOA (DO1866) for different configurations at 10°C and 20°C, under an applied constant current of 1 A and 1.5 A.

OC	Temperature	Current	nm	nm	Tunability, nm
20%	10°C	1.5 A	1132	1295	163
20%	20°C	1.5 A	1136.6	1280	143.4
96%	10°C	1.5 A	1132.4	1275	142.6
96%	20°C	1.5 A	1138.4	1273	134.6
20%	10°C	1 A	1138	1310	172
20%	20°C	1 A	1143	1288	145
96%	10°C	1 A	1139.6	1281	141.4
96%	20°C	1 A	1146	1279	133

The tuning range for different bias (300 mA - 1500 mA), temperature conditions (10°C - 20°C) and configuration of the QD-ECDL incorporating the SOA (DO1866) was investigated. The obtained results, as depicted in Fig. 3.12 and Fig. 3.13, show that the tuning range is enhanced for lower temperatures and higher pump currents.

For the 96% OC, in agreement with the EL spectra depicted in Fig. 3.6, this enhancement is asymmetric and occurs predominantly on the shorter wavelength side of the tuning range, whereas the longer wavelength side remains practically unaltered, particularly for high current bias.

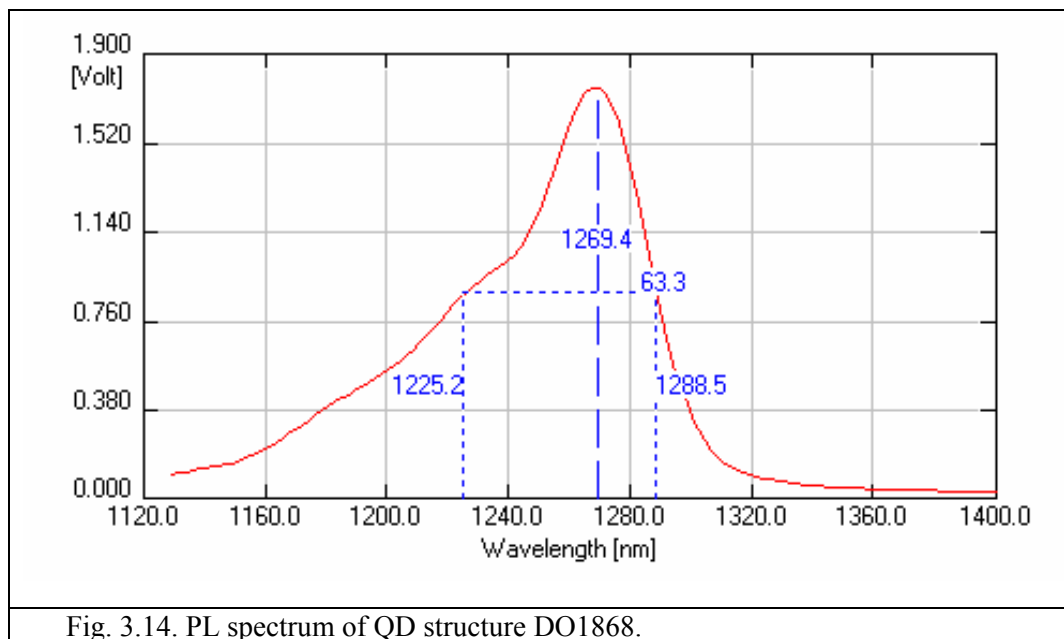
For the 20% OC, an enhancement of the tuning range occurred predominantly on the longer wavelength side, as the lower cavity losses favoured laser emission via the ground-state levels of the QD gain material, as had been previously proposed by Li *et al.* [3.12]. An increase of the cavity feedback by the addition of the 20% OC has been shown to extend the tuning range, particularly at the red side of the spectrum. However, a trade-off exists, as the presence of an OC in the cavity reduces its maximum output power.



3.3. Semiconductor Optical Amplifier (Structure DO1868)

3.3.1. Structure and Device Design of InAs/GaAs Quantum Dot Diode Laser

The SOA used in this work was fabricated from the QD wafer structure (DO1868), with active medium different from that described in the previous Section 3.2. An active region containing 10 non-identical InAs QD layers was incorporated into $\text{Al}_{0.35}\text{Ga}_{0.65}\text{As}$ cladding layers and grown on a GaAs substrate by MBE. These 10 layers contained 3 groups of QDs: Group 1 consisted of 4 QD layers while Groups 2 and 3 consisted of 3 QD layers each with different photoluminescence (PL) peak positions (1270 nm, 1243 nm and 1211 nm, respectively). This structure was fabricated with 3 different PL peak positions for continuous tuning between the ground and excited-state optical transitions of the different QD groups. The PL spectrum of QD structure DO1868 is presented in Fig. 3.14.



The SOA ridge waveguide fabricated from this structure had a width of $5\ \mu\text{m}$ and length of $4\ \text{mm}$ (Fig. 3.15), and was angled at 5° relative to the normal of the facets, in order to significantly reduce its reflectivity. Additionally, both facets also had conventional AR coatings, resulting in total estimated reflectivities of 10^{-5} for each.

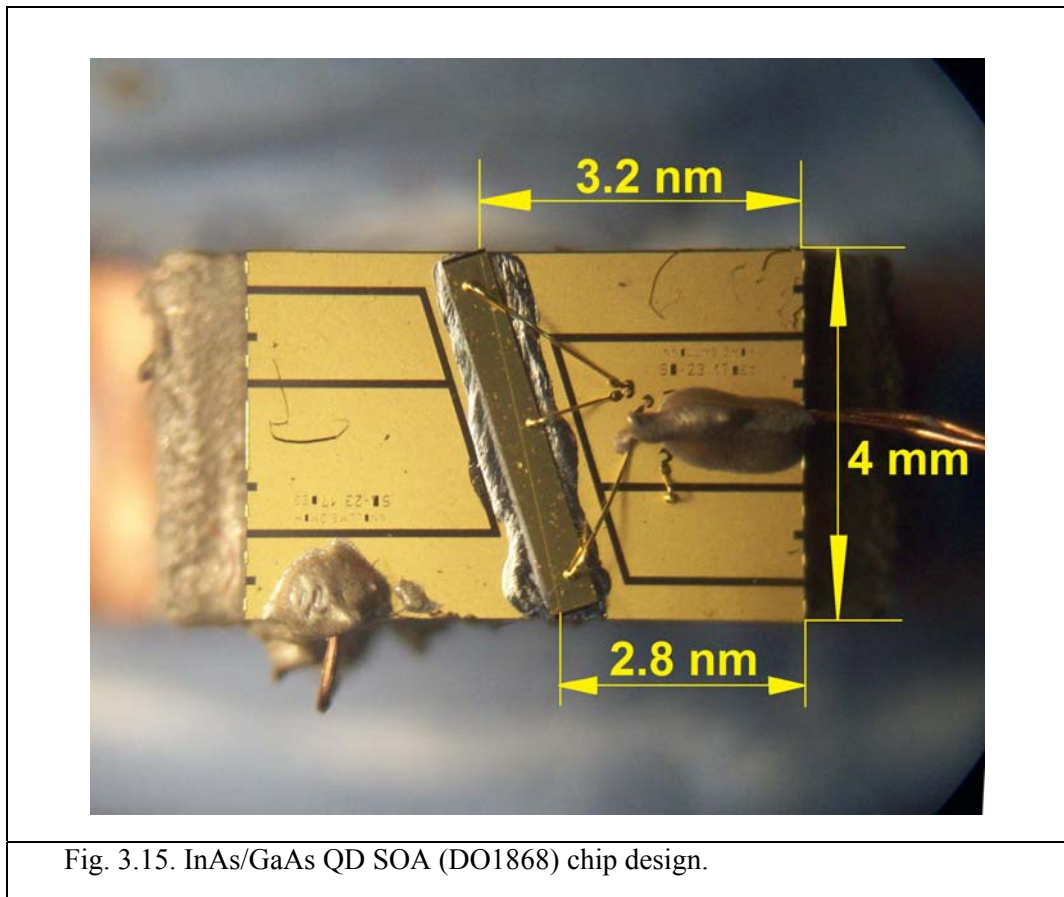


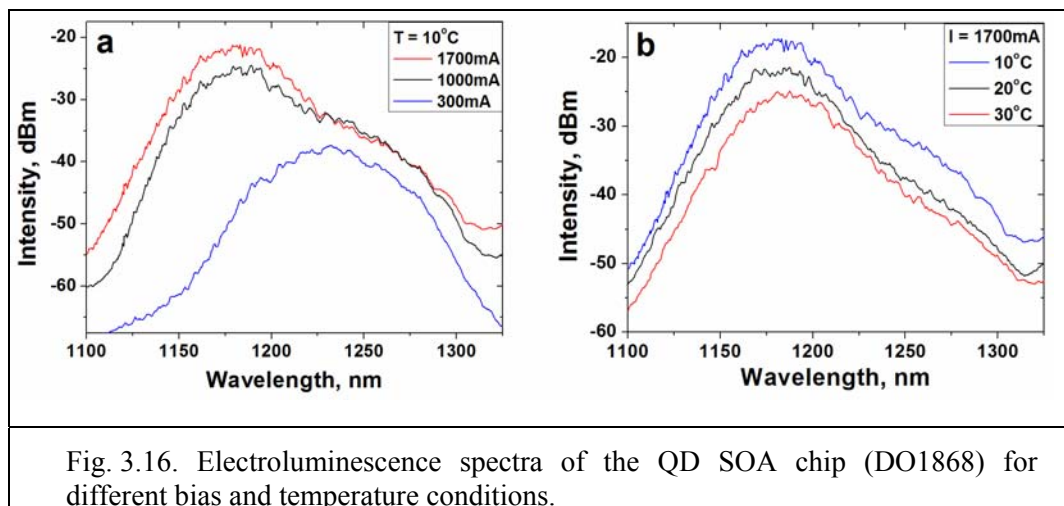
Fig. 3.15. InAs/GaAs QD SOA (DO1868) chip design.

3.3.2. Experimental Setup

The experimental setup (Fig. 3.4) was similar to that which was already described in the previous Section 3.2.2. The QD-ECDL with the SOA (DO1868) was examined for two configurations by utilising a 20% OC and a 96% OC (output couplers are similar to those used in the previous Section 3.2).

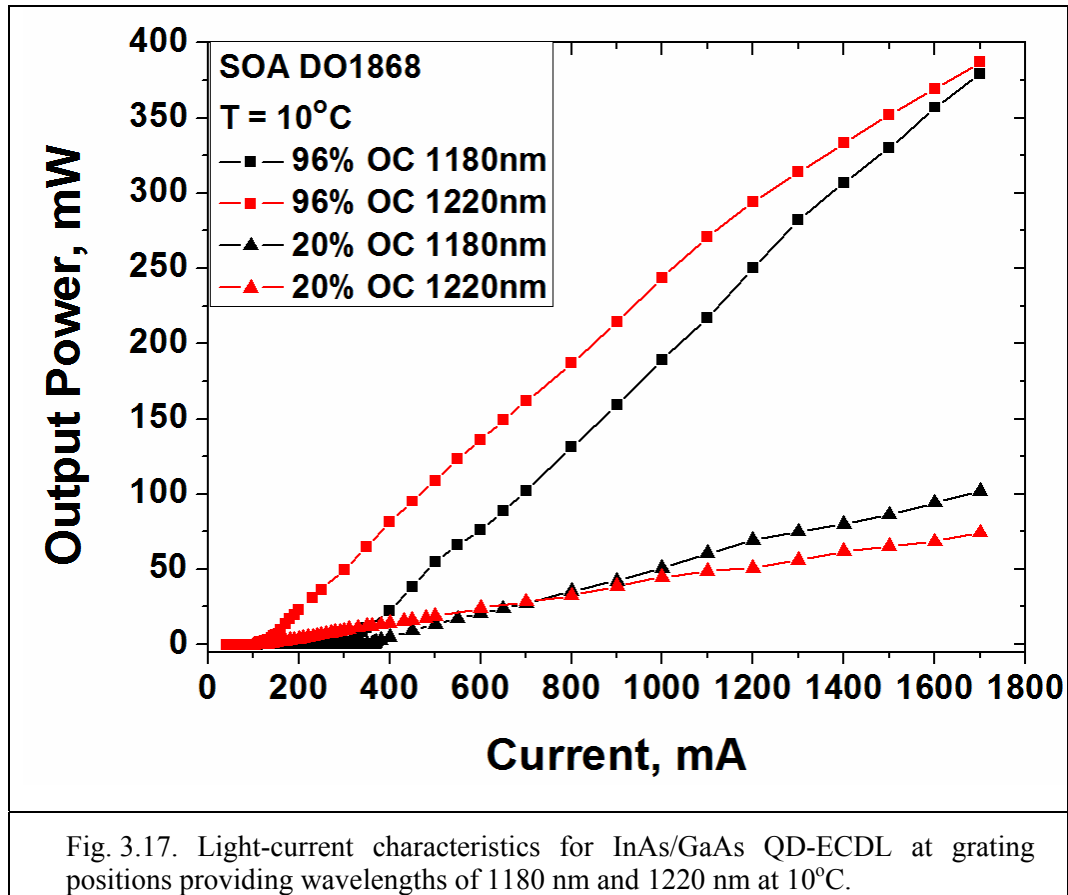
3.3.3. Results

The EL spectra obtained from the SOA (DO1868) for various bias and temperature conditions are shown in Fig. 3.16. At a fixed temperature, the measured EL spectra broaden with increasing current, with greater emphasis at the blue side of the spectrum. Such behaviour can be attributed to the saturation of the ground states and increasingly high carrier filling of the higher-energy excited states, which also have higher degeneracy, as is widely known in literature [3.22]. For a given injected current, the peak of the EL spectrum red-shifts with increasing temperature, as has also been previously observed [3.23]. The spectra also become broader when the temperature is increased, particularly towards the longer wavelengths. This effect can be understood by taking into account the thermal excitation of the carriers out of the QDs into the wetting layer. This escape process will be stronger for the carriers in the higher energy states (in smaller dots), which then become less populated than the lower energy states (in larger dots) [3.24].



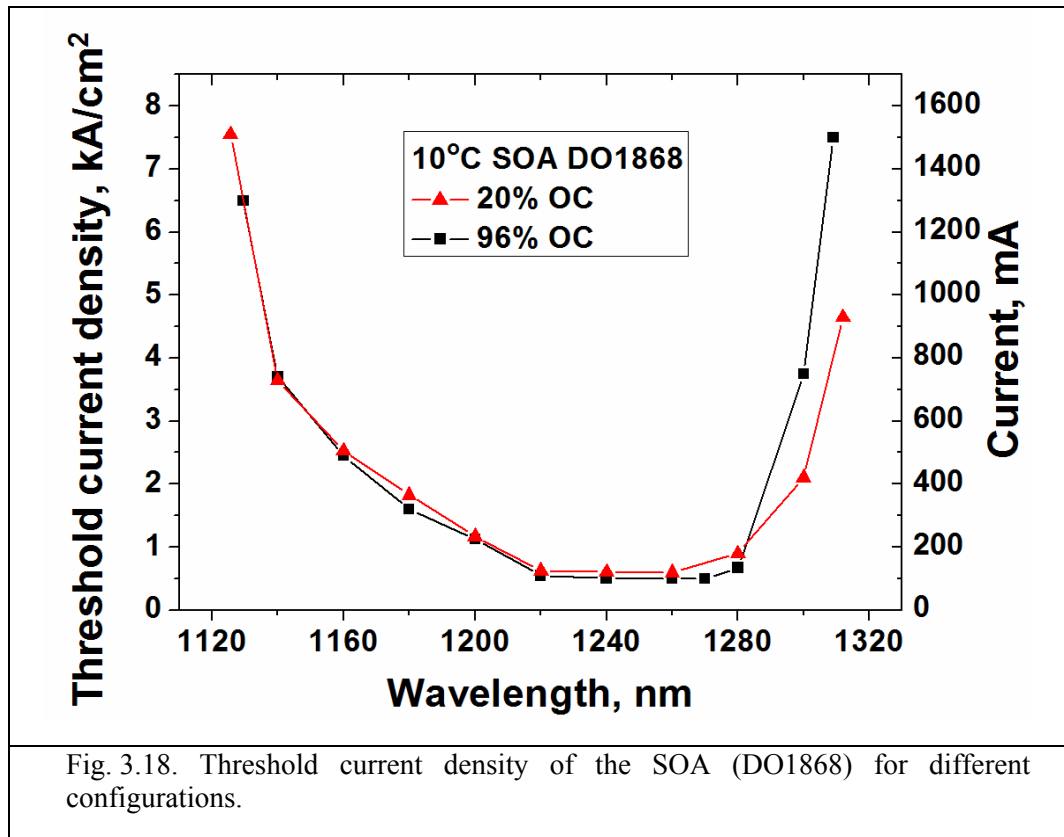
The light-current characteristics of the external cavity laser, as shown in Fig. 3.17, were taken with the QD-ECDL tuned at the wavelengths providing a maximum output power. This corresponded to 1220 nm with the 96% OC, and to 1180 nm with the

20% OC. A maximum optical output power of 387 mW for the 96% OC for a CW-pump current of 1.7 A, at 10°C was observed for the SOA (DO1868).

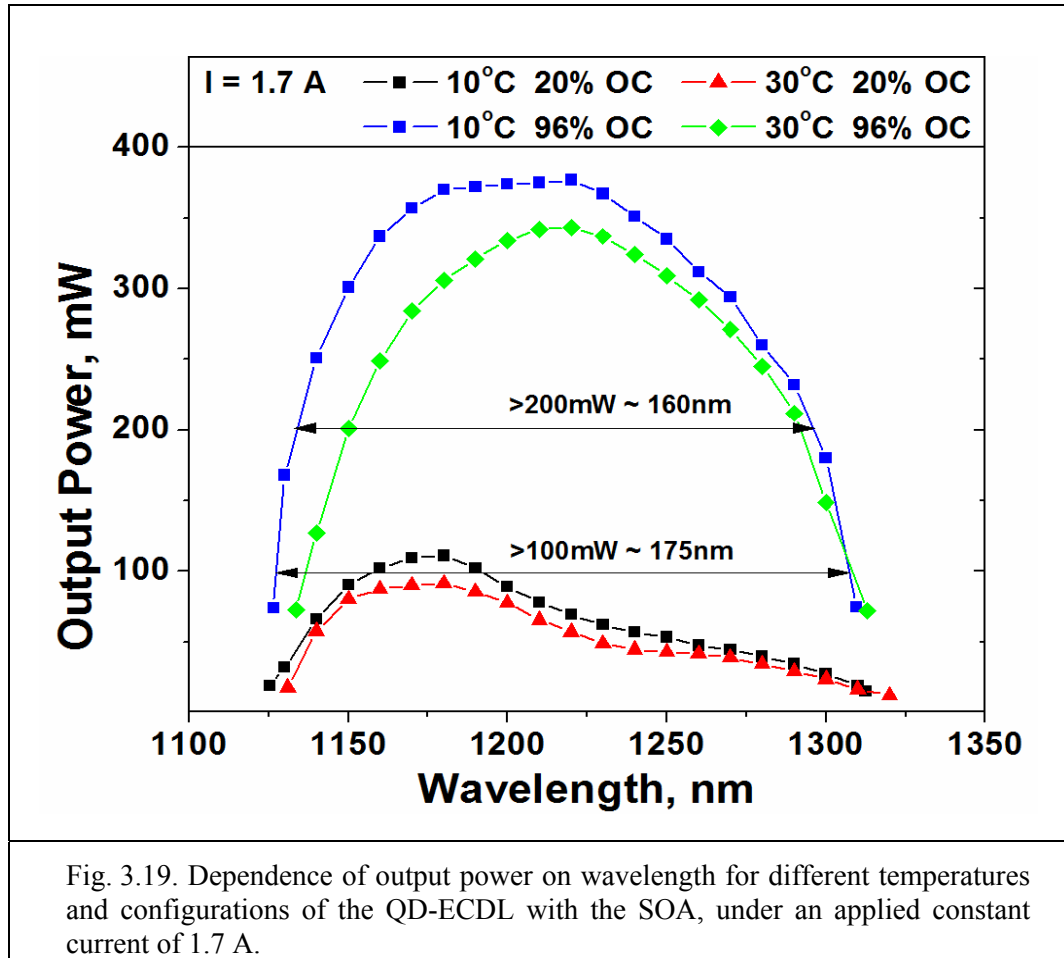


For the different configurations, the threshold current density (Fig. 3.18) was consistently lower than 2 kA/cm^2 in most of the central part of the tuning range (between 120-130 nm), with a steep increase close to the extremes of the tuning region. For the SOA at 10°C and with the 96% OC, the minimum threshold current density was 0.49 kA/cm^2 , while the maximum was 7.5 kA/cm^2 . At this point, it should be stressed that in general, broadly tunable QD-based lasers present a much lower threshold and operation current than their counterpart QW lasers. Indeed, in QW-based lasers, an injection current typically greater than a few tens of kA/cm^2 needs to be injected in order to reach broad tuning ranges by accessing not only the first but also the second quantized states ($n=1$ and $n=2$) that corresponds to shorter wavelengths [3.25]. On the

other hand, it is well known that in QD-based lasers the ground state can saturate at a fairly low current, thus enabling a transition to the ES at much lower values of bias current [3.12], which is extremely relevant not only to achieve a tunable laser with higher efficiency but also to enable a longer device lifetime.



The dependence of the output power with the different wavelengths for the SOA QD-ECDL is represented in Fig. 3.19, for the configurations with 20% OC and 96% OC and for two distinct temperatures of 10°C and 30°C. For the QD-ECDL configuration with the 96% OC, a maximum optical output power of 387 mW was achieved for a CW-pump current of 1.7 A, at 10°C (when tuned to $\lambda=1220$ nm, as previously shown in Fig. 3.17). In comparison, only 111 mW was achieved (when tuned to $\lambda=1180$ nm), when the 20% OC was included in the cavity (Figures 3.17 and 3.19).



The various optical spectra obtained while tuning this laser across the 1125.5 nm – 1320 nm wavelength range, are presented in Fig. 3.20. The emission spectrum exhibited a side-mode suppression ratio in excess of 45 dB in the central part of the tuning range. The resulting optical spectrum exhibited a full-width half-maximum spectral bandwidth around 0.13 nm (Fig. 3.21), limited only by the instrumental resolution of the spectrometer. Using a CW-pump current of 1.7 A, a tuning range exceeding 186 nm was achieved for InAs/GaAs QD-ECDL in the SOA chip configuration with the 96% OC. By changing the configuration of the cavity by the addition of the 20% OC instead of the 96% OC, the tuning range could be extended, with the same laser demonstrating 194.5 nm continuous tuning between 1125.5 nm and 1320 nm (Fig. 3.20). An average output power in excess of 200 mW was achieved for a tuning range of 160 nm.

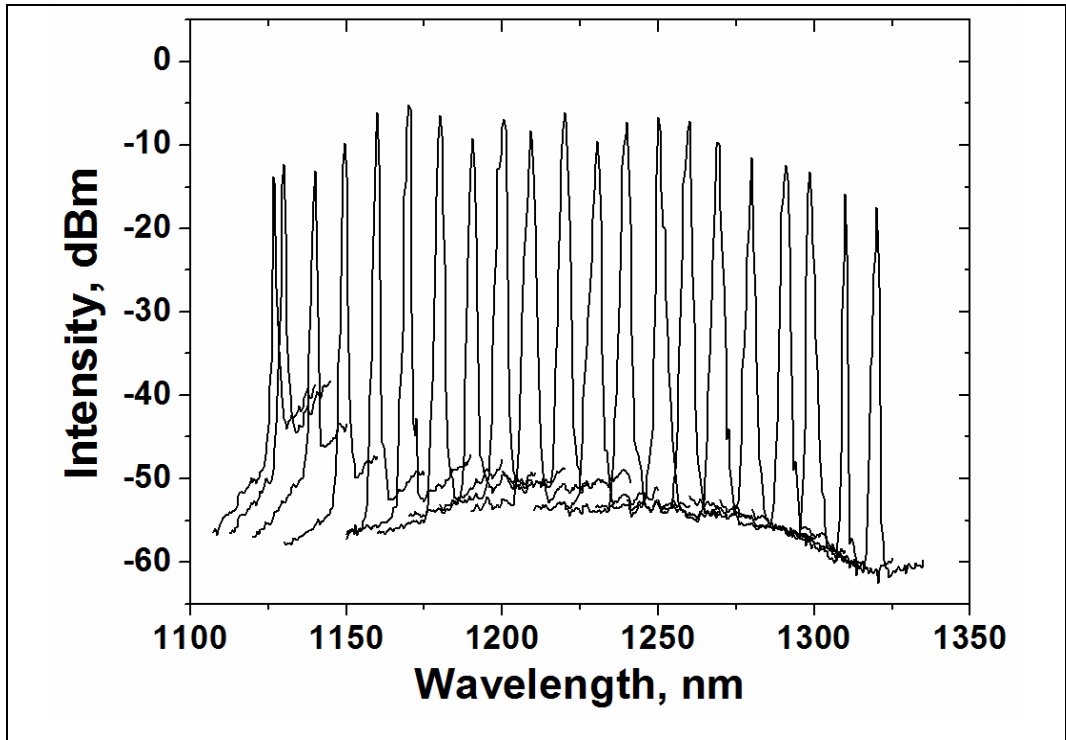


Fig. 3.20. Spectra of the QD-ECDL with the SOA (DO1868), tuned across the 1125.5 nm – 1320 nm wavelength range, under an applied constant current of 1.7 A.

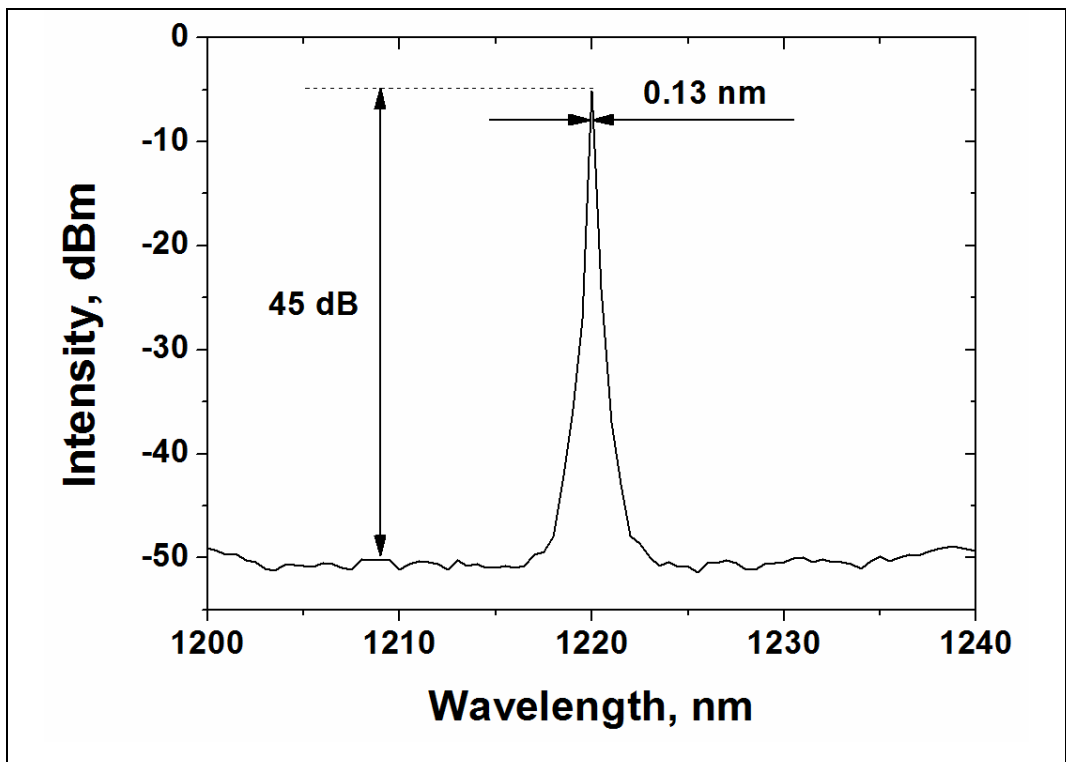
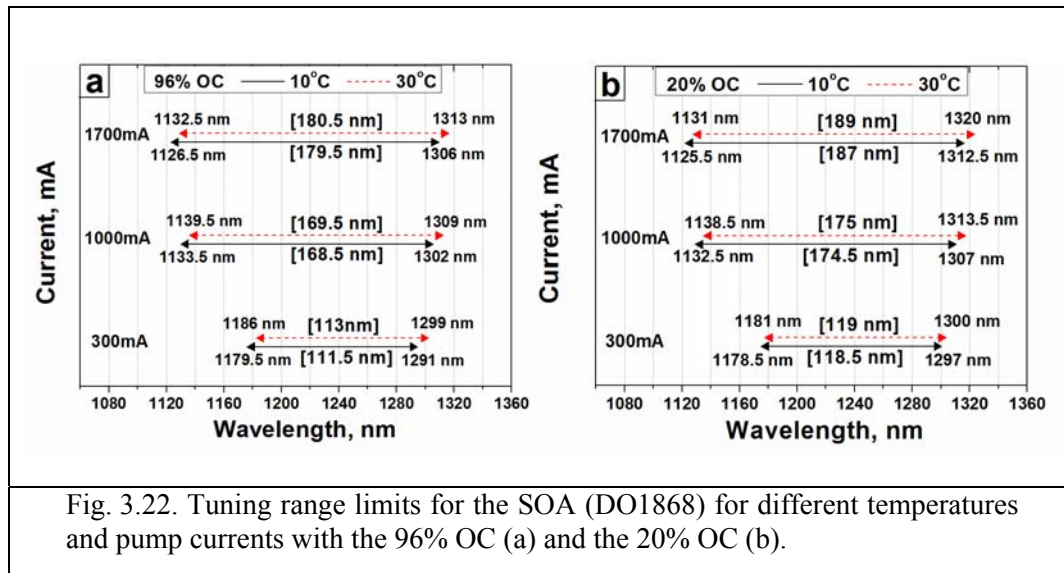


Fig. 3.21. The resulting optical spectrum exhibited a bandwidth around 0.13 nm.

The tuning range for different bias (300 mA - 1700 mA), temperature conditions (10°C - 30°C) and configuration of the QD-ECDL incorporating the SOA was also investigated. The obtained results, as depicted in Fig. 3.22, show that the tuning range is enhanced for higher pump currents. In agreement with the EL spectra depicted in Fig. 3.16, this enhancement is asymmetric and occurs predominantly on the shorter wavelength side of the tuning range, whereas the longer wavelength side remains practically unaltered, particularly for high current bias. Moreover, a shift of the tuning range to the longer wavelength side of the spectra was observed, when the temperature was increased from 10°C to 30°C (Fig. 3.22).



For the 20% OC, an enhancement of the tuning range occurred predominantly on the longer wavelength side, as the lower cavity losses favoured laser emission via the ground-state levels of the QD gain material. Furthermore, due to the fact that the temperature red-shift was more accentuated on the longer wavelength side of the spectra than on the shorter side, the tuning range was actually slightly extended with increasing temperature, which is related to the thermalisation effect previously described and also observed in the EL spectra (Fig. 3.16).

Using the results presented in this Section, the prototype of the QD-ECDL has been realised by Toptica Photonics AG (Graefelfing, Germany), as depicted in Figure 3.23.



Fig. 3.23. The prototype of the QD-ECDL.

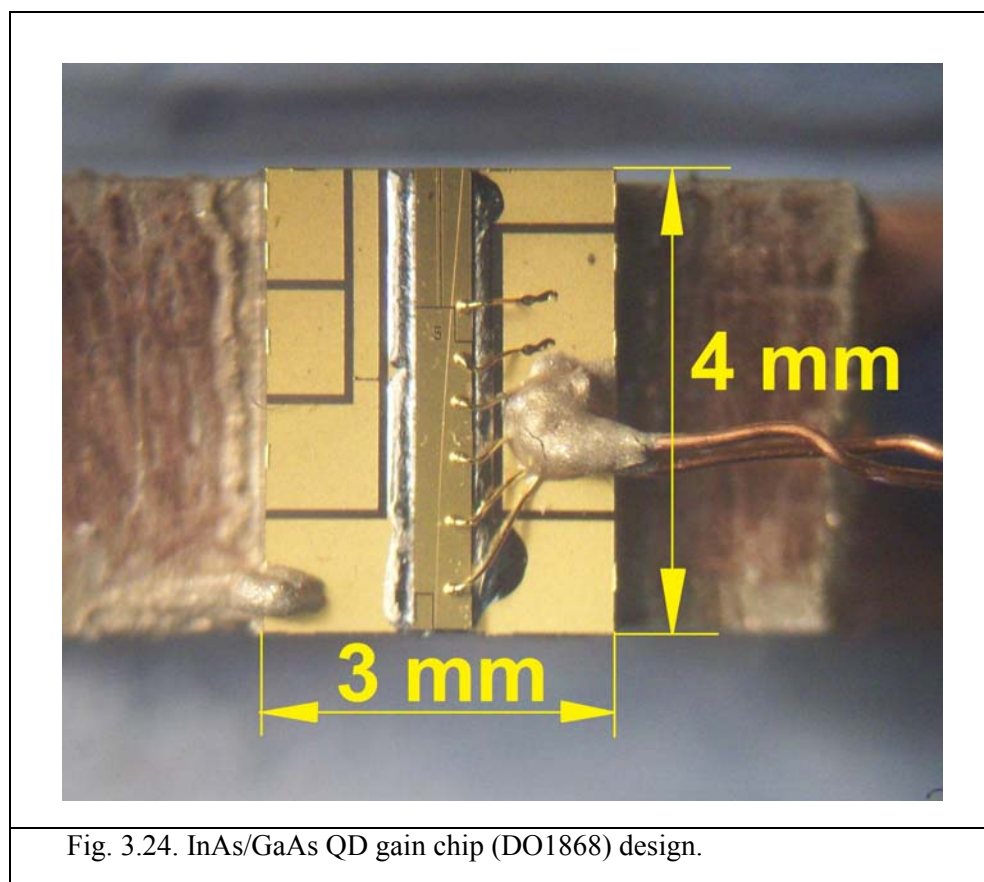
3.4. Gain Chip (Structure DO1868)

3.4.1. Structure and Device Design of InAs/GaAs Quantum Dot Diode

Laser

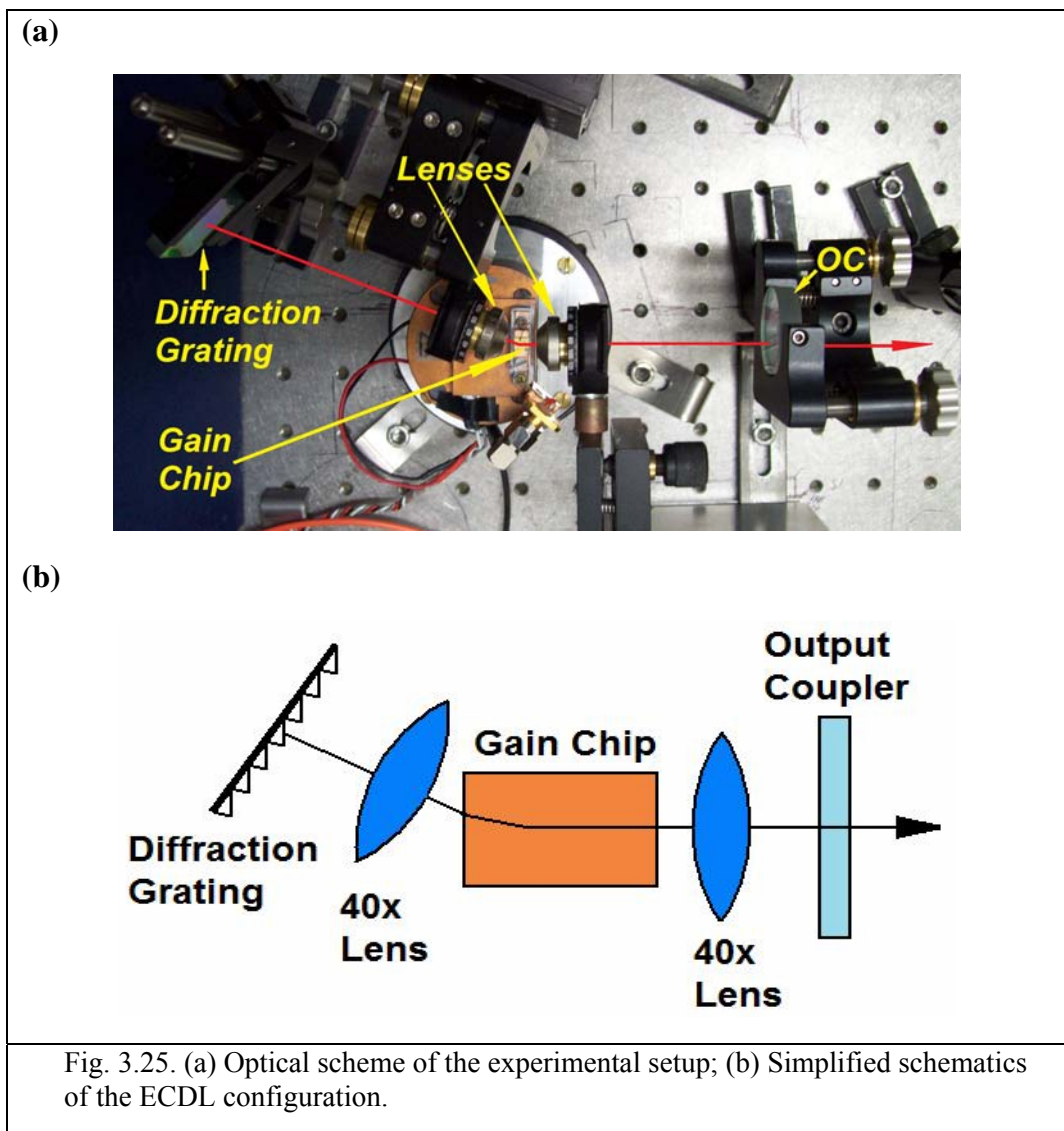
The gain chips investigated in this Section were fabricated from the QD wafer structure (DO 1868) described in Section 3.3.

The gain chip ridge waveguide had a width of $5\ \mu\text{m}$ and length of $4\ \text{mm}$ (Fig. 3.24), and was angled at 5° relative to the normal of the back facet, in order to significantly reduce its reflectivity. Additionally, both facets also had conventional AR coatings, resulting in total estimated reflectivities of $2 \cdot 10^{-3}$ for the front facet and less than 10^{-5} for the angled facet.



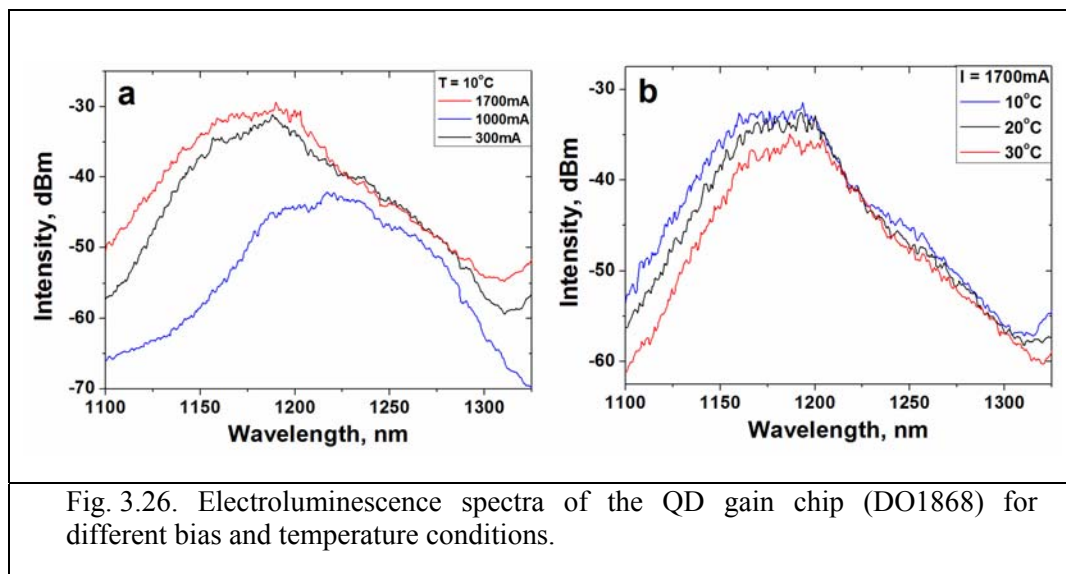
3.4.2. Experimental Setup

The gain chip operated under CW forward bias was mounted on a copper heat sink and its temperature was controlled by a thermo-electric cooler. The QD-ECDL was set-up in a quasi-Littrow configuration (Fig. 3.25), which consisted of a diffraction grating with 1200 grooves/mm, 40x (numerical aperture of 0.55) AR-coated aspheric lenses and output coupler. Coarse wavelength tuning was made possible by changing the incidence angle of the grating. The performance of the QD-ECDL with the gain chip was investigated for two configurations by utilising a 20% OC and without an output coupler. The 20% OC is similar to that used in the previous Sections.



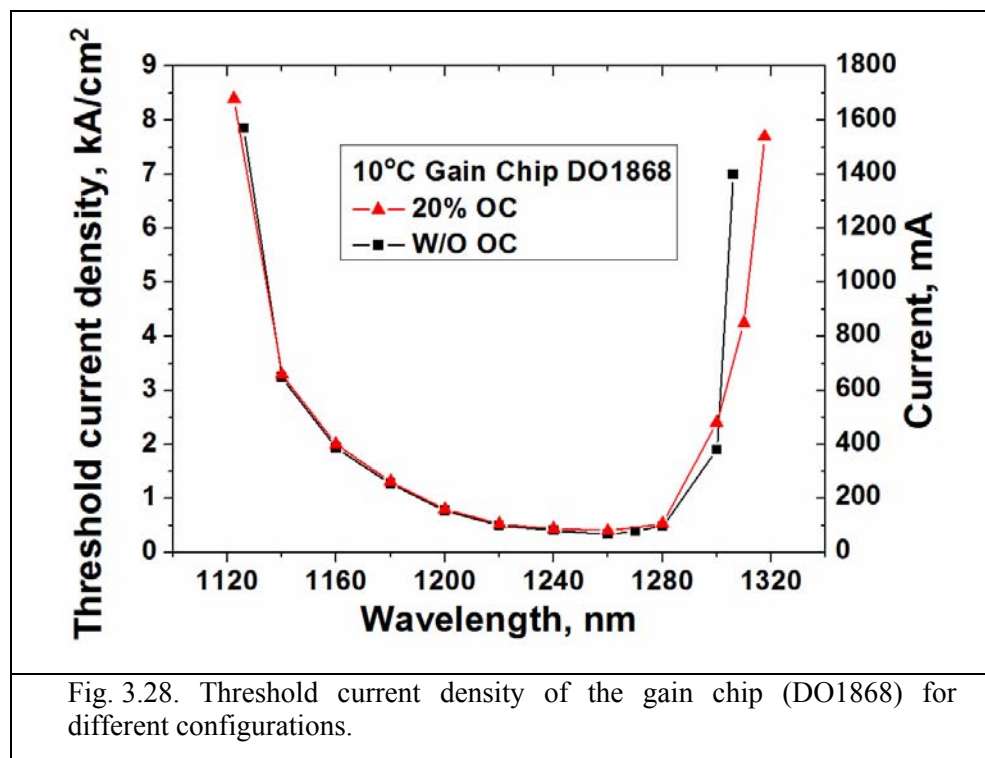
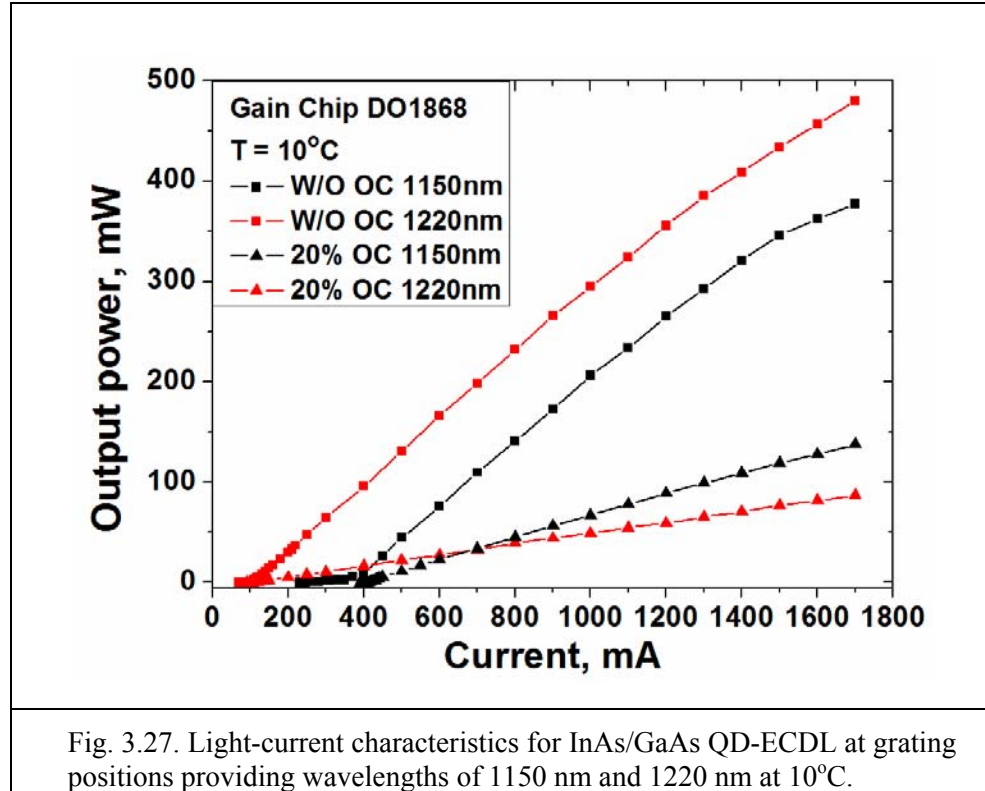
3.4.3. Results

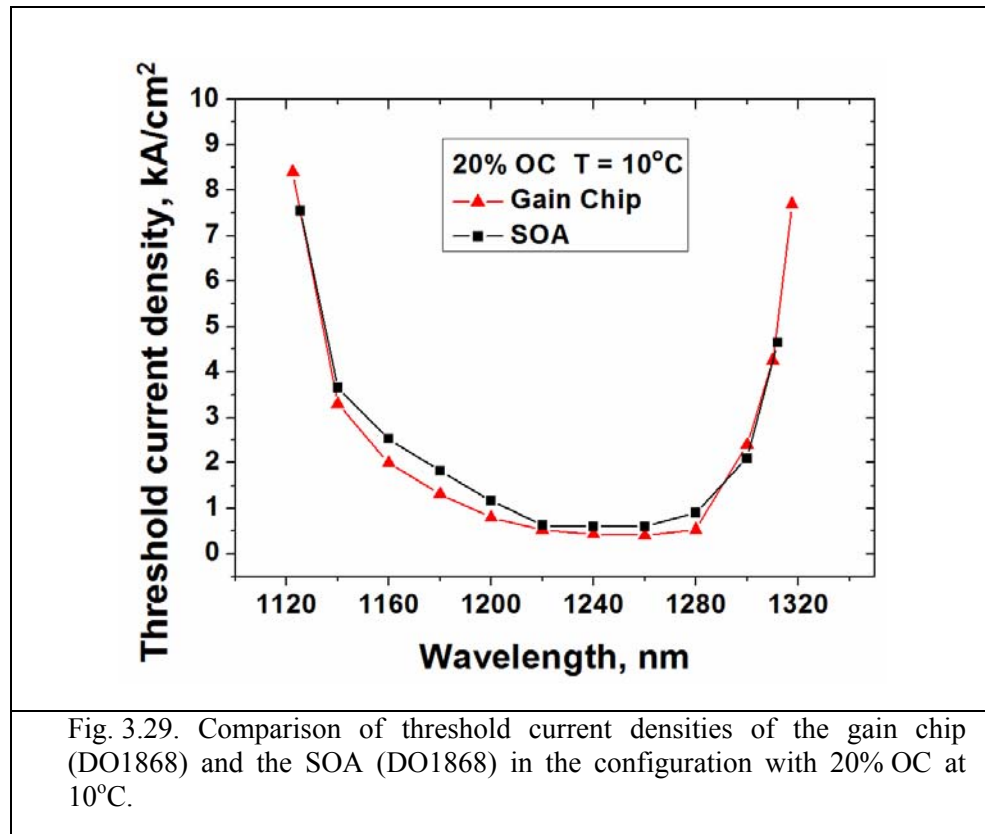
The EL spectra of the QD gain chip for various bias and temperature conditions are shown in Fig. 3.26. The EL spectra for the gain chip exhibit similar behaviour as the EL for the SOA (Fig. 3.16) fabricated from the same structure (DO1868). Under a fixed temperature, the measured EL spectra broaden with increasing current and with greater emphasis at the blue side of the spectrum. For a given injected current, the peak of the EL spectrum red-shifts with increasing temperature. The spectra also become broader when the temperature is increased, particularly towards the longer wavelengths.



The light-current characteristics of the external cavity laser, as shown in Fig. 3.27, were taken with the QD-ECDL tuned at the wavelengths providing a maximum output power. In the gain chip configuration, this corresponded to 1220 nm without an OC, and to 1150 nm, with the 20% OC. A maximum optical output power of 480 mW for a CW-pump current of 1.7 A, at 10°C was observed for the gain chip (DO1868). For the different configurations, the threshold current density (Fig. 3.28) was consistently lower than 2 kA/cm² for most of the central part of the tuning range (between 130 - 140 nm), with a steep increase close to the extremes of the tuning region. For the gain chip at 10°C and without an OC, the minimum threshold current density was 0.34 kA/cm²,

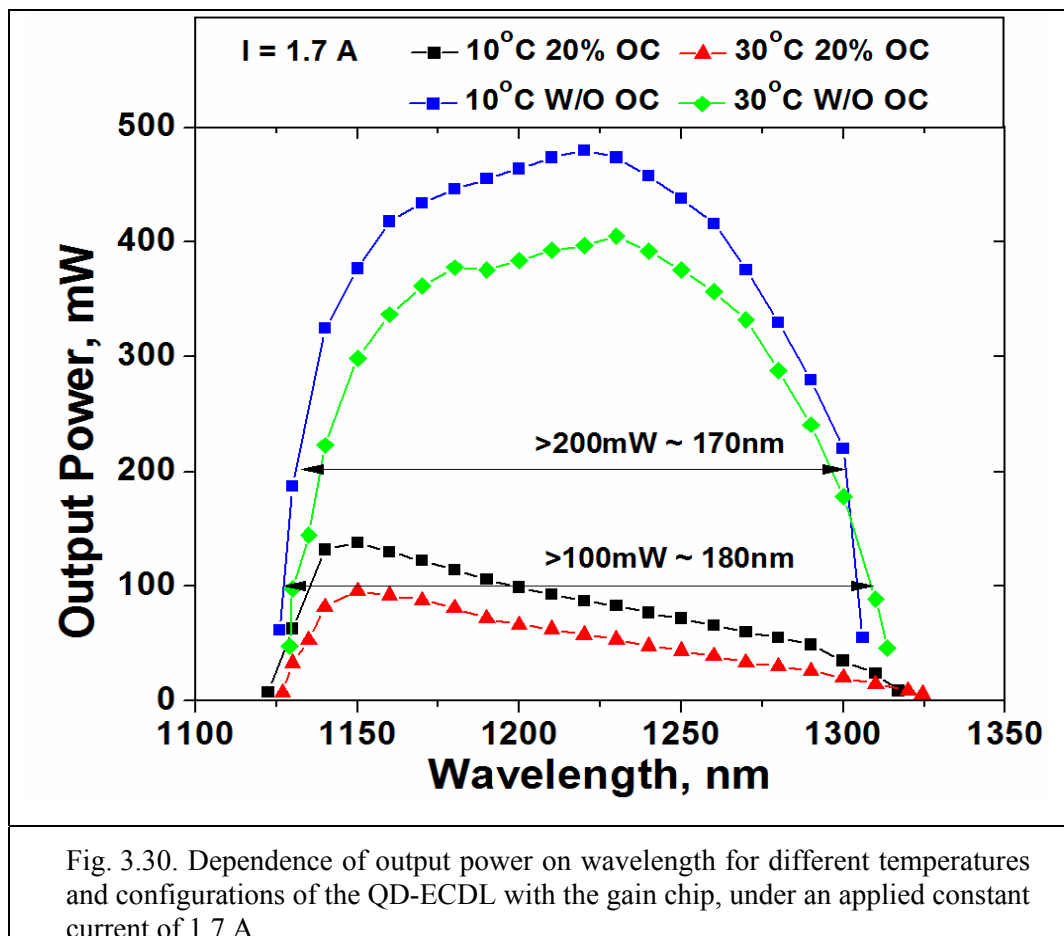
while the maximum was 7.85 kA/cm^2 . Comparison of the threshold current densities for the SOA and gain chip (fabricated from the same structure DO1868) in the configuration with the 20% OC at 10°C is shown in Fig. 3.29.





The dependence of the output power on wavelength for the gain chip QD-ECDL is presented in Fig. 3.30, for the configurations with 20% OC and without an OC, for two distinct temperatures of 10°C and 30°C. Notably, for the QD-ECDL configuration without the OC, a maximum optical output power of 480 mW was achieved for a CW-pump current of 1.7 A, at 10°C (when tuned to $\lambda=1220$ nm, and as previously shown in Fig. 3.27). In comparison, only 138 mW was achieved (when tuned to $\lambda=1150$ nm), when the 20% OC was included in the cavity (Fig. 3.27 and Fig. 3.30). The various optical spectra obtained while tuning this laser across the 1122.5 nm – 1324.5 nm wavelength range, are presented in Fig. 3.31. The emission spectrum exhibited a side-mode suppression ratio in excess of 45 dB in the central part of the tuning range. The resulting optical spectrum exhibited a full-width half-maximum spectral bandwidth around 0.13 nm (Fig. 3.32), limited only by the instrumental resolution of the spectrometer. Using a cw-pump current of 1.7 A, a tuning range exceeding 187 nm was

achieved for InAs/GaAs QD-ECDL in the gain chip configuration without the OC. It should be stressed that an output power in excess of 400 mW was achieved for a tuning range of 110 nm, as depicted in Fig. 3.30. Furthermore, it can be seen that the output power only varies by $\sim 10\%$ in the central part of the tuning range under a constant forward bias of 1.7 A, which is an extremely desirable feature for the development of a fast swept tunable laser source with high output power. Likewise, the threshold current is also relatively constant across this spectral range. The tuning range can be extended by changing the configuration of the cavity by the addition of the OC. The same laser demonstrated 202 nm continuous tuning in the configuration with the 20% OC (Fig. 3.31). Moreover, it should be emphasised that the lasing wavelength of 1324 nm is the longest GaAs-based QD lasing wavelength reported until now from a tunable GaAs-based QD laser.



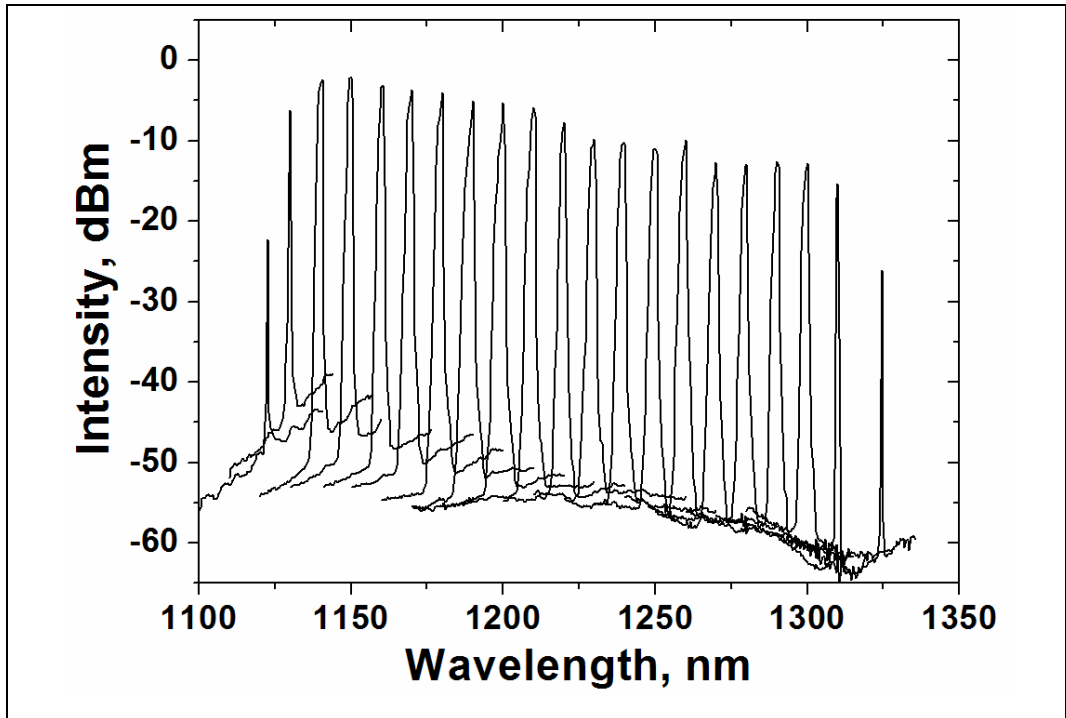


Fig. 3.31. Spectra of the QD-ECDL with the gain chip (DO1868), tuned across the 1122.5 nm – 1324.5 nm wavelength range, under an applied constant current of 1.7 A.

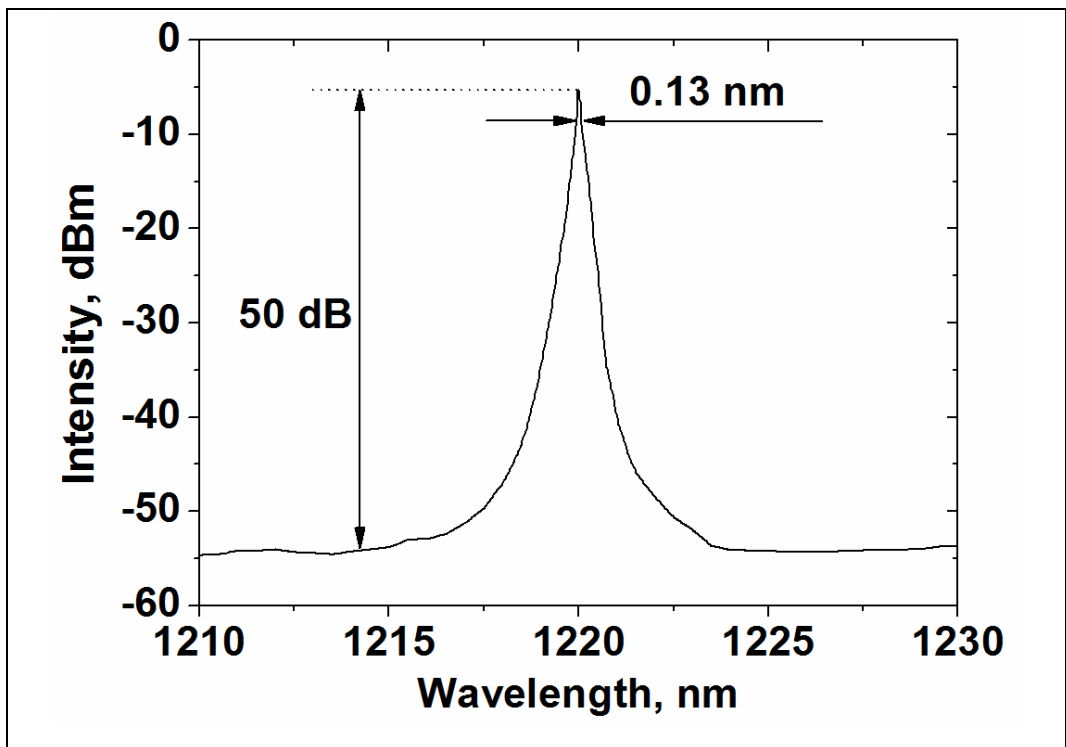
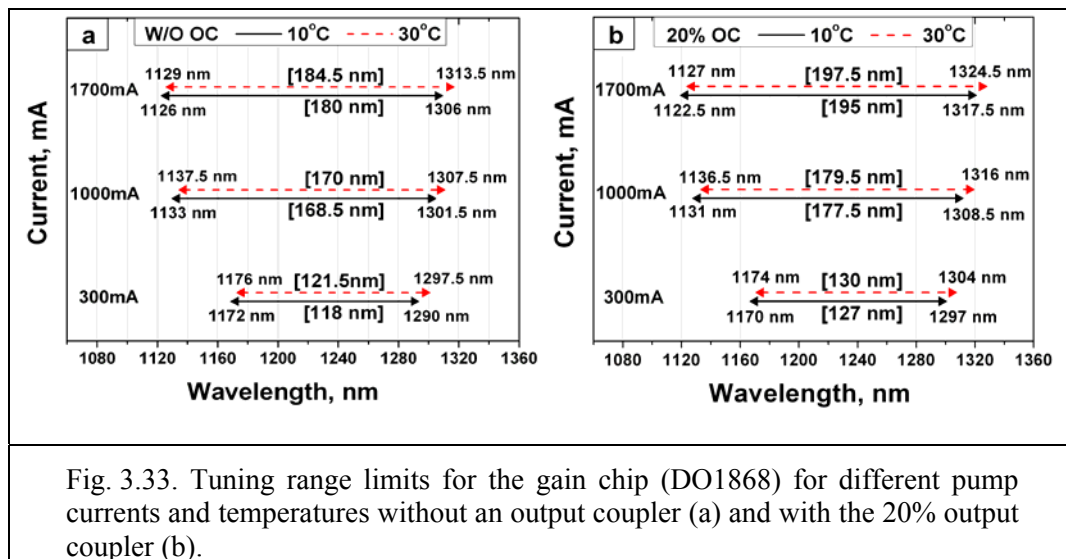


Fig. 3.32. The resulting optical spectrum exhibited a bandwidth around 0.13 nm.

Similarly to the SOA described in the previous Section 3.3, the QD-ECDL with the gain chip (DO 1868) was tested in configurations that included the 20% OC and without an OC, and exhibited the same trend in the dependence of the tuning range on bias (300 mA - 1700 mA) and temperature (10°C - 30°C) conditions as the SOA QD-ECDL. The obtained results, as depicted in Fig. 3.33, show that the tuning range is enhanced for higher pump currents. In agreement with the EL spectra depicted in Fig. 3.26, this enhancement is asymmetric and occurs predominantly on the shorter wavelength side of the tuning range, whereas the longer wavelength side remains practically unaltered, particularly for high current bias. Moreover, a shift of the tuning range to the longer wavelength side of the spectra was observed, when the temperature was increased from 10°C to 30°C.



For the 20% OC, an enhancement of the tuning range occurs predominantly on the longer wavelength side. Furthermore, due to the fact that the temperature red-shift was more accentuated on the longer wavelength side of the spectra than on the shorter wavelength side, the tuning range was actually slightly extended with increasing temperature, which is related to the thermalisation effect previously described and also observed in the EL spectra.

3.4.4. Comparison of Different Configurations (SOA and Gain Chip)

For both gain chip and SOA configurations, an increase of the cavity feedback by the addition of an OC has been shown to extend the tuning range, particularly at the red side of the spectrum. However, a trade-off exists, as the presence of an OC in the cavity reduces its maximum output power.

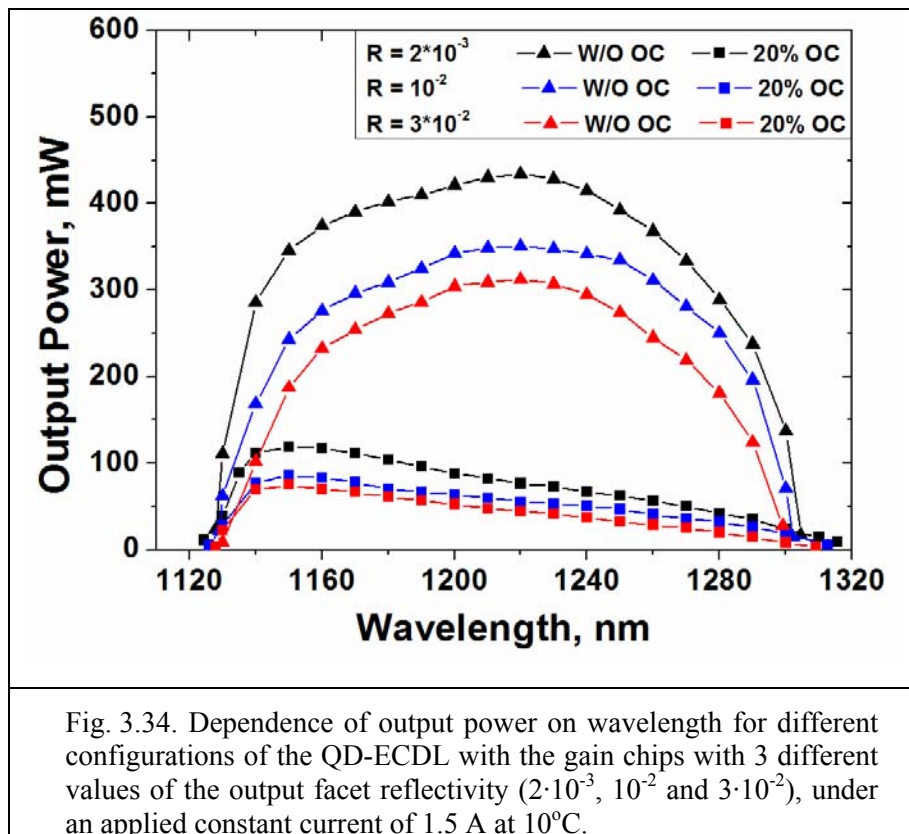
The primary advantage of the gain chip over the SOA is the fact that there is no need to use an OC in conjunction with the gain chip, because the front facet of the gain chip together with the diffraction grating can create a cavity, whereas the presence of an OC is always necessary for the SOA, owing to the lower reflectivities of the facets. Moreover, the waveguide tilt at an angle with respect to the emission facet results not only in a reduction in the effective facet reflectivity but also strongly affects the shape of the emitted beam, which becomes slightly asymmetric [3.26]. For this reason, the coupling of light feedback from the OC and diffraction grating is more inefficient for the SOA than for the gain chip, where only the back facet is angled. These higher coupling losses are therefore one of the main factors that determine the lower performance of the SOA as opposed to the gain chip, which exhibits higher output power and tuning range.

3.5. Gain Chips with Different Output Facet Reflectivities

Gain chips with 3 different values of the output facet reflectivity (fabricated from the structure DO1868) were also examined for the same laser configurations and operation conditions (pump current and temperature). The gain chips were similar to those described in the Section 3.4. The ridge waveguides had a width of 5 μm and length of

4 mm (Fig. 3.23), and were angled at 5° relative to the normal of the back facet. Additionally, both facets also had conventional AR coatings, resulting in total estimated reflectivities of less than 10^{-5} for the angled facet and $2 \cdot 10^{-3}$, 10^{-2} or $3 \cdot 10^{-2}$ for the front facet.

The dependence of the output power on wavelength for the 3 gain chips with different output facet reflectivities is presented in Fig.3.33, for the configurations with 20% OC and without an OC at 10°C . An increase of the value of the output facet reflectivity has been shown to reduce the output power (Fig. 3.34).



Similarly to the work in the previous Section 3.4, the QD-ECDLs with these 3 gain chips were tested in configurations that included the 20% OC and without an OC, and exhibited the same trend in the dependence of the tuning range on bias (300 mA - 1500 mA) and temperature (10°C - 20°C) conditions as the SOA and the gain chip described in Sections 3.3 and 3.4.

The obtained results, as depicted in Fig. 3.35, show that an increase of the value of the output facet reflectivity leads to reduction of the tuning range of the QD-ECDL.

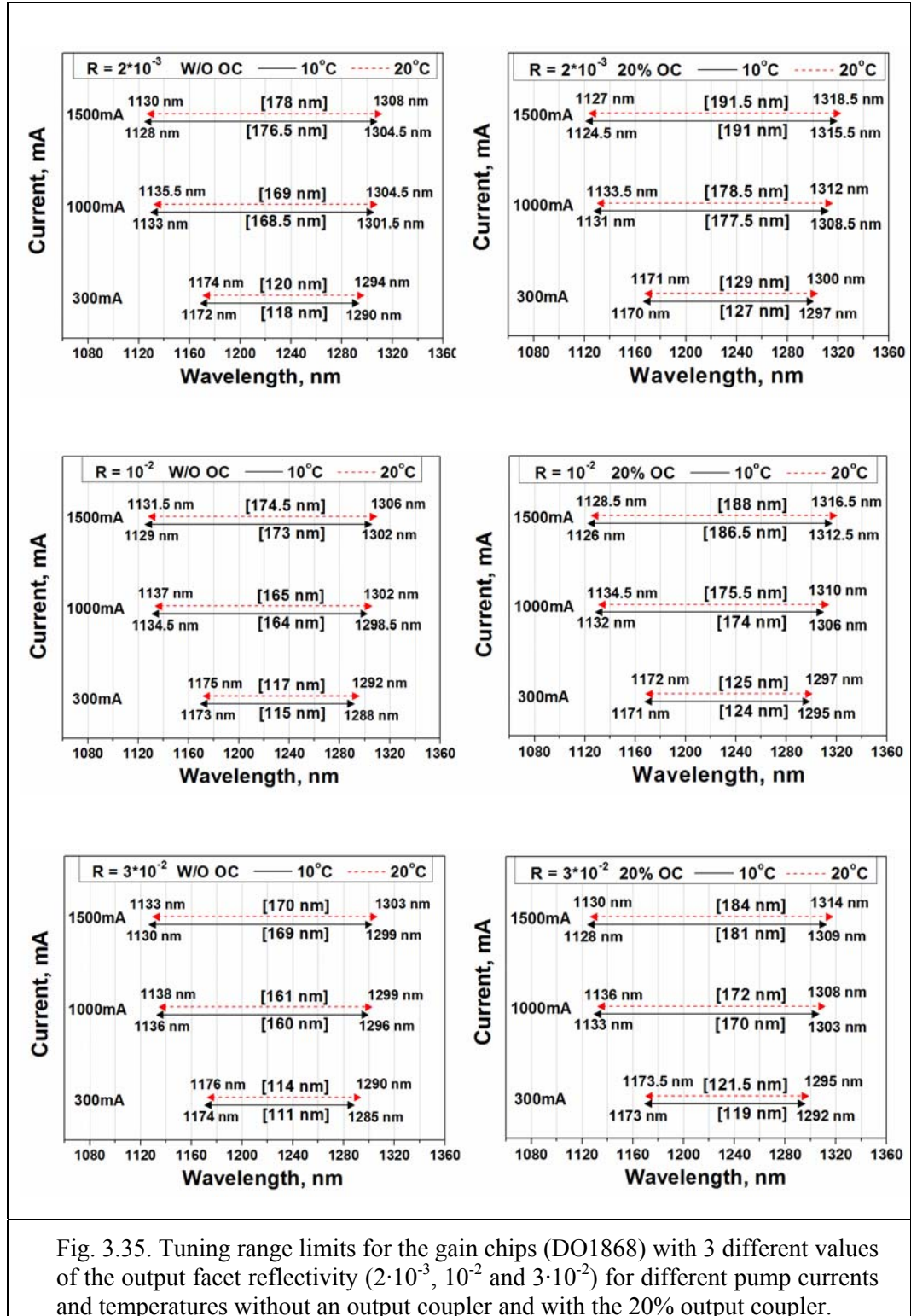


Fig. 3.35. Tuning range limits for the gain chips (DO1868) with 3 different values of the output facet reflectivity ($2 \cdot 10^{-3}$, 10^{-2} and $3 \cdot 10^{-2}$) for different pump currents and temperatures without an output coupler and with the 20% output coupler.

3.6. Summary

In this Chapter, a range of diode lasers fabricated from two different QD structures were examined. The influence of extrinsic conditions on the tuning range of QD-ECDLs was systematically investigated. It is shown that the tuning range can be mostly enhanced on the blue side of the spectrum via bias conditions, whereas reducing the cavity losses assists in the enhancement of the tuning range on the red side of the spectrum. Different waveguide structure designs were investigated, and the improved performance of the QD-ECDL with the gain chip configuration in comparison with the SOA has been demonstrated. The influence of the output facet reflectivity of the gain chips on the tuning range were also carried out.

A record broadly tunable high-power InAs/GaAs QD-ECDL with tuning range of 202 nm, between 1122.5 nm and 1324.5 nm was demonstrated. A maximum CW output power of 480 mW and a side-mode suppression ratio greater than 45 dB were achieved in the central part of the tuning range. An average output power in excess of 400 mW was achieved for a tuning range of 110 nm. This represents a promising achievement for the development of a high-power fast swept tunable laser and compact nonlinear frequency generation schemes for the green-yellow-orange-red spectral range (Fig. 3.36).

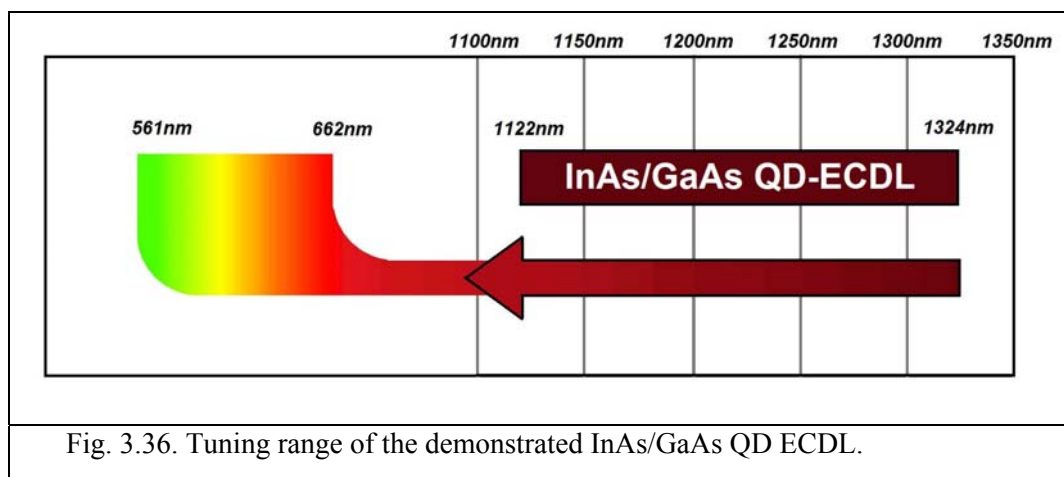


Fig. 3.36. Tuning range of the demonstrated InAs/GaAs QD ECDL.

Future work which could yield improved performance of these QD ECDLs relates to the modification of QD structures for broader wavelength coverage and re-design of QD chips for the use in mode-locking regime.

3.7. References

- [3.1] S.C. Woodworth, D.T. Cassidy, M.J. Hamp, “Sensitive absorption spectroscopy by use of an asymmetric multiple-quantum-well diode laser in an external cavity,” *Appl. Opt.* **40**, pp.6719–6724 (2001).
- [3.2] N. Kuramoto, K. Fujii, “Volume determination of a silicon sphere using an improved interferometer with optical frequency tuning,” *IEEE Trans. Instrum. Meas.* **54**, pp.868–871 (2005).
- [3.3] S.J.B. Yoo, “Wavelength conversion technologies for WDM network applications,” *IEEE J. Lightwave Technol.* **14**, pp.955-966 (1996).
- [3.4] B.J. Stevens, D.T.D. Childs, K.M. Groom, M. Hopkinson, R.A. Hogg, “All semiconductor swept laser source utilizing quantum dots,” *Appl. Phys. Lett.* **91**, pp.121119 (2007).
- [3.5] S.H. Yun, C. Boudoux, G.J. Tearney, B.E. Bouma, “High-speed wavelength-swept semiconductor laser with a polygon-scanner-based wavelength filter,” *Opt. Lett.* **28**, pp.1981-1983 (2003).
- [3.6] N. Krstajic, D.T.D. Childs, S.J. Matcher, D. Livshits, A. Shkolnik, I. Krestnikov, R.A. Hogg, “Swept-source laser based on quantum-dot semiconductor optical amplifier – applications in optical coherence tomography,” *IEEE Photon. Tech. Lett.* **23**(11), pp.739-741 (2011).
- [3.7] M.E. Brezinski, J.G. Fujimoto, “Optical coherence tomography: High-resolution imaging in nontransparent tissue,” *IEEE J. Sel. Top. Quant. Electron.* **5**, pp.1185-1192 (1999).
- [3.8] K.A. Fedorova, M.A. Cataluna, P.R. Battle, C.M. Kaleva, I.L. Krestnikov, D.A. Livshits, E.U. Rafailov, “Orange light generation from a PPKTP waveguide end-pumped by a cw quantum-dot tunable laser diode,” *Appl. Phys. B* **103**, pp.41-43 (2011).
- [3.9] K.A. Fedorova, M.A. Cataluna, P.R. Battle, I.L. Krestnikov, D.A. Livshits, E.U. Rafailov, “Broadly tunable CW green-to-red laser source based on frequency doubling of a quantum-dot external cavity diode laser in a PPKTP waveguide,” *CLEO/Europe-EQEC 2011, CD3.3, Munich, Germany (2011)*.
- [3.10] E.U. Rafailov, M. A. Cataluna, W. Sibbett, “Mode-locked quantum-dot lasers,” *Nature Photon.* **1**, pp.395 (2007).

- [3.11] A. Kovsh, I. Krestnikov, D. Livshits, S. Mikhlin, J. Weimert, A. Zhukov, "Quantum dot laser with 75 nm broad spectrum of emission," *Opt. Lett.* **32**(7), pp.793-795 (2007).
- [3.12] H. Li, G.T. Liu, P.M. Varangis, T.C. Newell, A. Stintz, B. Fuchs, K.J. Malloy, L.F. Lester, "150-nm tuning range in a grating-coupled external cavity quantum-dot laser," *IEEE Photon. Technol. Lett.* **12**, pp.759-761 (2000).
- [3.13] P.M. Varangis, H. Li, G.T. Liu, T.C. Newell, A. Stintz, B. Fuchs, K.J. Malloy, L.F. Lester, "Low-threshold quantum dot lasers with 201 nm tuning range," *Electron. Lett.* **36**, pp.1544-1545 (2000).
- [3.14] A.Yu. Nevsky, U. Bressel, I. Ernsting, Ch. Eisele, M. Okhapkin, S. Schiller, A. Gubenko, D. Livshits, S. Mikhlin, I. Krestnikov, A. Kovsh, "A narrow-line-width external cavity quantum dot laser for high-resolution spectroscopy in the near-infrared and yellow spectral range," *Appl. Phys. B* **92**, pp.501 (2008).
- [3.15] X.Q. Lv, P. Jin, W.Y. Wang, Z.G. Wang, "Broadband external cavity tunable quantum dot lasers with low injection current density," *Opt. Express* **18**(9), pp.8916-8922 (2010).
- [3.16] P.M. Varangis, H. Li, G.T. Liu, T.C. Newell, A. Stintz, B. Fuchs, K.J. Malloy, L.F. Lester, "183nm Tuning range in a grating-coupled external-cavity quantum dot laser," ISLC-2000, Conf. Digest, pp.137-138, Monterey, USA (2000).
- [3.17] A. Biebersdorf, C. Lingk, M. De Giorgi, L. Feldmann, J. Sacher, M. Arzberger, C. Ulbrich, G. Bohm, M.-C. Amann, G. Abstreiter, "Tunable single and dual mode operation of an external cavity quantum-dot injection laser," *J. Phys. D: Appl. Phys.* **36**, pp.1-3 (2003).
- [3.18] A. Tierno, T. Ackemann, "Tunable, narrow-band light source in the 1.25 μ m region based on broad-area quantum dot lasers with feedback," *Appl. Phys. B* **89**, pp.585-588 (2007).
- [3.19] X.Q. Lv, P. Jin, Z.G. Wang, "A broadband external cavity tunable InAs/GaAs quantum dot laser by utilizing only the ground state emission," *Chin. Phys. B* **19**(1), pp.018104 (2010).
- [3.20] K.A. Fedorova, M.A. Cataluna, I.L. Krestnikov, D.A. Livshits, E.U. Rafailov, "Broadly Tunable High-Power InAs/GaAs Quantum-Dot External Cavity Diode Lasers," *Opt. Express* **18**(18), pp.19438-19443 (2010).

- [3.21] M. Sugawara, K. Mukai, Y. Nakata, H. Ishikawa, A. Sakamoto, "Effect of homogeneous broadening of optical gain on spectra in self-assembled $\text{In}_x\text{Ga}_{1-x}\text{As}/\text{GaAs}$ quantum dot lasers," *Phys. Rev. B* **61**(11), pp.7595-7603 (2000).
- [3.22] M. Rossetti, L. Lianhe, A. Markus, A. Fiore, L. Occhi, C. Velez, S. Mikhrin, I. Krestnikov, A. Kovsh, "Characterization and Modeling of Broad Spectrum InAs-GaAs Quantum-Dot Superluminescent Diodes Emitting at 1.2-1.3 μm ," *IEEE J. Quantum Electron.* **43**(8), pp.676-686 (2007).
- [3.23] P.G. Eliseev, H. Li, T. Liu, T.C. Newell, L.F. Lester, K. J. Malloy, "Ground-state emission and gain in ultralow-threshold InAs-InGaAs quantum-dot lasers," *IEEE J. Sel. Top. Quant. Electron.* **7**(2), pp.135-142 (2001).
- [3.24] H. Huang, D.G. Deppe, "Rate equation model for nonequilibrium operating conditions in a self-organized quantum-dot laser," *IEEE J. Quantum Electron.* **37**(5), pp.691-698 (2001).
- [3.25] H. Tabuchi, H. Ishikawa, "External grating tunable MQW laser with wide tuning range of 240 nm," *Electron. Lett.* **26**(11), pp.742-743 (1990).
- [3.26] L. Ching-Fuh, J. Chaur-Shiuann, "Superluminescent diodes with bent waveguide," *IEEE Phot. Tech. Lett.* **8**(2), pp.206-208 (1996).

4. Nonlinear Frequency Conversion Theory

In the previous Chapters the subject matter was concerned with the direct emission from laser devices. The next part of the thesis is directed towards induced nonlinear processes.

In this Chapter, a brief theoretical description of second-order nonlinear processes, focusing on nonlinear optical frequency conversion and including phase-matching techniques is presented. The theory and design considerations for optical parametric oscillator are also briefly discussed.

4.1. Introduction

Following the invention of the laser in 1960 by Maiman [4.1], nonlinear optics has been an important and commonly used application of lasers. In 1961, light frequency doubling in a crystal using the nonlinearity of a material was the first nonlinear optical effect to be experimentally demonstrated [4.2] shortly after the invention of the laser. Soon after this result showing non-phase-matched second harmonic generation (SHG), a few scientific groups [4.3-4.5] demonstrated that phase matching could be achieved by using crystal birefringence to compensate the index dispersion of the crystal. The quasi-phase-matching (QPM) enabling efficient frequency up-conversion was also introduced in 1962 by Armstrong *et al.* in bulk configuration [4.6]. One of the important advantages of QPM is that it can be used to produce phase-matching in optically isotropic materials that have no birefringence at all and can be realised at any wavelength in the transparency region of the medium by only appropriate design of the QPM period, and thus potentially makes a wider range of materials available [4.7]. Nowadays, QPM is widely used in both – bulk and waveguide configurations. The waveguide offers strong optical wave confinement and maintain high optical intensity over a long propagation length, and hence, makes it possible to show very high optical conversion efficiencies even at low pump power, thus making guided wave nonlinear optical conversion ideal for applications requiring CW or low peak power quasi-CW lasers [4.8].

Another important application of nonlinear phenomena which offers a wide wavelength coverage and tunability (typically several hundred nanometers) is optical parametric oscillation (OPO). This was reported for the first time by Giordmaine and Miller in 1965 [4.9]. Nowadays, second-order nonlinear processes are commonly used

to generate new frequencies, allowing coverage of those wavelength regions which are not directly accessible to conventional lasers.

4.2. Second-Order Nonlinear Optical Processes

Second-order nonlinear processes allow extending the available wavelength range of coherent radiation via frequency conversion. In particular, second harmonic generation (SHG) and optical parametric oscillation (OPO) are two of the most important applications of nonlinear phenomena.

The second-order nonlinearity involves three waves which can be input or generated within the nonlinear media. Frequency up-conversion or sum frequency generation (SFG) involves the interaction of two waves with lower frequencies ω_1 and ω_2 , which are mixed with each other to generate a wave with a higher frequency ω_3 :

$$\omega_1 + \omega_2 = \omega_3 \quad (4.1)$$

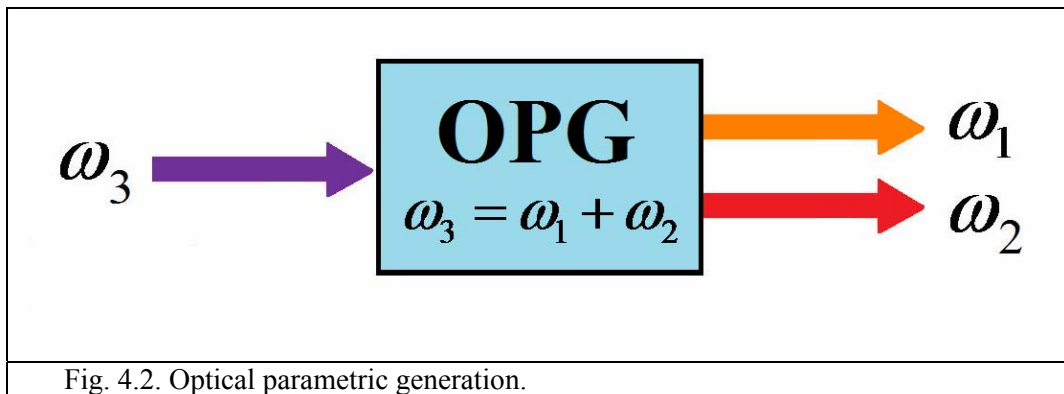
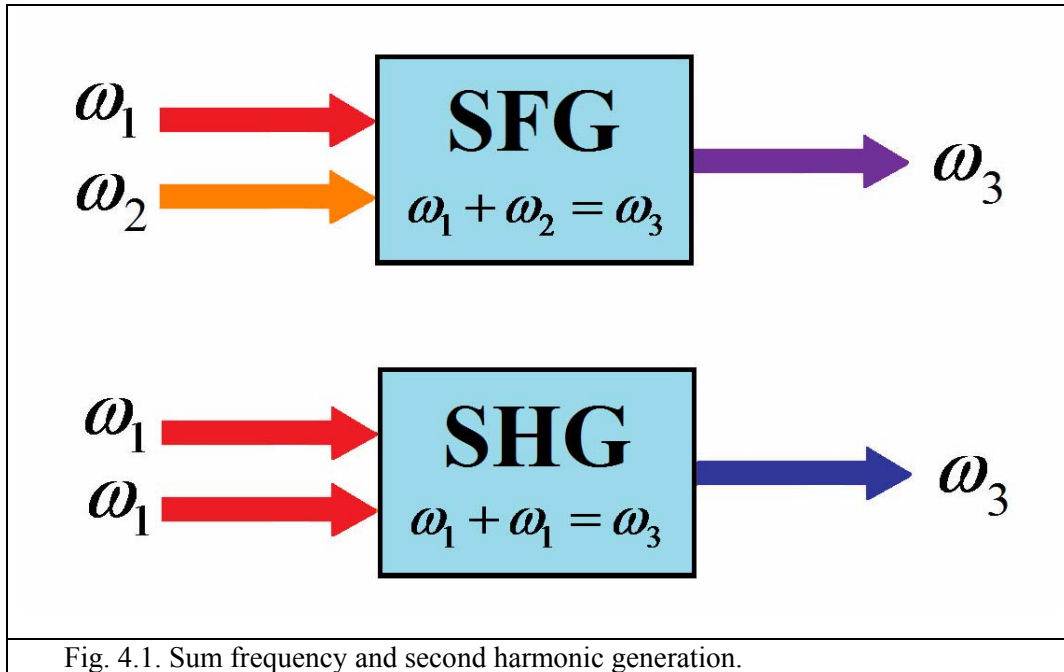
The degenerate case of sum frequency generation, with $\omega_1 = \omega_2$, is frequency doubling or second harmonic generation in which part of the energy of an optical wave of frequency ω_1 propagating through a crystal is converted to that of a wave with twice the optical frequency $2\omega_1$. A schematic description of these processes is shown in Fig. 4.1.

Frequency down-conversion or optical parametric generation (OPG) correspond to situation when a strong pump wave with high frequency ω_3 causes generation of radiation at two lower frequencies ω_1 and ω_2 (Fig. 4.2):

$$\omega_3 = \omega_1 + \omega_2 \quad (4.2)$$

Traditionally, the generated wave at higher frequency ω_1 is called the signal, and low frequency ω_2 wave - the idler ($\omega_2 < \omega_1$).

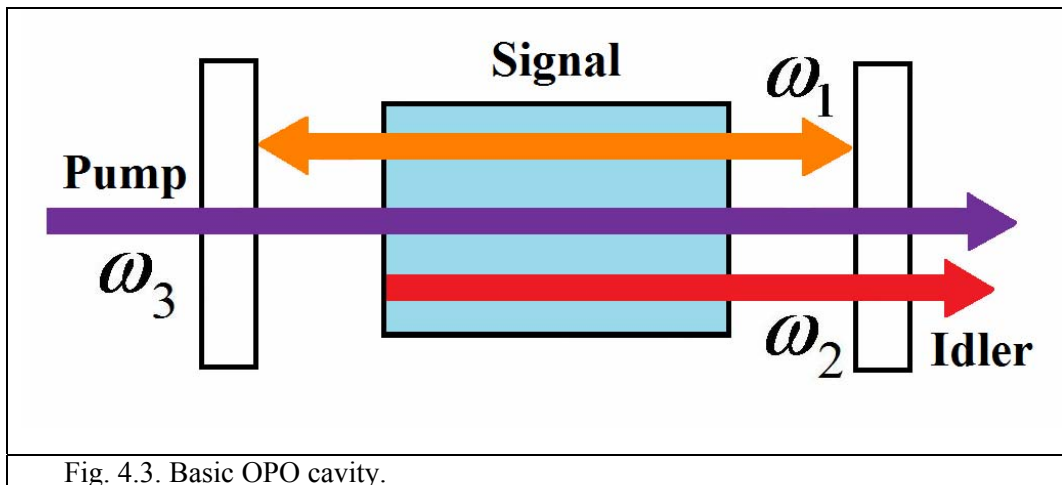
The special case when $\omega_1 = \omega_2$ is the exactly reverse of SHG, and this process is said to be degenerate [4.10].



If the nonlinear crystal is placed into an optical cavity with an appropriate optical feedback and the parametric gain exceeds the cavity loss, then oscillation can occur [4.11]. Depending on the mirror characteristics, OPOs can be designed to resonate either the signal or idler waves (singly-resonant oscillator, SRO), or both signal and idler waves together (doubly-resonant oscillator, DRO). Both mirrors are usually

transparent for the pump wave. These designs mainly differ by their spectral fine tuning properties, threshold and conversion efficiency [4.12].

For an SRO where the signal is resonated (Fig. 4.3), threshold is reached when the signal gain equals the roundtrip signal loss. As the pump power increases past its threshold, the signal and idler output powers grow dramatically. If high output power and conversion efficiency together with stable continuous tuning are required, the singly resonant OPO is preferred in comparison with the doubly resonant OPO, which suffers from stability problems, and hence rarely used in practice [4.13]. On the other hand, a DRO configuration has lower threshold than an SRO.



The fact that the wavelengths generated in OPO can be tuned over a broad spectral range whilst the pump wavelength is kept the same, makes the OPO an important and widely used application of nonlinear optics.

4.3. Phase-Matching

4.3.1. Phase-Matching and Coherence Length

For efficient frequency conversion in parametric processes such as frequency doubling or optical parametric oscillation, phase-matching is required to be efficient. This means that the interacting waves have a proper phase relationship between them along the propagation direction. This leads to the condition that the phase mismatch Δk must be close to zero [4.14].

For frequency doubling, the phase-mismatch can be written as:

$$\Delta k = k_{2\omega} - 2 \cdot k_{\omega} = 2\pi \frac{2}{\lambda} (n_{2\omega} - n_{\omega}) \quad (4.3)$$

where $n_{2\omega}$ and n_{ω} are refractive indexes for pump and harmonic waves, respectively, $k_{2\omega}$ and k_{ω} are the wavevectors of each wave, and λ is the wavelength of the pump wave in vacuum.

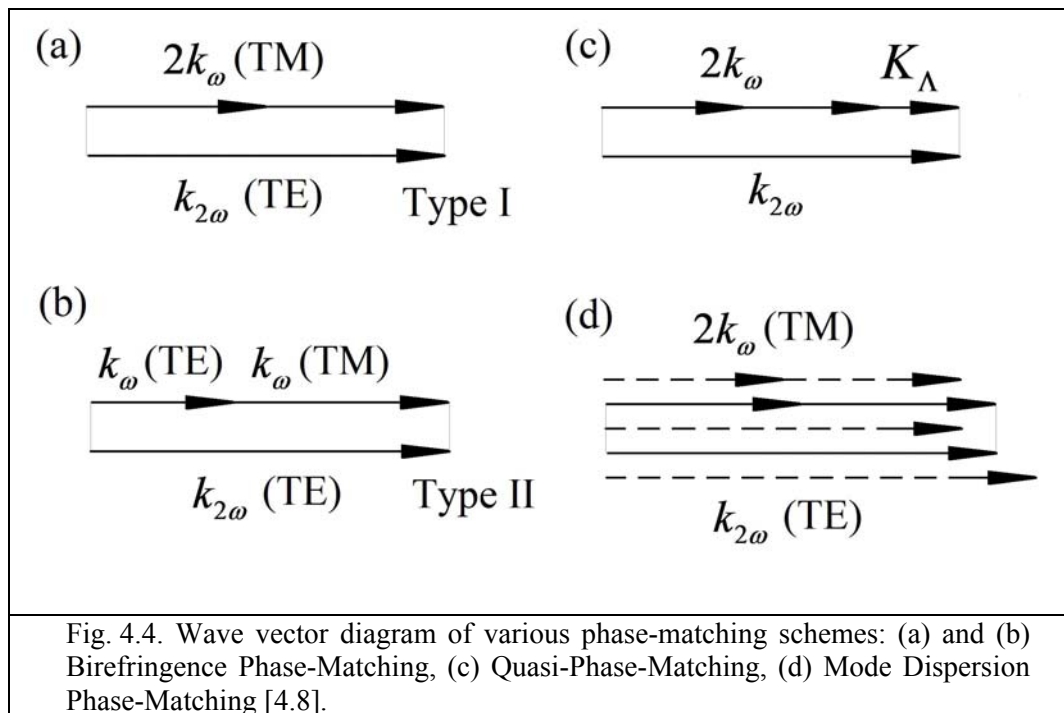
If the phase mismatch is not zero, the intensity of the generated light will oscillate back and forth with a certain periodicity of the length called the coherence length l_c :

$$l_c = \frac{\pi}{\Delta k} \quad (4.4)$$

4.3.2. Birefringence Phase-Matching

The refractive index of a material is a function of frequency. One of the traditional techniques to solve the problem that material dispersion introduces and achieve phase-matching is through use of the birefringence of the anisotropic nonlinear materials [4.15]. In uniaxial crystals, the refractive index of the extraordinary (e) wave (n_e) depends on the direction of propagating wave, while the refractive index of the ordinary (o) wave (n_o) does not. Generation of the e wave from two o waves at an angle where

$n_o^\omega = n_e^{2\omega}$ is called Type I ($o+o \rightarrow e$) phase-matching. In Type II ($o+e \rightarrow e$) phase-matching, the e wave is generated from the o and e pump waves at an angle where $(n_o^\omega + n_e^\omega)/2 = n_e^{2\omega}$. In waveguides in z-cut crystals, TE and TM modes correspond to the o and e waves, respectively. The wave vector diagrams of Type I and Type II phase-matching are shown in Fig. 4.4 (a) and (b), correspondingly.



4.3.3. Quasi-Phase-Matching

Quasi-phase-matching is an alternative technique to birefringence phase-matching allowing compensating the momentum mismatch imposed by the material dispersion. The important advantage of QPM is that it extends the utility of existing materials enabling the use of materials with no birefringence and even optically isotropic materials. The idea of QPM is to correct the phase-mismatch between the interacting fields at certain intervals by artificially modifying the material structure. The crystal

domain is reversed periodically with a period which corresponds to the double coherence length:

$$\Lambda = 2 \cdot l_c = 2\pi / K_\Lambda \quad (4.5)$$

In case of SHG, the phase-matching condition (Fig. 4.4 (c)) for QPM has the following dependence:

$$\Delta k_{QPM} = k_{2\omega} - 2 \cdot k_\omega - K_\Lambda = 0 \quad (4.6)$$

As it can be seen from Fig. 4.5, in case of QPM the conversion process will reinstate at the coherence length, leading to a sum up of the intensity after each l_c .

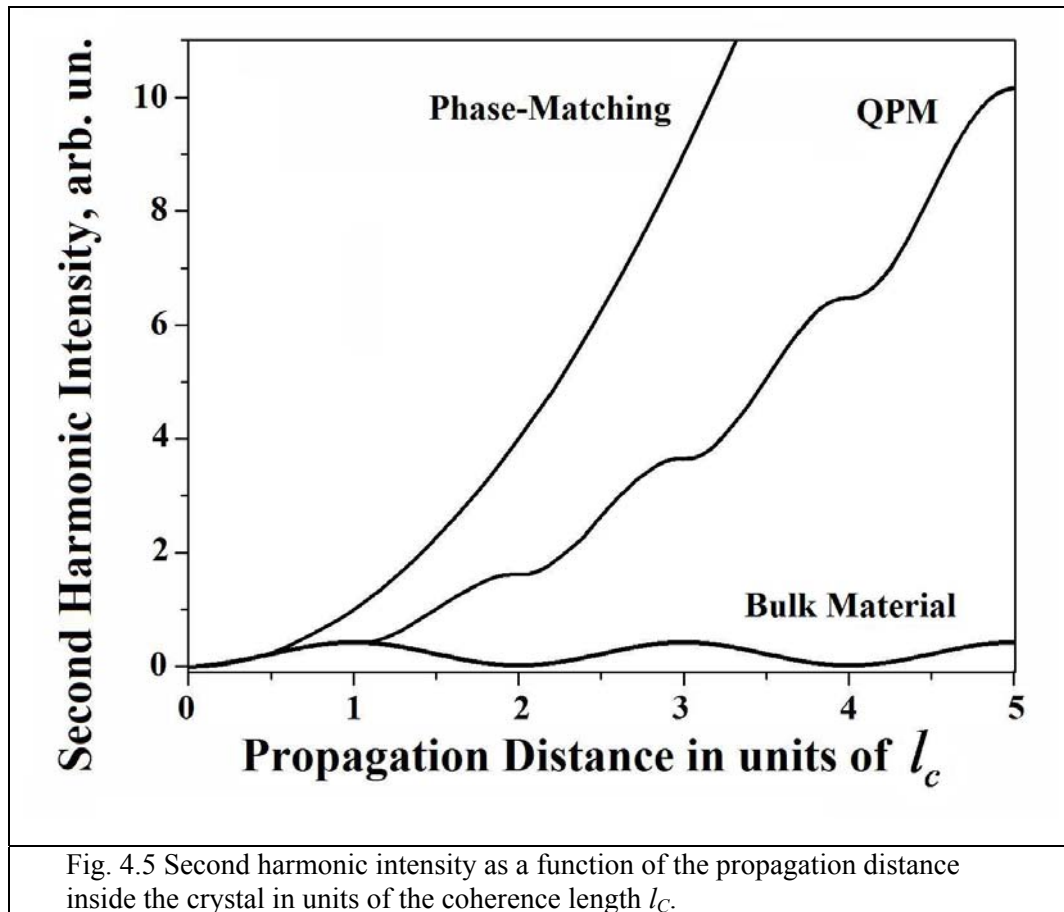
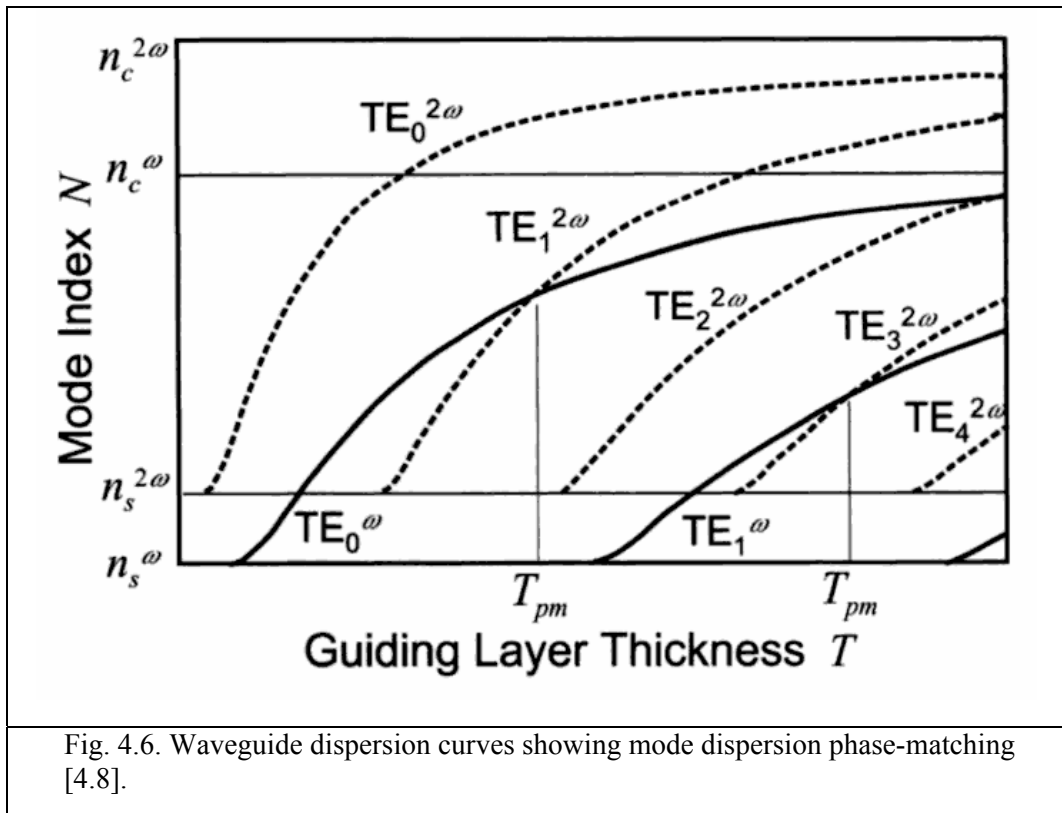


Fig. 4.5 Second harmonic intensity as a function of the propagation distance inside the crystal in units of the coherence length l_c .

To date, by far the most commonly used approach to fabricate QPM structure is the periodical poling of the ferroelectric nonlinear crystals by periodically reversing the crystals polarization under the influence of a sufficiently large electric field [4.16].

4.3.4. Mode Dispersion Phase-Matching

The use of crystal waveguides allows phase-matching by mode dispersion. A wave vector diagram for mode dispersion phase-matching is shown in Fig. 4.4 (d). When mode dispersion alone is used to achieve phase-matching, it is typical for the SHG beam to emerge in a higher-order mode [4.17]. Because of the material dispersion, the SHG wave tends to travel more slowly than the fundamental wave, and hence, the second harmonic needs to be speeded up by placing it in a higher-order waveguide mode, which travels faster than a low order mode. The mode dispersion curves for the pump and second harmonic waves are depicted in Fig. 4.6 where intersections of the curves for two wavelengths correspond to phase-matching. As shown in this Figure, the fundamental mode of the pump wave matches a higher order mode of the second harmonic wave. This matching is possible between modes with the same polarization and between modes with different polarizations.



4.4. Summary

In this Chapter, a brief discussion on second-order nonlinear processes which are commonly used to extend the available wavelength range of coherent radiation via frequency conversion was presented. In particular, sum frequency and second harmonic generation allow the generation of coherent radiation in the visible and mid-IR spectral region, which are of interest for many applications ranging from biophotonics and photomedicine to laser projection displays.

Optical parametric oscillation, which is another very important application of nonlinear optics, was also briefly discussed. OPO allows wide coverage and tunability in the wavelength regions which are not directly accessible to conventional lasers, and potentially can be used in many applications, such as spectroscopy, gas sensing, digital projection displays, military applications etc.

Experimental demonstration of SHG and OPO will be presented in the next two Chapters.

4.5. References

- [4.1] T.H. Maiman, “Stimulated optical radiation in Ruby,” *Nature* **187**(4736), p.493–494 (1960).
- [4.2] P.A. Franken, A.E. Hill, C.W. Peters, G. Weinreich, “Generation of optical harmonic,” *Phys. Rev. Lett.* **7**(4), p.118-119 (1961).
- [4.3] D.A. Kleinman, “Nonlinear dielectric polarization in optical media,” *Phys. Rev.* **126**, pp.1977-1979 (1962).
- [4.4] J.A. Giordmaine, “Mixing of light beam in crystals,” *Phys. Rev. Lett.* **8**, pp.19-21 (1962).
- [4.5] P.D. Maker, R.W. Terhune, M. Nisenoff, C.M. Savage, “Effect of dispersive and focussing on the production of optical harmonics,” *Phys.Rev.Lett.* **8**, pp.21-24 (1962).
- [4.6] I.A. Armstrong, N. Bloembergen, I. Ducuing, P.S. Pershan, “Interactions between Light Waves in a Nonlinear Dielectric,” *Phys. Rev.* **127**, pp. 1918-1939 (1962).
- [4.7] D.S. Hum, M.M. Fejer, “Quasi-phasematching,” *C.R. Physique* **8**, pp.180-198 (2007).
- [4.8] T. Suhara, M. Fujimura, *Waveguide Nonlinear-Optic Devices* (Springer, Berlin, 2003).
- [4.9] J.A. Giordmaine, R.C. Miller, “Tunable Coherent Parametric Oscillation in LiNbO₃ at Optical Frequencies,” *Phys.Rev.Lett.* **14**, pp.973-976 (1965).
- [4.10] A. Yariv, *Optical Electronics* (Holt, Rinehart and Winston, Inc., Orlando, 1991).
- [4.11] D.M. Finlyanson, B.D. Sinclar, *Advances in Lasers and Applications* (J W Arrowsmith Ltd, Bristol, 1999).
- [4.12] M. Ebrahim-Zadeh, I.T. Sorokina, *Mid-Infrared Coherent Sources and Applications* (Springer, Dordrecht, 2008).
- [4.13] Y.R. Shen, *Nonlinear Infrared Generation* (Springer-Verlag, Berlin, 1977).
- [4.14] R. Paschotta, *Encyclopedia of Laser Physics and Technology* (Wiley-VCH, Berlin, 2008).
- [4.15] F. Zernike, J.E. Midwinter, *Applied Nonlinear Optics* (Wiley, New York, 1973).

- [4.16] M.M. Fejer, G.A. Magel, D.H. Jundt, R.L. Byer, "Quasi-phase-matched second harmonic generation: tuning and tolerances," *IEEE J. Quantum Electron.* **28**, pp.2631-2654 (1992).
- [4.17] W.P. Gosnell, A.V. Nurmikko, *Compact Blue-Green Lasers* (Cambridge University Press, Cambridge, 2003).

5. Frequency Doubling of Quantum Dot External-Cavity Diode Laser in PPKTP Waveguides

In this Chapter, an all-room-temperature CW second harmonic generation at 612.9 nm and 591.5 nm in periodically poled potassium titanyl phosphate waveguides pumped by a broadly tunable quantum dot external-cavity diode laser is demonstrated. A frequency-doubled power of up to 4.3 mW at the wavelength of 612.9 nm and 4.1 mW at 591.5 nm with a conversion efficiency of 10.5% and 7.9%, respectively, is achieved.

A green-to-red tunable laser source with tunability of over 60nm (567.7 nm – 629.1 nm) based on SHG in a single periodically poled potassium titanyl phosphate waveguide pumped by a single broadly tunable quantum dot laser is demonstrated.

5.1. Introduction

In recent years, there has been a growing interest in the development of compact coherent sources emitting in the visible spectral region at around 550 nm - 650 nm, which are of interest for many applications, such as laser projection displays [5.1], spectroscopy, optical atomic clock in ytterbium [5.2], photodynamic therapy [5.3,5.4], ophthalmology and biophotonic applications such as flow cytometry, where a range of important fluorescent probes are optimally excited in the yellow-orange range [5.5]. This spectral region is currently unreachable for conventional diode lasers due to a lack of suitable direct band gap materials providing sufficient carrier confinement in the quantum wells. An attractive approach is frequency doubling of infrared light.

Efficient nonlinear optical frequency conversion requires phase matching, large pump intensities, long interaction lengths and materials with large nonlinear optical coefficients. The limitations imposed on nonlinear optical mixing processes due to the low peak powers found in most quasi-CW and CW lasers can be overcome by creating waveguides in the nonlinear material [5.6]. The waveguide offers strong optical wave confinement, allowing for a high intensity over long interaction lengths, and hence, makes it possible to show very high optical conversion efficiencies even at low level pump power, thus making guided wave nonlinear optical conversion ideal for applications requiring CW or low peak power quasi-CW lasers. Furthermore, efficient optical conversion over the entire transparency range of the crystal can be achieved by utilising a quasi-phase-matching (QPM) process [5.7,5.8], using a modification of a structure in which the ferroelectric domain periodically inverted to correct the relative phase at regular intervals.

Potassium titanyl phosphate (KTiOPO₄ or KTP) is the most commonly used material for the fabrication of a QPM structure in the crystal when high power densities

of the visible light are generated such as in waveguides, and hence, KTP is especially suitable to serve as the nonlinear crystal for second-harmonic generation (SHG). Moreover, there is the opportunity to make a periodically poled KTP crystal to satisfy QPM conditions and to fabricate a waveguide [5.9] in the crystal, that would make it possible to increase the second harmonic conversion efficiency.

Recently, second and third-harmonic generation in a periodically poled potassium titanyl phosphate (PPKTP) waveguide using a compact femtosecond Yb-based laser with conversion efficiencies of up to 33% (532 nm) and 2% (355 nm), respectively, were demonstrated [5.10]. Green (532 nm) and yellow (560 nm) picosecond pulse sources that utilise SHG of Yb-doped fibre based pump source in PPKTP waveguide with maximum average power of 41.7 μ W and 2.3 mW, respectively, were also presented [5.11]. It has also been reported for a diode-pumped femtosecond Cr:LiSAF laser (fundamental wavelength of 860 nm) that frequency doubling in a PPKTP waveguide afforded SH conversion efficiency of up to 37% [5.12].

The recent availability of low-cost good quality InAs/GaAs QD diode lasers, allowing the coverage of a broad spectral range between 1.0 μ m and 1.3 μ m [5.13,5.14], in combination with well established techniques to fabricate good quality waveguides in nonlinear crystals, enables compact laser sources in the visible spectral region to be realised.

5.2. KTP Waveguide: Fabrication and Design

The KTP waveguides used in the experiments described in this Chapter were fabricated by AdvR Inc. (Bozeman, USA) using photolithography to transfer a mask containing the waveguide patterns to a KTP wafer and then using an ion-exchange technique to embed the waveguide [5.9]. With this technique, the masked KTP crystals were individually immersed in the ion-exchange bath consisting of a mixture of molten nitrate salts of Rb and Ba (RbNO_3 and $\text{Ba}(\text{NO}_3)_2$) [5.6]. Within this bath, the Rb ions diffused through a mask into the substrate, while the K ions diffused out of the KTP crystal. In the diffused regions, the Rb ions increased the refractive index relatively to the undiffused KTP and thus formed the optical waveguide. The addition of a few percent of $\text{Ba}(\text{NO}_3)_2$ salt to the melt improved the uniformity of the waveguides [5.15]. An example of end-view of a Ba/Rb-exchanged channel waveguide in KTP crystal is shown in Fig.5.1.

The KTP waveguides used in the experiments had a cross-sectional area of $\sim 4 \times 4 \mu\text{m}^2$ and a refractive index step of ~ 0.01 . The crystals facets were not AR coated.

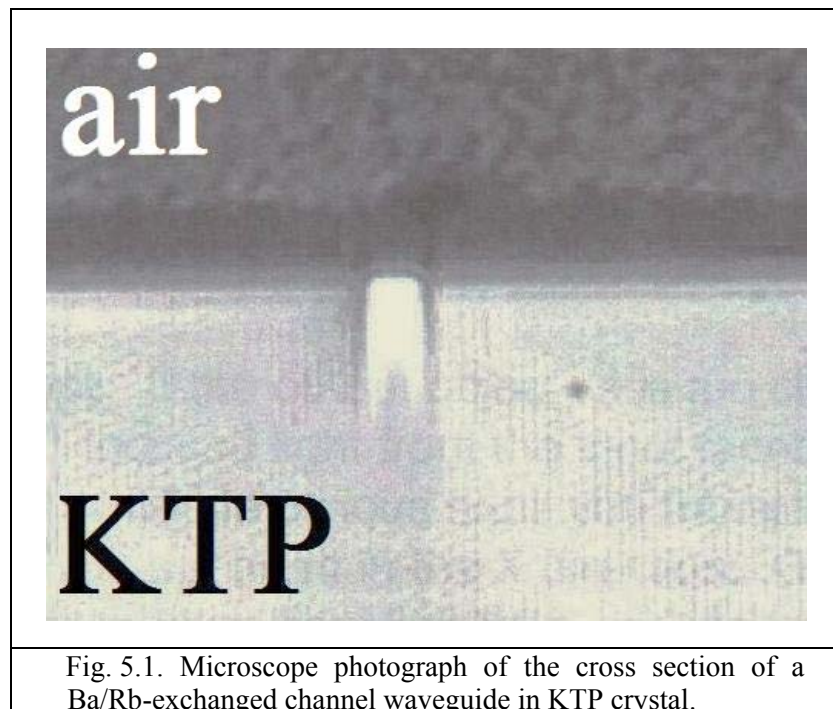


Fig. 5.1. Microscope photograph of the cross section of a Ba/Rb-exchanged channel waveguide in KTP crystal.

5.3. Loss Measurement in KTP Waveguides

The waveguide insertion loss ($\alpha_{\text{insertion}}$) consists of the coupling losses (α_{coupling}) and the propagation losses ($\alpha_{\text{propagation}}$):

$$\alpha_{\text{insertion}} = \alpha_{\text{coupling}} + \alpha_{\text{propagation}} \cdot L \quad (5.1)$$

where L – is the length of a waveguide. The simplest method to estimate the propagation losses of a waveguide is the cutback method, which requires the transmitted power of waveguides of different length, whilst the input power and the coupling conditions are kept constant. In this method, the propagation loss can be calculated using the following Equation:

$$\text{Loss (dB/cm)} = \alpha_{\text{dB}} = 10 \cdot \log_{10}(P_1/P_2)/(L_2 - L_1) \quad (5.2)$$

where P_1 and P_2 are the transmitted powers and L_1 and L_2 – the lengths of the short and the long waveguide [5.16]. Theoretically, only two waveguides of different length are required for the cutback method, but in this work three identical waveguides of different length (24 mm, 14 mm, 9 mm) were used to increase the accuracy.

The experimental setup is shown in Fig.5.2. The core element of the QD-ECDL pump source was the gain chip (DO1868), previously described in Chapter 3 (Section 3.4). The KTP waveguides used in this work were fabricated by an ion-exchange technique [5.9,5.17] and had different lengths: 24 mm, 14 mm and 9 mm. All waveguides were identical and had a cross-sectional area of $\sim 4 \times 4 \mu\text{m}^2$.

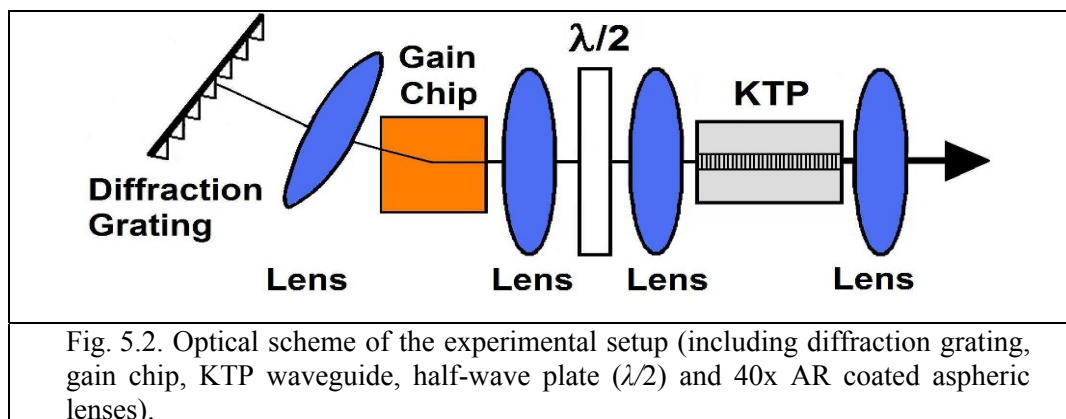


Fig. 5.2. Optical scheme of the experimental setup (including diffraction grating, gain chip, KTP waveguide, half-wave plate ($\lambda/2$) and 40x AR coated aspheric lenses).

Waveguide loss measurements were made at wavelengths of 1183 nm and 1226 nm. By using the Equation 5.2, the propagation losses were estimated to be around 1.75 dB/cm at 1183 nm and 1.93 dB/cm at 1226nm, which are close to typical values of losses in ion-exchanged KTP waveguides [5.18]. The total losses shown in Fig.5.3 were calculated using a similar equation containing input power coupled to the waveguide and output power for each sample. In Fig.5.3, the trendlines cut the y-axis above the origin. This is because the data shows insertion loss, and hence the loss corresponding to zero propagation length is the coupling loss to the waveguide [5.19]. The coupling losses were estimated to be around 3.39 dB and 3.41 dB (at 1183 nm and 1226 nm, respectively).

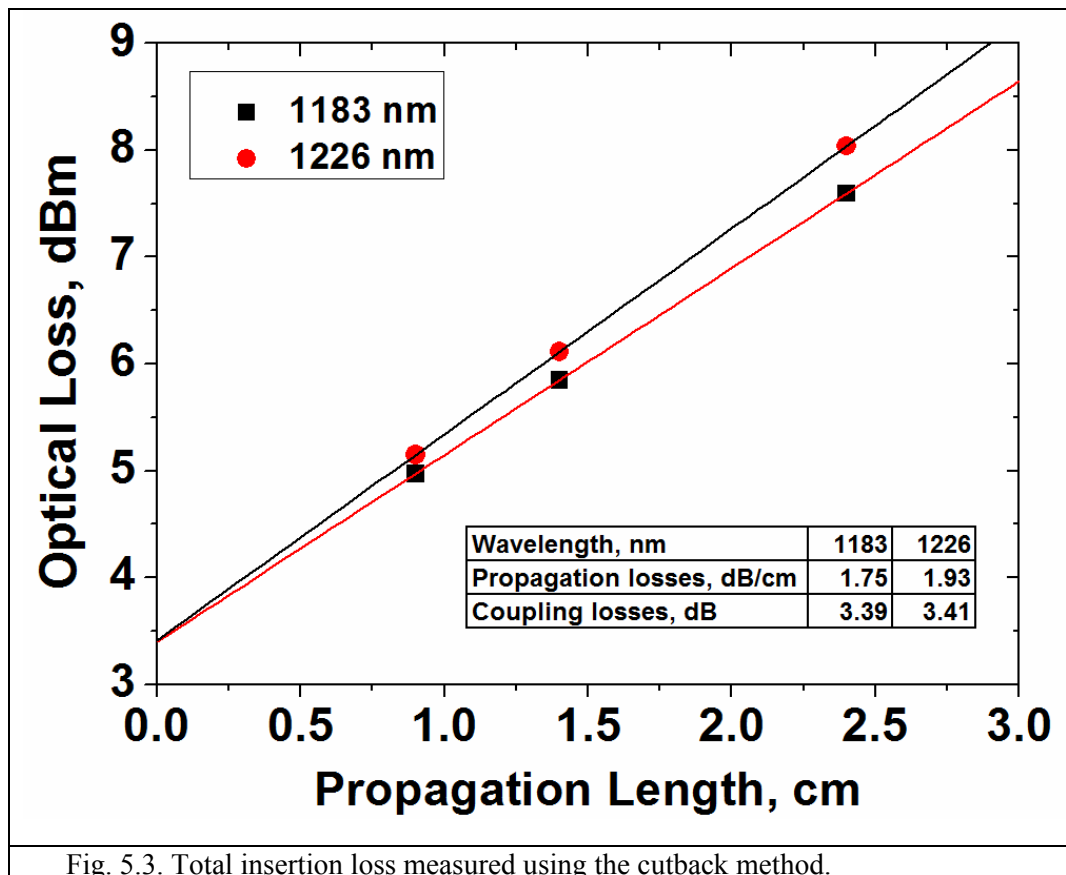
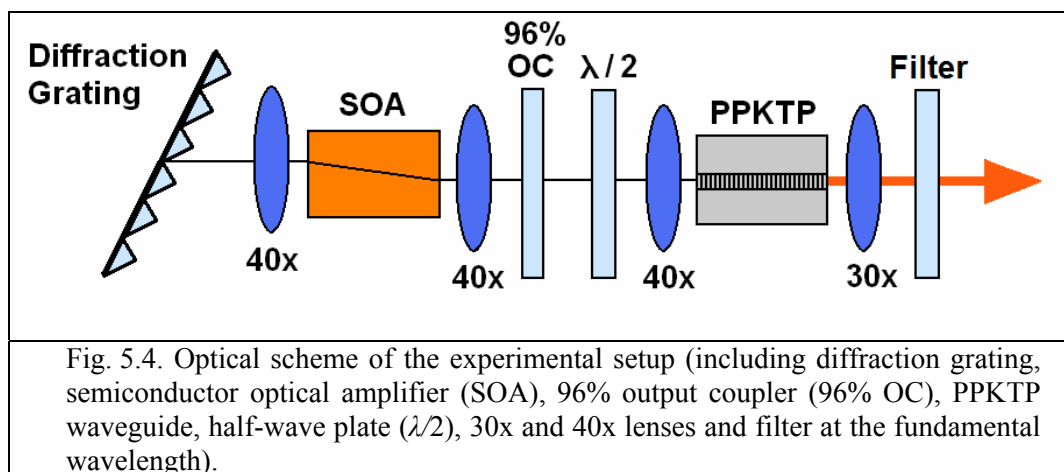


Fig. 5.3. Total insertion loss measured using the cutback method.

5.4. Second Harmonic Generation at 612.9 nm

5.4.1. Experimental Setup

The experimental setup is shown in Fig.5.4. The core element of the QD-ECDL pump source consisted of a QD semiconductor optical amplifier (SOA) fabricated from the structure DO1866, previously described in Chapter 3 (Section 3.2). The ridge waveguide of the SOA had a width of 5 μm and a length of 4 mm, and was angled at 6.5° relative to the normal of the facets, which also had a conventional antireflective (AR) coating, resulting in total estimated reflectivities of 10^{-5} in each facet. The QD-SOA was mounted on a copper heat sink and its temperature was controlled by a thermo-electric cooler. The QD-ECDL was set up in a quasi-Littrow configuration (Fig.5.4), which consisted of a diffraction grating with 1200 grooves/mm, 40x (NA of 0.55) AR-coated aspheric lenses and the output coupler (OC) with 96% transmission. Coarse wavelength tuning of QD-ECDL between 1146 and 1279 nm at 20°C was made possible by changing the incidence angle of the grating. The QD-ECDL was tuned to the 1226-nm target wavelength at 20°C, and then the collimated output from the QD-ECDL was coupled into the PPKTP waveguide using a 40x aspheric lens. ECDL was coupled into the PPKTP waveguide using a 40x aspheric lens.



The PPKTP frequency-doubling crystal used in this work was 13 mm in length and was periodically poled for SHG at 612.9 nm (with the poling period of $\sim 13.82 \mu\text{m}$). The waveguide with a cross-sectional area of $\sim 4 \times 4 \mu\text{m}^2$ (as shown in Fig.5.1) was fabricated by an ion-exchange technique that provided a refractive index step $\Delta n \approx 0.01$. The crystal facets were not AR coated. The PPKTP crystal was mounted on a copper heat sink and its temperature was controlled by a thermo-electric cooler. Both the pump laser and the PPKTP crystal were operating at room temperature.

The output of the laser system was collimated with a 30x (NA of 0.40) AR-coated aspheric lens and then coupled into a broadband thermopile power meter or via an optical fibre into an optical spectrum analyser (OSA Advantest Q8384) for the fundamental wavelength or Ocean Optics spectrometer for the second harmonic wavelength.

5.4.2. Results

Figure 5.5 shows the SHG output power versus the launched pump power. The maximum SHG output power of 4.3 mW at 612.9 nm was achieved for 41 mW of launched power at 1225.8 nm, resulting in a conversion efficiency of 10.5%. The SHG output power of 3.5 mW at 613.6 nm was achieved for 41 mW of launched pump power at 1227.2 nm with a conversion efficiency of 8.5%. A photograph of the SHG at 612.9 nm in the PPKTP waveguide pumped by the QD-ECDL is shown in Fig. 5.6.

Figure 5.7 shows the measured optical spectrum of the second-harmonic (612.9 nm) and fundamental (1225.8 nm) wavelengths. The optical spectrum of the fundamental wavelength exhibited a bandwidth of around 0.12 nm, limited only by the instrumental resolution of the spectrometer (OSA Advantest Q8384). A spectral width

of the SH was measured to be 0.65 nm (limited only by the instrumental resolution of the Ocean Optics spectrometer used).

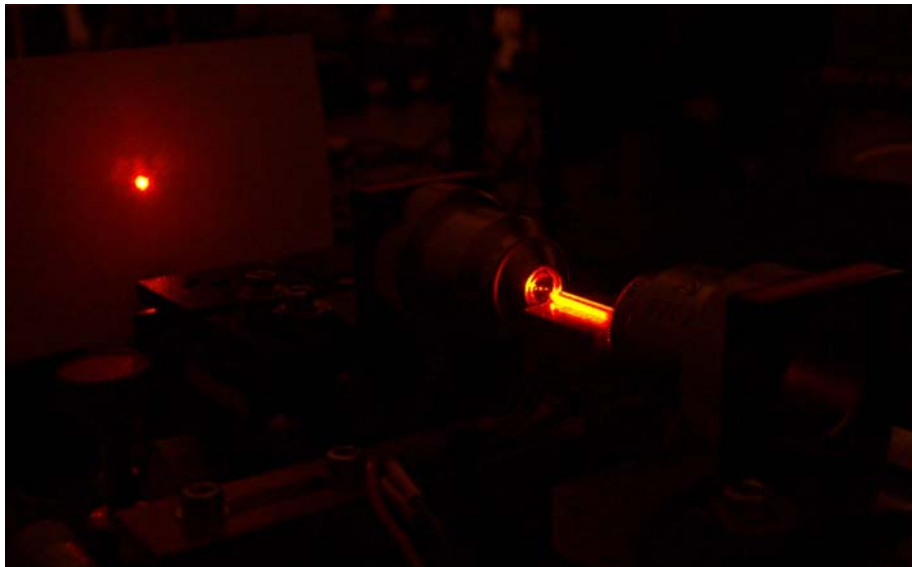
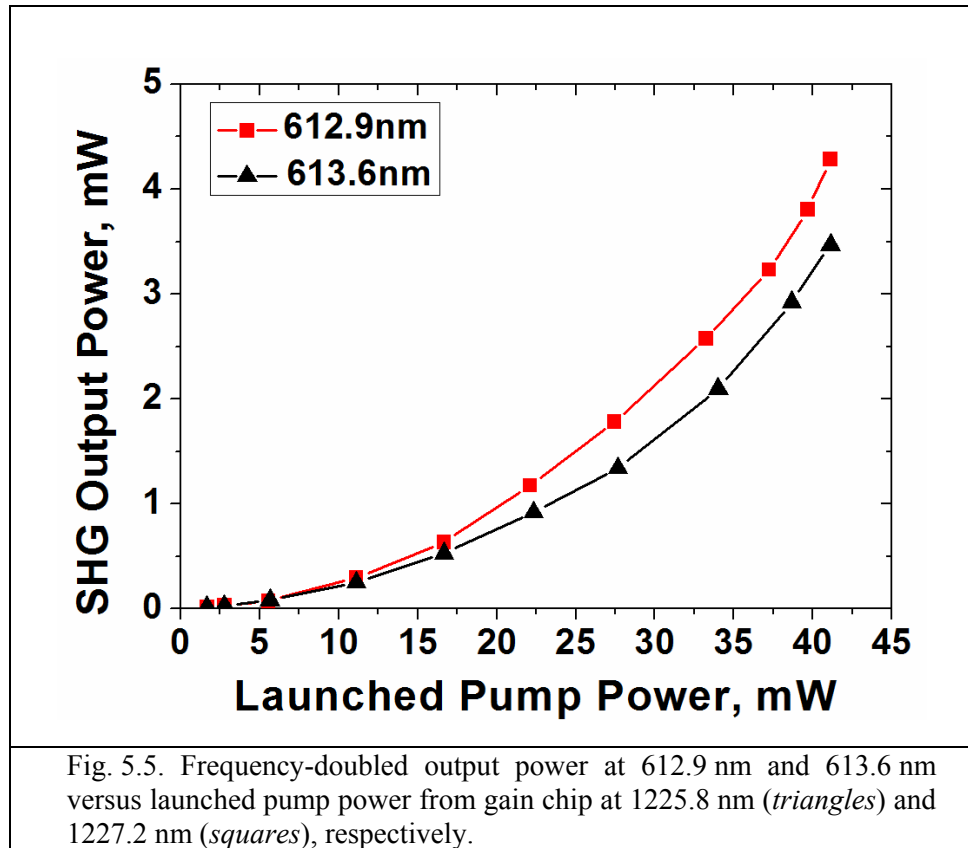
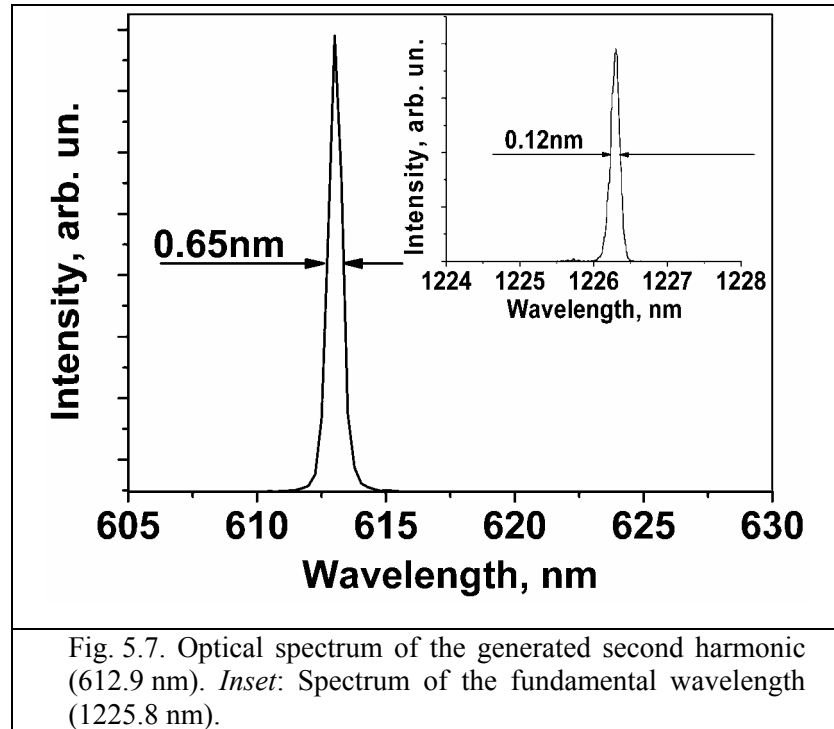
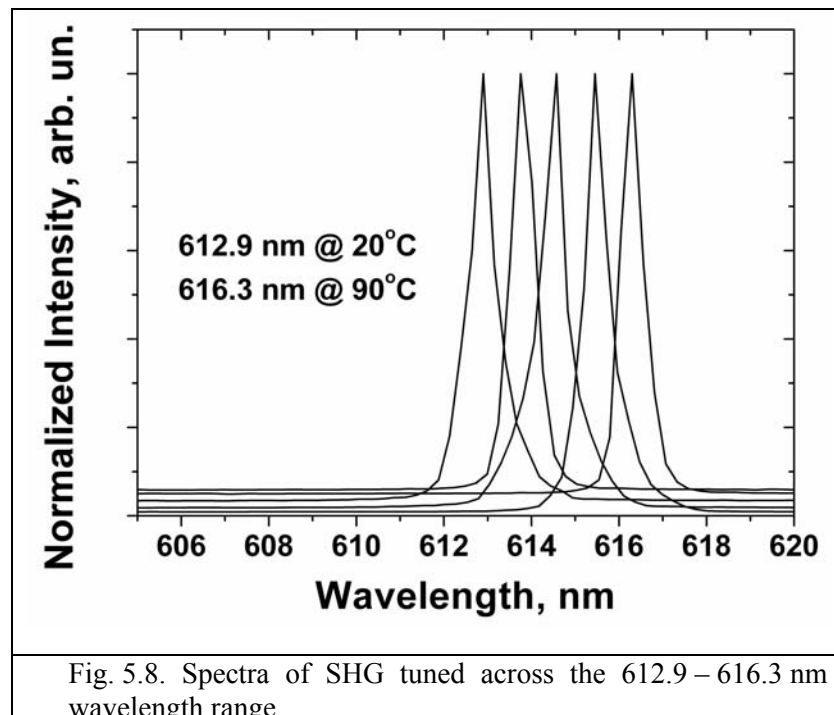


Fig. 5.6. Photograph of the efficient SHG at 612.9 nm from the QD-ECDL and the PPKTP waveguide.



The tunability of the second harmonic generated wavelength (Fig.5.8) was also investigated. It was done by increasing the temperature of the PPKTP crystal from 20°C to 90°C while simultaneously tuning the QD laser. A tuning range of 3.4 nm between 612.9 nm and 616.3 nm was achieved. The SHG conversion efficiency was similar across the range of crystal temperatures investigated in this work.



5.5. Second Harmonic Generation at 591.5 nm

5.5.1. Experimental Setup

The experimental setup is shown in Fig. 5.9. The core element of the QD-ECDL pump source consists of a QD gain chip fabricated from the structure DO1868, previously described in Chapter 3 (Section 3.4). The ridge waveguide of the SOA had a width of $5\ \mu\text{m}$ and a length of 4 mm, and was angled at 5° relative to the normal of the back facet. Additionally, both facets had a conventional AR coating, resulting in total estimated reflectivities of $2 \cdot 10^{-3}$ for the front facet and less than 10^{-5} for the angled facet. The QD gain chip was mounted on a copper heat sink and its temperature was controlled by a thermo-electric cooler. The QD-ECDL was set up in a quasi-Littrow configuration (Fig.5.9), which consists of a diffraction grating with 1200 grooves/mm and 40x (NA of 0.55) AR-coated aspheric lenses. Coarse wavelength tuning of QD-ECDL between 1130 and 1308 nm at 20°C was made possible by changing the incidence angle of the grating. The QD-ECDL was tuned to the 1183-nm target wavelength at 20°C , and then the collimated output from the QD-ECDL was coupled into the PPKTP waveguide using a 40x aspheric lens. The collimated output from the QD-ECDL was coupled into the PPKTP waveguide using a 40x aspheric lens.

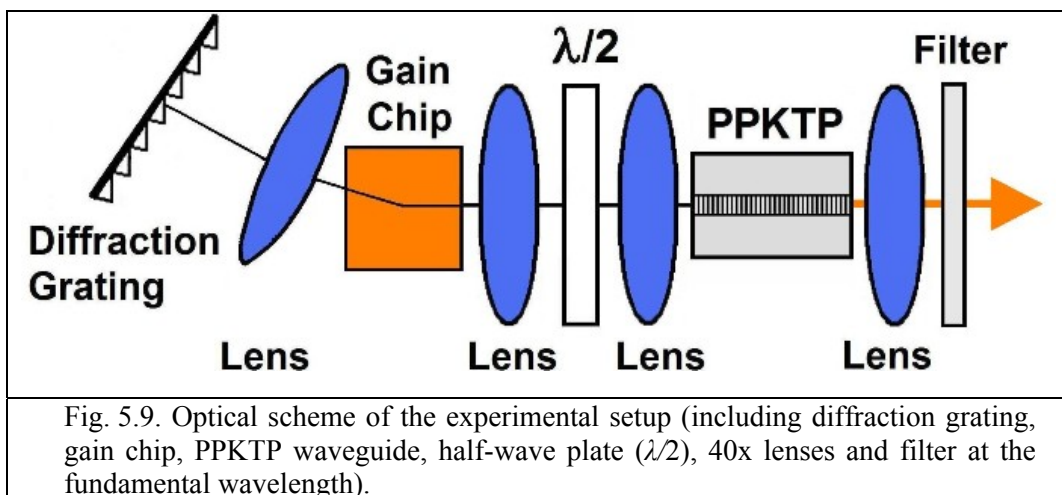
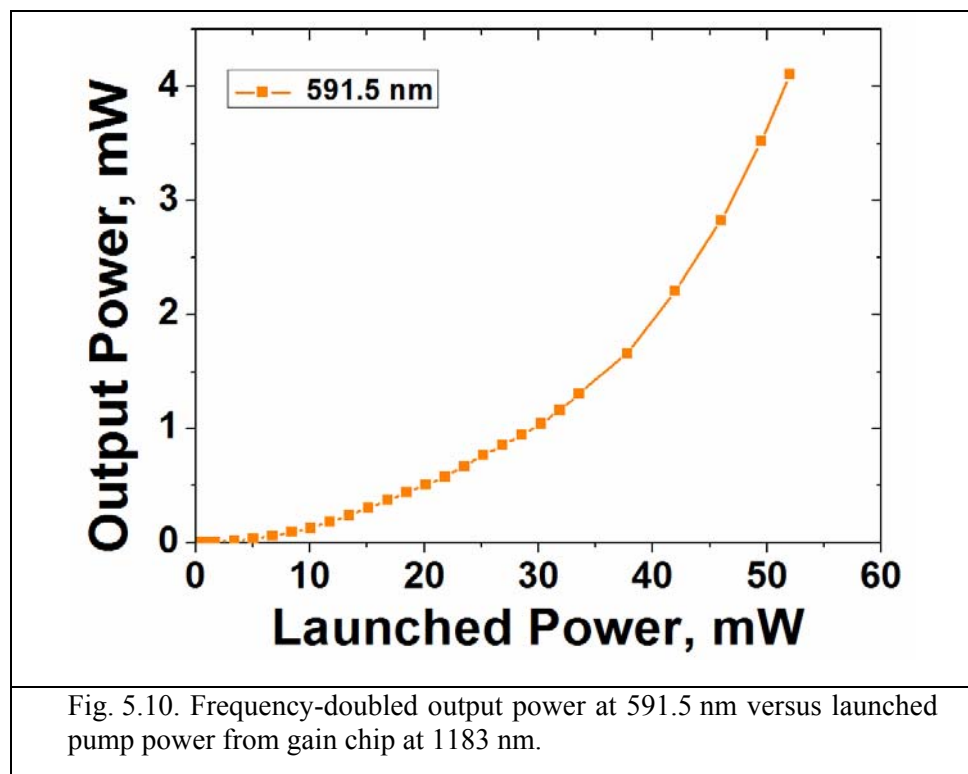


Fig. 5.9. Optical scheme of the experimental setup (including diffraction grating, gain chip, PPKTP waveguide, half-wave plate ($\lambda/2$), 40x lenses and filter at the fundamental wavelength).

The PPKTP frequency-doubling crystal used in this work was 16 mm in length and was periodically poled for SHG at 591.5 nm (with the poling period of $\sim 12.47 \mu\text{m}$). The waveguide with a cross-sectional area of $\sim 4 \times 4 \mu\text{m}^2$ (as shown in Fig. 5.1) and a refractive index step $\Delta n \approx 0.01$ was fabricated by an ion-exchange technique. The crystal facets were not AR coated. The PPKTP crystal was mounted on a copper heat sink and its temperature was controlled by a thermo-electric cooler. Both the pump laser and the PPKTP crystal were operating at room temperature.

5.5.2. Results

Figure 5.10 shows SHG output power versus launched pump power. The maximum SHG output power of 4.11 mW at 591.5 nm was achieved for 52 mW of launched pump power at 1183 nm, resulting in a conversion efficiency of 7.9%. A photograph of the SHG at 591.5 nm in the PPKTP waveguide pumped by the QD-ECDL is shown in Fig. 5.11.



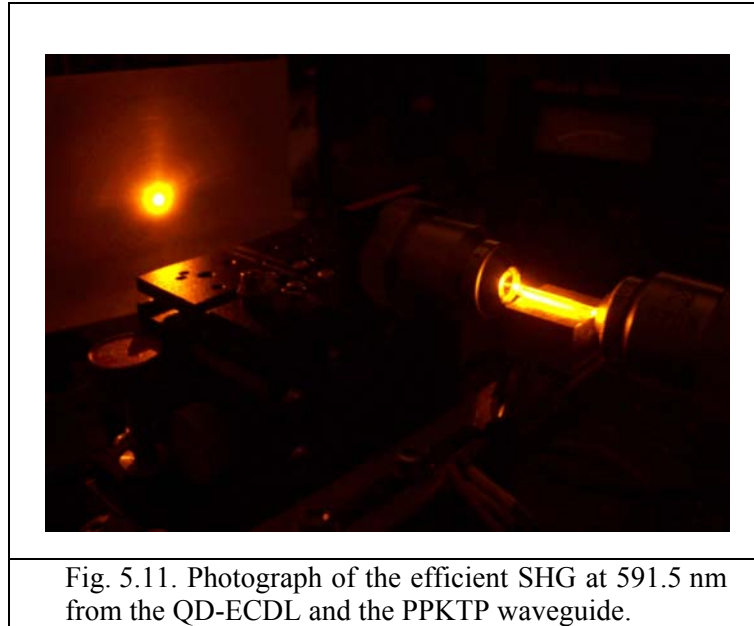


Fig. 5.11. Photograph of the efficient SHG at 591.5 nm from the QD-ECDL and the PPKTP waveguide.

Figure 5.12 shows the measured optical spectrum of the second-harmonic (591.5 nm) and fundamental (1183 nm) wavelengths. The optical spectrum of the fundamental wavelength exhibited a bandwidth of around 0.13 nm, limited only by the instrumental resolution of the spectrometer (OSA Advantest Q8384). A spectral width of the SH was measured to be 0.63 nm (limited only by the instrumental resolution of the Ocean Optics spectrometer used).

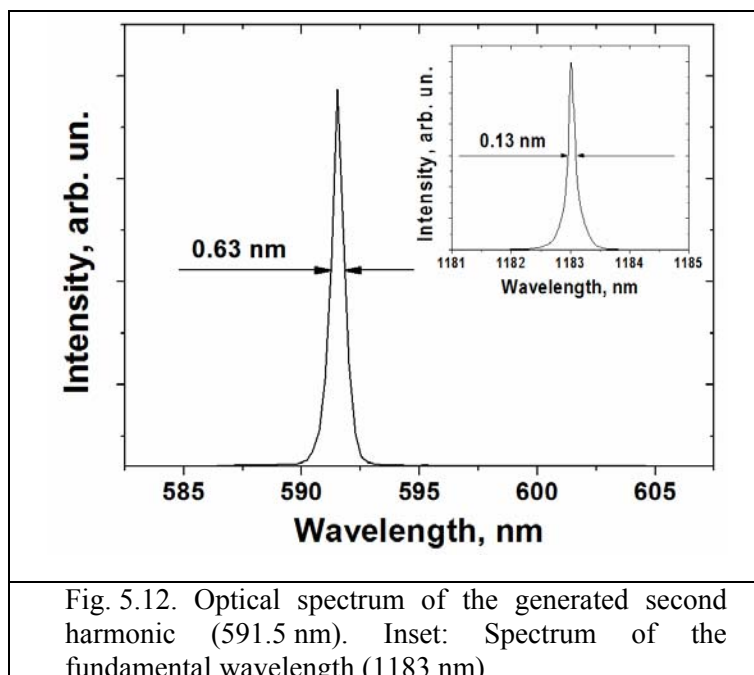
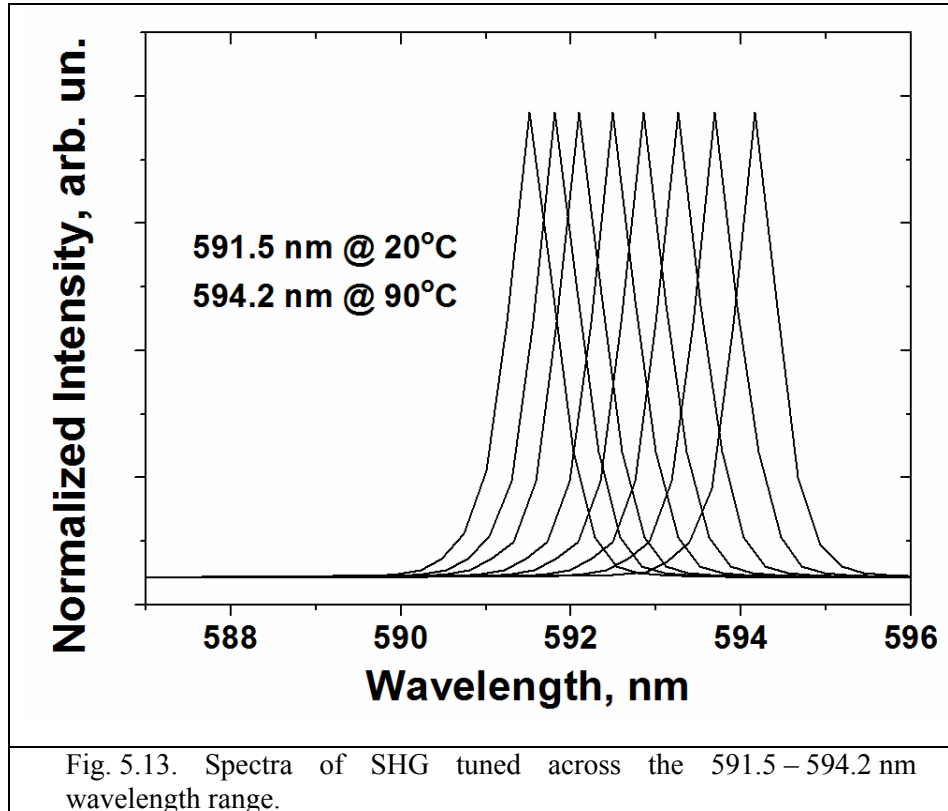


Fig. 5.12. Optical spectrum of the generated second harmonic (591.5 nm). Inset: Spectrum of the fundamental wavelength (1183 nm).

The tunability of the second harmonic generated wavelength (Fig. 5.13) was also investigated. It was done by increasing the temperature of the PPKTP crystal from 20°C to 90°C while simultaneously tuning the QD laser. A tuning range of 2.7 nm between 591.5 nm and 594.2 nm was achieved. The SHG conversion efficiency was similar across the range of crystal temperatures investigated in this work.



5.6. Tunable Visible Laser Source Based on Second Harmonic Generation in PPKTP Waveguide

5.6.1. Discussion

Quasi-phase-matching is an important and widely-used technique in nonlinear optics enabling efficient frequency up-conversion. However, since its introduction almost half a century ago [5.7], this technique is intrinsically limited in spectral tunability by the strict conditions set by the spatial modulation which compensates the momentum mismatch imposed by the dispersion. In this Section, a fundamental generalisation of quasi-phase-matching based on the utilisation of a significant difference in the effective refractive indices of the high- and low-order modes in multimode waveguides will be provided. This concept enables the period of poling to be matched over a very broad wavelength range and opens up a new avenue for an order-of-magnitude increase in wavelength range for frequency conversion from a single crystal.

Frequency doubling of infrared (IR) light based on the generation of new laser wavelengths via a material's nonlinearity $\chi^{(2)}$ in so-called 'nonlinear' crystals is one of the most attractive ways for the realisation of compact laser sources in the visible spectral region with a number of cutting-edge applications ranging from biophotonics [5.5] and photomedicine [5.3,5.20] to laser projection displays [5.1]. This trend is backed both by the market and technical sides by the availability of compact and highly efficient IR semiconductor lasers in the spectral range encompassing 0.9-1.3 μm . To enable efficient conversion, or SHG, both photon energy conservation $E_\lambda = 2 \cdot E_{2\lambda}$ and momentum conservation $k_\lambda = 2 \cdot k_{2\lambda}$ are to be achieved simultaneously. However, requirement of the photon momentum conservation (also called "phase-matching"

constraint) is difficult to achieve due to dispersion of the refractive index in the nonlinear crystal (i.e. due to the obvious fact that the refractive index for IR light is different from that for light in the visible spectral range resulting in difference of phase velocities for IR and visible light waves propagating through the crystal).

Without phase matching, the generated second harmonic grows and decays as the fundamental (IR) and second harmonic (visible) waves go in and out of phase over each coherence length l_c [5.7]:

$$l_c = \frac{\lambda}{2|n_\lambda - n_{2\lambda}|}, \quad (5.3)$$

where λ is the second harmonic wavelength, n_λ and $n_{2\lambda}$ are the refractive indices for the visible and IR light. In other words, out-of-phase SHG leads to the total suppression of the second harmonic light by radiation generated in the distance of coherence length l_c due to the opposite phases of these waves. Therefore phase matching between interacting waves is mandatory in order to achieve efficient frequency conversion. To date, by far the most commonly used approach for this is the periodical poling (or QPM) of the ferroelectric nonlinear crystals by periodically reversing the crystals polarization under the influence of a sufficiently large electric field [5.8]. When the poling period corresponds to double the coherence length $\Lambda = 2l_c$, then the proper phase relationship between the propagating waves is maintained and the SHG efficiency is maximised with the quasi-wave-vector of the periodically poling grating enabling momentum conservation, $k_\lambda = 2 \cdot k_{2\lambda} + k_\Lambda$:

$$\frac{2\pi n_\lambda}{\lambda} = 2 \frac{2\pi n_{2\lambda}}{2\lambda} + \frac{2\pi}{\Lambda}, \quad (5.4)$$

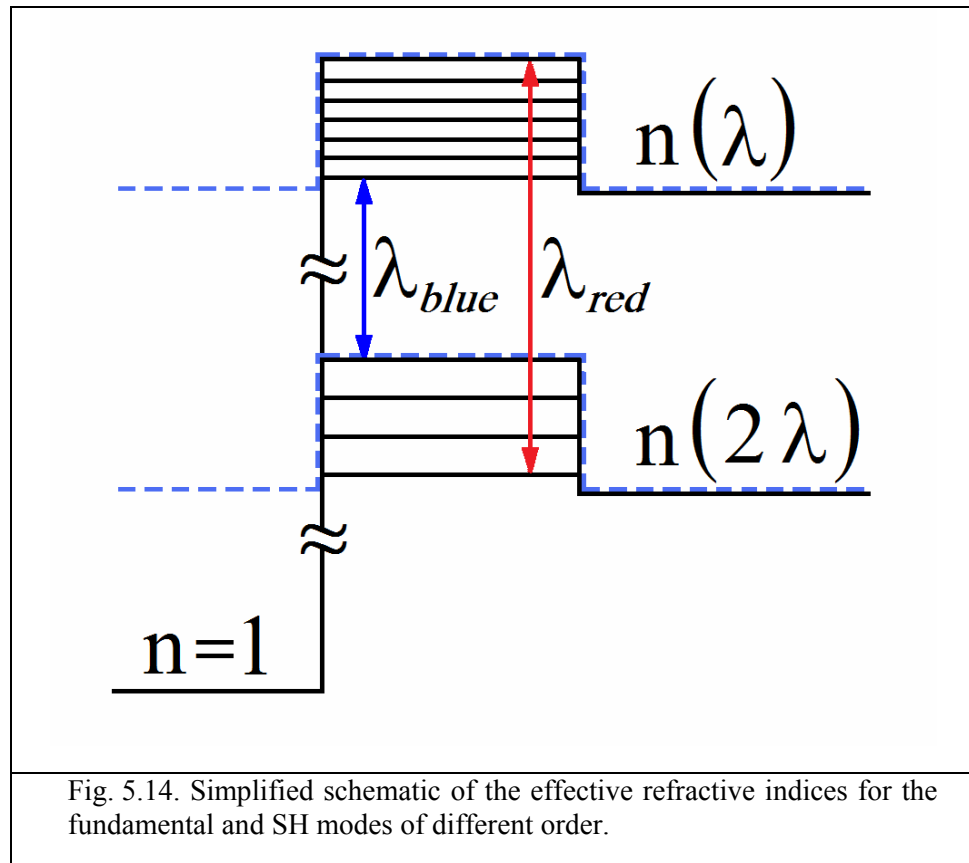
Equation (5.4) means that almost no tunability can be introduced to the SHG system involving periodical poling of the nonlinear crystal. Until now, regardless of the availability of extremely broadly tunable semiconductor lasers thanks to the utilisation

of size-variable QDs [5.13], QPM crystals have not been used for broadly tunable SHG. However, if similar tunability was made available, then the utilisation of a single-chip QD laser emitting in a broad range exceeding 200 nm [5.21] could make full-colour SHG already within reach.

Current state-of-the-art SHG tuning approaches include multiple-grating and temperature-assisted tuning with short-pulsed and CW pumping (including diode pumping) but both are limited to only few nm tuning range [5.11,5.18,5.22-5.25].

Great progress in tunability was achieved with ‘random’ quasi-phase-matching in polycrystalline materials enabling the generation of second harmonic from green to red [5.26] with the obvious drawback being an extremely low conversion efficiency even with short-pulsed pumping. The most promising approaches to the broadly tunable SHG involve Fibonacci or Fourier-constructed quasi-periodical poling that opens the avenue for general solutions of the multiple-phase-matching problem [5.27,5.28]. Unfortunately, this technique suffers from complicated poling mask requirements and is obviously not free from the compromise of conversion efficiency. Another very promising approach utilises counter-propagating light pulses enabling the enhancement of high-harmonic emission by scrambling the quantum phase of the generated short-wavelength light, to suppress emission from the out-of-phase regions [5.29], but to date, this technique has only been applied to X-ray and extreme ultra-violet generation [5.30,5.31]. The most outstanding recent advancement, ‘spatiotemporal’ quasi-phase-matching [5.32] was proposed and demonstrated to enable momentum and energy conservation through a combination of spatial and temporal modulation of pumping light. This technique, being intrinsically not applicable for CW regime, is absolutely free of the compromise of conversion efficiency when extremely short-pulsed pumping is available.

However, nonlinear crystal waveguides that offer an order-of-magnitude increase in IR-to-visible conversion efficiency [5.10,5.12] also enable a very different approach to SHG tunability in periodically poled crystals, promising order-of-magnitude increase of wavelength range for SHG conversion. The idea of enabling such broad tunability has been almost overlooked in earlier publications [5.33-5.35]. However, only 4.5 nm tuning range was demonstrated [5.34] even with assistance of temperature-control and solid-state pumping. In contrast, our approach is based on the utilisation of a significant difference in the effective refractive indices of the high-order and low-order modes in the waveguide, that enables to shift the difference between the effective refractive indices of the fundamental and second-harmonic waves to match the period of poling in a very broad wavelength range limited mainly by the waveguide refractive index step Δn , as shown schematically on Fig. 5.14.



Deriving the effective poling period as $\Lambda \approx \lambda_{red/blue} / (n_{\lambda_{red/blue}} - n_{2\lambda_{red/blue}} \pm \Delta n)$, from Equations (5.3) and (5.4), it is easy to see that for the multimode waveguide the total tunable range can be approximated as:

$$\Delta\lambda = \lambda_{red} - \lambda_{blue} \approx \Lambda(2\Delta n + \delta n_{disp}), \quad (5.5)$$

where $\Delta\lambda$ is the difference between the most ‘red’ (λ_{red}) and ‘blue’ (λ_{blue}) visible wavelengths that can be generated in the nonlinear crystal with poling period Λ , Δn is the waveguide refractive index step (approximated to be the same for IR and visible range), and δn_{disp} is the refractive index change due to dispersion being combination of refractive indices corresponding to the most ‘red’ and ‘blue’ IR and visible wavelengths:

$$\delta n_{disp} = n_{2\lambda_{blue}} - n_{2\lambda_{red}} - n_{\lambda_{blue}} + n_{\lambda_{red}}. \quad (5.6)$$

With a poling period of 5 - 20 μm and a refractive index step Δn on the order of 0.01 (which is typical for ion-exchange waveguides in the nonlinear crystals), one can see that SHG tunability from 10’s to 100’s of nanometres can easily be achieved. Moreover, taking into account the refractive index change due to the dispersion δn_{disp} , SHG tunability on the order of, or even exceeding, the whole visible spectrum is feasible with some crystals having a suitable dispersion curve. Calculated dependence of the poling period on wavelength illustrating SHG tunability due to significant difference of the effective refractive indices of the high- and low-order modes in a PPKTP waveguide with $\Delta n = 0.01$ is shown in Fig. 5.15. In this Figure, according to Equation (5.3), the small difference between refractive indices of low-order IR and high-order SHG modes enables a ‘‘blue-shift’’ of the effective poling period (shown by blue curve), while a larger difference between refractive indices of high-order IR and low-order visible modes introduces a ‘‘red-shift’’ (shown in red). Horizontal black dashed line represents the physical poling period of the crystal used in experiments ($\sim 12.47 \mu\text{m}$).

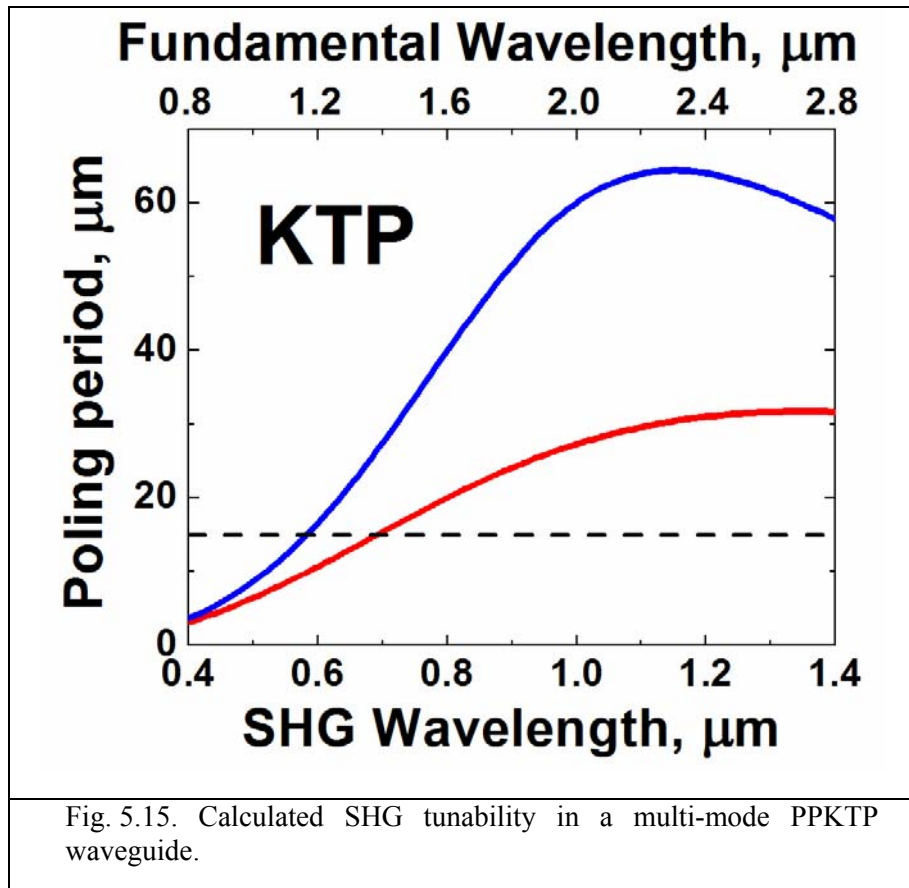


Fig. 5.15. Calculated SHG tunability in a multi-mode PPKTP waveguide.

The range of tunability can be extended by increasing the refractive index step of the waveguide Δn (Fig. 5.16) or by choosing material with an appropriate refractive index change due to dispersion δn_{disp} . The latter is illustrated in Fig. 5.17, where the total tunable range $\Delta\lambda$ vs. waveguide refractive index step Δn is calculated according to Equation (5.5) for lithium niobate (LN) and KTP known for the highest $\chi^{(2)}$ as well as for potassium dihydrogen phosphate (KDP) and lithium iodate (LI) having the highest δn_{disp} . The refractive indices for KTP, LN, KDP and LI crystals were calculated using the Sellmeier equations from Reference [5.36].

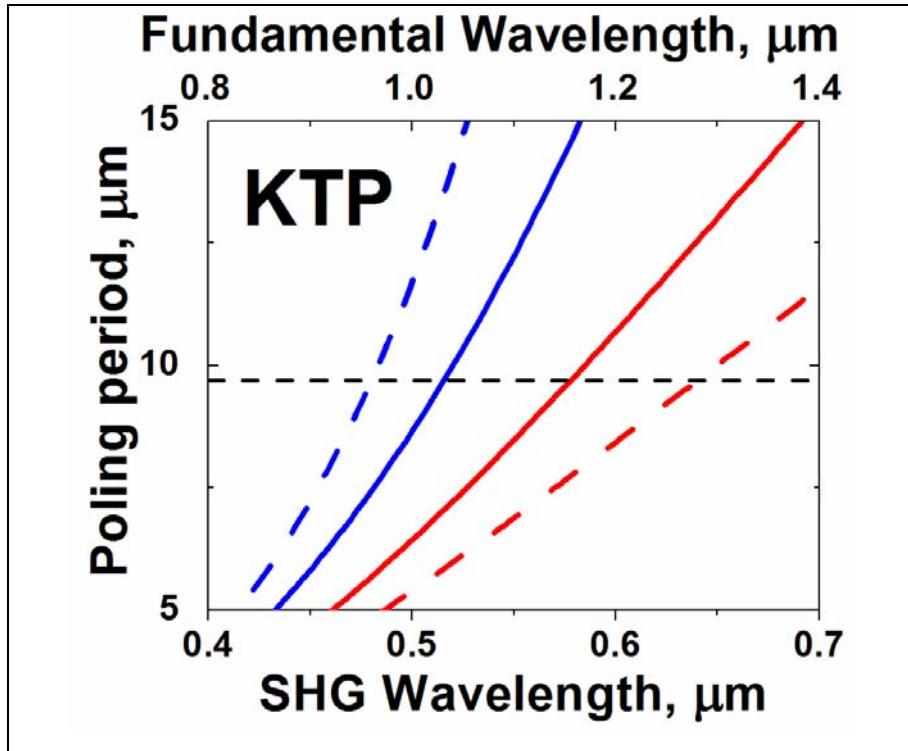


Fig. 5.16. Calculated SHG tunability for the PPKTP waveguides with $\Delta n = 0.01$ (solid lines) and 0.025 (dashed lines). Horizontal dashed line represents the physical poling period of $\sim 9.7 \mu\text{m}$, which corresponds to the QPM in the spectral region between 480 and 640 nm for $\Delta n = 0.025$.

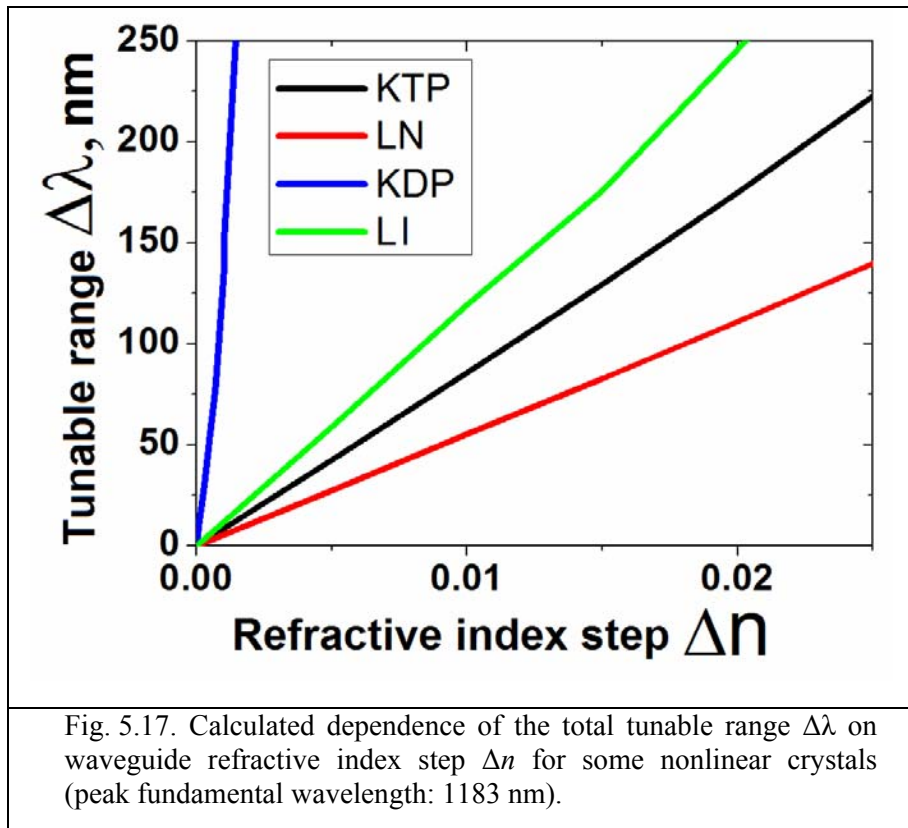
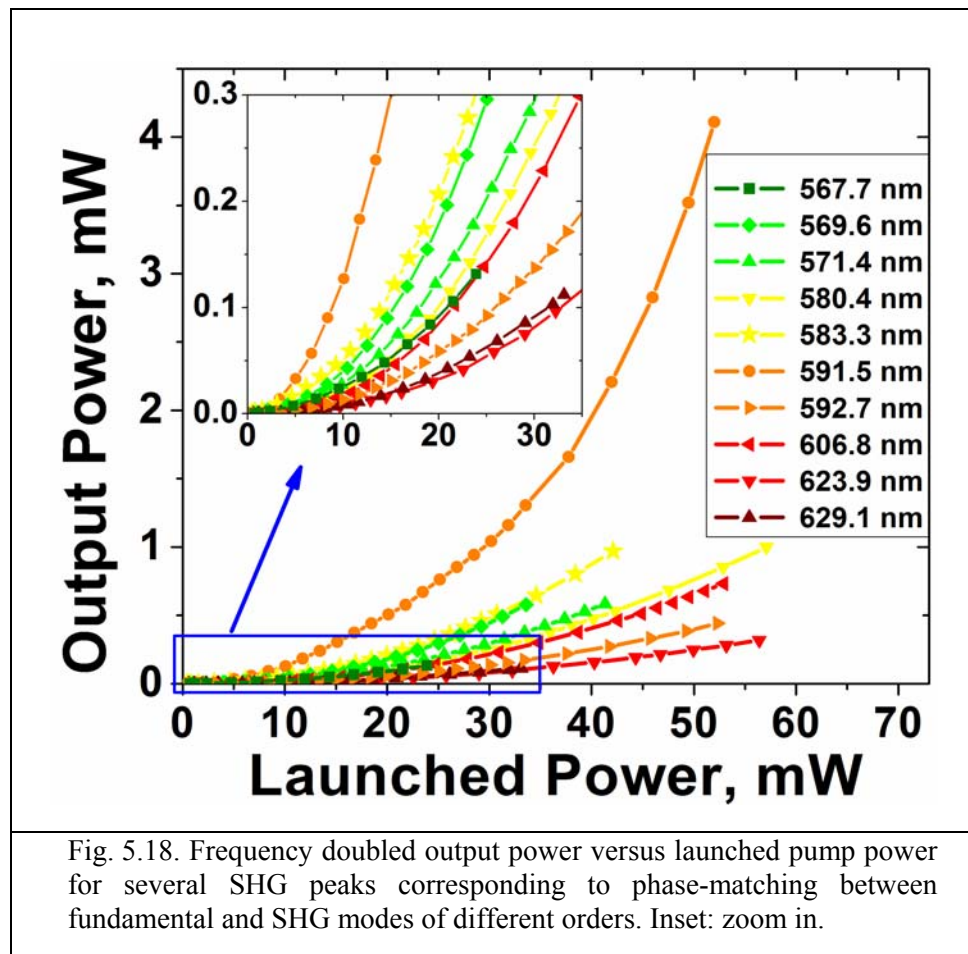


Fig. 5.17. Calculated dependence of the total tunable range $\Delta\lambda$ on waveguide refractive index step Δn for some nonlinear crystals (peak fundamental wavelength: 1183 nm).

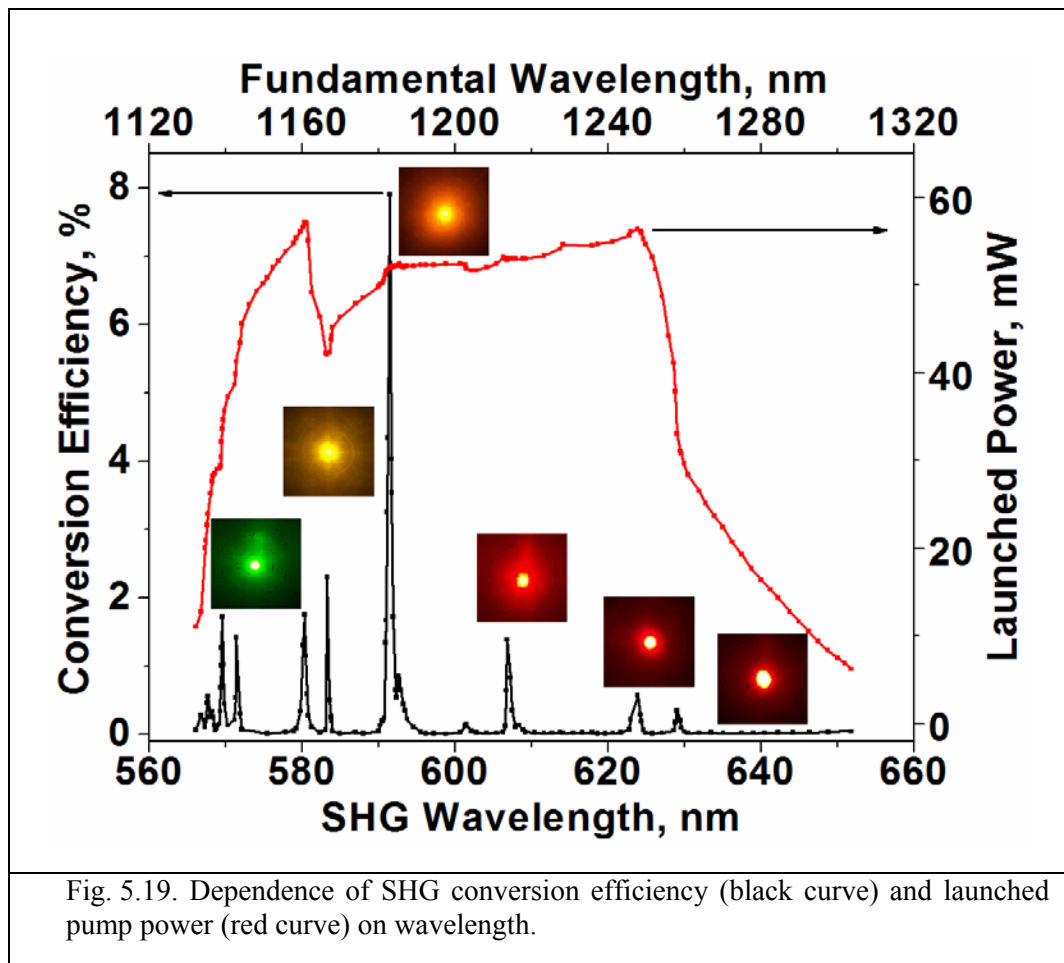
5.6.2. Experimental Results

For an experimental demonstration of the extremely broad tunability I used the experimental setup described in Section 5.5 of this Chapter with the same uncoated 16 mm long KTP crystal which was periodically poled for SHG at 591.5 nm (with the poling period of 12.47 μm) and had the waveguide with a cross-sectional area of $4 \times 4 \mu\text{m}^2$ and a refractive index step $\Delta n \approx 0.01$. A simplified scheme of the experimental setup is shown in Fig. 5.9. Both the pump laser and the PPKTP crystal were operating at room temperature.

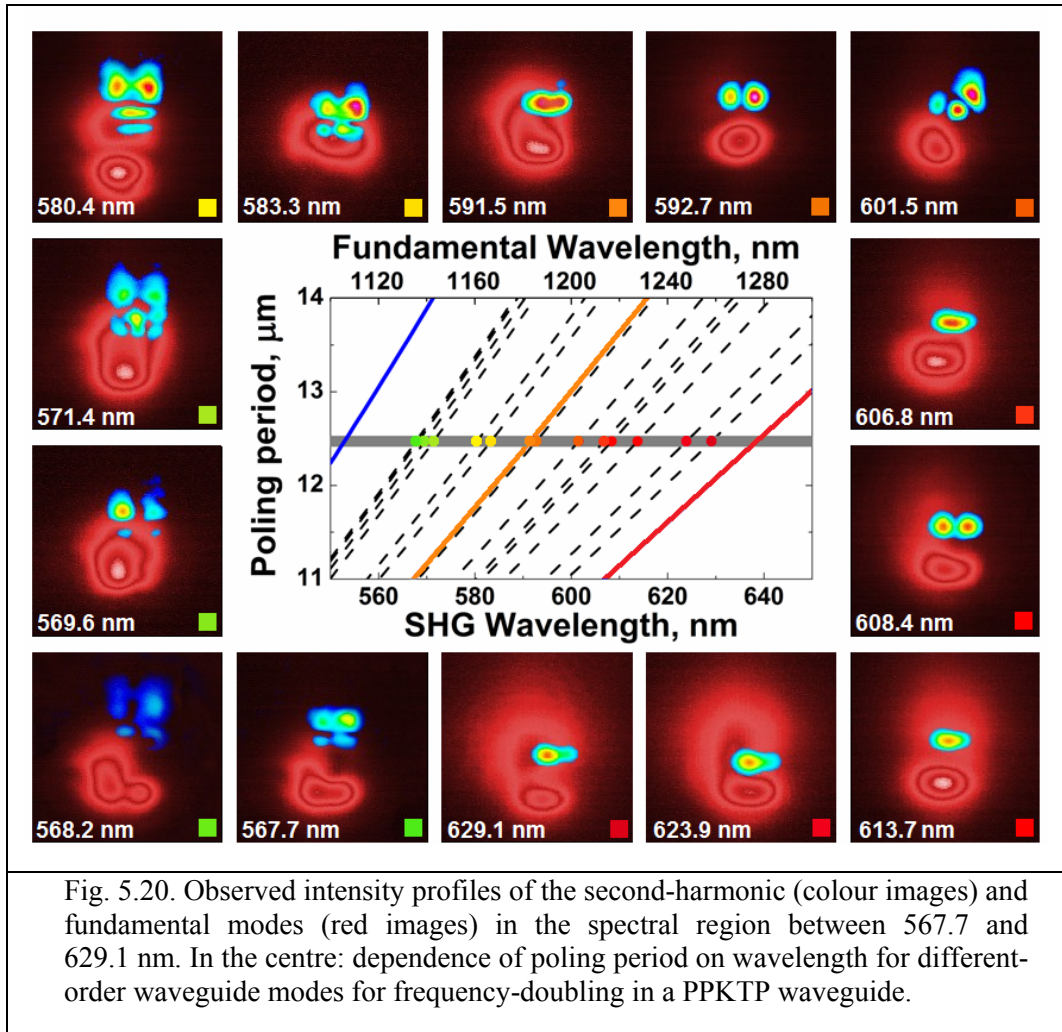
Figure 5.18 shows SHG output power versus launched pump power for several wavelengths related to the main peaks of SHG efficiency as shown in Fig. 5.19, which were observed by wavelength tuning of the QD-ECDL.



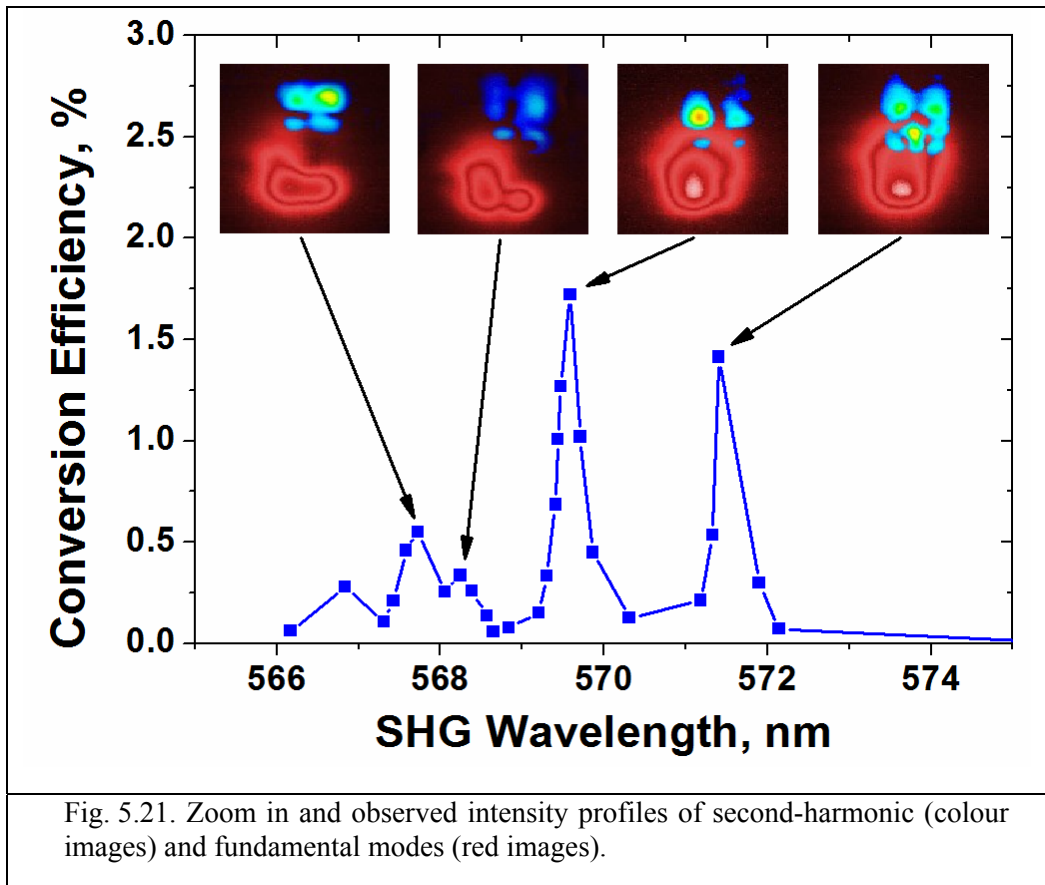
The maximum SHG output power of 4.11 mW at 591.5 nm was achieved for 52 mW of launched pump power at 1183 nm, resulting in a conversion efficiency of 7.9%. All other SHG peaks in the spectral region between 567.7 and 629.1 nm corresponded to phase-matching between fundamental and SHG modes of different order (simulated dispersion curves are depicted schematically in Fig. 5.20).



The influence of the waveguide refractive index step on the effective poling period is shown in the centre of Fig. 5.20, where the horizontal grey line represents the physical poling period of the crystal used in experiments ($\sim 12.47 \mu\text{m}$), the thick orange line is the central dispersion curve (crossing the grey line at the designed wavelength of 1183 nm) and the thick blue and red lines represent “blue” and “red” SHG margins for the waveguide refractive index step $\Delta n = 0.01$.



The effect of excitation of different-order modes on SHG wavelength can be seen very clearly in Fig. 5.21, where only ~ 4 nm tuning involves four different pairs of fundamental and SHG modes. As it can be seen from the observed intensity profiles of the fundamental and SHG modes in Fig. 5.20, phase-matching between the low-order fundamental (red images) and high-order second harmonic modes (colour images) corresponds to the SHG on the blue side of tuning range, and the high-order fundamental and low-order SHG modes are attributed to the frequency doubling on the red side of tuning range. These results are in excellent agreement with our multi-mode interaction model.



5.7. Summary

In this Chapter, an all-room-temperature CW second harmonic generation at 612.9 nm and 591.5 nm in periodically poled potassium titanyl phosphate waveguides pumped by a broadly-tunable quantum-dot external cavity diode laser was demonstrated. A frequency-doubled power of up to 4.3 mW at the wavelength of 612.9 nm and 4.1 mW at 591.5 nm with a conversion efficiency of 10.5% and 7.9%, respectively, was achieved.

A fundamental generalisation of quasi-phase-matching based on the utilisation of a significant difference in the effective refractive indices of the high-order and low-order modes in multimode waveguides were provided. This concept enables us to match the period of poling in a very broad wavelength range and opens up a new avenue for an order-of-magnitude increase in wavelength range for frequency conversion from a single crystal.

A green-to-red tunable laser source with tunability of over 60nm (567.7 nm – 629.1 nm) and maximum conversion efficiencies in range of 0.34 - 7.9% based on SHG in a single periodically poled potassium titanyl phosphate waveguide pumped by a single broadly-tunable quantum dot laser was demonstrated.

The results demonstrate an important step towards a compact tunable coherent visible light source, operating at room temperature. Further work on the improvement of launching efficiency into the nonlinear crystal and the extension of operation to different spectral regions is currently under way.

In future experiments, for materials with high nonlinearity $\chi^{(2)}$ but inconvenient dispersion (such as LN and KTP), tunability over entire red-green-blue region can be

achieved with the introduction of a higher waveguide refractive index step, as shown in Fig. 5.17. For LN, Δn up to 0.14 was reported by Korkishko *et al.* [5.37], and for KTP, Δn up to 0.04, a four-fold measure over the value used in this work, was demonstrated by Risk *et al.* [5.38]. Therefore, thoughtful engineering of the waveguide structure and poling along with careful choice of the nonlinear material and improvement of the laser-to-crystal coupling efficiency can further increase the demonstrated second-harmonic generation tunability and conversion efficiency. Additionally, utilisation of slightly aperiodically (i.e. “chirped”) poling of the nonlinear crystal and SHG mode reshaping via direct coupling of the output beam into a multimode fibre will make the proposed breakthrough approach the preferred way for realisation of the compact full-colour laser source.



5.8. References

- [5.1] Z. Xu, Y. Bi, “Large laser projection displays utilizing all-solid-state RGB lasers,” *Proc. SPIE* **5632**, pp.114-122 (2005).
- [5.2] C.W. Hoyt, Z.W. Barber, C.W. Oates, T.M. Fortier, S.A. Diddams, and L. Hollberg, “Observation and Absolute Frequency Measurements of the 1S_0 - 3P_0 Optical Clock Transition in Neutral Ytterbium”, *Phys. Rev. Lett.* **95**, pp. 083003 (2005).
- [5.3] S. Karrer, W. Baumler, C. Abels, U. Hohenleutner, M. Landthaler, R.M. Szeimies, “Long-pulse dye laser for photodynamic therapy: investigations in vitro and in vivo,” *Lasers Surg. Med.* **25**, pp.51 (1999).
- [5.4] M. Blank, G. Kostenich, G. Lavie, S. Kimel, Y. Keisari, A. Orenstein, “Wavelength-dependent properties of photodynamic therapy using hypericin in vitro and in an animal model,” *Photochemistry and Photobiology* **76**(3), pp.335-340 (2002).
- [5.5] V. Kapoor, F.V. Subach, V.G. Kozlov, A. Grudinin, V.V. Verkhusha, W.G. Telford, “New lasers for flow cytometry: filling the gaps,” *Nat. Methods* **4**, pp.678-679 (2007).
- [5.6] B. Agate, E.U. Rafailov, W. Sibbett, S.M. Saltiel, K. Koynov, M. Tihonen, S.Wang, F. Laurell, P. Battle, T. Fry, T. Roberts, E. Noonan, “Efficient frequency-doubling of femtosecond pulses in waveguide and bulk nonlinear crystals: Design, fabrication, theory and experiment,” in *Frontiers in Planar Lightwave Circuit Technology. NATO Sci. Ser. II: Math. Phys. Chem.*, **216**, pp.189–227 (Springer, Dordrecht, 2006).
- [5.7] J.A. Armstrong, N. Bloembergen, J. Ducuing, P.S. Pershan, “Interactions between light waves in a nonlinear dielectric,” *Phys. Rev.* **127**, pp.1918-1939 (1962).
- [5.8] M.M. Fejer, G.A. Magel, D.H. Jundt, R.L. Byer, “Quasi-phase-matched second harmonic generation: tuning and tolerances,” *IEEE J. Quantum Electron.* **28**, pp.2631-2654 (1992).
- [5.9] J.D. Bierlein, A. Ferretti, L.H. Brixner, W.Y. Hsu, “Fabrication and characterisation of optical waveguides in KTiOPO_4 ,” *Appl. Phys. Lett.* **50**(18), pp.1216-1218 (1987).

- [5.10] M. Rusu, E.U. Rafailov, R. Herda, O.G. Okhotnikov, S.M. Saltiel, P. Battle, S. McNeil, A.B. Grudinin, W. Sibbett, "Efficient generation of green and UV light in a single PP-KTP waveguide pumped by a compact all-fibre system," *Appl. Phys. Lett.* **88**, pp.121105 (2006).
- [5.11] D.A. Chestnut, S.V. Popov, J.R. Taylor, T.D. Roberts, "Second-harmonic generation to the green and yellow using picosecond fibre pump sources and periodically poled waveguides," *Appl. Phys. Lett.* **88**, pp.071113 (2006).
- [5.12] B. Agate, E.U. Rafailov, W. Sibbett, S.M. Saltiel, K. Koinov, M. Tihonen, S.Wang, F. Laurell, P. Battle, T. Fry, T. Roberts, E. Noonan, "Portable ultrafast blue light sources designed with frequency doubling in KTP and KNbO₃," *IEEE J. Sel. Top. Quantum Electron.* **10**, pp.1268-1276 (2004).
- [5.13] E.U. Rafailov, M.A. Cataluna, W. Sibbett, "Mode-locked quantum-dot lasers," *Nature Photon.* **1**, pp.395-401 (2007).
- [5.14] A. Kovsh, I. Krestnikov, D. Livshits, S. Mikhrin, J. Weimert, and A. Zhukov, "Quantum dot laser with 75 nm broad spectrum of emission," *Opt. Lett.* **32**(7), pp.793-795 (2007).
- [5.15] J.D. Bierlein, H. Vanherzeele, "Potassium titanyl phosphate: properties and new applications," *J. Opt. Soc. Am. B* **6**(4), pp.622-633 (1989).
- [5.16] G.P. Agrawal, *Nonlinear Fiber Optics* (Academic Press, New York, 1989).
- [5.17] G.W. Arnold, G. De Marchi, F. Gonella, P. Mazzoldi, A. Quaranta, G. Battaglin, M. Catalano, F. Garrido, R.F. Haglund, *Nucl. Instrum. Methods B* **116**, pp.507 (1996).
- [5.18] J. Webjorn, S. Siala, D.W. Nam, R.G. Waarts, R.J. Lang, "Visible laser sources based on frequency doubling in nonlinear waveguides," *IEEE J. Quantum Electron.* **33**, pp.1673-1686 (1997).
- [5.19] G.T. Reed, A.P. Knights, *Silicon Photonics. An Introduction* (Wiley, Chichester, 2004).
- [5.20] R.E. Fitzpatrick, "Lasers in dermatology & plastic surgery," *Opt. Photon. News*, **6**, p.24 (1995).
- [5.21] K.A. Fedorova, M.A. Cataluna, I. Krestnikov, D. Livshits, E.U. Rafailov, "Broadly tunable high-power InAs/GaAs quantum-dot external cavity diode lasers," *Opt. Express* **18**, pp.19438-19443 (2010).
- [5.22] J.L. Mortensen, A. McWilliam, C.G. Leburn, P. Tidemand-Lichtenberg, M. Thorhauge, J. Janousek, C.T.A. Brown, A.A. Lagatsky, P. Buchhave, W.

- Sibbett, "Up to 30 mW of broadly tunable CW green-to-orange light, based on sum-frequency mixing of Cr⁴⁺:forsterite and Nd:YVO₄ lasers," *Opt. Commun.* **260**, pp.637-640 (2006).
- [5.23] A. Sennaroglu, "Continuous-wave broadly tunable intracavity frequency-doubled Cr⁴⁺:forsterite laser", *IEEE J. of Selected Areas in Quant. Electron.* **8**(3), pp.474-478 (2002).
- [5.24] E.U. Rafailov, D.J.L. Birkin, W. Sibbett, P. Battle, T. Fry, D. Mohatt, "Efficient frequency doubling of a pulsed laser diode by use of a periodically poled KTP waveguide crystal with Bragg gratings," *Opt. Lett.* **26**, 1961-1962 (2001).
- [5.25] K.A. Fedorova, M.A. Cataluna, P.R. Battle, C.M. Kaleva, I.L. Krestnikov, D.A. Livshits, E.U. Rafailov, "Orange light generation from a PPKTP waveguide end-pumped by a cw quantum-dot tunable laser diode," *Appl. Phys. B* **103**, pp.41-43 (2011).
- [5.26] P.T. Lin, B.W. Wessels, J.I. Jang, J.B. Ketterson, "Highly efficient broadband second harmonic generation using polydomain epitaxial barium titanate thin film waveguides," *Appl. Phys. Lett.* **92** pp.221103 (2008).
- [5.27] A. Bahabad, N. Voloch, A. Arie, R. Lifshits, "Experimental confirmation of the general solution of the multiple-phase-matching problem," *J. Opt. Soc. Am. B* **24**, pp.1916-1921 (2007).
- [5.28] S.N. Zhu, Y.Y. Zhu, N.B. Ming, "Quasi-phase-matched third-harmonic generation in a quasi-periodic optical superlattice," *Science* **278**, pp.843-846 (1997).
- [5.29] X. Zhang, A.L. Lytle, T. Popmintchev, X. Zhou, H.C. Kapteyn, M.M. Murnane, O. Cohen, "Quasi-phase-matching and quantum-path control of high-harmonic generation using counterpropagating light," *Nature Phys.* **3**, pp.225-229 (2007).
- [5.30] A. Bahabad, O. Cohen, M.M. Murnane, H.C. Kapteyn, "Quasi-phase-matching and dispersion characterization of harmonic generation in the perturbative regime using counterpropagating beams," *Opt. Express* **16**, pp.15923-15931 (2008).
- [5.31] O. Cohen, X. Zhang, A.L. Lytle, T. Popmintchev, H.C. Kapteyn, M.M. Murnane, "Grating-assisted phase matching in extreme nonlinear optics," *Phys. Rev. Lett.* **99**, pp.053902 (2007).

- [5.32] A. Bahabad, M.M. Murnane, H.C. Kapteyn, “Quasi-phase-matching of momentum and energy in nonlinear optical processes,” *Nature Photon.* **4**, pp.570-575 (2010).
- [5.33] A. Christ, K. Laiho, A. Eckstein, T. Lauckner, P.J. Mostley, C. Silberhorn, “Spatial modes in waveguided parametric down-conversion,” *Phys. Rev. A* **80**, pp.033829 (2009).
- [5.34] M. Karpinski, C. Radzewicz, K. Banaszek, “Experimental characterization of three-wave mixing in a multimode nonlinear KTiOPO₄ waveguide,” *Appl. Phys. Lett.* **94**, pp.181105 (2009).
- [5.35] Y.L. Lee, W. Shin, B.-A. Yu, C. Jung, Y.-C. Noh, D.K. Ko, “Mode Tailoring in a ridge-type periodically poled Lithium Niobate waveguide,” *Opt. Express* **18**, pp.7678-7684 (2010).
- [5.36] D.N. Nikogosyan, *Nonlinear Optical Crystals: A Complete Survey*. (Springer, New York, 2005).
- [5.37] Y.N. Korkishko, V.A. Fedorov, F. Laurell, “The SHG-response of different phases in proton exchanged lithium niobate waveguides,” *IEEE J. Sel. Top. Quantum Electron.* **6**, pp.132-142 (2000).
- [5.38] W.P. Risk, S.D. Lau, R. Fontana, L. Lane, Ch. Nadler, “Type-II second-harmonic generation and sum-frequency mixing in uniform KTiOPO₄ channel waveguides,” *Appl. Phys. Lett.* **63**, pp.1301-1303 (1993).

6. Frequency Conversion in OP-GaAs Waveguides

In this Chapter, the possibility of obtaining second harmonic generation in orientation-patterned GaAs waveguides is investigated. Frequency doubled light at 1621 nm in a periodically poled GaAs waveguide is demonstrated. For this work, an OPO system used as a pump source and based on the periodically poled 5 mol% MgO-doped Congruent Lithium Niobate crystal, generating light in the wavelength range between 1430 nm and 4157 nm, is developed.

6.1. Introduction

The development of broadly tunable optical sources covering the mid-IR (3 - 16 μm and beyond) spectral region is an important research area for a wide range of applications relating to gas sensing, atmospheric transmission, biomedicine and potentially for the detection of concealed explosive materials. For maximum applicability, the laser sources that generate these wavelengths should be compact (potentially portable) and cheap. The devices presently used for mid-IR spectral range are typically based on narrow band-gap semiconductors and quantum cascade lasers, but these are restricted to low CW or average pulsed output power levels at room temperature or require cooling to liquid nitrogen temperature and have limited tunability range.

Recent progress in the development of electric-field poling (or periodic-poling) techniques for patterning the domain structure of ferroelectric materials has led to the implementation of different quasi-phase-matched (QPM) structures for efficient nonlinear optical interactions [6.1]. Such QPM devices have been fabricated in LiNbO_3 [6.2-6.6], LiTaO_3 [6.7-6.8], KTiOPO_4 [6.9-6.11], RbTiOAsO_4 [6.11,6.12], and KNbO_3 [6.13] crystals. Other methods for fabricating QPM structures in ferroelectric nonlinear crystals [6.14,6.15] and semiconductor materials [6.16-6.18] have also been reported and a number of candidates for frequency up/down conversion such as $\text{GaAs}/\text{AlGaAs}$ [6.19], GaP/AlP [6.20] and InSb [6.21], have also been identified. The semiconductor materials such as GaAs and AlAs and their alloys are especially promising, because of high transparency in the infrared region, large nonlinear coefficients and high thresholds for optical damage. For example, GaAs exhibits a very broad optical transparency, extending from 870 nm through to 16 μm and has nonlinearity as large as $d_{14}=119$ pm/V at 1.53 μm wavelength [6.22].

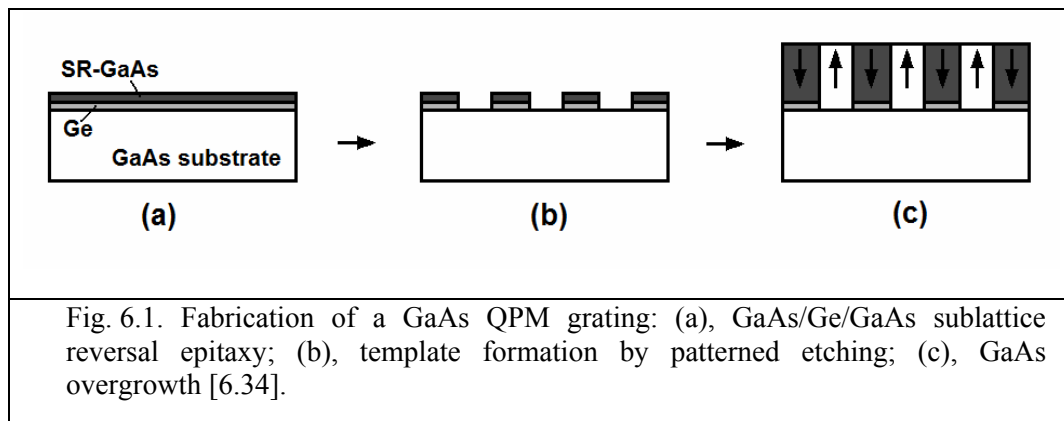
Well established semiconductor processing techniques can produce high quality, micro-structured GaAs devices. Hence, a ridge waveguide configuration can be employed to ensure good optical confinement and efficient nonlinear conversion and thus to permit the exploitation of low power (potentially diode laser) pump sources. The optically isotropic, non-ferroelectric nature of GaAs makes it unsuitable for common phase-matching methods based on birefringence or periodic poling and so alternative methods have been implemented to utilise it as a medium for nonlinear optical frequency conversion.

Gordon et al. has developed a QPM structure for SHG using diffusion-bonded GaAs stack of plates [6.23]. Yoo *et al.* used direct wafer bonding combined with microfabrication and regrowth techniques to fabricate periodically domain-inverted AlGaAs waveguides for SHG [6.24] and DFG [6.25]. However, these techniques require complicated fabrication processes, and furthermore, defects in the overgrown epitaxial layers occur due to inevitable misorientation in the bonding process.

A recently proposed novel method involving a periodically-switched-nonlinearity (PSN) in a semiconductor structure [6.26] enables first-order quasi-phase-matching to be achieved for the near- and mid-IR wavelength ranges [6.19,6.27]. In these PSN structures, the nonlinear optical coefficient in the material is either switched-off or decreased periodically using either an ion-implantation technique or an etch and regrowth process [6.28].

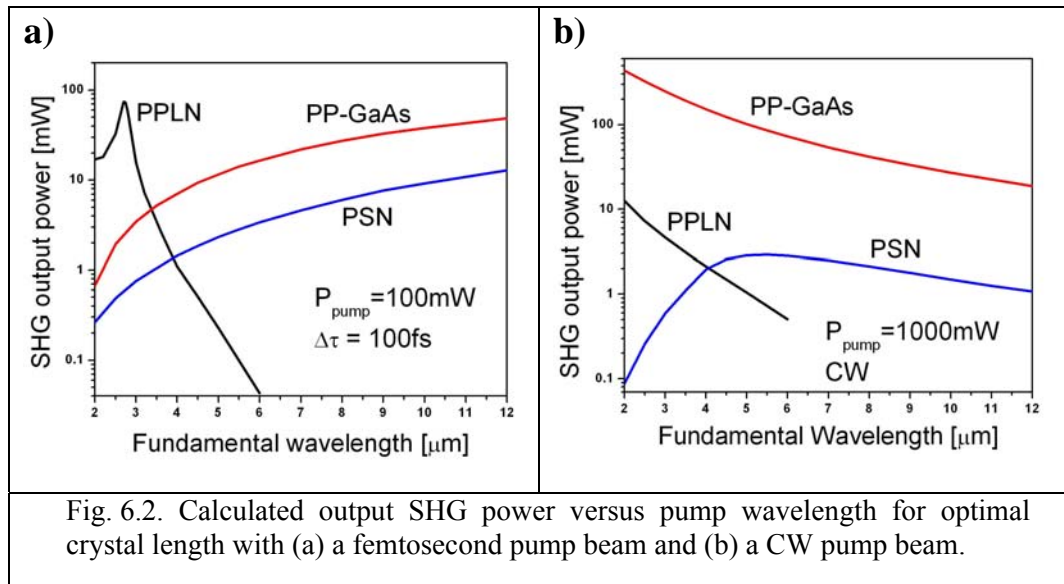
However, novel technology for QPM of semiconductors, so-called orientation-patterning or sublattice reversal epitaxy (SRE), [6.29-6.31] allows the fabrication of high quality domain inverted semiconductor structures (for example, periodically-poled GaAs-based crystals [6.32]), which demonstrate significantly better conversion efficiency. The idea of this technology is to deposit a thin non-polar buffer layer (such

as germanium, which has a very similar lattice constant to GaAs with $\sim 0.1\%$ mismatch [6.33]) to reverse sublattice occupation, followed by subsequent overgrowth of GaAs layer in antiphase to the substrate. Without this buffer layer, deposited GaAs layers nucleate in the same orientation as the preceding layer. Selective removal of inverted GaAs material and buffer layers followed by MBE regrowth allows the creation of positive and negative material in a side-by-side totally epitaxially grown structure. Regions of domain-inverted material exhibit sign reversal of all their non-vanishing nonlinear coefficients resulting in a nonlinear coefficient variation identical to the case of PPLN, to provide forward conversion at each coherence length. The schematic of the fabrication steps of orientation-patterned GaAs (OP-GaAs) structure is shown in Fig. 6.1.



According to our calculations (Fig. 6.2) periodically poled GaAs devices demonstrate significantly higher efficiency than either PPLN or PSN devices. The model was based on that used in references [6.27,6.35] and was developed by Dr. David Artigas. The calculations show (Fig. 6.2 (a)) that the GaAs-based devices are superior to PPLN crystals (at femtosecond pump) for wavelengths longer than $3.5 \mu\text{m}$. For the CW case (Fig. 6.2 (b)) it has been demonstrated that PP-GaAs-based devices show a significantly better conversion efficiency than that from a PPLN crystal in all wavelength range. Fig. 6.2 also shows that semiconductors such as GaAs may cover the

wavelength range from 6 to 16 μm which cannot be reached with conventional periodically-poled nonlinear crystals such as PPLN. These calculations also illustrate that PP-GaAs nonlinear crystal perform significantly better in terms of conversion efficiency compared with PSN-GaAs crystal.



Some of the earliest experimental studies on waveguide SHG were made with AlGaAs material. Using the OP-GaAs structure as a template, AlGaAs layers were over-grown by MBE to fabricate the QPM structure for SHG [6.36,6.37]. However, QPM AlGaAs waveguides fabricated using this technique suffered from large propagation losses due to the corrugation formation during the regrowth process [6.38,6.39]. GaAs material is more attractive in comparison with AlGaAs due to large nonlinear coefficients [6.40]. OP-GaAs bulk devices for frequency conversion have been recently reported [6.41,6.42]. However, the fabrication of bulk devices requires long growth time (more than 24 hours) and is very expensive. The fabrication of a waveguide design of OP-GaAs offers strong optical wave confinement and increases the optical power density inside the crystal, and this correspondingly reduces the pump power threshold for non-linear phenomena and provides better compatibility for diode

lasers with such a crystal. Therefore, the waveguide design of orientation-patterned semiconductor structure is better suited to, and can be successfully realised for up- and down-frequency conversion with “low-power” laser sources. Several papers on OP-GaAs waveguided wavelength conversion devices have recently been published [6.43-6.45].

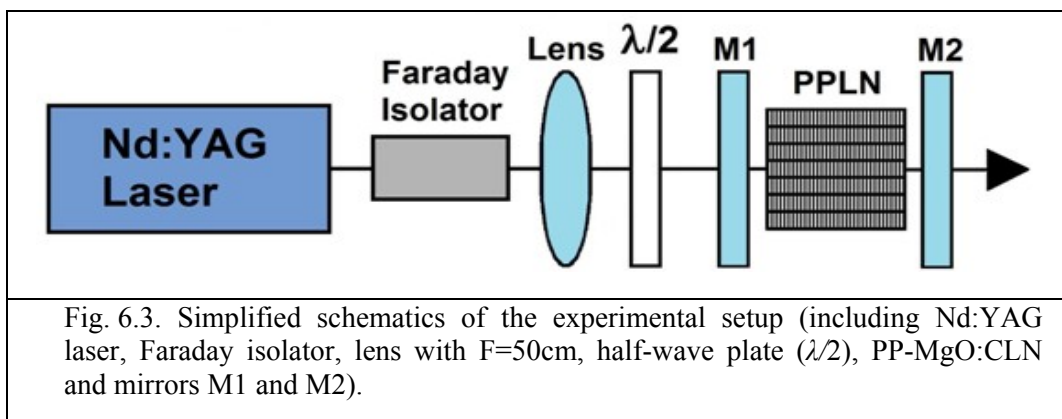
6.2. Optical Parametric Oscillator Based on PP-MgO:CLN

In order to investigate the frequency conversion properties of the orientation-patterned GaAs waveguides, a continuously tunable laser source was required. This motivated the development of an optical parametric oscillator (OPO) based on periodically poled lithium niobate (PPLN) and pumped by a Q-switched Nd:YAG laser. OPOs are very promising as versatile sources, being broadly tunable and with coherent radiation for spectral regions inaccessible to conventional lasers. The most important recent advances in OPO technology have been brought about by the advent of quasi-phase-matched nonlinear crystals [6.46]. PPLN is the most extensively used periodically poled material in OPOs due to its high nonlinear coefficient ($d_{\text{eff}}=27\text{pm/V}$), a wide transparency range (0.4 - 5 μm) and is easily fabricated by means of electric field poling [6.47,6.48]. The first PPLN crystals were made of undoped congruent lithium niobate, which suffers from photorefractive damage at temperature below 150°C [6.49]. In order to solve this problem, doping of PPLN crystals with Mg, In or Zn were introduced. As compared to undoped crystals, doped PPLN crystals offer several advantages [6.46] such as three orders of magnitude higher damage threshold, reduced thermal lensing resulting in better power and temperature stability, reduced photorefractive damage and room temperature operation of the crystal [6.50,6.51].

Over the last decade, numerous OPO systems based on periodically poled MgO-doped lithium niobate have been reported [6.52-6.61], offering unprecedented performance, having wide wavelength tuning, output power, pulse energy, conversion efficiency and fine tuning capability. These OPO systems, covering the spectral region of 2 - 5 μm , are of great interest for numerous applications, such as spectroscopy, trace gas monitoring, biomedicine, etc. Furthermore, the mid-infrared wavelength range available from OPO systems based on PPLN crystals in combining with latest advances in fabrication of QPM semiconductor structures provide an opportunity to develop laser sources in the wavelength region beyond $\sim 5 \mu\text{m}$.

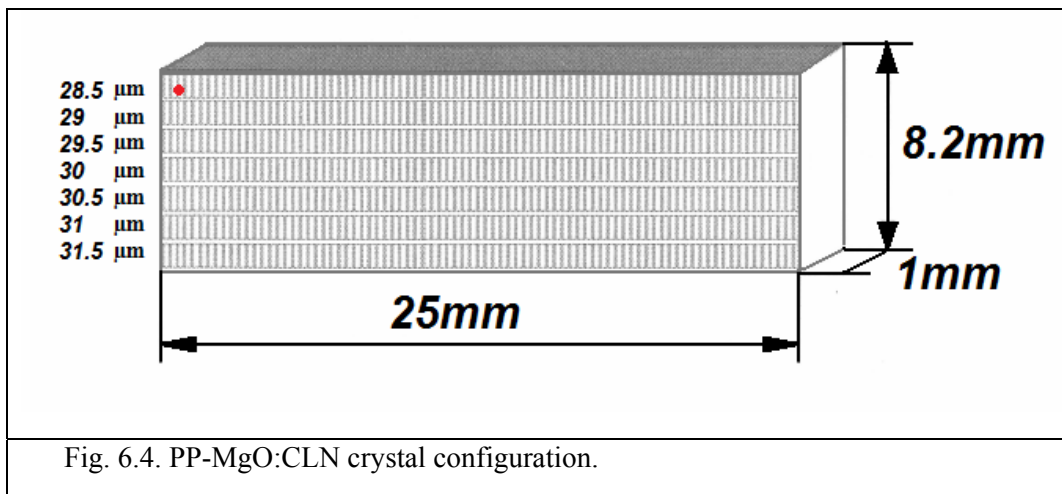
6.2.1. Experimental Setup

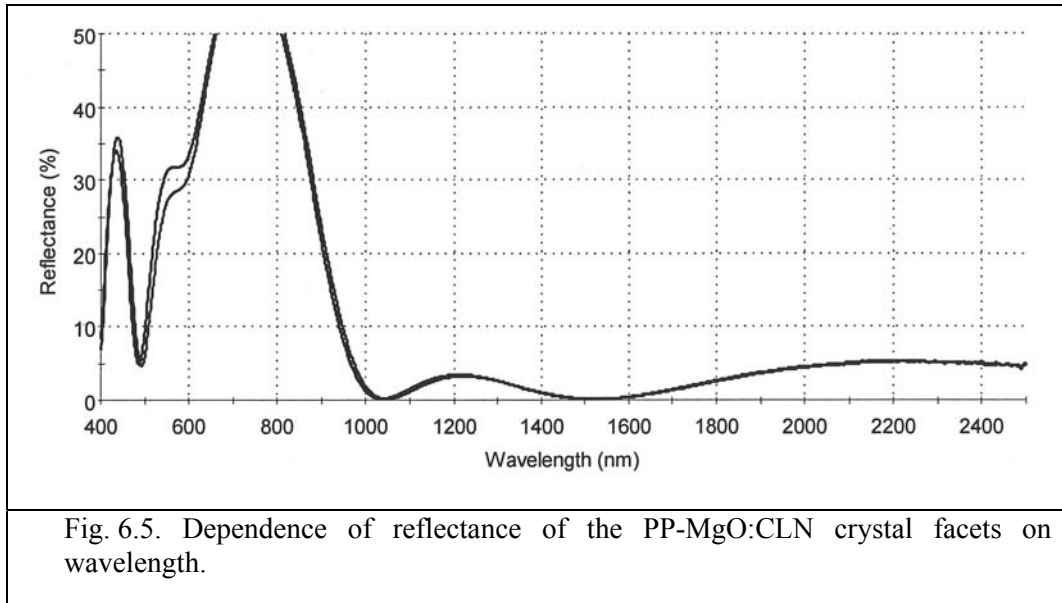
In this work, the linear geometry of an OPO was used due to its superiority in terms of the reduced complexity and mechanical instabilities of the system [6.62]. The experimental setup is shown in Fig. 6.3. It consisted of the pump Q-switched Nd:YAG laser, optical isolator, an uncoated lens with 50 cm focal length, half-wave plate ($\lambda/2$), the periodically poled 5 mol% MgO-doped Congruent Lithium Niobate (PP-MgO:CLN or PPLN) crystal in a temperature stabilised oven with an overall temperature stability and precision control of 0.1°C (Thorlabs TC200) and input (M1) and output (M2) mirrors.



The pump source was a Q-switched Nd:YAG laser (LCS-DTL-324QT), manufactured by Laser-Export Co. LTD (Moscow, Russia), which had a wavelength of 1064 nm, a maximum pulse energy of 30 μ J, a pulse duration of 15 ns and 10 kHz repetition rate. The laser beam was focused at the centre of the PPLN crystal by a 50 cm focal length lens to transform it into an appropriate form for the OPO experiments and maximise the signal and idler output powers. A focused beam diameter of approximately 525 μ m was measured by the moving knife edge method.

The PP-MgO:CLN crystal, manufactured by HP Photonics (Hsinchu, Taiwan), was 25 mm in length and was poled with seven different QPM periods evenly spaced with 0.5 μ m step between 28.5 μ m and 31.5 μ m (Fig. 6.4). The crystal facets were anti-reflective (AR) coated to give a reflectivity $R < 0.49\%$ at the pump wavelength 1064 nm and $R < 0.41\%$ over the signal wavelength range between 1500 nm and 1600 nm (Fig. 6.5).



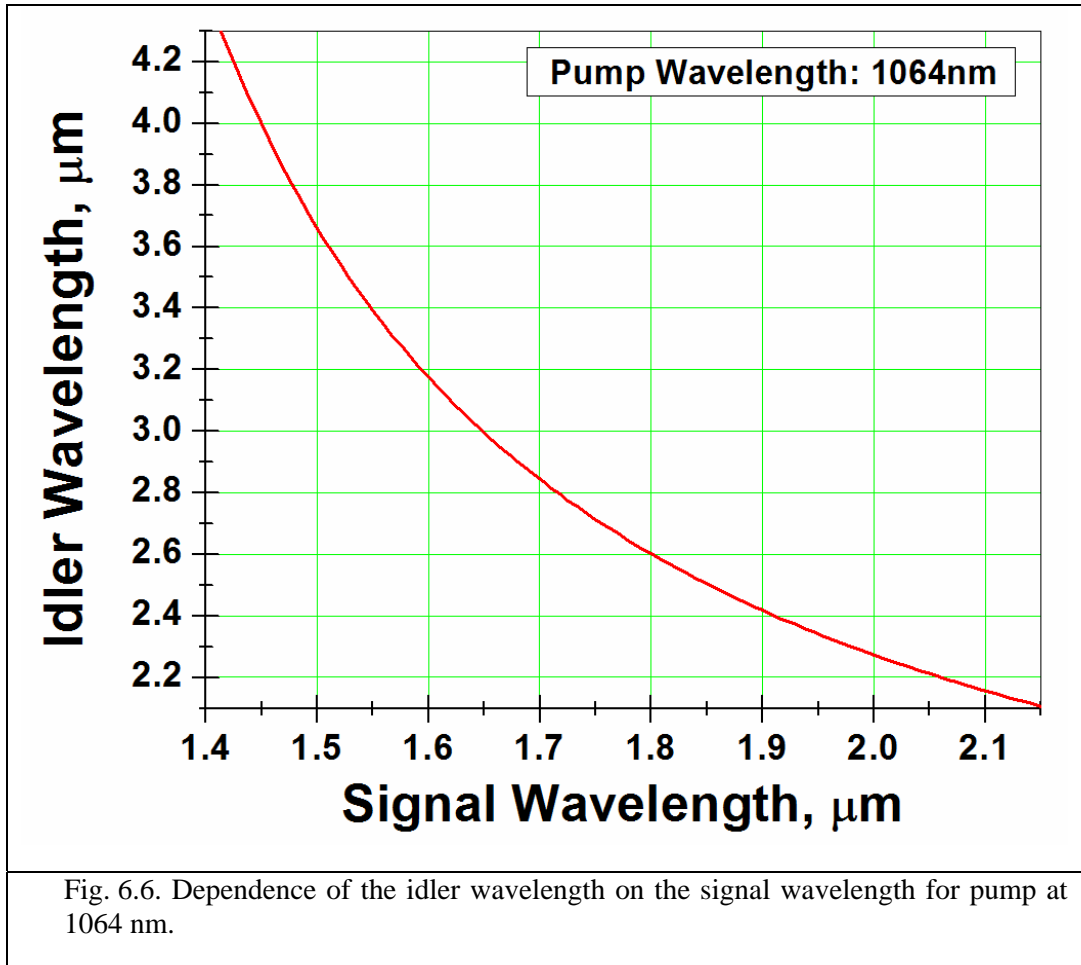


The OPO resonator was formed by a pair of mirrors with 65 mm distance between them. The input mirror M1 (with the radius of curvature $r = 75$ mm) was coated to give a high-reflectance (HR) at the signal wavelength, and the output mirror M2 (with the radius of curvature $r = -75$ mm) had HR at the pump and signal wavelengths and AR at the idler wavelength.

6.2.2. Results and Discussion

The OPO signal and idler spectra were measured for seven grating periods ($\Lambda = 28.5$ - $31.5 \mu\text{m}$) in the temperature range between 24° and 201.3°C . The signal wavelengths in the range between 1430 nm and 1750 nm were measured with an optical spectrum analyser (OSA Advantest Q8383), and the signal wavelengths above 1750 nm were measured with a monochromator/spectrograph (Digikrom DK 480) and PbSe Photoconductive detector (P9696-02). The idler wavelengths were calculated (Fig. 6.6)

using the signal wavelengths and the energy conservation law
$$\frac{1}{\lambda_{\text{pump}}} = \frac{1}{\lambda_{\text{signal}}} + \frac{1}{\lambda_{\text{idler}}}.$$



The measured dependence of the signal and idler wavelengths against temperature for the PP-MgO:CLN crystal is shown in Fig. 6.7 (dots). The combined signal and idler spectra continuously covered the spectral range between 1430 nm and 4157 nm. These results are in good agreement with the theoretical curves (shown in Fig. 6.7 with solid lines) based on the Sellmeier equations for this crystal composition [6.49].

The Sellmeier equation used for the calculation of the theoretical curves is like the one used by Jundt for undoped congruent lithium niobate [6.54].

$$n_e^2 = a_1 + b_1 f + \frac{a_2 + b_2 f}{\lambda^2 - (a_3 + b_3 f)^2} + \frac{a_4 + b_4 f}{\lambda^2 - a_5^2} - a_6 \lambda^2 \quad (6.1)$$

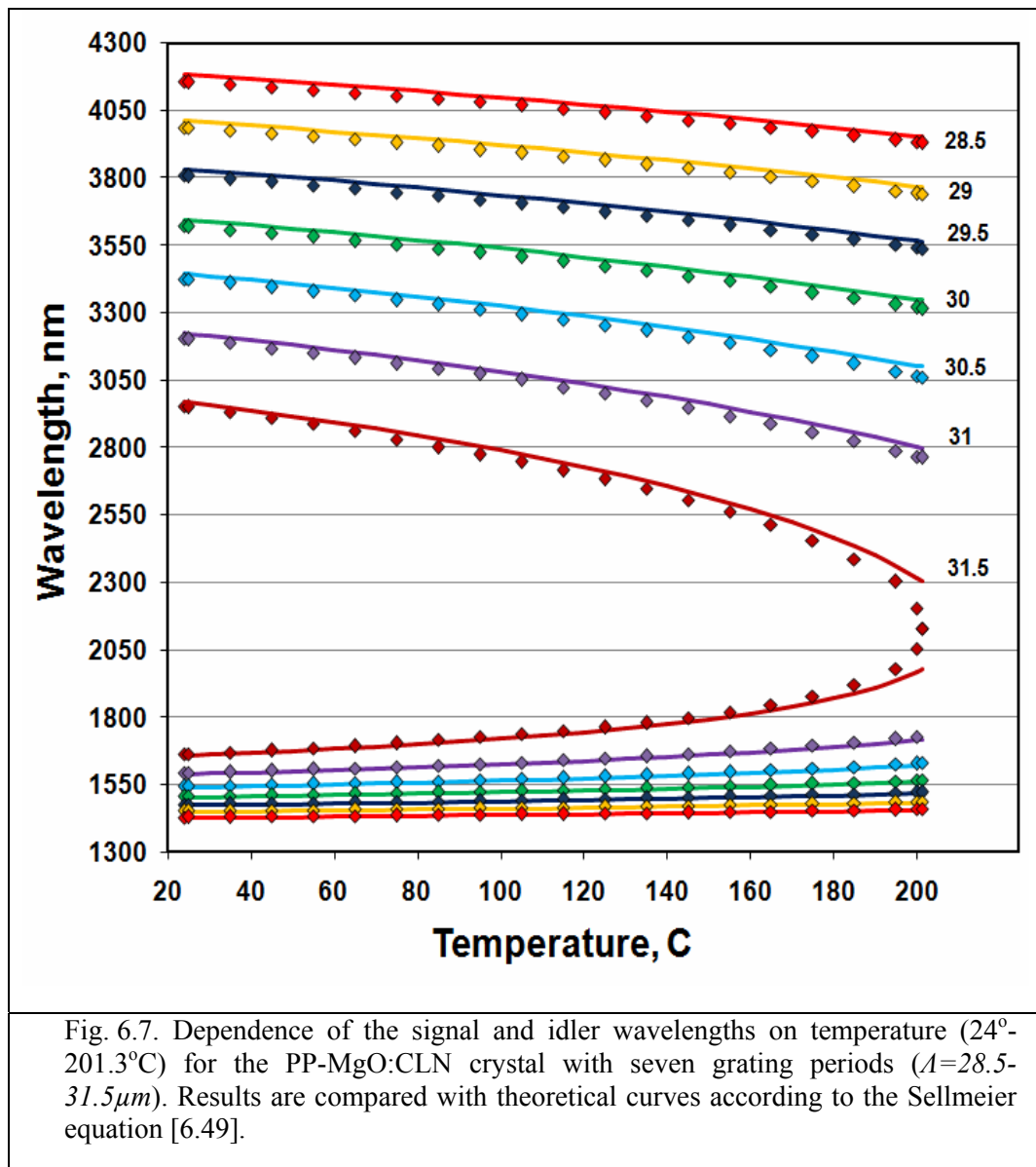
The temperature dependent parameter f is defined as:

$$f = (T - T_0)(T + T_0 + 2 \cdot 273.16) = (T - 24.5^\circ\text{C})(T + 570.82) \quad (6.2)$$

The Sellmeier coefficients for 5 mol% PP-MgO:CLN were taken from reference [6.49]:

$$a_1=5.756; a_2=0.0983; a_3=0.2020; a_4=189.32; a_5=12.52; a_6=1.32 \cdot 10^{-2};$$

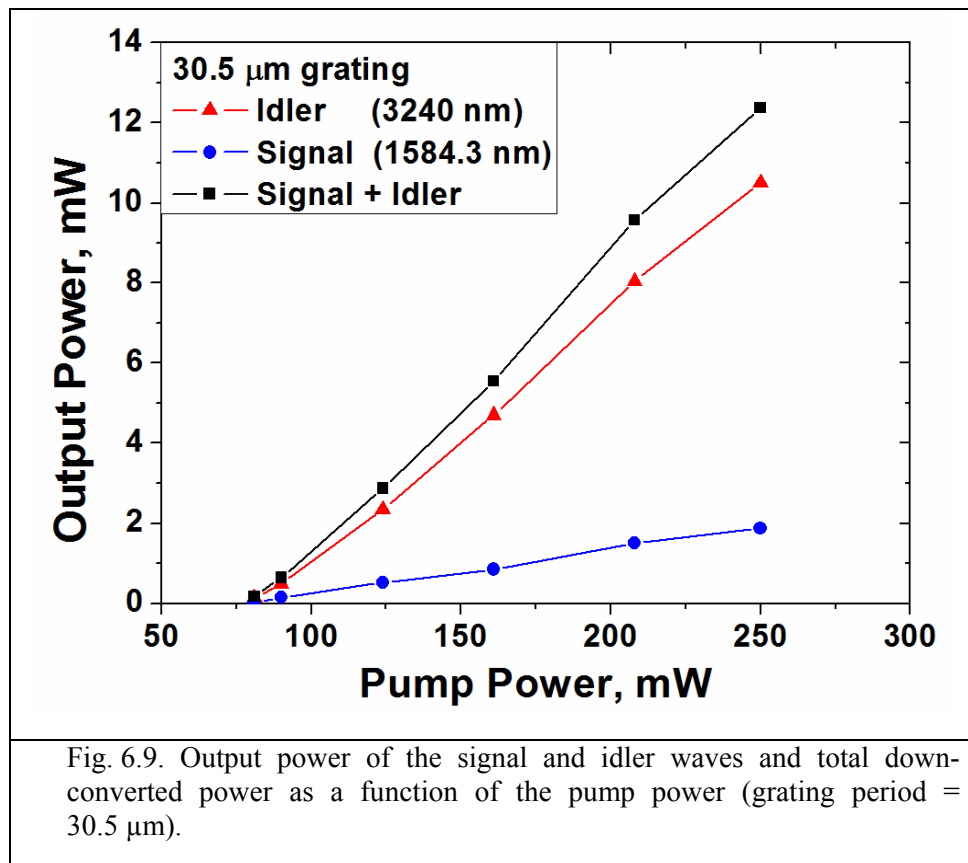
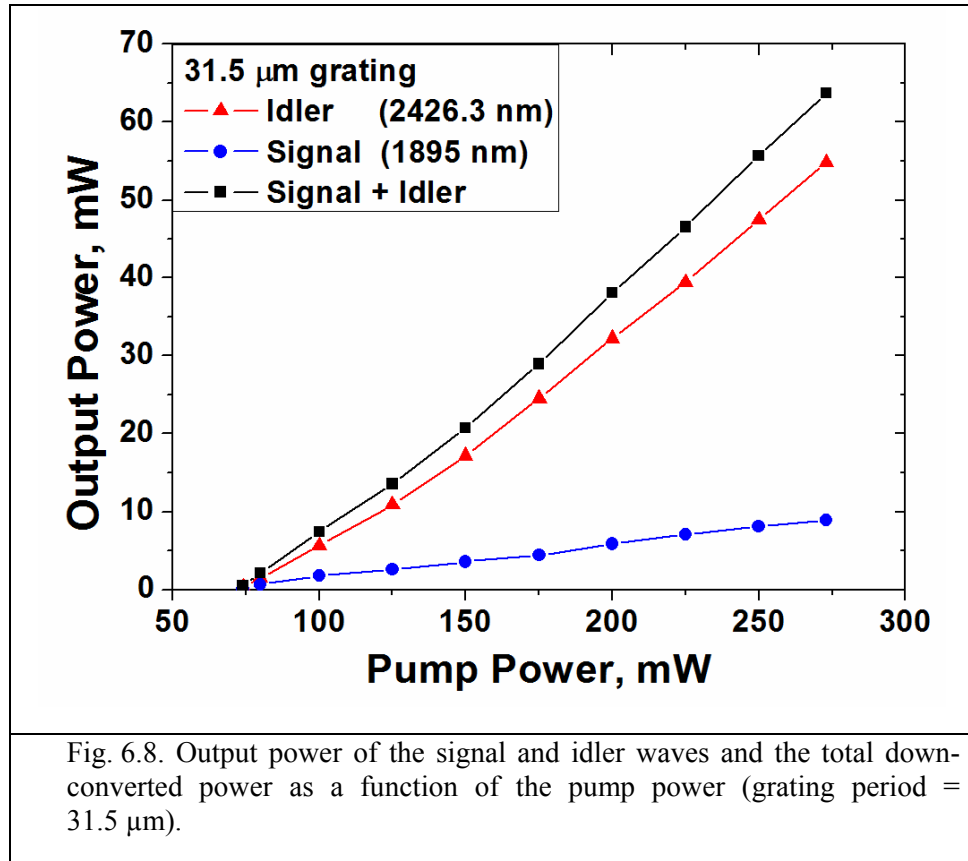
$$b_1=2.860 \cdot 10^{-6}; b_2=4.700 \cdot 10^{-8}; b_3=6.113 \cdot 10^{-8}; b_4=1.516 \cdot 10^{-4}.$$

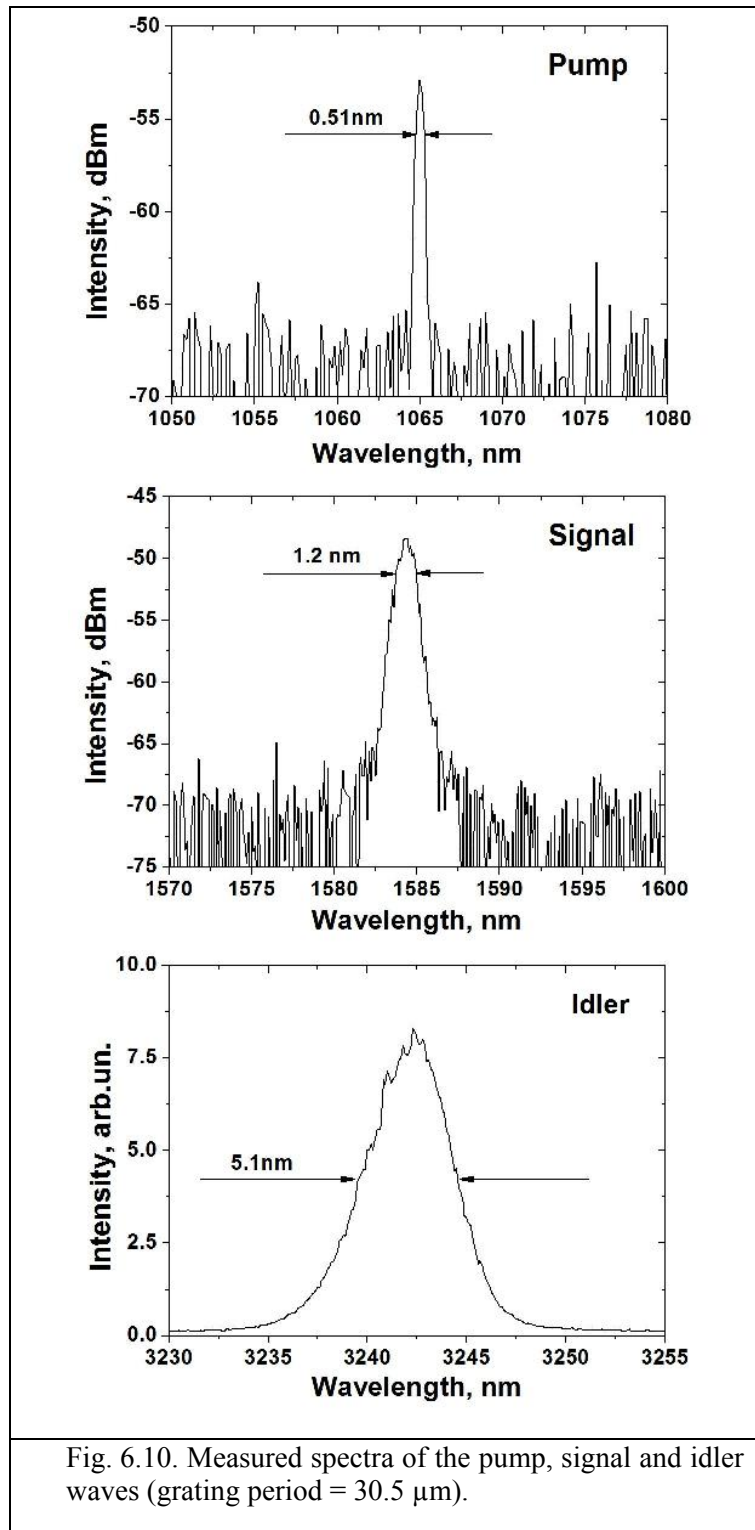


For each PP-MgO:CLN grating period, measurements concerning the output power that could be generated in the signal and idler waves were made (using a broadband powermeter Melles Griot 13PEM001). A maximum average idler output power of 54.82 mW at 2426.3 nm and total down-converted average power of 63.75 mW (at 2426.3 nm and 1895 nm) were achieved for 273 mW of the pump average power at 1064 nm with a PP-MgO:CLN grating period of 31.5 μm (Fig. 6.8). The idler and total down-conversion slope efficiencies were measured to be 27.34 % and 31.8 %, respectively.

Figure 6.9 shows the dependence of the signal (1584.3 nm) and idler (3240 nm) output power and the total down-converted power on the pump power for the PP-MgO:CLN crystal with a 30.5 μm grating period. The maximum idler average output power of 10.5 mW and idler slope efficiency of 6.13 % at 3240 nm were achieved for 250 mW of pump average power at 1064 nm. The total generated power of the signal and idler waves was 12.38 mW at 250 mW of pump average power (Fig. 6.9), corresponding to the total down-conversion slope efficiency of 7.2 %.

The pump, signal and idler wave spectra measured for the grating period 30.5 μm are shown in Fig. 6.10. The optical spectrum of the pump (1064 nm) and signal (1584.3 nm) wavelength exhibited a bandwidth of around 0.51 nm and 1.2 nm, respectively, limited only by the instrumental resolution of the spectrometer (OSA Advantest Q8383). A spectral bandwidth of the idler wave (3242 nm) of ~ 5.1 nm was measured with a monochromator (Digikrom DK 480) and PbSe Photoconductive detector (P9696-02).





The development of the OPO system described in this section was an attempt to obtain a continuously tunable laser source for investigating the possibility of obtaining SHG and development of an OPO system based on orientation-patterned GaAs waveguides, which can potentially cover the wavelength range up to $\sim 16 \mu\text{m}$.

6.3. Orientation-Patterned GaAs Waveguides

The GaAs-based materials have a high damage threshold, low absorption in the IR range (from 1 μm to 16 μm [6.20]) and high thermal conductivity, which make them attractive for IR applications. However, these materials have very high absorption losses particularly at shorter wavelengths [6.63]. Therefore, the periodically poled design in GaAs semiconductor structure is better suited to, and can be successfully realised for frequency conversion (SHG or OPO) into the short-wavelength infrared (1.4 - 3 μm) and mid-infrared (3 - 8 μm) spectral region.

Table 6.1 shows grating coherence lengths required to facilitate conversion in both second harmonic and optical parametric configurations for a range of wavelengths.

The calculations were made using the following Sellmeier equation for GaAs [6.64]:

$$n(\lambda) = \sqrt{1 + 0.186 \cdot \ln\left(\frac{9 \cdot \lambda^2 - 1.537}{2.039 \cdot \lambda^2 - 1.537}\right) + \frac{39.194}{9 - \frac{1.537}{\lambda^2}} + \frac{136.08}{26.01 - \frac{1.537}{\lambda^2}} + \frac{0.00218}{0.00111 - \frac{1.537}{\lambda^2}}} \quad (6.3)$$

Table 6.1. Coherence lengths required for SHG and OPO.

Coherence length, μm	Pump wavelength for SHG, μm	Pump Wavelength for OPO, μm	Signal, μm	Idler, μm
14.5	3.240	1.430	1.799	6.972
		1.450	1.857	6.611
		1.500	2.028	5.761
		1.5843	2.498	4.331
15.75	3.330	1.430	1.746	7.901
		1.450	1.796	7.527
		1.500	1.939	6.625
		1.600	2.363	4.955
25	3.899	1.465	1.613	15.970
		1.500	1.675	14.357
		1.600	1.867	11.188
		1.700	2.100	8.925
		1.800	2.412	7.094

The pump wavelengths in these calculations were chosen because of the available suitable wavelengths from the OPO system described in Section 6.2. The signal and idler wavelengths were chosen to produce light at a variety of wavelengths in an optical parametric generation (OPG).

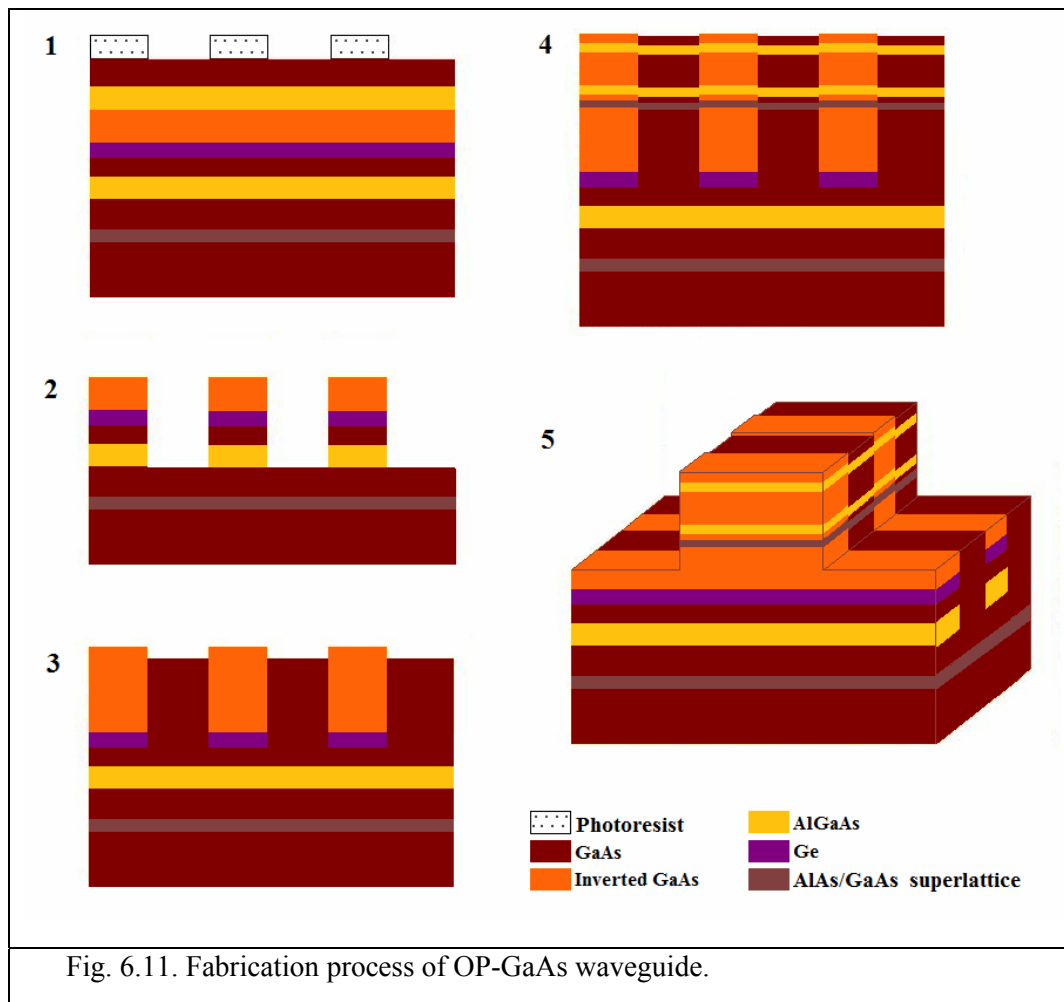
6.3.1. Sample Fabrication: First Structure

The OP-GaAs structures used in our experiment were grown by BAE Systems (Chicago, USA) using our growth design recipe. The preparation of the samples involved a few growth steps (Fig. 6.11). The first growth was initiated on a (100) GaAs substrate misoriented 4° towards (111) with an AlAs/GaAs superlattice buffer growth ($\sim 1 \mu\text{m}$). Then the 1000\AA layer of GaAs and 200\AA of $\text{Al}_{0.75}\text{Ga}_{0.25}\text{As}$ were grown, and after that the growth was completed by a 100\AA layer of GaAs. Then a buffer layer of Ge (40\AA) was grown on top of the GaAs, followed by growth of a 1200\AA GaAs layer, whose crystallographic orientation is rotated 90° around the [100] direction with respect to the substrate equivalent to an inversion in the $\bar{4}3m$ zincblende structure. Then 200\AA of $\text{Al}_{0.75}\text{Ga}_{0.25}\text{As}$ and 200\AA of GaAs were grown to protect GaAs layer from contaminants such as photoresist used for patterning of QPM gratings.

Exposure and development of a photoresist etch mask (with appropriate designed periods) followed by chemical or ion beam etching down to the GaAs layer that lay below Ge layer which produced an orientation grating pattern across the wafer surface. The patterned orientation template produced by such a process after appropriated cleaning was then placed back into the MBE system for re-growth of a thick layer of GaAs ($12.5 \mu\text{m}$) to produce an OP-GaAs template, which was covered by AlAs/GaAs superlattice buffer layer (2000\AA). The next phase in the manufacture was re-growth to

form the active region of GaAs and subsequent AlGaAs deposition to form the upper waveguiding layer and complete the optical waveguide in the vertical direction, as shown in Fig. 6.12.

The final stage of the sample preparation was the etching of the waveguides (with widths of 4, 6, 9, 12, 15 μm) in a direction perpendicular to the grating which was performed using the ion beam etching technique that is particularly well suited to the high quality, high aspect ratio trenches required in such fabrication. This completed the necessary fabrication steps for the test devices.




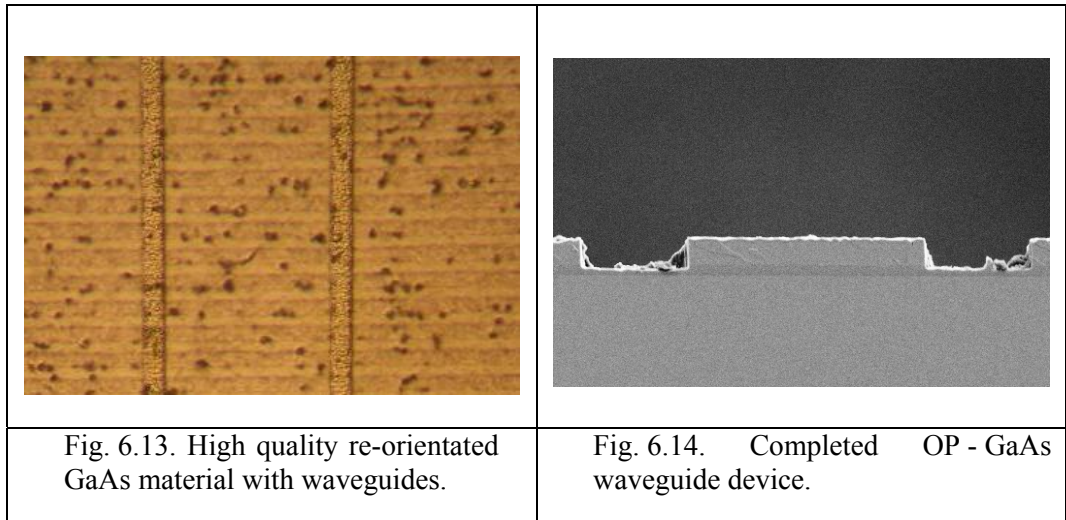
	Layer Thickness, Å	Material	
Cap	100	GaAs	
Waveguiding Layer	2000	Al.75Ga.25As	
GaAs	40000	GaAs	
Waveguiding Layer	5000	Al.75Ga.25As	
GaAs	3000	GaAs	
AlAs	500	AlAs	
SL (AlAs)	50	AlAs	5X
SL (GaAs)	450	GaAs	
GaAs	2500	GaAs	
MEE pause	-	-	
MEE As	-	As	50X
MEE pause	-	-	
MEE Ga	3	GaAs	
Photolithography for MBE REGROWTH			
Cap	200	GaAs	
Etch stop	200	Al.75Ga.25As	
slow GaAs	1200	GaAs	
Inversion layer	40	Ge	
buffer	100	GaAs	
Etch stop	200	Al.75Ga.25As	
GaAs	1000	GaAs	
SL (AlAs)	50	AlAs	20X
SL (GaAs)	450	GaAs	
3" DSP GaAs SI 4° Off Orientation			

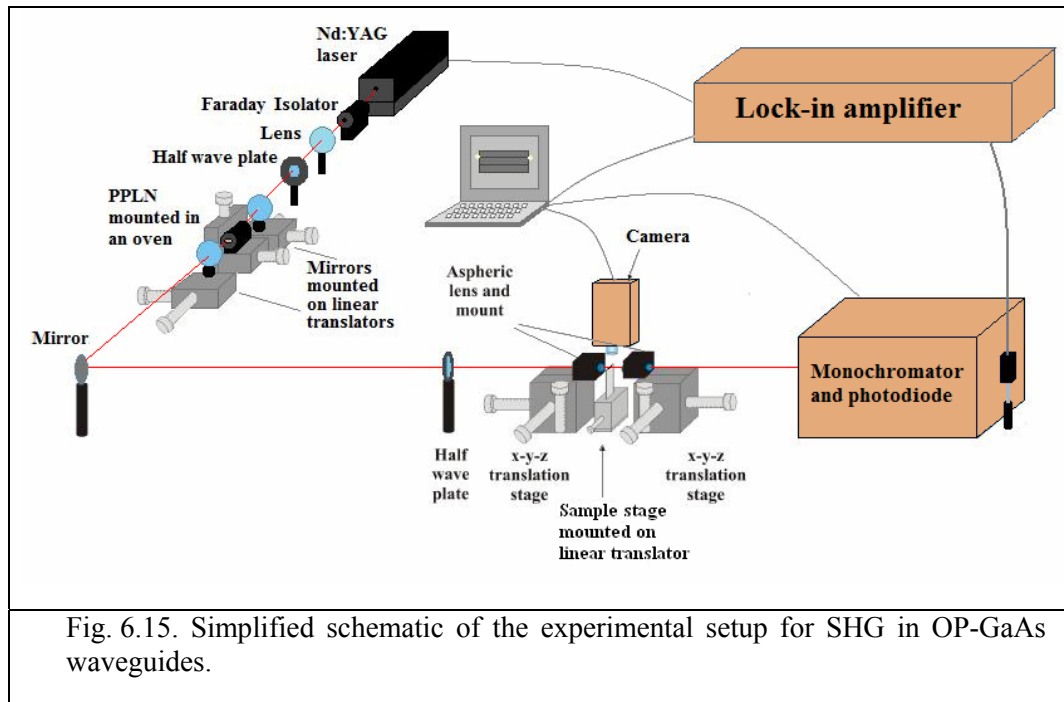
Fig. 6.12. First epitaxial layer structure.

Figures 6.13 and 6.14 demonstrate the high quality periodically re-orientated GaAs waveguides manufactured by the domain inverted methodology outlined above. In Fig. 6.13, two vertical etched channels defining a ridge waveguide with adjacent bulk areas. The horizontal grating defines the planes of oppositely oriented GaAs. Fig. 6.14 shows completed OP-GaAs waveguide device, where the central ridge waveguide formed by the two etched channels (etch depth is about 5.2 μm). Material in the channels is photoresist remaining after the etching process.



6.3.2. Experimental Setup

The experimental setup is shown in Fig. 6.15. This consisted of the OPO system described in Section 6.2, half-wave plate, 40x aspheric lenses (NA of 0.55) and sample mount with a copper heat sink (temperature was controlled by a thermo-electric cooler) on positioning stage. For SHG experiment, the OP-GaAs waveguide samples were fabricated with several grating periods (8 μm , 10 μm and 12 μm) to be tested at different pump wavelengths (2.172 μm , 2.318 μm and 2.449 μm , respectively). The samples were cleaved to several lengths between ~ 0.5 mm and 6 mm. A high resolution CMOS camera (Thorlabs DCC1545M) with long working distance microscope objective was used in the experiment to enable imaging of the waveguide facets and appraisal of the coupling conditions taking place. The OPO produced output at several wavelengths: the SHG beam at 532 nm was used for alignment of the system and the idler beam at around 2 μm was used as the pump for GaAs waveguided samples. After the alignment of the system, an appropriate filter situated after the OPO was used to block “unwanted” light from the OPO.



The investigation of the nonlinear properties of the highest quality devices was performed. During this nonlinear evaluation, the samples were observed to be extremely lossy and no nonlinear signal was observed. It can be explained by the presence of the high corrugation formation during the re-growth process. As seen in Fig. 6.11, the height difference between the inverted GaAs and the original GaAs is conserved during the re-growth process and contributes the final template corrugations. These corrugations impose difficulty in the fabrication of low-loss nonlinear waveguides.

During the course of our investigations, Ota et al. [6.65] reported that low-temperature ($\sim 420^\circ\text{C}$) growth technique can assist to reduce the corrugation formation at the core/clad interface during the re-growth process and the propagation losses in waveguide devices.

6.3.3 Sample Fabrication: Second Structure

The new orientation-patterned GaAs structure was grown by BAE Systems, using low-temperature growth-technique [6.65] to reduce the corrugation formation during the re-growth process. The epitaxial layer structure was also modified, as depicted in Fig. 6.16, in order to optimise our OP-GaAs devices and reduce losses.


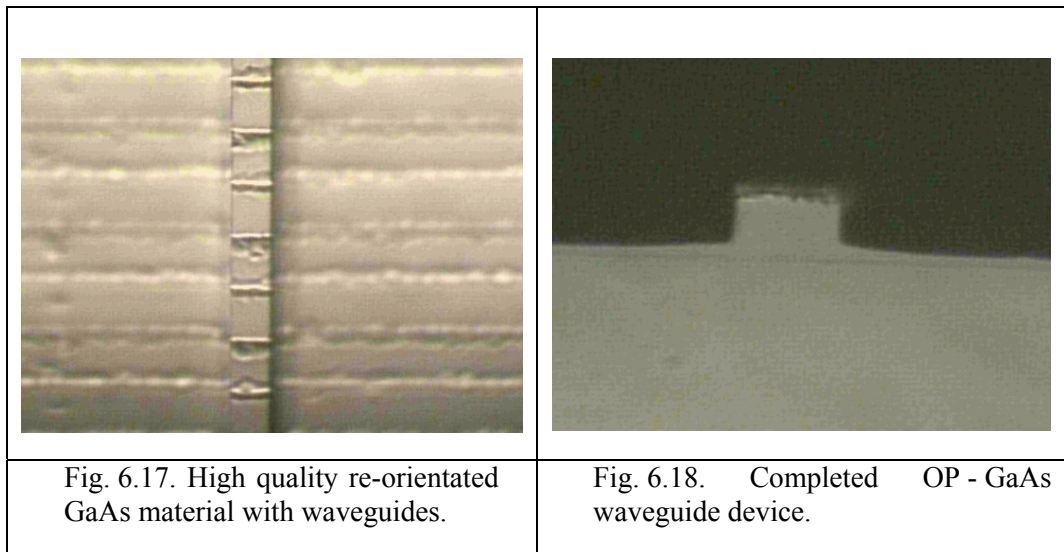
	Layer Thickness, Å	Material	
Cap	100	GaAs	
Waveguiding Layer	2000	Al _{0.3} Ga _{0.7} As	
Waveguiding Layer	5000	Al _{0.1} Ga _{0.9} As	
GaAs	60000	GaAs	
Waveguiding Layer	5000	Al _{0.1} Ga _{0.9} As	
Waveguiding Layer	2000	Al _{0.3} Ga _{0.7} As	
GaAs	3000	GaAs	
AlAs	500	AlAs	
SL (AlAs)	50	AlAs	5X
SL (GaAs)	450	GaAs	
GaAs	2500	GaAs	50X
MEE pause	-	-	
MEE As	-	As	
MEE pause	-	-	
MEE Ga	3	GaAs	
Photolithography for MBE REGROWTH			
Cap	200	GaAs	
Etch stop	200	Al _{0.75} Ga _{0.25} As	
slow GaAs	1200	GaAs	
Inversion layer	40	Ge	
buffer	100	GaAs	
Etch stop	200	Al _{0.75} Ga _{0.25} As	
GaAs	1000	GaAs	
SL (AlAs)	50	AlAs	20X
SL (GaAs)	450	GaAs	
3" DSP GaAs SI 4° Off Orientation			

Fig. 6.16. Second epitaxial layer structure.

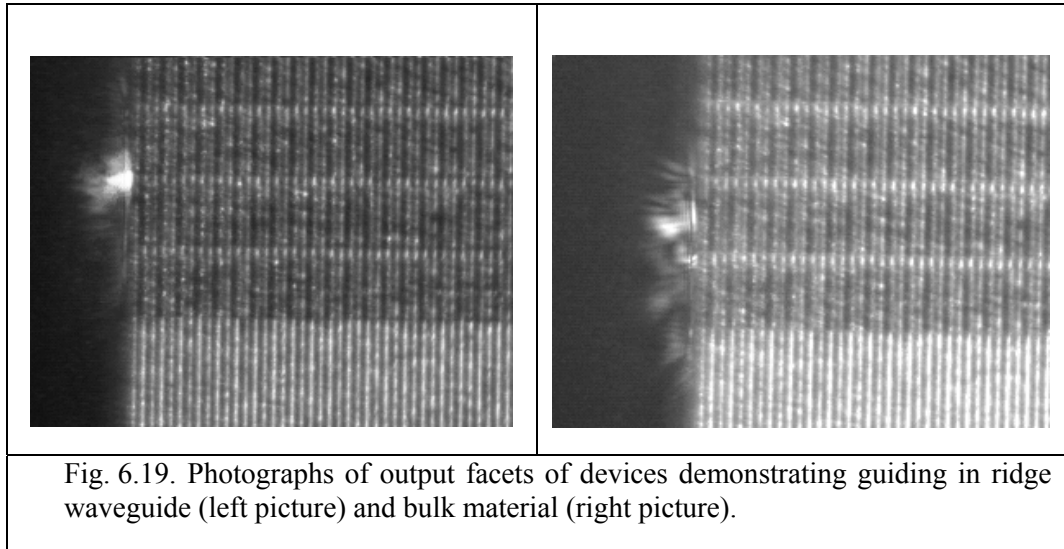
At the final stage of the sample preparation, the waveguides of width 4, 6, 9, 12 and 15 μm were defined in the material in a direction perpendicular to the grating. Figures 6.17 and 6.18 show an orientation-patterned GaAs waveguided structure. It was etched down to a depth of 7.6 μm to define the mesa waveguides. Figure 6.17 shows one vertical etched ridge waveguide channel. Cross-section of the waveguide after etching is shown in Fig.6.18.



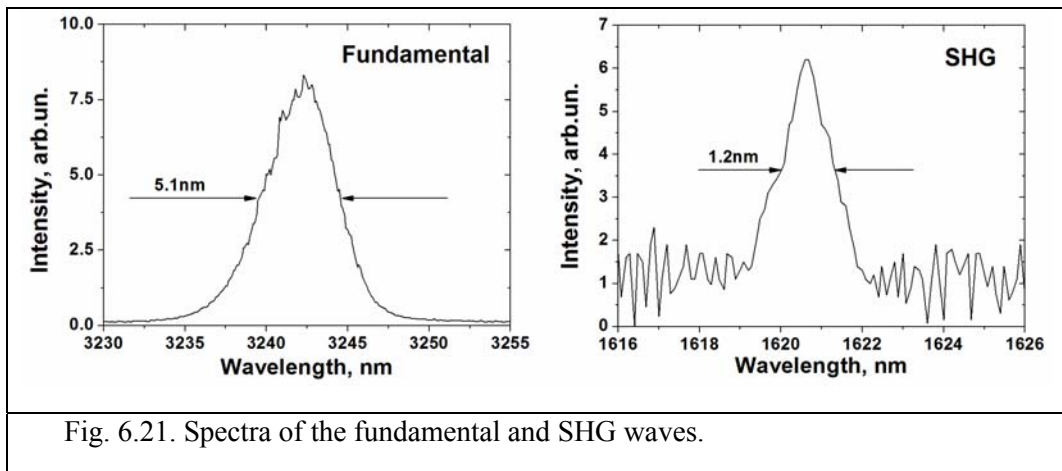
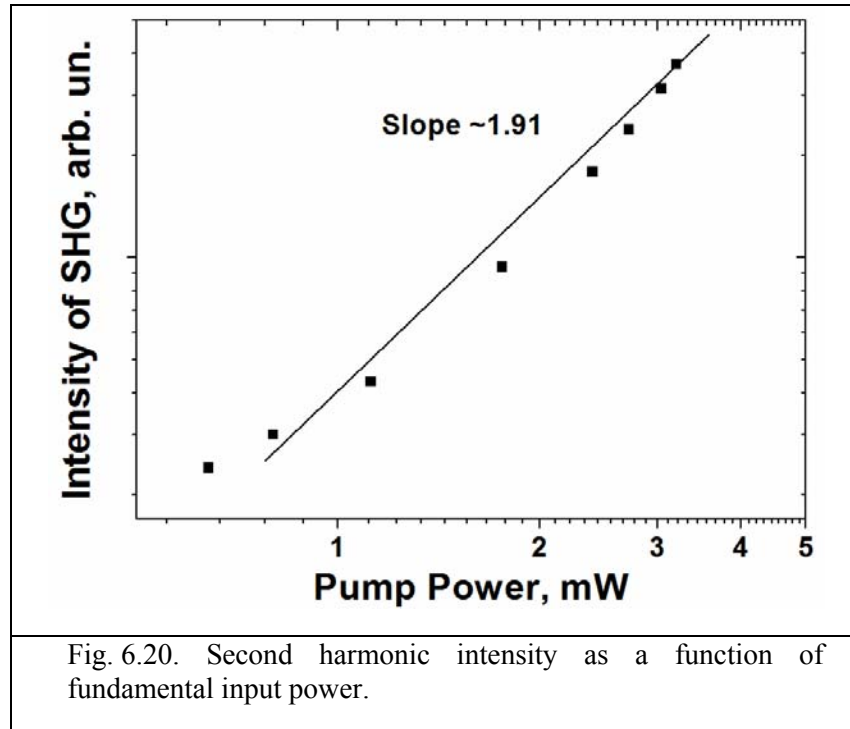
6.3.4. Experimental Results

The experimental setup was similar to that already been described in Section 6.3.2. The OP-GaAs structure was fabricated with several grating periods. The samples of different length with coherence length of 14.5 μm were tested to observe SHG. The idler wave from OPO at 3.240 μm was used as the pump for GaAs samples. Alignment of the system and appraisal of the coupling conditions taking place was aided by the use of a high resolution CMOS camera (Thorlabs DCC1545M) with long distance microscope objective, which was situated above the sample and focused in the plane of the waveguides. The SHG beam at 532 nm from OPO system assisted in this alignment. A dense bright spot at both the input and output waveguide facets was a sign that

successful waveguide coupling was taking place. Figure 6.19 shows guiding in ridge waveguide and bulk material, which were observed during the experiment.



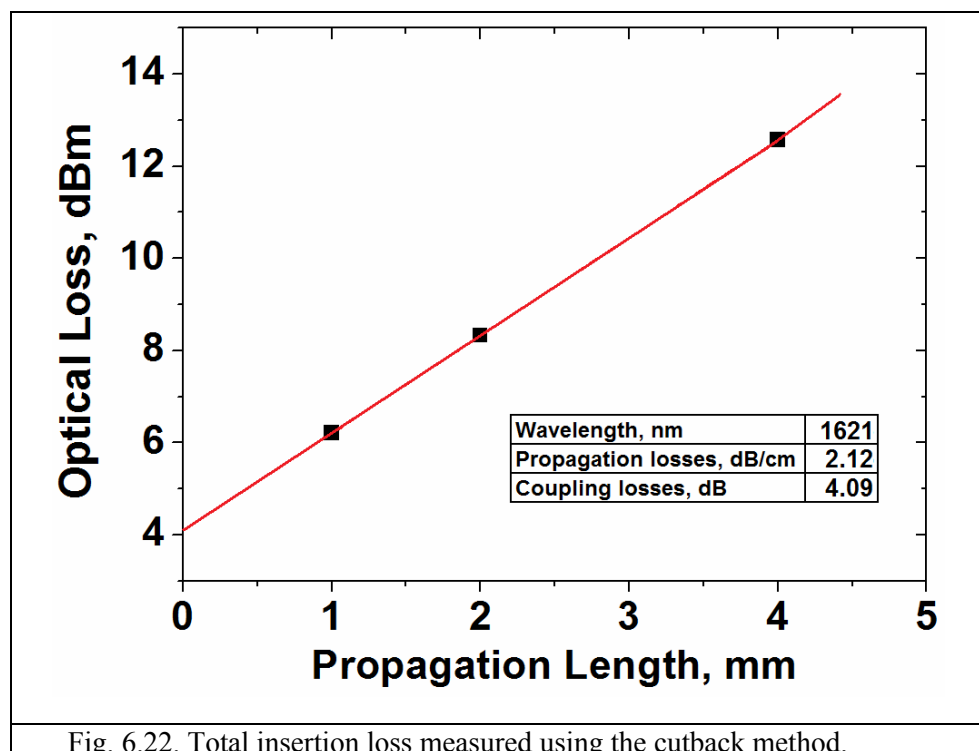
An OP-GaAs waveguide with a length of ~ 4 mm and a width of $15 \mu\text{m}$ was selected to examine the possibility of obtaining second harmonic generation. According to our calculation (Table 6.1), a wavelength of 3240 nm was chosen as a suitable pump for the sample with coherence length of $14.5 \mu\text{m}$. For measurements of the frequency doubled light a high speed InGaAs detector, assisted via lock-in amplifier, was used to register the SHG signal. The SHG intensity is plotted in Fig. 6.20 as a function of the fundamental wavelength launched into the OP-GaAs waveguide. The data shows the expected quadratic response for a QPM-SHG process, as can be seen from the linear fit which has a slope of ~ 1.91 (Fig. 6.20). The SHG signal vanished when the polarization of the fundamental wavelength was rotated by 90° . The spectra of the fundamental (3242 nm) and SHG (1621 nm) wavelengths were measured with a monochromator (Digikrom DK 480) and PbSe Photoconductive detector (P9696-02), as shown in Fig. 6.21. The optical spectrum of the fundamental and second harmonic waves exhibited a bandwidth of around 5.1 nm and 1.2 nm, respectively.



These results show experimental evidence of possibility to fabricate a QPM structure in GaAs waveguide for SHG. The use of antireflection coatings on the nonlinear crystal facets and the optimisation of focusing optics to minimise coupling losses can assist in the improvement of the system.

6.3.5. Loss Measurement in OP-GaAs Waveguides

OP-GaAs waveguide loss measurements were made using the cutback method, previously described in Section 5.3. The OP-GaAs waveguides used in this work were identical and had a width of 15 μm and 3 different lengths: 4 mm, 2 mm and 1 mm. The experimental setup for loss measurements is shown in Fig.6.15. The 1621 nm wavelength from the OPO system was chosen as a pump for the OP-GaAs waveguide loss measurements. By using Equation 5.2, the propagation losses were estimated to be around 2.12 dB/cm, which is comparable to the lowest losses reported to date for OP-GaAs waveguides [6.45]. The total losses shown in Fig. 6.22 were calculated using the similar equation containing input power coupled to the waveguide and output power for each sample. In Fig. 6.22, the trendline cuts the y-axis above the origin. This is because the data shows insertion loss, and hence the loss corresponding to zero propagation length is the coupling loss to the waveguide [6.66]. The coupling losses were estimated to be around 4.09 dB.



6.4. Summary

The investigations undertaken in this chapter sought to evaluate the suitability of new developed QPM technique (orientation-patterning) to fabricate low-loss “periodically poled” GaAs waveguided devices for nonlinear frequency conversion, as the laser sources based on the orientation-patterned semiconductor crystals can be suitable for studies in gas sensing, atmospheric transmission, telecommunications and medical applications.

The possibility of obtaining second harmonic generation in orientation-patterned GaAs waveguide was demonstrated. For this experimental work, an optical parametric oscillator based on the periodically poled 5 mol% MgO-doped congruent lithium niobate, which is tunable between 1430 nm and 4130 nm, was built. Using this extremely versatile source, frequency doubled light at 1621 nm in periodically poled GaAs waveguide was demonstrated. The losses in OP-GaAs waveguides were also estimated.

In the future, the use of antireflection coatings on the GaAs crystal facets and the optimisation of focusing optics to minimise coupling losses could assist in the improvement of the system. Another approach which could also yield improved performance relates to the minimisation of corrugation and its associated losses in the waveguide core.

Orientation-patterned GaAs waveguides have shown extremely promising results and the optimisation of the system and subsequent implementation of the orientation-patterning technique in optical parametric oscillator can lead to generation of wavelengths up to 16 μm . This work is currently under way.

6.5. References

- [6.1] M.M. Fejer, G.A. Magel, D.H. Jundt, R.L. Byer, "Quasi-phase-matched second harmonic generation: tuning and tolerances," *IEEE J. Quantum Electron.* **28**(11), pp.2631-2634 (1992).
- [6.2] M. Yamada, N. Nada, M. Saitoh, K. Watanabe, "First-order quasiphase matched LiNbO₃ waveguide periodically poled by applying an external field for efficient blue second-harmonic generation", *Appl. Phys. Lett.* **62**, pp.435-436 (1993).
- [6.3] M. Nakamura, M. Kotoh, H. Taniguchi, K. Tadamoto, "Bulk Periodically Poled MgO-doped LiNbO₃ by External Electric Field Application," *Jpn. J. Appl. Phys.* **38**, pp.L512-L514 (1999).
- [6.4] V. Gopalan, T.E. Mitchell, "In situ video observation of 180° domain switching in LiTaO₃ by electro-optic imaging microscopy," *J. Appl. Phys.* **85**, pp.2304-2311 (1999).
- [6.5] M.J. Missey, S. Russel, V. Dominic, R.G. Batchko, K.L. Schepler, "Real-time visualization of domain formation in periodically poled lithium niobate," *Opt. Exp.* **6**, pp.186-195 (2000).
- [6.6] V.Y. Shur, E.L. Romyantsef, E.V. Nikolaeva, E.I. Shishkin, D.V. Fursov, R.G. Batchko, L.A. Eyres, M.M. Fejer, R.L. Byer, "Nanoscale backswitched domain patterning in lithium niobate," *Appl. Phys. Lett.* **76**, pp.143-145 (2000).
- [6.7] K. Mizuuchi, K. Yamamoto, "Harmonic blue light generation in bulk periodically poled LiTaO₃," *Appl. Phys. Lett.* **66**, pp. 2943-2945 (1995).
- [6.8] S.N. Zhu, Y.Y. Zhu, Z.Y. Zhang, H. Shu. H.F. Wang, N.B. Ming, "LiTaO₃ crystal periodically poled by applying an external pulsed field," *J. Appl. Phys.* **77**(10), pp.5481-5483 (1995).
- [6.9] Q. Chen, W.P. Risk, "Periodic poling of KTiOPO₄, using an applied electric field," *Electron. Lett.* **30**, pp.1516-1517 (1994).
- [6.10] D. Eger, M. Oron, M. Katz, A. Reizman, G. Rosenman, A. Skliar, "Quasi-phase-matched waveguides in electric field poled, flux grown KTiOPO₄," *Electron. Lett.* **33**, pp.1548-1550 (1997).
- [6.11] M. Peltz, U. Bader, A. Borsutzky, R. Wallenstein, J. Hellstrom, H. Karlsson, V. Pasiskevicius, F. Laurell, "Optical parametric oscillators for high pulse

- energy and high average power operation based on large aperture periodically poled KTP and RTA,” *Appl. Phys. B* **73**, pp.663-670 (2001).
- [6.12] H. Karlsson, F. Laurell, P. Henriksson, G. Arvidsson, “Frequency doubling in periodically poled RbTiOAsO₄,” *Electron. Lett.* **32**, pp.556-557 (1996).
- [6.13] J.-P. Meyn, M.E. Klein, D. Woll, R. Wallenstein, D. Rytz, “Periodically poled potassium niobate for second-harmonic generation at 463nm,” *Opt. Lett.* **24**, pp.1154–1156 (1999).
- [6.14] T.Sugita, K.Mizuuchi, Y.Kitaoka and K.Yamamoto, “31%-efficient blue second-harmonic generation in a periodically poled MgO:LiNbO₃ waveguide by frequency doubling of an AlGaAs laser diode,” *Opt. Lett.* **24**, pp.1590 (1999).
- [6.15] D.J.L. Birkin, E.U. Rafailov, G.S. Sokolovskii, W. Sibbett, G.W. Ross, P.G.R. Smith, D.C. Hanna, “3.6 mW blue light by direct frequency doubling of a diode laser using an aperiodically poled lithium niobate crystal,” *Appl. Phys. Lett.* **78** (21), pp.3172 (2001).
- [6.16] M.W. Street, N.D. Whitbread, C.J. Hamilton, B. Vogel, C.R. Stanley, D.C. Hutchings, J.H. Marsh, J.S. Aitchison, G.T. Kennedy, W. Sibbett, “Modification of the second-order optical nonlinearities in AlGaAs asymmetric multiple quantum well waveguides by quantum well intermixing,” *Appl. Phys. Lett.* **70**, pp.2804 (1997).
- [6.17] D. Zheng, L.A. Gordon, Y.S. Wu, R.S. Feigelson, M.M. Fejer, R.L. Byer, K.L. Vodopyanov, “16- μ m infrared generation by difference-frequency mixing in diffusion-bonded-stacked GaAs,” *Opt. Lett.* **23**, pp.1010-1012 (1998).
- [6.18] A. Saher Helmy, D.C. Hutchings, T.C. Kleckner, J.H. Marsh, A.C. Bryce, J.M. Arnold, C.R. Stanley, J.S. Aitchison, C.T.A. Brown, K. Moutzouris, M. Ebrahimzadeh, “Quasi-phase matched second harmonic generation by modulation bulk-like $\chi^{(2)}$ coefficients in GaAs-AlAs superlattices by quantum well intermixing,” Tech. Digest, CLEO’2000, San Francisco, Postdeadline PD25 (2000).
- [6.19] E.U. Rafailov, P. Loza-Alvarez, C.T.A. Brown, W. Sibbett, R.M. De La Rue, P. Millar, D.A. Yanson, J.S. Roberts, P.A. Houston, “Second-harmonic generation from a first-order quasi-phase-matched GaAs/AlGaAs waveguide crystal,” *Opt. Lett.* **26**(24), pp.1984-1986 (2001).

- [6.20] D.V. Petrov, "Nonlinear phase shift by cascaded quasi-phase-matched second harmonic generation," *Opt. Commun.* **131**, pp.102-106 (1996).
- [6.21] H. Komine, W.H. Long, Jr. J.W. Tully, E.A. Stappaerts, "Quasi-phase-matched second-harmonic generation by use of a total-internal-reflection phase shift in gallium arsenide and zinc selenide plates," *Opt. Lett.* **23**, pp.661 (1998).
- [6.22] I. Shoji, T. Kondo, A. Kitamoto, M. Shirane, R. Ito, "Absolute scale of second-order nonlinear-optical coefficients," *J. Opt. Soc. Am. B* **14**, pp.2268-2294 (1997).
- [6.23] L. Gordon, G.L. Woods, R.C. Eckardt, R.R. Route, R.S. Feigelson, M.M. Fejer, R.L. Byer, "Diffusion-bonded stacked GaAs for quasiphasematched second-harmonic generation of a carbon dioxide laser," *Electron. Lett.* **29**, pp.1942 (1993).
- [6.24] S.J.B. Yoo, R. Bhat, C. Caneau, M.A. Koza, "Quasi-phase-matched second-harmonic generation in AlGaAs waveguides with periodic domain inversion achieved by wafer-bonding," *Appl. Phys. Lett.* **66**, pp.3410 – 3412 (1995).
- [6.25] S.J.B. Yoo, C. Caneau, R. Bhat, M.A. Koza, A. Rajhel, N. Antoniadis, "Wavelength conversion by difference frequency generation in AlGaAs waveguides with periodic domain inversion achieved by wafer bonding," *Appl. Phys. Lett.* **68**, pp.2609–2611 (1996).
- [6.26] E.U. Rafailov, P. Loza-Alvarez, W. Sibbett, "Novel methods for quasi-phasematching in nonlinear optical crystals," UK Patent 0105415.4 (2001).
- [6.27] D. Artigas, E.U. Rafailov, P. Loza-Alvarez, W. Sibbett, "Periodically switched nonlinear structured for frequency conversion: theory and experimental demonstration," *IEEE J. Quantum Electron.* **40**(8), pp.1122-1130 (2004).
- [6.28] A.D. McRobbie, "Novel semiconductor based light sources," PhD Thesis, St.Andrews (2008).
- [6.29] S. Koh, T. Kondo, T. Ishiwada, C. Iwamoto, H. Ichinose, H. Yaguichi, T. Usami, Y. Shiraki, R. Ito, "Sublattice Reversal in GaAs/Si/GaAs (100) Heterostructures by Molecular Beam Epitaxy," *Jpn. J. Appl. Phys.* **37**, pp.L1493 – L1496 (1998).
- [6.30] C.B. Ebert, L.A. Eyres, M.M. Fejer, Jr. J.S. Harris, "MBE growth of antiphase GaAs films using GaAs/Ge/GaAs heteroepitaxy," *J. Crystal Growth* **201/202**, pp.187–193 (1999).

- [6.31] T. Kondo, S. Koh, R. Ito, "Sublattice reversal epitaxy: a novel technique for fabricating domain-inverted compound semiconductor structures," *Sci. Technol. Mater.* **1**, pp.173-179 (2000).
- [6.32] L.A. Eyres, P.J. Tourreau, T.J. Pinguet, C.B. Ebert, J.S. Harris, M.M. Fejer, L. Becouarn, B. Gerard, E. Lallier, "All-epitaxial fabrication of thick, orientation-patterned GaAs films for nonlinear optical frequency conversion," *Appl. Phys. Lett.* **79**(7), pp.904 (2001).
- [6.33] S. Strite, D. Biswas, N. S. Kumar, M. Fradkin, H. Morkoc, "Antiphase domain free growth of GaAs on Ge in GaAs/Ge/GaAs heterostructures," *Appl. Phys. Lett.* **56**(3), pp.244-246 (1990).
- [6.34] T. Suhara, M. Fujimura, *Waveguide Nonlinear-Optic Devices* (Springer, Berlin, 2003).
- [6.35] D. Artigas, P. Loza-Alvarez, E.U. Rafailov, A.D. McRobbie, W. Sibbett, "Design parameters of periodically switched nonlinear structures for efficient nonlinear processes," OSA Trends in Optics and Photonics series. Advanced Solid-State Photonics, I. Sorokina Ed., **98**, pp.86-91 (2005).
- [6.36] S. Koh, T. Kondo, Y. Shiraki, R. Ito, "GaAs/Ge/GaAs sublattice reversal epitaxy and its application to nonlinear optical devices," *J. Crystal. Growth* **227-228**, pp.183-192 (2001).
- [6.37] T.J. Pinguet, L. Scaccabarozzi, O. Levi, T. Scauli, L.A. Eyres, M.M. Fejer, J.S. Harris, "Second Harmonic Generation in Orientation-Patterned AlGaAs Waveguides Pumped at 1.55 μm ," The 14th Annual Meeting of the IEEE Lasers & Electro-Optics Society (LEOS 2001), San Diego, CA, pp.376-377 (2001).
- [6.38] X. Yu, L. Scaccabarozzi, O. Levi, T.J. Pinguet, M.M. Fejer, J.S. Harris Jr., "Template design and fabrication for low-loss orientation-patterned nonlinear AlGaAs waveguides pumped at 1.55 μm ," *J. Crystal Growth* **251**, pp.794-799 (2003).
- [6.39] X. Yu, L. Scaccabarozzi, J.S. Harris Jr., P.S. Kuo, M.M. Fejer, "Efficient continuous wave second harmonic generation pumped at 1.55 μm in quasi-phase-matched AlGaAs waveguides," *Opt. Exp.* **13**(26), pp.10742-10748 (2005).

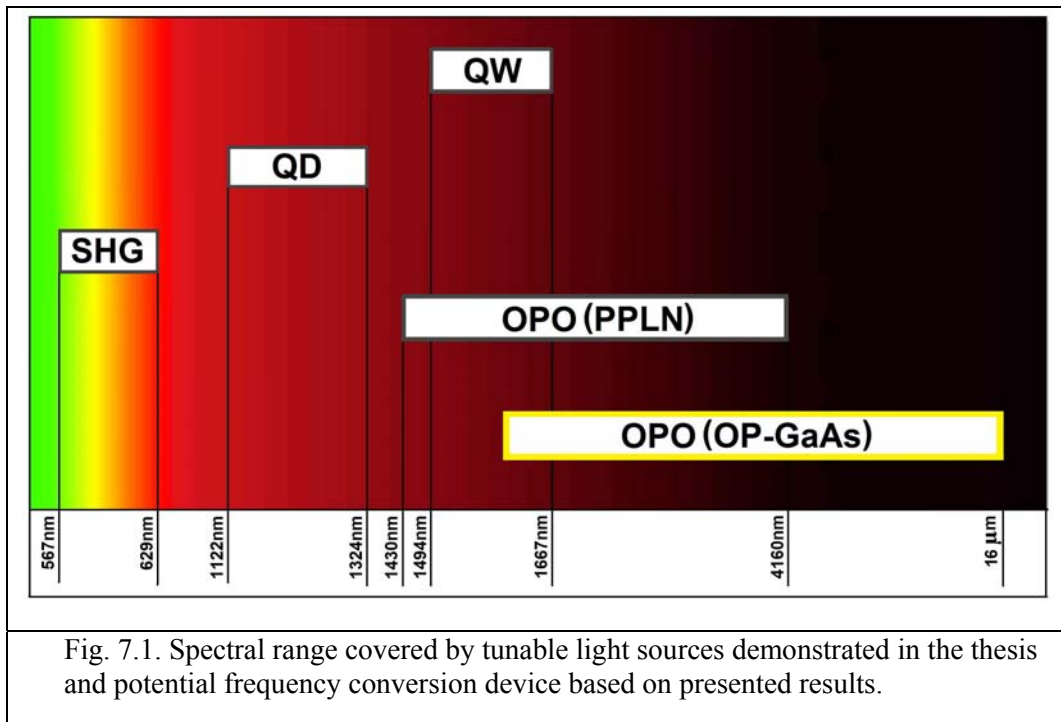
- [6.40] T. Kondo, I. Shoji, "Study on wavelength conversion by compound-semiconductor-based quasi phase-matching devices," *Photonics Based on Wavelength Integration and Manipulation IPAP Books* **2**, pp.155-160 (2005).
- [6.41] T. Skali, K.L. Vodopyanov, T.J. Pinguet, A. Schober, O. Levi, L.A. Eyres, M.M. Fejer, J.S. Harris, B. Gerard, L. Becouarn, E. Lallier, G. Arisholm, "Measurement of the nonlinear coefficient of orientation-patterned GaAs and demonstration of highly efficient second-harmonic generation," *Opt. Lett.* **27**(8), pp.628-630 (2002).
- [6.42] K.L. Vodopyanov, O. Levi, P.S. Kuo, T.J. Pinguet, J.S. Harris, M.M. Fejer, B. Gerard, L. Becouarn, E. Lallier, "Optical parametric oscillation in quasi-phase-matched GaAs," *Opt. Lett.* **29**(16), pp.1912-1914 (2004).
- [6.43] T. Kondo, "Semiconductor Guided-Wave Wavelength Conversion Devices," CLEO, Baltimore, CThD4 (2009).
- [6.44] I. Ohta, T. Matsushita, J. Ohta, T. Kondo, "Quasi Phase Matched Parametric Fluorescence in High-Quality GaAs/AlGaAs Waveguides," ASSP, Nara, p.MC31 (2008).
- [6.45] M.B. Oron, P. Blau, S. Pearl, S. Shusterman, "Efficient Second Harmonic Generation in Orientation Patterned GaAs Waveguides," CLEO, San Jose, CThEE3 (2010).
- [6.46] M. Ebrahim-Zadeh, I.T. Sorokina, *Mid-Infrared Coherent sources and Applications* (Springer, Dordrecht, 2008).
- [6.47] K. Mizuuchi, A. Morikawa, T. Sugita, K. Yamamoto, "Electric-field poling in Mg-doped LiNbO₃," *J. Appl. Phys.* **96**, pp.6585-6590 (2004).
- [6.48] Y.L. Chen, W.G. Yan, J. Guo, G.Y. Zhang, "Effect of Mg concentration on the domain reversal of Mg-doped LiNbO₃," *Appl. Phys. Lett.* **87**, pp.212904 (2005).
- [6.49] O. Gayer, Z.Sacks, E. Galun, A. Arie, "Temperature and wavelength dependent refractive index equations for MgO-doped congruent and stoichiometric LiNbO₃," *Appl. Phys. B* **91**, pp.343-348 (2008).
- [6.50] T. Andres, P. Haag, S. Zelt, J.-P. Meyn, A. Borsutzky, R. Beigang, R. Wallenstein, "Synchronously pumped femtosecond optical parametric oscillator of congruent and stoichiometric MgO-doped periodically poled lithium niobate," *Appl. Phys. B* **76**(3), pp.241-244 (2003).

- [6.51] A.K.Y. Ngai, S. T. Persijn, G. Von Basum, F.J.M. Harren, "Automatically tunable continuous-wave optical parametric oscillator for high-resolution spectroscopy and sensitive trace-gas detection," *Appl. Phys. B* **85**, pp.173-180 (2006).
- [6.52] N. Nakamura, M. Sugihara, M. Kotoh, H. Taniguchi, K. Tadatomo, "Quasi-phase-matched optical parametric oscillator using periodically poled MgO-doped LiNbO₃ crystal," *Jpn. J. Appl. Phys.* **38**, pp.L1234-6 (1999).
- [6.53] H. Ishizuki, I. Shoji, T. Taira, "High-energy quasi-phase-matched optical parametric oscillation in a 3-mm-thick periodically poled MgO:LiNbO₃ device," *Opt. Lett.* **29**, pp.2527 (2004).
- [6.54] D.H. Jundt, "Temperature-dependent Sellmeier equation for the index of refraction, n_e , in congruent lithium niobate," *Opt. Lett.* **22**(20), pp.1533-1555 (1997).
- [6.55] J. Yi, H. Ishizuki, I. Shoji, T. Taira, S. Kurimura, "Infrared laser spectra from an optical parametric oscillator using 5 mol.% MgO-doped periodically poled lithium niobate," *J. Korean Phys. Soc.* **47**(3), pp.439-443 (2005).
- [6.56] H. Ishizuru, T. Taira, "High-energy quasi-phase-matched optical parametric oscillation in a periodically poled MgO:LiNbO₃ device with a 5 μ m \times 5 μ m aperture," *Opt. Lett.* **30**, pp.2918 (2005).
- [6.57] H.P. Li, D.Y. Tang, S.P. Ng, J. Kong, "Temperature -tunable nanosecond optical parametric oscillator based on periodically poled MgO:LiNbO₃," *Optics&Laser Technology* **38**, pp.192-195 (2006).
- [6.58] J. Saikawa, M. Fujii, H. Ishizuku, T. Taira, "High-energy, narrow-bandwidth periodically poled Mg-doped LiNbO₃ optical parametric oscillator with a volume Bragg grating," *Opt. Lett.* **32**(20), pp. 2996-2998 (2007).
- [6.59] Y.L. Chen, J.W. Yuan, C.F. Yan, J.J. Xu, G.Y. Zhang. "Low-pump-threshold tunable optical parametric oscillator using periodically poled MgO:LiNbO₃," *Opt. Comm.* **273**, pp.560-563 (2007).
- [6.60] O. Paul, A. Quisig, T. Bauer, M. Nittmann, J. Bartschke, G. Anstett, J.A. L'Huillier, "Temperature - dependent Sellmeier equation in the MIR for the extraordinary refractive index of 5% MgO doped congruent LiNbO₃," *Appl. Phys. B* **86**, pp.111-115 (2007).

- [6.61] X. Zhang, B. Yao, Y. Wang, Y. Ju, Y. Zhang, "Middle-infrared intracavity periodically poled MgO:LiNbO₃ optical parametric oscillator," *Chinese Opt. Lett.* **5**(7), pp.426-427 (2007).
- [6.62] W.R. Bosenberg, A. Drobshoff, J.I. Alexander, L.E. Myers, R.L. Byer, "93% pump depletion, 3.5-W continuous-wave, singly resonant optical parametric oscillator," *Opt. Lett.* **21**(17), pp.1336-1338 (1996).
- [6.63] F.A. Katsriku, B.M.A. Rahman, K.T.V. Grattan, "Numerical modelling of second harmonic generation in optical waveguides using the finite element method," *IEEE J. Quantum Electron.* **36**, 282 (2000).
- [6.64] E.D. Palik, Handbook of optical constant of solids (Academic Press, New York, 1998).
- [6.65] J. Ota, W. Narita, I. Ohta, T. Matsushita, T. Kondo, "Fabrication of periodically-inverted AlGaAs waveguides for quasi-phase-matched wavelength conversion at 1.55 μ m," *Jpn. J. Appl. Phys.* **48**, pp.04C110 (2009).
- [6.66] G.T. Reed, A.P. Knights, Silicon Photonics. An Introduction (Wiley, Chichester, 2004).

7. Summary and Outlook

The work presented in this thesis focused on the development and characterisation of a number of compact broadly tunable laser sources operating in the visible, near-infrared and mid-infrared spectral regions, which are of considerable interest for a wide range of applications, but are unattainable for conventional lasers due to fundamental limitations. The main results on wavelength coverage by laser devices presented in the thesis are summarised in Fig. 7.1.



In the thesis, Chapter 1 presented a review of tunable diode lasers and described the need for compact tunable external-cavity diode lasers and the brief history of their development. The introduction to growth techniques, possible semiconductor diode laser structures and commonly used external-cavity configurations were also provided.

In Chapter 2, a broadly tunable InGaAs/InP strained multi-quantum well external cavity diode laser, which operates in the spectral range of 1494 nm – 1667 nm was demonstrated. Different pump current and temperature regimes were investigated. A maximum CW output power in excess of 81 mW and side-mode suppression ratio higher than 50 dB was achieved in the central part of the tuning range. This represents the highest output power and side-mode suppression ratio ever to be generated in this spectral region - which due to its extended coverage, could prove extremely useful for the deployment of these sources in dense wavelength division multiplexing applications, and also for high-speed swept sources.

In Chapter 3, a range of diode lasers with two waveguide designs (gain chip and semiconductor optical amplifier), processed from two different structures with chirped QD layers, were characterised. A comparison of their performances was undertaken. A number of strategies for enhancing the tuning range of external cavity quantum-dot lasers were exploited. Different waveguide designs, output facet reflectivities, laser configurations and operation conditions (pump current and temperature) were investigated for optimisation of output power and tunability.

A record broadly tunable high-power external cavity InAs/GaAs quantum-dot diode laser with a tuning range of 202 nm (1122 nm - 1324 nm) was demonstrated. A maximum output power of 480 mW and a side-mode suppression ratio greater than 45 dB were achieved in the central part of the tuning range. An average output power in excess of 400 mW was achieved for a tuning range of 110 nm. This represents a promising achievement for the development of a high-power fast swept tunable laser and compact nonlinear frequency generation schemes for the green-yellow-orange-red spectral range.

In Chapter 4, a brief theoretical introduction to second-order nonlinear processes, focusing on nonlinear optical frequency conversion and including phase-matching techniques was presented.

In Chapter 5, an all-room-temperature CW second harmonic generation at 612.9 nm and 591.5 nm in periodically poled potassium titanyl phosphate waveguides pumped by a broadly-tunable quantum-dot external cavity diode laser was demonstrated. A frequency-doubled power of up to 4.3 mW at the wavelength of 612.9 nm and 4.1 mW at 591.5 nm with a conversion efficiency of 10.5% and 7.9%, respectively, was achieved.

For the first time, a green-to-red tunable laser source with tunability of over 60 nm (567.7 nm – 629.1 nm) based on SHG in a single periodically poled potassium titanyl phosphate waveguide pumped by a single broadly-tunable quantum dot laser was demonstrated.

These results are an important step towards a compact tunable coherent visible light source, operating at room temperature. Further design work on the engineering of the waveguide structure along with careful choice of the nonlinear material and improvement of the laser-to-crystal coupling efficiency can further increase the demonstrated second-harmonic generation tunability and conversion efficiency and make the proposed breakthrough approach the preferred way for realisation of the compact full-colour laser source.

In Chapter 6, the possibility of obtaining second harmonic generation in orientation-patterned GaAs waveguides was investigated. Low-loss OP-GaAs waveguides were designed and fabricated. Frequency doubled light at 1621 nm in periodically poled GaAs waveguide was demonstrated. For this work, an optical

parametric oscillator system used as the pump source and based on the periodically poled 5 mol% MgO-doped Congruent Lithium Niobate crystal, generating light in the wavelength range between 1430 nm and 4157 nm, was developed.

Extremely promising results for fabrication of high-performance frequency conversion devices shown by orientation-patterned GaAs waveguides and their further optimisation can lead to realisation of significantly higher power nonlinear devices and extending the generated wavelength up to 16 μm by using optical parametric oscillation technology.